SMRI

Society for Magnetic Resonance Imaging

EIGHTH ANNUAL MEETING
FEBRUARY 24 - 28, 1990

Washington Hilton and Towers, Washington, D.C.

ORGANIZING COMMITTEE

E. Mark Haacke, Ph.D. R. Mark Henkelman, Ph.D.	ORGANIZING COMMITTEE CHAIRMEN
Kenneth R. Maravilla, M.D. Jeffrey C. Weinreb, M.D.	EDUCATIONAL PROGRAM CHAIRMEN
C. Leon Partain, M.D., Ph.D. Ronald R. Price, Ph.D.	SCIENTIFIC PROGRAM CHAIRMEN
Michael W. Weiner, M.D. Joanne S. Ingwall, Ph.D.	SPECTROSCOPY PROGRAM CHAIRMEN
David Thickman, M.D.	POSTER PROGRAM CHAIRMAN
Steven E. Harms, M.D. Michael L. Wood, Ph.D.	EVENING TUTORIAL PROGRAM CHAIRMEN
Shelley Field, R.T. Leslee Watson, R.T.	TECHNOLOGIST PROGRAM CHAIRMEN

OFFICERS

R. Edward Hendrick, Ph.D
PRESIDENT

Robert B. Lufkin, M.D.
PRESIDENT-ELECT

William G. Bradley, Jr., M.D., Ph.D.
PAST PRESIDENT

David D. Stark, M.D.
TREASURER

Felix W. Wehrli, Ph.D.
SECRETARY

BOARD OF DIRECTORS

Thomas J. Brady, M.D. (1992)
Michael T. Brant-Zawadski, M.D. (1992)
Graeme Bydder, M.D. (1991)
W. Thomas Dixon, Ph.D. (1992)
Margaret Foster, Ph.D. (1991)
John C. Gore, Ph.D. (Co-Editor)
E. Mark Haacke, Ph.D. (1992)
Steven E. Harms, M.D. (1992)
R. Mark Henkelman, Ph.D. (1991)
Robert J. Herfkens, M.D. (1990)
Shirley McCarthy, M.D., Ph.D.(1990)
Michael T. Modic, M.D. (1991)
Lawrence R. Muroff, M.D. (1991)
C. Leon Partain, M.D., Ph.D. (1991)
Ronald R. Price, Ph.D. (1992)
Francis W. Smith, M.D. (Co-Editor)
Gerald L. Wolf, M.D. (1990)
Michael L. Wood, Ph.D. (1991)

SMRI

SOCIETY HISTORY

The Society for Magnetic Resonance Imaging (SMRI) was chartered in 1982 to:

- provide an equal opportunity to clinical and basic scientists to contribute to the development of MRI.
- provide an international multidisciplinary forum for the advancement of magnetic resonance imaging.
- promote the applications of magnetic resonance techniques to medicine and biology, with specific emphasis on imaging.
- prepare and disseminate technical and product information related to research techniques, equipment and clinical applications of magnetic resonance.
- develop educational and training material and methods for the application of magnetic resonance to medicine and biology.

Since its conception, the SMRI has grown to an international association of clinical and basic scientists dedicated to research and the application of MR as a diagnostic technique in medicine. The professionalism and experience of its members has guided the Society to its current position as the major resource for the clinical MRI practitioner.

ANNUAL BUSINESS MEETING

The Annual Business Meeting of the SMRI is scheduled in the International Ballroom East on the date and time listed below:

Monday, February 26
- 12 Noon – 1:00 p.m.

All members are invited and encouraged to attend this very important meeting of the Society.

PAST MEETINGS

Organizational Meeting (1982)
Houston, Texas

First Annual Meeting (1983)
Broadmoor Hotel
Colorado Springs, Colorado

Second Annual Meeting (1984)
Greenlefe Hotel
Orlando, Florida

Third Annual Meeting (1985)
Town and Country Hotel
San Diego, California

Fourth Annual Meeting (1986)
Wyndham Franklin Plaza
Philadelphia, Pennsylvania

Fifth Annual Meeting (1987)
Palacio del Rio
San Antonio, Texas

Sixth Annual Meeting (1988)
Westin Copley Place
Boston, Massachusetts

Seventh Annual Meeting (1989)
Century Plaza Hotel
Los Angeles, California

Eighth Annual Meeting (1990)
Washington Hilton and Towers
Washington, D.C.

FUTURE MEETINGS

Ninth Annual Meeting (1991)
Chicago Hilton and Towers
Chicago, Illinois
April 13 – 17

Tenth Annual Meeting (1992)
New York Hilton and Towers
New York, New York
April 25 – 29

Eleventh Annual Meeting (1993)
San Francisco Hilton
San Francisco, California
March 27 – 31

SMRI HONORARY MEMBER AWARD

Honorary SMRI Membership is the highest honor of the Society and is awarded by the Board of Directors to that individual who, in the judgement of the Board, has rendered unusual service to the science of magnetic resonance imaging.

In 1990, the Society for Magnetic Resonance Imaging is pleased to award Honorary Membership to Francis W. Smith, M.D., Aberdeen Royal Infirmary.

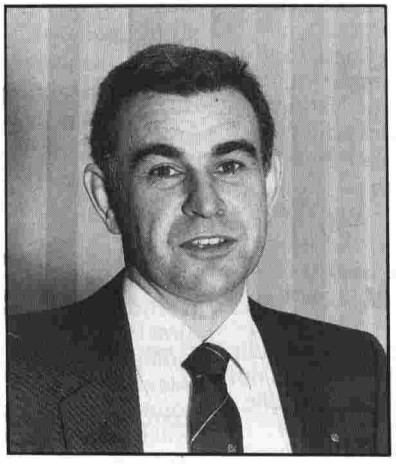

FRANCIS W. SMITH, M.D.
Aberdeen Royal Infirmary

1990 HONORARY MEMBER

Francis W. Smith, M.D.
Aberdeen Royal Infirmary

After earning his doctorate at the University of Aberdeen in 1970, Dr. Smith began active involvement in magnetic resonance imaging in 1980, being the first radiologist to use MRI for routine clinical diagnosis. Since that time, he has pioneered research into the clinical applications of MRI to the body, with special emphasis on the examination of the abdomen and pelvis. His early work in examining human pregnancy pointed the direction for this application of MRI.

Dr. Smith served as SMRI President pro tem in 1983–1984 during the formative years of the SMRI's development. In drafting the original SMRI constitution, Dr. Smith displayed great legal expertise and fine attention to detail which marks all his work.

Since 1984, he has been Co-Editor in Chief of the Society's journal, *Magnetic Resonance Imaging.* Under his guidance, the clinical component of the journal has grown substantially, cinching *MRI's* international position as the dominant clinical publication devoted to magnetic resonance imaging.

In 1988, Dr. Smith was elected a Fellow of the Society for Magnetic Resonance Imaging. Now, the SMRI is pleased to bestow Honorary Membership upon Dr. Frank Smith and to count him among its most valued members.

1989 HONORARY MEMBER AWARD

Ian R. Young, Ph.D.
Middlesex, England

1988 HONORARY MEMBER AWARD

Paul C. Lauterbur, Ph.D.
University of Illinois

GENERAL MEETING INFORMATION

REGISTRATION

All meeting registration will take place on the Concourse Level of the Washington Hilton and Towers during the following hours:

Saturday, Feb. 24
7:00 am – 5:30 pm

Sunday, Feb. 25
7:00 am – 6:00 pm

Monday, Feb. 26
7:00 am – 6:00 pm

Tuesday, Feb. 27
7:00 am – 6:00 pm

Wednesday, Feb. 28
7:00 am – 3:00 pm

SMRI SESSION DESIGNATIONS AND LOCATIONS

Education Program sessions will be presented in the International Ballroom East.

PS designates a Plenary Symposium. Plenary Symposia will be presented in the Lincoln Room on Sunday and the International Ballroom thereafter.

IT designates an Invited Talk. Presented as an introduction to select Proffered Paper Sessions, Invited Talks will be presented at the time and place indicated on the appropriate abstracts.

ET designates an Evening Tutorial presentation. Evening Tutorial sessions will be presented in the rooms indicated on page x.

P designates a Poster Scientific Paper. Poster Papers will be presented in the Poster Exhibit Area, accessible through the Technical Exhibits Area, Concourse Level. Posters will be on display Sunday – Wednesday.

DAILY LUNCHEONS

Complimentary luncheon service will be provided by the SMRI in the Crystal Corridor on Saturday and the Technical Exhibits Area thereafter.

TECHNICAL EXHIBITS

An expanded collection of leading-edge Technical Exhibitors will again complement the SMRI scientific program. Please plan to visit this integral component of the Annual Meeting in the Technical Exhibit Area, during the following hours:

Saturday, Feb. 24
5:30 pm – 7:30 pm

Sunday, Feb. 25
9:30 am – 6:00 pm

Monday, Feb. 26
9:30 am – 6:00 pm

Tuesday, Feb. 27
9:30 am – 6:00 pm

Wednesday, Feb. 28
9:30 am – 1:00 pm

SOCIAL PROGRAM

The SMRI cordially invites all attendees (single day registrants must visit the Social Program Desk for tickets) to join in an evening of fellowship at the following receptions:

Technical Exhibits Opening Reception

Technical Exhibit Area
Saturday, February 24
5:30 pm – 7:30 pm

Poster Exhibit Reception

Poster Exhibit Area
Monday, February 26
7:00 pm – 9:00 pm

Gala Reception: A Taste of America

International Ballroom
Tuesday, February 27
7:30 pm – 10:00 pm

A Social Program Desk will be staffed in the registration area for participants wishing to attend the above receptions with an accompanying guest.

Additional events, listed at right, are scheduled around Washington, D.C. and its environs. Don't miss this opportunity to explore our nation's capital...

SOCIAL PROGRAM TOUR DESCRIPTIONS

I've Never Been Here Before

Sunday, February 25, 1990
2:00 p.m. – 5:00 p.m.

Depart the hotel for an interesting tour about our Nation's Capital. Our tour takes you past the Capital, the Supreme Court, the Library of Congress and along the Mall, continuing on to the Lincoln and Vietnam Memorials. Next, stop at the Iwo Jima and Jefferson Memorials and the world famous John F. Kennedy Center for the Performing Arts. Conclude with a riding tour of historic Georgetown, passing by the National Cathedral and riding down Embassy Row.

Fee: $20.00 per person
Minimum: 43 persons

Capitol Hill

Monday, February 26, 1990
9:30 a.m. – 3:30 p.m.

Your guide will conduct you through passages not ordinarily seen on public tours as well as to the House and Senate Chambers and Statuary Hall. The next stop will be the Library of Congress and finally, the Supreme Court. Lunch will be "on your own" at the newly renovated Union Station.

Fee: $25.00 per person
Minimum: 43 persons

Dignity and Glory

Monday, February 26, 1990
9:30 a.m. – 1:00 p.m.

Visit Arlington Cemetary, where you will view the very moving Changing of the Guard ceremony. Stops will also be made at the graves of President Kennedy and Senator Robert Kennedy. Next visit the Air and Space Museum and see one of the multi-screened films in the museum theatre.

Fee: $26.00 per person
Minimum: 43 persons

The Federal City

Tuesday, February 27, 1990
7:30 a.m. – Noon

The first stop will be the White House. After the White House tour, guests will go to the Decatur House, an early 19th century residence built for Commodore Stephen Decatur, for a continental breakfast. Guests will enjoy a riding tour of Embassy Row and Georgetown. Finally, guests will have a special tour of the Washington National Cathedral.

Fee: $33.00 per person
Minimum/Maximum: 43 persons

Mount Vernon/ Historical Alexandria

Wednesday, February 28, 1990
8:30 a.m. – 1:30 p.m.

Step back into colonial history on a visit to Mount Vernon, the estate of our first President. Next take a riding tour of historic Alexandria, which was founded in 1749. There will be time in Alexandria to have lunch on your own and shop in the boutiques and shops along King Street.

Fee: $25.00 per person
Minimum: 43 persons

Georgetown

Wednesday, February 28, 1990
9:30 a.m. – 3:30 p.m.

Enjoy a tour of Georgetown, one of the most charming residential sections of Washington. Visit three of these lovely private homes. Lunch will be on your own. Enjoy shopping at Georgetown Park and at the shops and boutiques in Georgetown.

Fee: $33.00 per person
Minimum: 43 persons

Please contact the Social Program Desk to verify tour schedule and for further information.

TABLE OF CONTENTS

WEEK AT A GLANCE

SATURDAY FEBRUARY 24

EDUCATIONAL PROGRAM

7:00 am – 5:30 pm
General Registration

8:00 am – 10:45 am
Introduction to MRI/ Practical Technical Considerations

New Techniques for MRI

Hemorrhage & Hemorrhagic Lesions

Intravenous Contrast Agents: CNS

Cerebrovascular Disease

10:45 am – 11:15 am
Coffee Break

11:15 am – 12:45 pm
Intracranial Tumors

CNS AIDS

White Matter Disease

12:45 pm – 2:15 pm
Luncheon

2:15 pm – 5:00 pm
Head and Neck

Spinal Cord Disease

Degenerative Disease of the Spine

Spinal Trauma

Pediatric Spine

MRI of Syrinx

Questions and Answers

TECHNOLOGIST PROGRAM

7:30 am – 9:30 am
Physics of MR

Surface and Body Coils

Optimizing Image Quality in Difficult Exams

9:30 am – 10:00 am
Coffee Break

10:00 am – 12:00 pm
Applications of Fast Scan

Patient & System Induced Artifacts

Matched Bandwidth Technology

12:00 pm – 1:00 pm
Luncheon

1:00 pm – 3:00 pm
Futures of MRI

Cross Sectional Anatomy: An Overview

Echo Planar Imaging: An Overview

3:00 pm – 3:30 pm
Coffee Break

3:30 pm – 6:00 pm
Proffered Papers
see page ix for details

Organizational Meeting

TECHNICAL EXHIBITS RECEPTION

5:30 pm – 7:30 pm

SUNDAY FEBRUARY 25

EDUCATIONAL PROGRAM

7:00 am – 6:00 pm
General Registration

9:30 am – 6:00 pm
Technical Exhibits/Poster Sessions

8:00 am – 9:30 am
Flow and Angiography

Cardiac

Thorax and Aorta

9:30 am – 10:30 am
Coffee Break

10:30 am – 12:30 pm
Liver

Kidney and Adrenals

Prostate and Bladder

Gynecology

12:30 pm – 1:30 pm
Luncheon

1:30 pm – 3:00 pm
Knee

Shoulder

Wrist and Fingers

3:00 pm – 3:45 pm
Coffee Break

3:45 pm – 5:30 pm
TMJ

Practical Safety Considerations

New Horizons

SPECTROSCOPY PROGRAM

SMRI/SMRM JOINT SYMPOSIUM

8:00 am – 9:30 am
^{13}C Studies of Metabolic Pathways in Liver and Brain

^{31}P of Cardiac Ischemia

Proton MRI of the Brain

9:30 am – 10:30 am
Coffee Break

10:30 am – 12:15 pm
Proffered Papers
see page xii for details

12:15 pm – 1:30 pm
Luncheon

1:30 pm – 3:00 pm
Spectroscopic Imaging

Spectroscopic Imaging of ^{31}P

Spectroscopy of Proton Metabolites

Spectroscopic Imaging at 4.0 T

3:00 pm – 3:45 pm
Coffee Break

3:45 pm – 5:30 pm
Proffered Papers
see page xii for details

EVENING TUTORIAL PROGRAM

5:30 pm – 7:30 pm
Body

Introductory MRI Physics

Advanced MRI Physics

WEEK AT A GLANCE

MONDAY FEBRUARY 26

SCIENTIFIC PROGRAM

7:00 am – 6:00 pm
General Registration

9:30 am – 6:00 pm
Technical Exhibits/ Poster Sessions

8:00 am – 8:45 am
Award Presentations

8:45 am – 10:15 am
MR of the Shoulder

MR of the Knee

MR of Muscle

10:15 am – 10:45 am
Coffee Break

10:45 am – 12:30 pm
Proffered Papers
see page xiv for details

12:30 pm – 1:30 pm
Luncheon

1:30 pm – 3:00 pm
MR Angiographic Techniques

MR Applications

MR Perfusion/ Diffusion

3:00 pm – 3:45 pm
Coffee Break

3:45 pm – 5:30 pm
Proffered Papers
see page xiv for details

EVENING TUTORIAL PROGRAM

5:30 pm – 7:30 pm
Musculoskeletal

Spine

Quality Assurance & Acceptance Testing

POSTER SESSION SCIENTIFIC RECEPTION

7:00 pm – 9:00 pm

TUESDAY FEBRUARY 27

SCIENTIFIC PROGRAM

7:00 am – 6:00 pm
General Registration

9:30 am – 6:00 pm
Technical Exhibits/ Poster Sessions

8:00 am – 9:30 am
Image Contrast in Gradient Echo Sequences

Ultra Fast MRI

Acquisition and Processing of 3-D MR Imaging

9:30 am – 10:30 am
Coffee Break

10:30 am – 12:15 pm
Proffered Papers
see page xv for details

12:15 pm – 1:30 pm
Luncheon

1:30 pm – 3:00 pm
New Developments in Dynamic Cardiac Cine

MRI of Congenital Heart Disease

MRI/S of Cardiac Function

3:00 pm – 3:45 pm
Coffee Break

3:45 pm – 5:30 pm
Proffered Papers
see page xv for details

EVENING TUTORIAL PROGRAM

5:30 pm – 7:30 pm
Brain

Practice Management

GALA RECEPTION

7:30 pm – 10:00 pm

WEDNESDAY FEBRUARY 28

SCIENTIFIC PROGRAM

7:00 am – 3:00 pm
General Registration

9:30 am – 1:00 pm
Technical Exhibits/ Poster Sessions

8:00 am – 9:30 am
Neurosurgical Applications of Integrated 3-D Display of MRI/PET

Neuro Correlative Studies: MRI/MRS/PET

Clinical Spine MR: Pulse Sequences, Gradient Echo Techniques & Contrast Agents

9:30 am – 10:30 am
Coffee Break

10:30 am – 12:15 pm
Proffered Papers
see page xvi for details

12:15 pm – 1:00 pm
Luncheon

1:00 pm – 2:30 pm
Developments in Upper Abdomen Imaging: MRI & Correlative Modalities

Kidney & Retroperitoneum: Clinical Experience with MRI & Correlative Modalities

Female Pelvis: Clinical Results & Correlative Imaging with MRI/US/CT

2:30 pm – 2:45 pm
Coffee Break

2:45 pm – 4:30 pm
Proffered Papers
see page xvi for details

SATURDAY, FEBRUARY 24

Moderators:
K.R. Maravilla, M.D., J.C. Weinreb, M.D.

8:00 am – 10:45 am
- Intro. to MRI/Practical Technical Considerations ..... G.D. Fullerton, Ph.D.
- New Techniques for MRI ..... M.L. Wood, Ph.D.
- Hemorrhage and Hemorrhagic Lesions ..... S.W. Atlas, M.D.
- Intravenous Contrast Agents: CNS ..... V.M. Runge, M.D.
- Cerebrovascular Disease ..... R.N. Bryan, M.D.

10:45 am - 11:15 am
- Coffee Break ..... Crystal Corridor

11:15 am – 12:45 pm
- Intracranial Tumors ..... J.R. Hesselink, M.D.
- CNS AIDS ..... D.O. Davis, M.D.
- White Matter Disease .... O. Boyko, M.D.

12:45 pm – 2:15 pm
- Luncheon ..... Crystal Corridor

2:15 pm - 5:00 pm
- Head and Neck ..... I.K. Braun, M.D.
- Spinal Cord Disease ..... G. Sze, M.D.
- Degenerative Disease of the Spine ..... M.T. Modic, M.D.
- Spinal Trauma ..... J.L. Sherman, M.D.
- Pediatric Spine ..... A.J. Barkovich, M.D.
- MRI of the Syrinx ..... C.M. Citrin, M.D.
- Questions and Answers ..... Faculty

SUNDAY, FEBRUARY 25

Moderators:
K.R. Maravilla, M.D., J.C. Weinreb, M.D.

8:00 am – 9:30 am
- Flow and Angiography .. E.K. Fram, M.D.
- Cardiac ..... C.E. Spritzer, M.D.
- Thorax and Aorta ..... D.P. Naidich, M.D.

9:30 am – 10:30 am
- Coffee Break ..... Crystal Corridor

10:30 am – 12:30 pm
- Liver ..... M.E. Bernardino, M.D.
- Kidney and Adrenals ..... P.L. Choyke, M.D.
- Prostate and Bladder ..... M.D. Rifkin, M.D.
- Gynecology ..... S. McCarthy, M.D., Ph.D.

12:30 pm – 1:30 pm
- Luncheon ..... Crystal Corridor

1:30 pm – 3:00 pm
- Knee ..... D.L. Burk, M.D.
- Shoulder ..... M. Rafii, M.D.
- Wrist and Fingers ..... J.B. Kneeland, M.D.

3:00 pm – 3:45 pm
- Coffee Break ..... Crystal Corridor

3:45 pm – 5:30 pm
- TMJ ..... S.E. Harms, M.D.
- Practical Safety Considerations ..... E. Kanal, M.D.
- New Horizons ..... G. Bydder, M.B., Ch.B.

SATURDAY, FEBRUARY 24

Moderators:
S.A. Field, R.T., L. Watson, R.T.

7:30 am – 9:30 am
Physics of MR ..... L.A. Culbreath, R.T.
Surface & Body Coils ..... B. Farrar, R.T.
Optimizing Image Quality
in Difficult Exams ..... T.J. Robertson, R.T.

9:30 am – 10:00 am
Coffee Break ..... Crystal Corridor

10:00 am – 12:00 pm
Applications of Fast
Scan ..... W.H. Faulkner, R.T.
Patient and System Induced
Artifacts ..... K.T. McEwan, R.T.
Matched Bandwidth
Technology ..... D.U. Feliz, R.T.

12:00 pm – 1:00 pm
Luncheon ..... Crystal Corridor

1:00 pm – 3:00 pm
Futures of MRI ..... E.K. Keeler, Ph.D.
Cross Sectional Anatomy:
An Overview ..... D.G. Mills, M.D.
Echo Planar Imaging:
An Overview ..... F. Farzaneh, Ph.D.

3:00 pm – 3:30 pm
Coffee Break ..... Crystal Corridor

3:30 pm – 6:00 pm
Proffered Papers
Organizational Meeting

EVENING TUTORIAL PROGRAM

SUNDAY, FEBRUARY 25

5:30 PM – 7:30 PM

Georgetown East Room

Body ..... P.L. Davis, M.D.
J.M. Fulmer, M.D.
E.A. Zerhouni, M.D.

Georgetown West Room

Introductory MRI Physics ..... M.J. Bronskill, Ph.D.
S.R. Thomas, Ph.D.

Monroe East Room

Advanced MRI Physics .. D.G. Nishimura, Ph.D.
W. Sattin, Ph.D.

MONDAY, FEBRUARY 26

5:30 PM – 7:30 PM

Georgetown East Room

Musculoskeletal System ..... J.V. Crues III, M.D.
S.E. Harms, M.D.
F.G. Shellock, Ph.D.

Georgetown West Room

Spine ..... A.W. Litt, M.D.
V.M. Runge, M.D.
G. Sze, M.D.

Monroe East Room

Quality Assurance & Acceptance Testing .... J.E. Gray, Ph.D.
S.K. Mun, Ph.D.
J.G. Och, M.S.
R.R. Price, Ph.D.

TUESDAY, FEBRUARY 27

5:30 PM – 7:30 PM

Georgetown East Room

Brain ..... R.N. Bryan, M.D.
E.R. McVeigh, Ph.D.
G.E. Wesby, M.D.

Georgetown West Room

Practice Management .... C.E. Citrin, M.D.
M.A. Solomon, M.D.

SPECTROSCOPY PROGRAM

▼

SUNDAY, FEBRUARY 25

8:00 am – 9:30 am

Moderators:
J.A. Ingwall, Ph.D., M.W. Weiner, M.D.

^{13}C Studies of Metabolic Pathways in Liver and Brain ..... R.G. Schulman, Ph.D.
^{31}P of Cardiac Ischemia ..... K. Ugurbil, Ph.D.
Proton MRI of the Brain ..... J. Frahm, Ph.D.

9:30 am – 10:30 am

Coffee Break ..... Technical Exhibits Area

10:30 – 12:15 pm

Proffered Papers ..... see page xii for details

12:15 pm – 1:30 pm

Luncheon ..... Technical Exhibits Area

1:30 pm – 3:00 pm

Moderators:
J.A. Ingwall, Ph.D., M.W. Weiner, M.D.

Spectroscopic Imaging ..... I.R. Young, Ph.D.
Spectroscopic Imaging of ^{31}P ..... A.A. Maudsley, Ph.D.
Spectroscopy of Proton Metabolites ..... P.R. Luyten, Ph.D.
Spectroscopic Imaging at 4.0T ..... P.A. Bottomley, Ph.D.

3:00 pm – 3:45 pm

Coffee Break ..... Technical Exhibits Area

3:45 pm – 5:30 pm

Proffered Papers ..... see page xii for details

10:30 AM – 12:15 PM

Papers 001 – 008

SPECTROSCOPY I

Lincoln Room

Moderators:
T.R. Brown, Ph.D.
J.H. Park, Ph.D.

001 10:30
002 10:42
003 10:54
004 11:06
005 11:18
006 11:30
007 11:42
008 11:54

3:45 PM – 5:30 PM

Papers 009 – 016

SPECTROSCOPY II

Lincoln Room

Moderators:
G.D. Fullerton, Ph.D.
P.L. Davis, M.D.

009 15:45
010 15:57
011 16:09
012 16:21
013 16:33
014 16:45
015 16:57
016 17:09

SCIENTIFIC PROGRAM

MONDAY, FEBRUARY 26

8:00 am – 8:45 am
Award Presentations ..... R.E. Hendrick, Ph.D.

8:45 am – 10:15 am
Moderators:
H.K. Genant, M.D., F.G. Shellock, Ph.D.

MR of the Shoulder ..... H.K. Genant, M.D.
MR of the Knee ..... S.E. Harms, M.D.
MR of Muscle ..... W.A. Murphy, M.D.

10:15 am – 10:45 am
Coffee Break ..... Technical Exhibits Area

10:45 am – 12:30 pm
Proffered Papers ..... see page xiv for details

12:30 pm – 1:30 pm
Luncheon ..... Technical Exhibits Area

1:30 pm – 3:00 pm
Moderators:
E.M. Haacke, Ph.D., T.J. Masaryk, M.D.

MR Angiographic Techniques ..... P.J. Keller, Ph.D.
MRA Applications ..... J.L. Creasy, M.D.
MRA Perfusion/ Diffusion ..... T.J. Brady, M.D.

3:00 pm – 3:45 pm
Coffee Break ..... Technical Exhibits Area

3:45 pm – 5:30 pm
Proffered Papers ..... see page xiv for details

TUESDAY, FEBRUARY 27

8:00 am – 9:30 am
Moderators:
R.E. Hendrick, Ph.D., J. Tkach, Ph.D.

Image Contrast in Gradient Echo Sequences ..... F.W. Wehrli, Ph.D.
Ultra Fast MRI ..... M.S. Cohen, Ph.D.
Acquisition and Processing of 3-D MR Imaging ..... M.L. Wood, Ph.D.

9:30 am – 10:30 am
Coffee Break ..... Technical Exhibits Area

10:30 am – 12:15 pm
Proffered Papers ..... see page xv for details

12:15 – 1:30 pm
Luncheon ..... Technical Exhibits Area

1:30 pm – 3:00 pm
Moderators:
R.M. Henkelman, Ph.D., R.J. Herfkens, M.D.

New Developments in Dynamic Cardiac Cine ..... M. S. Silver, Ph.D.
MRI of Congenital Heart Disease ..... R.D. White, M.D.
MRI/S of Cardiac Function ..... C.B. Higgins, M.D.

3:00 pm – 3:45 pm
Coffee Break ..... Technical Exhibits Area

3:45 pm – 5:30 pm
Proffered Papers ..... see page xv for details

WEDNESDAY, FEBRUARY 28

8:00 am – 9:30 am
Moderators:
R.B. Lufkin, M.D., V.M. Runge, M.D.

Neurosurgical Applications of Integrated 3-D Display of MRI/PET ..... D.N. Levin, Ph.D.
Neuro Correlative Studies: MRI/MRS/PET ..... R.M. Kessler, M.D.
Clinical Spine MR: Pulse Sequences, Gradient Echo Techniques & Contrast Agents ..... J.S. Ross, M.D.

9:30 am – 10:30 am
Coffee Break ..... Technical Exhibits Area

10:30 am – 12:15 pm
Proffered Papers ..... see page xvi for details

12:15 pm – 1:00 pm
Luncheon ..... Technical Exhibits Area

1:00 pm – 2:30 pm
Moderators:
D.D. Stark, M.D., H.D. Sostman, M.D.

Developments in Upper Abdomen Imaging: MRI & Correlative Modalities ..... H.Y. Kressel, M.D.
Kidneys & Retroperitoneum: Clinical Experience with MRI & Correlative Modalities ..... T.A. Powers, M.D.
Female Pelvis: Clinical Results and Correlative Imaging with MRI/US/CT ..... S. McCarthy, M.D., Ph.D.

2:30 pm – 2:45 pm
Coffee Break ..... Technical Exhibits Area

2:45 pm – 4:30 pm
Proffered Papers ..... see page xvi for details

SCIENTIFIC PROGRAM PROFFERED PAPERS
MONDAY, FEBRUARY 26

10:45 AM – 12:30 PM

Papers 101 – 108
MUSCULOSKELETAL
Georgetown East Room

Moderators:
S.E. Harms, M.D.
P. Lang, M.D.

101 10:45
102 10:57
103 11:09
104 11:21
105 11:33
106 11:45
107 11:57
108 12:09

Papers 109 – 116
FLOW I
Georgetown West Room

Moderators:
R.D. White, M.D.
S.R. Underwood, M.D.

109 10:45
110 10:57
111 11:09
112 11:21
113 11:33
114 11:45
115 11:57
116 12:09

Papers 117 – 124
BRAIN I
Monroe East Room

Moderators:
W.G. Bradley, M.D., Ph.D.
J.L. Creasy, M.D.

117 10:45
118 10:57
119 11:09
120 11:21
121 11:33
122 11:45
123 11:57
124 12:09

Papers 125 – 132
SPECTROSCOPY III
Monroe West Room

Moderators:
R.E. Lenkinski, Ph.D.
M.R. Willcott, Ph.D.

125 10:45
126 10:57
127 11:09
128 11:21
129 11:33
130 11:45
131 11:57
132 12:09

Papers 133 – 140
MOTION SUPPRESSION/ CORRECTION
Military Room

Moderators:
S.J. Riederer, Ph.D.
L.P. Clark, Ph.D.

133 10:45
134 10:57
135 11:09
136 11:21
137 11:33
138 11:45
139 11:57
140 12:09

3:45 PM – 5:30 PM

Papers 141 – 147
PERFUSION/ DIFFUSION
Georgetown East Room

Moderators:
D.J. LeBihan M.D., Ph.D.
T.J. Brady, M.D.

IT-01 15:45
141 15:57
142 16:09
143 16:21
144 16:33
145 16:45
146 16:57
147 17:09

Papers 148 – 155
PELVIS
Georgetown West Room

Moderators:
S. McCarthy, M.D., Ph.D.
C.P. Semba, M.D.

148 15:45
149 15:57
150 16:09
151 16:21
152 16:33
153 16:45
154 16:57
155 17:09

Papers 156 – 163
BASIC NMR
Monroe East Room

Moderators:
S.R. Thomas, Ph.D.
M.A. Foster, Ph.D.

156 15:45
157 15:57
158 16:09
159 16:21
160 16:33
161 16:45
162 16:57
163 17:09

Papers 164 – 171
CONTRAST I
Monroe West Room

Moderators:
G.L. Wolf, M.D.
W.A. Murphy, M.D.

164 15:45
165 15:57
166 16:09
167 16:21
168 16:33
169 16:45
170 16:57
171 17:09

Papers 172 – 179
BRAIN II
Military Room

Moderators:
R.M. Kessler, M.D.
J.L. Sherman, M.D.

172 15:45
173 15:57
174 16:09
175 16:21
176 16:33
177 16:45
178 16:57
179 17:09

SCIENTIFIC PROGRAM PROFFERED PAPERS
TUESDAY, FEBRUARY 27

10:30 AM – 12:15 PM

Papers 201 – 208
IMAGING I – FAST
Georgetown East Room

Moderators:
F.W. Wehrli, Ph.D.
J.L. Duerk, Ph.D.

201 10:30
202 10:42
203 10:54
204 11:06
205 11:18
206 11:30
207 11:42
208 11:54

Papers 209 – 216
MRA I
Georgetown West Room

Moderators:
P.J. Keller, Ph.D.
D.G. Nishimura, Ph.D.

209 10:30
210 10:42
211 10:54
212 11:06
213 11:18
214 11:30
215 11:42
216 11:54

Papers 217 – 224
COMBINED CORRELATIVE IMAGING
Monroe East Room

Moderators:
D.N. Levin, M.D., Ph.D.
J.C. Weinreb, M.D.

217 10:30
218 10:42
219 10:54
220 11:06
221 11:18
222 11:30
223 11:42
224 11:54

Papers 225 – 232
SPINE I
Monroe West Room

Moderators:
M.T. Modic, M.D.
E.R. McVeigh, Ph.D.

225 10:30
226 10:42
227 10:54
228 11:06
229 11:18
230 11:30
231 11:42
232 11:54

Papers 233 – 240
SPECTROSCOPY IV
Military Room

Moderators:
H.C. Charles, Ph.D.
P.A. Narayana, Ph.D.

233 10:30
234 10:42
235 10:54
236 11:06
237 11:18
238 11:30
239 11:42
240 11:54

3:45 PM – 5:30 PM

Papers 241 – 248
CARDIAC
Georgetown East Room

Moderators:
C.B. Higgins, M.D.
W.J. MacIntyre, Ph.D.

241 15:45
242 15:57
243 16:09
244 16:21
245 16:33
246 16:45
247 16:57
248 17:09

Papers 249 – 256
IMAGE PROCESSING
Georgetown West Room

Moderators:
M.L. Wood, Ph.D.
R.F. Johnson, Ph.D.

249 15:45
250 15:57
251 16:09
252 16:21
253 16:33
254 16:45
255 16:57
256 17:09

Papers 257 – 264
JOINTS
Monroe East Room

Moderators:
T.A. Powers, M.D.
E.E. Kim, M.D.

257 15:45
258 15:57
259 16:09
260 16:21
261 16:33
262 16:45
263 16:57
264 17:09

Papers 265 – 272
BRAIN III
Monroe West Room

Moderators:
G. Bydder, M.B., Ch.B.
K.R. Maravilla, M.D.

265 15:45
266 15:57
267 16:09
268 16:21
269 16:33
270 16:45
271 16:57
272 17:09

10:30 AM – 12:15 PM

Papers 301 – 307
CONTRAST II
Georgetown East Room

Moderators:
E.C. Unger, M.D.
D.C. Thickman, M.D.

IT–02 10:30
301 10:42
302 10:54
303 11:06
304 11:18
305 11:30
306 11:42
307 11:54

Papers 308 – 315
CINE/DYNAMIC MRI
Georgetown West Room

Moderators:
L. Axel, M.D., Ph.D.
M. Silver, Ph.D.

308 10:30
309 10:42
310 10:54
311 11:06
312 11:18
313 11:30
314 11:42
315 11:54

Papers 316 – 323
BRAIN IV
Monroe East Room

Moderators:
J.S. Ross, M.D.
T.L. Chenevert, Ph.D.

316 10:30
317 10:42
318 10:54
319 11:06
320 11:18
321 11:30
322 11:42
323 11:54

Papers 324 – 331
MRA II
Monroe West Room

Moderators:
V. Haughton, M.D.
T. Vogl, M.D.

324 10:30
325 10:42
326 10:54
327 11:06
328 11:18
329 11:30
330 11:42
331 11:54

2:45 PM – 4:30 PM

Papers 332 – 339
ABDOMEN
Georgetown East Room

Moderators:
H.Y. Kressel, M.D.
E.A. Zerhouni, M.D.

332 14:45
333 14:57
334 15:09
335 15:21
336 15:33
337 15:45
338 15:57
339 16:09

Papers 340 – 347
MRA III
Georgetown West Room

Moderators:
R.I. Pettigrew, M.D.
D.J. Pennell, M.D.

340 14:45
341 14:57
342 15:09
343 15:21
344 15:33
345 15:45
346 15:57
347 16:09

Papers 348 – 355
HARDWARE SYSTEMS & CHARACTERISTICS
Monroe East Room

Moderators:
M.S. Cohen, M.D.
J.C. Gore, Ph.D.

348 14:45
349 14:57
350 15:09
351 15:21
352 15:33
353 15:45
354 15:57
355 16:09

Papers 356 – 363
PULSE SEQUENCE DEVELOPMENT & OPTIMIZATION
Monroe West Room

Moderators:
W.T. Dixon, Ph.D.
M.I. Hrovat, Ph.D.

356 14:45
357 14:57
358 15:09
359 15:21
360 15:33
361 15:45
362 15:57
363 16:09

SMRI

LETTER FROM THE ORGANIZING CHAIRMEN

Welcome to SMRI '90, the 8th Annual Meeting of the Society for Magnetic Resonance Imaging.

The role of the Organizing Chairman is one of drawing together the time–consuming and diligent efforts of each Program Chairman. This is, in practice, done in the Central Office which has made our job all the easier. Nevertheless, this responsibility continues throughout the Meeting, and we invite you to approach us with your comments about the operations and contents of any aspect of SMRI '90.

SMRI '90 opens with a two-day Educational Program. This is an opportunity to learn basic material from recognized experts in the field or to brush up on the basics and, at the same time, familiarize yourself with new advances.

SMRI is again hosting a one-day Technologist Program designed by and for MRI technologists. The Program may stand alone or provide an excellent introduction to the week-long Scientific Program.

SMRI '90 continues the topical conference on Sunday and introduces the first scientific symposium jointly sponsored by SMRI and the Society for Magnetic Resonance in Medicine. This Sunday program focuses on the Clinical Applications of MR Spectroscopy and, as usual, has no concurrent parallel sessions to interfere with your enjoyment of the presentations.

Following the Sunday program, SMRI '90 presents the most ambitious Scientific Program ever offered by SMRI. Due to the overwhelming response to the Call for Papers, there will be six parallel sessions each day. Including contributed papers, posters, and Works in Progress presentations, over 550 abstracts were reviewed with over 420 accepted. The Works in Progress sessions have expanded and will continue to offer registrants a fascinating look into the future of MRI. This enhanced program offers significant learning opportunities for the diverse SMRI attendee.

To facilitate more intensive discussion and interchange between presenters and their audience, SMRI '90 again includes an Evening Tutorial Program. Limited attendance allows for an informal atmosphere where newcomers may review a variety of clinical and basic topics with the "experts".

The Technical Exhibits have expanded for 1990 to provide you with a comprehensive demonstration of MR equipment, supplies, services, and exciting new developments.

To assist you in planning your personal itinerary during SMRI '90, we have provided this 1990 SMRI Printed Program, in what we hope is an improved format for easier abstract and information access. As usual, the program is unsurpassed as it strives to meet your scientific needs.

On behalf of the entire Program Committee, without whose efforts this superb program would not have been possible, we look forward to your participation in the SMRI 8th Annual Meeting.

E. Mark Haacke, Ph.D.
R. Mark Henkelman, Ph.D.
ORGANIZING COMMITTEE CHAIRMEN

NOTES

SPECTROSCOPY I

MODERATORS: T. R. BROWN, Ph.D., J. H. PARK, Ph.D.

► 001 10:30AM

A Comparison of Short TE STEAM Sequences for Volume Localized Proton Spectroscopy of the Brain

Robert E. Lenkinski and Duane Flamig
Department of Radiology, University of Pennsylvania and Baylor University Medical Center

The recent interest in solvent suppressed proton spectrocopy of the brain has led us to evaluate several different implementations of the stimulated echo(STEAM) sequence with TE's as short as 10 msec in terms of their signal-to-noise, suppression of solvent, minimum voxel size achievable and sensitivity to artifacts. In these evaluations we systematically investigated the effects of employing different types and numbers of frequency selective (CHESS) pulses for solvent suppression.We also employed various RF phase cycling schemes in combination with the studies described above in order to determine which phase cycling scheme was most effective. All of these evaluations were performed in phantoms and in normal volunteers. We found that suppression ratios in excess of 500 to 1 were routinely achievable with a combination of three CHESS pulses applied before the STEAM 90 degree pulse train. The precise order of spoiler gradients applied was critically important. The sequence with a TE of 10 msec gave the best signal-to-noise. We also found that an eight step phase cycling scheme in which the phase of the three STEAM pulses were varied by 180 degrees gave the best results.Spectra could be obtained from 1.7 cm^3 vovels in the brain with an optimized sequence. We found that the use of processing schemes such as alternate data shift additions could improve the apparent baseline in the spectra.

► 002 10:42AM

THE EFFECT OF LOCALISATION SCHEMES USING SELECTIVE PULSES FOR DIRECT SPECTRA LOCALISATION ON THE SPECTRA OF COUPLED SYSTEMS

Th.Ernst, J.Hennig
Radiol.Klinik, University Freiburg, FRG

Volume selection techniques, which use three selective pulses under orthogonal gradients to generate the stimulated echo (STEAM) or the (second) spin echo (PRESS) of spins inside the selected voxel have found widespread application at least in proton spectroscopy, where the relaxation times T2 of the metabolites are long. Care has to be taken, however, that the amplitudes of signals measured with these techniques does not only depend on the relaxation times T2 and T1. For coupled systems like lactate, glutamine, glutamate and others, the exact value of the flipangles of pulses and the timing of the sequence with respect to the coupling constant play an important role, which has been widely neglected in spectra interpretations so far.

These factors can be quantified by applying well–known density–matrix algorithm to the time evolution of the spin system. The major and highly significant difference of a localised spectroscopy experiment and a high–resolution experiment lies in the fact, that the gradients used for localistion lead to a loss of coherence of the total signal phase of transverse magnetisation during most of the experiment.

One important consequence of this fact is, that the stimulated echo of coupled spin systems will be affected by gradients in the tm–intervall whenever te is unequal 2/J. Especially at te = 1/J, all signal from the stimulated echo will be destroyed and only zero–quantum coherence can be observed. In a practical case this means, that lactate does not invert at te= 135 ms or te= 405 ms in a STEAM–experiment, the signal rather vanishes.

In order to demonstrate these effects, we have measured the spectra of all common metabolites under the conditions of in vivo spectroscopy experiments using STEAM– and PRESS–sequences at different timing intervalls. The spectra show, that the signal amplitudes for coupled systems with complicated coupling patterns like glutamate and glutamine, is significantly reduced compared to control spectra especially for the stimulated echo sequence. The signal modulation is much less pronounced for the PRESS–sequence as long as the flipangle of the refocussing pulses does not deviate appreciable from 180 degrees.

► **003** 10:54AM

VAPOR FOR SOLVENT SUPPRESSED, SHORT ECHO, VOLUME-LOCALIZED PROTON SPECTROSCOPY

RH Griffey,[1] D Flamig[2]

Center for Non-Invasive Diagnosis, University of New Mexico School of Medicine, Albuquerque, NM[1] and Dept of Radiology, Baylor University Med Ctr, Dallas, TX[2]

For gradient-localized proton spectroscopic techniques such as the stimulated echo, excellent suppression of the strong resonance from water is achieved with a preliminary frequency-selective stimulated echo (SUBMERGE, D.M. Doddrell, G.J. Galloway, W.M. Brooks, et al., *J. Magn. Reson.* 70: 176 (1986)) containing dephasing gradients applied sequentially along each of the three orthogonal axes to uniformly dephase longitudinal magnetization from water in the rotating frame. Combined with STEAM for localization, this VAPOR technique offers improved suppression compared to a single narrow band pulse followed by dephasing gradients or presaturation. Additional pulses beyond the three required to effect formation of the stimulated echo offer no improvement in suppression and can lead to the formation of spurious echoes in the digitization period. The minimum strengths and durations of gradient pulses required to effect the dephasing are described. Examples of 750-fold solvent suppression are shown in patients from a whole body system with well-compensated gradients. Localized spectra from 4 cc volume elements are presented which demonstrate that solvent suppression and localization to very small regions can be achieved with echo times of 10 msec. Proton NMR spectra can thus be acquired from patients without the phase and amplitude errors associated with incorporation of hard pulse binomial solvent suppression pulses into the localization scheme.

► **004** 11:06AM

THE PERFORMANCE OF LOCALIZED PROTON NMR SPECTROSCOPY OF THE HUMAN BRAIN *IN VIVO* ON MR IMAGING SYSTEMS OPERATING AT A MEDIUM FIELD STRENGTH OF 1.0 TESLA

R Sauter, W Loeffler, H Bruhn *, J Frahm *

SIEMENS AG, Bereich Medizinische Technik, D-8520 Erlangen, Fed. Rep. of Germany

* Max-Planck-Institut für biophysikalische Chemie, D-3400 Göttingen, Fed. Rep. of Germany

On a whole-body MR imaging system operating at a medium field strength of 1.0 T, water-suppressed localized proton NMR spectra from different regions of the normal human brain *in vivo* have been acquired using the stimulated echo (STEAM) technique [1]. Typically, a VOI of 27 ml was selected and multiple spectra with different echo times (TE = 34 ms, 270 ms) and repetition times (TR = 1500 ms, 3000 ms, and 6000 ms) were obtained. The in vivo 1.0T STEAM proton spectra from the insular region, occipital region, cerebellum and pons show well resolved resonances from N-acetylaspartate (CH_3 and CH_2), creatine and phosphocreatine, cholines, and inositols. Compared with a 1.5 T study [2] reported previously, the relative concentrations of the major cerebral metabolites as well as the T_2 relaxation times found at 1.0 T are in good agreement, while the T_1 relaxation times were found to be approximately 25 % shorter at 1.0 T.

STEAM proton spectra from the same VOI of the same volunteer were obtained at field strengths of 1.0 T and 2.0 T using identical measurement parameters and applying the same postprocessing. At both field strengths, virtually the same spectral resolution has been achieved. For the given repetition time of 1500 ms, the gain in SNR at the higher field strength is only 1.2. The surprisingly small field dependence of SNR and spectral resolution can be explained by the fact that the linewidths of cerebral metabolites observed in proton MRS are determined by susceptibility differences in the tissue and consequently scale with the field strength. Hence, proton MRS of the human *brain* has to be considered as a special case where in deviation from most *in vivo* studies, including proton MRS of muscle and phosphorous MRS in general, the observed linewidths are *not* determined by the field-independent natural linewidth and consequently SNR as well as spectral resolution no longer increase in direct proportion to the applied field strengths.

From these results we expect that proton MRS of the human *brain* is feasible on cost-optimized clinical MR systems operating at medium field strengths.

[1] J Frahm, KD Merboldt, and W Hänicke; J. Magn. Reson. 72, 502 (1987)

[2] J Frahm, H Bruhn, ML Gyngell, KD Merboldt, W Hänicke, R Sauter; Magn. Reson. Med. 11, 47 (1989)

LOCALIZED PROTON NMR SPECTROSCOPY OF THE HUMAN BRAIN: COMPARISON OF THE STIMULATED ECHO TECHNIQUE AND THE SPIN ECHO TECHNIQUE

R Sauter, M Schneider, W Grodd *
SIEMENS AG, Bereich Medizinische Technik, D-8520 Erlangen, Fed. Rep. of Germany
* Universität Tübingen, Abt. für Neuroradiologie, D-7400 Tübingen, Fed. Rep. of Germany

On conventional whole-body MR imaging systems, one of the most frequently used localization techniques for high resolution proton NMR spectroscopy *in vivo* is the stimulated echo (STEAM) technique [1]:

$$90^\circ(sl.x) - TE/2 - 90^\circ(sl.y) - TM - 90^\circ(sl.z) - TE/2 - STE.$$

Applying only 90° pulses, the STEAM technique provides a high degree of spatial selectivity and limited requirements for rf power. Further advantages of the STEAM technique are easy integration of spectral editing schemes like zero quantum modulation and maintenance of spatial localization even at very short echo times due to the application of spoiler gradients in the middle interval TM. The major disadvantage of the STEAM technique is that the stimulated echo (STE) represents only 50 % of the available signal from the VOI as defined by the intersection of the three excited slices (sl.x, sl.y and sl.z). A double spin echo (SE) technique [2]:

$$90^\circ(sl.x) - TE_1/2 - 180^\circ(sl.y) - (TE_1/2 + TE_2/2) - 180^\circ(sl.z) - TE_2/2 - SE$$

should theoretically provide a gain in sensitivity by a factor of 2 when compared to the STEAM technique.

Both localization techniques, STEAM and SE, have been implemented on conventional whole-body MR imaging systems (Siemens Magnetom) operating at 1.5 T. Water suppression was achieved by chemical shift selective saturation of the water protons preceding the STEAM or SE localization pulse sequence. The two techniques are found to be comparable with respect to the effort for implementation and susceptibility to residual instrumental imperfections. Measurements on phantoms and volunteers provided an improved sensitivity of the SE technique close to the theoretical factor of 2 when compared to STEAM. Using a echo time of 270 ms (TE or TE_1+TE_2) , the two techniques showed no significant difference in spatial selectivity. In initial applications of the SE technique in a clinical environment, the gain in sensitivity was used to reduce the size of the VOI (2 cm x 2 cm x 2 cm), enabling the examination of smaller cerebral neoplasms.

[1] J Frahm, KD Merboldt, and W Hänicke, J. Magn. Reson. 72, 502 (1987)
[2] RE Gordon, and RJ Ordidge, SMRM Book of Abstracts, 272 (1984)

LOCALIZED ^{1}H-MRS OF FELINE BRAIN AT 2.0 T WITHOUT STRONG GRADIENTS

L.K. Hedges* and J.R. Alger+
*BEIB/DRS & +NIS/NINDS. National Institutes of Health, Bethesda, MD

This presentation describes practical methods for detecting ^{1}H metabolite resonances from defined volumes of cat brain at 2.0 T. A modified-PRESS localization technique, requiring gradients less than 4 gauss/cm, is used with an rf probe designed for optimal sensitivity. These methods permit routine MRS examination of arbitrarily-positioned brain volumes. Short acquisitions from small volumes in opposite hemispheres (see below) have well-resolved signals from several highly concentrated cerebral metabolites. Use of the methods eliminates need for surgical retraction of extracranial tissues, and permits lactate detection without spectral editing. Furthermore, water suppression pulses can be eliminated if long TE times are acceptable. The methods are well-suited for the identification of brain foci having abnormal lactate, choline or N-acetyl aspartate levels.

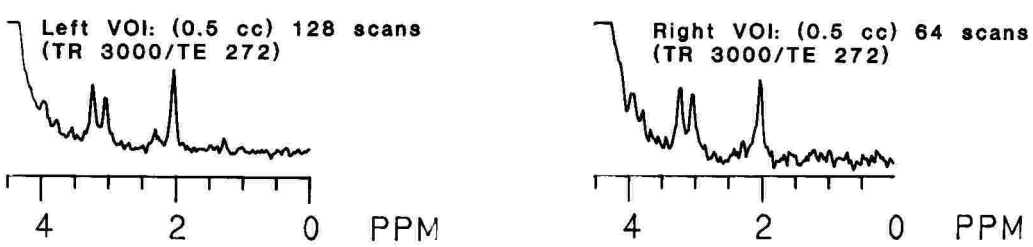

► **007** 11:42AM

LOCALIZED ^{1}H MRS OF HUMAN GLIOMAS AT 1.5 T

J.R. Alger, A. Bizzi, B.X. DeSouza, M.J. Fulham, S.W. Inscoe, J.L. Black, J.A. Frank, G. Di Chiro
Neuroimaging Section, NINDS, National Institutes of Health, and Georgetown University, Bethesda, Maryland.

A STEAM localization sequence was used to examine the ^{1}H MR spectra of volumes ranging from 18 cm^3 to 60 cm^3 in 25 patients referred for brain glioma using a 1.5 T GE Signa scanner. Most of the cases were recurrent tumors, which had previously been treated by surgical resection or radiotherapy, or both. Signals from lactate, N-acetylaspartate (NAA), cholines and creatine were evaluated. FDG-PET and Gd-DPTA MRI were also performed. Multi-slice GRASS scans (TR=600, TE=30, 10° flip angle) helped in the visualization of B_0 inhomogeneities. Artifacts complicated spectroscopic evaluation in seven cases. The NAA signal was decreased in 15 cases, but it was completely absent in only one lesion. The choline signal was elevated in 11 cases, was normal in four, with four additional cases in which it could not be detected. Lactate was clearly identified in nine of the 18 successful exams. It was present in four cases which were evaluated by FDG-PET as hypermetabolic (high grade), and in three hypometabolic (low grade) tumors. These results reveal variability in the spectral patterns of human glioma, which may be related to present restrictions on the size of the selected volume. On the other hand, this variability may be reporting fundamental and incompletely-understood aspects of individual brain tumors which may be of diagnostic and prognostic value.

► **008** 11:54AM

PROTON MAGNETIC RESONANCE SPECTROSCOPY OF ISCHEMIC BRAIN INJURY IN HUMANS: SERIAL STUDIES

PA Narayana, MJ Fenstermacher
Department of Radiology, The University of Texas Medical School at Houston

The purpose of these studies was to follow with <u>in vivo</u> proton magnetic resonance spectroscopy (MRS) the changes in the human stroke serially over a period of time, identify any potential specific markers of ischemic injury, and apply the relevant findings in a clinically useful prospective manner. Multislice coronal images with T_E = 80 ms and T_R = 2000 ms were obtained to locate the infarct. Spectra from the infarcted regions (8 cc volume) as well as contralateral matched normal regions were obtained using the stimulated echo sequence. Four patients were followed serially with proton MRS at times ranging from three days to ten weeks following a documented ischemic event.The time course of the concentrations of N-acetyl aspartate (NAA), creatine (Cr), and choline (Cho) were determined relative to the contralateral control. Lactate and lipid resonances were followed only qualitatively because of their absence in the contralateral control and their changes were related to the known pathophysiology of stroke. A conspicuous lack of significant change in the Cho resonance with concomittant decrease in NAA and Cr seems to be a possible marker of ischemic injury. These results were applied to a fifth patient with evidence of a non-ischemic cause for the acute stroke syndrome.

SPECTROSCOPY II

MODERATORS: G. D. FULLERTON, Ph.D., P. L. DAVIS, M.D.

► 009 15:45PM

METABOLITE MAPPING BY 1H NMR SPECTROSCOPIC IMAGING, COMPETITION FOR PET?

PR Luyten*, AJH Marië̈n*, PHJ van Gerwen*, JA den Hollander*, W.-D Heindel+, G. Friedman+
*Philips Medical Systems, P.O. Box 10.000, NL-5680 DA Best, The Netherlands.
+Department of Radiology, University of Cologne, Köln, F.R.G.

With the use of volume selection and water suppression techniques it is possible to measure different metabolites the human brain by 1H NMR spectroscopy, in particular N-acetyl aspartate (NAA), lactate (Lac), (phospho)creatine (Cr), choline compounds (Cho), alanine (Ala), and glutamate/glutamine (Glu). Recently, the extension of these techniques with phase encoding has enabled us to obtain 2D 1H NMR spectroscopic images over a 16x16 data matrix, with a field of view of 120x120 mm. With a slice thickness of 25 mm this leads to a nominal voxel size of 1.5 cc, obtained in a measurement time of 34 min. From these data sets metabolite maps can be reconstructed to visualize variations in metabolite concentrations with that spatial resolution.

We have applied this approach to examine a number of intracranial tumour patients with a 1.5 tesla clinical MR imager. Intracranial tumours usually show an increase of Cho, low NAA, and sometimes high Lac or Ala, with considerable differences between different tumours. However, the metabolite maps show that within the tumorous region large variations exist in metabolite distribution. In particular, in patient I (who suffered of a large glioma grade III) one portion of the tumour had high Cho and normal NAA level, while another part had high Cho, and no NAA. Within the tumour Lac was low, but Lac could be detected in the ventricles. Patient II (large astrocytoma, grade II) showed high lactate throughout the tumorous region, and no NAA. However, Cho was high in one portion of the tumour, and absent in the other. Patient III (oligoastrocytoma grade II/III) showed low NAA, and high Lac in the tumorous region.

Variations in metabolite concentration are most likely associated with tumour heterogeneity. Low NAA could indicate the absence of viable neurons, while high Lac can be a marker for high glycolytic activity. Increased Cho is observed in tumours, but not in infarcts or other pathologies. It is hoped that the 1H metabolite maps may be of help in staging, prognosis, and clinical management of intracranial tumour patients.

► 010 15:57PM

PRODUCTION OF ^{31}P METABOLIC IMAGES FROM CHEMICAL SHIFT IMAGING DATA.

SJ Nelson, JS Taylor, J Murphy-Boesch, DB Vigneron, TR Brown.
Dept. of NMR and Medical Spectroscopy, Fox Chase Cancer Center

The application of NMR spectroscopy to measuring changes in metabolism within specific regions of the body requires precise localization and correlation with anatomical features. Chemical shift imaging (CSI) produces spectra on well defined one, two or three dimensional grids which can be mapped directly onto corresponding proton images. To analyze the CSI data one must first quantify individual spectral and then estimate metabolic concentrations. We have developed automatic procedures for quantifying CSI spectra and extracting images of the spatial distribution of different metabolites. These use a modification of the PIQABLE algorithm to perform the quantification and peak specific Wiener filters to improve the signal to noise of the metabolic images. We have applied these procedures to the analysis of 2-D CSI data from the human forearm. A single turn 12.5 cm diameter surface coil was placed around the arm and 16x16 datasets collected with spatial resolution 1 cm. Localization perpendicular to the plane of the coil was provided by the drop-off in coil sensitivity, giving a slice thickness of approximately 8 cm. Metabolic images of P_i, PCr, γ-ATP, α-ATP and β-ATP were extracted from datasets with 8 acquisitions per voxel (total time 34 mins) and 1 acquisition per voxel (total time 4.5 mins). These metabolic images showed excellent correlation with the anatomy as seen in the proton images. A similar experimental set-up was used in conjunction with an exercise protocol in order to visualize changes in the ^{31}P metabolites during exercise. This showed specific changes in pH, P_i and PCr localized to three muscle groups: the flexor digitalis superficialis, the flexor digitalis profundis and the extensores carpi radialis. We have also obtained ^{31}P metabolic images from 3-D CSI data from the brain of normal volunteers. These latter data were obtained on an 8x8x8 grid of size 3 cm. The metabolic images of PCr, PDE and α-ATP showed clear variations in different regions of the brain which correlated well with anatomy.

► **011** 16:09PM

^{31}P NMR STUDIES OF A TRANSGENIC MOUSE MODEL EXPRESSING CREATINE KINASE IN LIVER

M.J. Brosnan*, L.Chen*, J.Chen#, T. VanDyke#, and A.P. Koretsky*
*Dept.Biol.Sciences, Carnegie Mellon Univ. and #Univ. of Pittsburgh

Little is known of the regulation of bioenergetics in the liver despite the highly metabolic nature of this organ. Free ADP has been proposed to be an important regulator in the liver as in other tissues such as heart and skeletal muscle. However, in the liver, quantification of this metabolite has been difficult. For this reason we have generated several lines of transgenic mice which express the B isozyme of creatine kinase in liver. Creatine kinase activity in these livers is comparable to that found in heart and brain. ^{31}P NMR spectra reveal a phosphocreatine peak from the transgenic livers. ^{31}P NMR examination of these livers, along with HPLC determination of total creatine content, allows the determination of free ADP levels using the creatine kinase equilibrium. A value of 0.059 ± 0.004 μmoles/g wet weight is found. This value is independent of total creatine content or CK activity indicating the reaction is at equilibrium.

We have used these mice to investigate the change in ADP which occurs upon infusion of fructose. The livers of creatine fed transgenic mice, like those of control creatine fed mice, show an elevated sugar phosphate and decreased inorganic phosphate peak after fructose infusion. In the case of the transgenic mice the fructose leads to a fall in PCr and protection of ATP levels. These results indicate that a fructose load leads to a doubling of free ADP levels. In addition, the combination of transgenic mice technology with in vivo NMR affords a powerful new approach to studying metabolic control.

► **012** 16:21PM

31P AND 1H NMR SPECTROSCOPY OF THE HUMAN BRAIN AND CLINICAL GRADING IN CHRONIC HEPATIC ENCEPHALOPATHY

Peter R. Luyten, Jan A. den Hollander, Diederik K. Bosman+, and Robert A.F.M. Chamuleau+
Philips Medical Systems, P.O. Box 10.000, NL-5680 DA Best, The Netherlands.
+Dept. of Experimental Medicine, Academic Medical Centre, Amsterdam

Spectroscopic studies of animal models during acute hepatic encephalopathy (HE) have resulted in the observation of abnormal metabolite levels in the brain. Changes in ATP levels have been detected by 31P NMR, while proton spectroscopy has revealed even more pronounced alterations in the levels of lactate, choline, glutamate and glutamine. We have employed spectroscopic techniques to obtain high quality localized (proton decoupled) phosphorus and proton brain spectra to asses metabolic changes in the brain of patients with HE.

Seven patients (age 23-63) have been examined, six having liver cirrhosis and one congenital liver fibrosis. For all patients the spectroscopic data have been correlated with several clinical classifications to grade the pathology (liver function tests (Child), HE tests (Reitan), plasma ammonia concentration , EEG).

The brain spectra of all patients clearly showed abnormal metabolite levels. The phosphorus data indicated abnormal mono- and diester levels, normal pH values and minor changes in ATP and PCr signals. However, all patients showed substantial changes in their choline (decreased), glutamate/glutamine (increased), and N-acetyl apartate (increased) levels relative to total creatine as detected by the localized proton NMR spectra (obtained using an echo time of 136 ms). These spectra show in particular that HE induced cerebral metabolic alterations can be detected by NMR spectroscopy. None of the patient proton NMR data showed any overlap with the control values. Moreover, the alterations were in agreement with the HE classification (grade 0,1,2) based on the conventional clinical observations.

PROTON LOCALIZED SPECTROSCOPY OF MS PATIENTS

P. Van Hecke, K. Johannik, P. Demaerel, G. Marchal, H. Carton, A.L. Baert
Department of Radiology, University Hospitals K.U. Leuven

Localized proton spectroscopy of the brain was performed on MS patients (n=12) and the results compared with those of a control group (n=5).

The experiments were performed on 1.5 T Siemens Magnetom using the stimulated echo method and selective water suppresion. Acquisition parameters were TR/TE/TM= 3000/270/30 ms, NA=256 and Acq= 13 min. Localized volumes ranged from 8 to about 30 cc. The size of the smallest volume was set by the S/N achievable within the acquisition time. The patients (ages 25 to 66) were at various stages of the disease. Three of the twelve patients did not show any plaques on the MR images. VOIs were chosen to contain as much plaque volume as possible. In the controls and in the patients with no plaques, the VOI were localized in the periventricular white matter.

All spectra were characterized by the presence of Cho (3,2 ppm), PCr+Cr (3,0 ppm) and NAA (2,0 ppm). The ratios NAA/Cho and NAA/Cr were calculated for both the MS and the control group. The results for the three MS patients with no detectable plaques did not differ significantly from the results of the control group. The former group is however too limited to draw any conclusion for the moment. For the MR positive patients, the following values were found (mean $\pm$1 SD) : NAA/Cho= 1,97 $\pm$0,35 and NAA/Cr= 2,14 $\pm$0,15. In the normals, these values were NAA/Cho= 2,49 $\pm$0,38 and NAA/Cr= 2,66 $\pm$0,17. The results quoted are TR and TE dependent.

It is concluded that these ratios are significantly lower in the MS patients (t-test at the 95% confidence level). The decrease is tentatively assigned to a decrease in NAA content in the MS patients. This is supported by the fact that the reduction in NAA/Cr and in NAA/Cho is about the same (0,79 and 0,80, respectively). The decrease in NAA could reflect the degradation of the neuronal tissue. Further work on specificity and sensitivity is in progress.

INTRACELLULAR FREE MG^{2+} CONCENTRATIONS IN THE HUMAN BRAIN.

JS Taylor, DB Vigneron, SJ Nelson, J Murphy-Boesch, TR Brown
Dept. of NMR and Medical Spectroscopy, Fox Chase Cancer Center

Recent development of a circularly polarized ^{31}P birdcage resonator for clinical studies of the head has allowed us for the first time to survey the entire brain with sufficient spatial resolution [$(3\ cm)^3$] and signal/noise to make accurate gray/white matter discrimination. Initial observations showed an upfield shift of the β-ATP peak in human brain relative to its position in muscle, as well as a significant difference in the β-ATP peak positions for gray and white matter. The β-ATP shifts from the central core of the cerebrum (white matter) in 3 volunteers were measured. The mean values and standard deviations for each of the 3 volunteers, obtained by averaging, respectively, 6, 7, and 7 voxels in white matter, were: -18.99 ± 0.06, -19.80 ± 0.21, and -18.97 ± 0.17 ppm. The simplest explanation for this upfield shift of the β-ATP resonance is that free Mg^{2+} levels are lower in this region of human brain than has been observed in brain from several species of animal (rat, rabbit). The above shifts correspond to Mg^{2+} concentrations of 0.2 mM in white matter. Spectra from regions of muscle in the same 3D datasets have β-ATP peak positions corresponding to Mg^{2+} concentrations greater than 1 mM.

Studies of the range of variation in spatial distribution of free Mg^{2+} and other ^{31}P observable brain metabolites are in progress. Representation of the spatial distributions as metabolite images as an effective way to deal with the information contained in the 3D datasets will be shown.

► **015** 16:57PM

PROTON MAGNETIC RESONANCE SPECTROSCOPY IN A CLINICAL MRI PRACTICE: INITIAL EXPERIENCE USING VAPOR AS AN ADD-ON SERIES FOR STUDIES OF THE BRAIN.

RH Griffey,[1] D Flamig,[3] NA Matwiyoff,[1] and LA Dell.[2]

Center for Non-Invasive Diagnosis, University of New Mexico;[1] Four Corners Radiological Assoc. Farmington NM;[2] Dept of Radiology, Baylor Univ Med Ctr, Dallas[3]

The utility of high resolution proton nuclear magnetic resonance (NMR) spectroscopy in a routine clinical setting has been evaluated in a series of twenty patients. In all cases, diagnostic MRI examinations of the brain were completed prior to spectroscopy which was implemented without modification of the hardware. The spectroscopic examination was performed using the VAPOR technique localized to a single 8 or 15.8 ml voxel. The localizing image, adjustment of magnetic field homogeneity, and acquisition of data was completed as a 25 minute add-on to a three-series MRI study. The twenty patients presented with tumor, stroke, headache, and multiple sclerosis. In eight patients, major differences related to the biochemistry/physiology of the lesion were observed in the spectral profile compared to controls or the contralateral hemisphere of the same individual. One study was compromised by patient motion. In ten cases the spectral profile was not altered significantly from control values. The results suggest that proton NMR spectroscopy may have a role for metabolic profiling of tissue in an add-on exam similar in duration to the use of GdDTPA.

► **016** 17:09PM

PHOSPHOCREATINE IMAGING AND SATURATION TRANSFER IN BRAIN

BN Mora[1,2], BD Ross[1], JM Allman[2] and PB Barker[1]

[1]Huntington Medical Research Institutes, [2]California Institute of Technology, Pasadena, CA 91105

Important metabolic changes accompany optical stimulation of the visual cortex in man (1). As part of a program to integrate Magnetic Resonance Imaging (MRI), Positron Emission Tomography (PET) and Nuclear Magnetic Resonance (NMR) Spectroscopy, we have implemented the techniques of Phosphocreatine (PCr) imaging and saturation transfer of the brain of the macaque monkey *Macaca fascicularus*.

Using a General Electric CSI-II 4.7T spectrometer and a solenoidal head coil which could be tuned to either ^{31}P (81 MHz) or ^{1}H (200 MHz), we have modified the spin echo imaging experiment proposed by Hsieh and Balaban (2) for use in muscle to take into account the different spin-spin relaxation times and concentrations of metabolites in brain. The animal preparation allowed experiments of up to eight hours to be performed, consisting of regular MRI imaging, followed by PCr imaging with and without saturation of γ-ATP.

PCr images of the brain were produced which could be superimposed over normal MRI images to confirm spatial localization. Saturation of γ-ATP produced the expected fall in PCr intensity, but sensitivity was not sufficiently high to permit regional comparison of creatine kinase fluxes. Techniques will be discussed for maximization of signal-to-noise ratios in localized saturation transfer experiments.

(1) Mora, BN, Carman, G, and Allman, JM, *Trends in NeuroScience* (in press)
(2) Hseih, PS, and Balaban, RS, *Journal of Magnetic Resonance*, **74**, 574-9.

MUSCULOSKELETAL I

MODERATORS: S. E. HARMS, M.D., P. LANG, M.D.

► 101 10:45AM

USE OF DYNAMIC Gd-DTPA ENHANCED MRI IN MUSCULOSKELETAL MALIGNANCIES

SL Hanna, BD Fletcher, DL Fairclough, A Le

Diagnostic Imaging and Biostatistics, St. Jude Children's Research Hospital

In an effort to improve specificity of MRI for determining viability and therapeutic response of malignant musculoskeletal tumors, we performed 32 dynamic Gd-DTPA-enhanced FLASH MR studies on 22 patients with osteosarcoma (9), Ewing sarcoma (9), lymphoma (1), rhabdomyosarcoma (2), and neuroblastoma metastasis (1). Ten studies were performed before and 22 during or following chemo/radiation therapy.

Changes in tumor signal intensity (SI) were measured on FLASH gradient-echo sequences (TR, 30 msec; TE, 10 msec; 2 NSA; flip angle, 40°) at 15 second intervals, starting before and continuing for at least three minutes after manual intravenous injection of Gd-DTPA. SI of regions of interest within the tumor were then plotted against time. Percent increase SI per minute over the baseline value i.e. slope of curve (Erlemann R., Radiology 1989; 171:767), was calculated and compared with histologic findings.

Slopes of pathologically proven lesions were greater ($p=0.003$) for viable tumors (mean=77; range=29-189) than for non-viable tumors (mean=22, range=11-34). In 15/16 exams, a slope >30% reflected tumor viability, while in 4/5 studies, a slope of <30% favored tumor inactivity.

Seven tumors were evaluated before and during induction chemotherapy, two did not respond and had increasing slopes, while in the remaining five responsive tumors, slopes decreased to below or remained at approximately 30%. Two patients with recurrent tumors showed slopes >30% while the three patients with stable lesions were <30%.

These data suggest that the rate of Gd-DTPA uptake in malignant tumors is modified by therapy and that dynamic-enhanced MRI may contribute to identification of tumor response and viability.

Supported in part by the National Cancer Institute, Cancer Center Support (CORE) grant P30CA21765 and by the American Lebanese Syrian Associated Charities.

► 102 10:57AM

Bone Marrow Imaging Using STIR at 0.5T and 1.5T

Kendall Jones, M.D., Per Granstrom, M.D., Evan Unger, M.D., Joachim Seeger, M.D., Raymond Carmody, M.D., Mark Yoshino, M.D., Rebecca Hunt, M.D.
University of Arizona, Department of Radiology, Tucson, Arizona 85724

We retrospectively evaluated MR images in a blinded study to evaluate the use of STIR inversion recovery images in bone marrow imaging at 0.5 and 1.5T. Firstly, these sequences were implemented on a 0.5T Toshiba MRT-50A and a Siemens 1.5T scanner and the sequences were adjusted for optimal image quality, contrast and fat nulling. The study included 50 patients examined at each field strength for a variety of bone marrow pathologies (principally oncologic) and compared the contrast to spin echo short TR/TE, long TR/TE sequences and FLASH gradient echo sequences.

The study indicates the following conclusions: **1)** STIR images are more reliable at 0.5T than at 1.5T; motion compensation is often necessary at 1.5T while this is generally not necessary at 0.5T and the contrast is generally greater at the lower field strength. Still, even at 0.5T STIR images are more prone to artifacts than FLASH or spin echo images. **2)** At 0.5T FLASH usually has as much contrast as STIR for imaging disease in hematopoietic marrow (e.g. the spine) but STIR has greater contrast for imaging disease in fatty marrow than either FLASH or the spin echo pulse sequences.

► **103** 11:09AM

EXTRASKELETAL MULTIPLE MYELOMA DEMONSTRATED BY MRI

EE Kim, JS Cho, LK Misra, S Wallace, B Barlogie
UT M D Anderson Cancer Center

Neoplastic plasma cells in multiple myeloma are typically concentrated within the medullary space. However, autopsy studies have demonstrated microscopic infiltrates of myeloma outside of bone in up to 70% of cases. Often the extramedullary myeloma involvement represents a direct extension from diseased bone.

We have retrospectively evaluated MRI studies in selected 40 patients with histologically proven multiple myeloma. MRI examination was performed using 1.5T magnet (Signa System; General Electric Co.) with spin-echo technique. T1, proton density and T2 weighted images were usually obtained in multiplanes and multislices. Of the 40 patients; there were 20 sites of extramedullary myeloma involvement in 18 patients; 5 epidural spaces, 4 paraspinous muscles, 2 liver, 2 gluteus muscles, 2 neck and mediastinal nodes, 1 psoas muscles, 1 spleen, 1 breast, 1 lung, 1 pericardium. Extraskeletal myelomas demonstrate low signal intensity on T1-weighted images and heterogenous intermediate to high signal intensity on T2-weighted images. In contrast to medullary myelomas, they were better shown on T2-weighted images.

It is concluded that MRI is very useful in assessment of the extraskeletal involvement of multiple myeloma.

► **104** 11:21AM

CHANGES IN MRI SIGNAL INTENSITY WITH RADIATION THERAPY

SL Hanna, BD Fletcher, LE Kun, MA Lemmi

Diagnostic Imaging and Radiation Oncology, St. Jude Children's Research Hospital & University of Tennessee, Memphis

Recognition of iatrogenic changes is essential in MRI evaluation of therapy of musculoskeletal tumors. We performed serial 1.0T MRI studies in six patients with Ewing sarcoma before and after hyperfractionated radiation therapy and in two patients with soft tissue malignancies who received conventionally fractionated therapy. T1-weighted, T2-weighted, STIR and Gd-DTPA-enhanced T1-weighted sequences were employed.

Diffuse increase in signal intensity of subcutaneous soft tissue and muscle corresponding to the radiation port was noted on T2-, STIR and enhanced T1-weighted images, consistent with radiation changes. Abnormal intensity was most marked on STIR and was observed on follow-up studies obtained from 1 week to 62 weeks after completion of radiation therapy ranging from 24-60 Gy. All cases showed corresponding enhancement following Gd-DTPA administration. Fatty deposition developed in the irradiated marrow of six patients and bladder wall thickening was observed in three of four patients receiving pelvic radiation.

Differentiation of abnormal soft tissue MRI signal intensity from malignant infiltration may be facilitated by knowledge of radiation therapy volumes and comparison with pre-radiation MR studies.

Supported in part by the National Cancer Institute, Cancer Center Support (CORE) grant P30CA21765 and by the American Lebanese Syrian Associated Charities.

► **105** 11:33AM

PYOMYOSITIS: EARLY DETECTION UTILIZING MAGNETIC RESONANCE IMAGING

GR Applegate, AJ Cohen

University of Pittsburgh, Department of Radiology, Pittsburgh NMR Institute and the University of California, Irvine, Department of Radiological Sciences

Pyomyositis accounts for 3% to 4% of surgical admissions in East Africa, however, there were no reported cases in the United States prior to 1971. Since then there have been numerous reports of this entity utilizing ultrasound, nuclear medicine and CT. Diagnosis is often delayed using these modalities due to the non-specific findings and unfamiliarity with this entity. Recent cases are presented utilizing multiple modalities including plain films, CT, ultrasound, indium-111 labeled white blood cells, Gallium-67 citrate with SPECT, bone scans and five magnetic resonance studies. We report the MR appearance of 4 recent cases of pyomyositis evaluated at our Institutions and compare the MR appearance to other imaging modalities.

Although pyomyositis is a rare clinical entity in the United States, its prompt diagnosis can lead to effective clinical management. In all cases MRI was accurate in the diagnosis of pyomyositis. MR can reliably differentiate fluid collections from soft tissue masses or evolving hematomas. In addition, MR is very sensitive for the early changes of osteomyelitis combined with the ability to demonstrate these focal muscle abscesses with superior anatomical localization. Therefore, if there is a clinical suspicion as to the presence of pyomyositis, we advocate initial evaluation with magnetic resonance imaging. If there is a question of remote sites of pyomyositis, nuclear medicine whole-body white cell or Gallium scans would be helpful to localize areas for further MR scanning.

► **106** 11:45AM

LOW FIELD MRI OF THE MUSCULOSKELETAL SYSTEM

L Ekelund

Department of Diagnostic Radiology, University Hospital, S-901 85 Umeå, Sweden

Musculoskeletal imaging has become one of the most important nonneurologic applications of magnetic resonance imaging (MRI). The experience so far has been limited to MR systems with intermediate or high field strengths. If ultra-low field MRI could provide diagnostic information comparable to that obtained from systems with higher field strengths, this would have important economical implication.

MR examinations were performed with a low field resistive magnet operating at 0.02 T (Acutscan, Instrumentarium, Finland). While poor signal-to-noise ratio and long imaging times make extremely low field MRI less useful in abdominal imaging, more promising results have been obtained in the imaging of musculoskeletal disorders, where the lack of motion of the object results in better image quality. In patients with bone and soft tissue tumors (n=18) the diagnostic information was at least comparable to that obtained from CT. With a non-ferromagnetic osteosynthesis the healing course after femoral neck fractures was evaluated in 14 patients and avascular necrosis of the femoral head could be diagnosed earlier than on conventional radiographs. It was also possible to diagnose tears of the cruciate ligaments of the knee (5 patients).

Ultra-low field MRI may provide important diagnostic information in the evaluation of many musculoskeletal disorders. The magnet has recently been upgraded to 0.04 T, which has improved image quality.

► **107** 11:57AM

MRI AND THE DIABETIC FOOT INFECTION
A Wang, D Weinstein, L Chiu, L Greenfield, R Chambers, W Weaver, R Diaz
Rancho Los Amigos Medical Center

Fifty patients with known diabetus mellitus and clinical suspicion of osteomyelitis were studied. All had plain x-ray films and MRI examinations.
Sequences: Picker 0.5T - 27 pts., 1.5T - 23 pts.
Sagittal, Coronal, & Axial SE 700/26 STIR 2000/125/40 or SE 2000/20/100 5 mm.
43/50 patients had surgery & culture: resection 43, biopsy 3.
Sites of Infection: Phalanges 24, Metatarsus 26, Talus 1, Calcaneus 2.
Pathology: The bones were resected and decalcified. Microscopic determination of osteomyelitis was made.
All patients treated medically or surgically were followed-up clinically.
MRI findings of osteomyelitis: Acute: 48% ↓ T1WI, iso. or ↑ T2WI, ↑↑ STIR
Chronic: 50% ↓ T1WI, iso. T2WI, inhomogenous ↑ STIR
True positive: 63% True negative: 30% False positive: 6% False negative: 0%
X-ray Findings: True pos.: 25% True neg.: 18% False pos.: 7% False neg.: 50%
Pitfalls - Fracture: ↓ T1WI ↑↑STIR (fracture line seen)
Charcot Joint: ↓ /iso. T1WI ↓/↑ or mixed STIR (occur at tarsal joints)
Bone Cyst: ↓ T1WI ↑↑STIR (well circumscribed)
We were usually able to make the differentiation clinically or with a bone biopsy.
Conclusion: MRI offers superior detection for osteomyelitis. The anatomic extent of infection can be localized to an individual bone or portion of bone which allows a clear margin of resection which will preserve as much functional foot as possible. Three views are usually required to avoid partial volume effect from surrounding cellulitis. Accurate positioning is important. MRI offers the best management of foot infection in diabetic patients.

► **108** 12:09AM

ACUTE FEMORAL NECK FRACTURE: UNENHANCED AND GD-DTPA ENHANCED MR IMAGING

Philipp Lang, Gunther Schwetlick, Mathias Langer, Michael Mauz, Ulrich Weber, Harry K. Genant, and Roland Felix
Dept. of Radiology, University Clinic Rudolf Virchow/Charlottenburg, Free University Berlin,
Dept. of Orthopaedic Surgery, Oskar-Helene-Heim, Free University Berlin,
Dept. of Radiology, University of California San Francisco

Femoral neck fracture frequently leads to interruption of blood supply to the femoral head with resultant traumatic osteonecrosis. Although scintigraphy may be employed to assess the perfusion of the femoral head after acute femoral neck fracture, reports on its sensitivity and thus its ultimate clinical value have been controversial. In the present study, 10 patients with traumatic femoral neck fracture were prospectively studied with unenhanced and Gd-DTPA-enhanced (0.1mmol/kg body weight, Magnevist, Schering, Berlin, FRG) MR imaging (0.5T, Magnetom, Siemens, Erlangen, FRG; *precontrast:* multiecho, TR=1600msec, TE=30-240msec; *pre- and postcontrast:* spin-echo, TR=400msec, TE=30msec; gradient-echo, TR=315, TE=14msec, θ=90°). In 7 patients, superselective digital subtraction angiography was performed and correlated to MR imaging findings. DSA demonstrated complete interruption of blood supply to the femoral head in 5 patients. In 2 patients, the femoral head arteries were intact. The fracture line had low signal intensity on precontrast MR images. In all patients, the femoral head showed normal, high signal intensity on all of the precontrast sequences. In the 2 patients with intact femoral head arteries, the femoral head, neck, and shaft demonstrated an increase in signal intensity after i.v. administration of Gd-DTPA which was comparable to the unaffected side. In the 5 patients with impaired blood supply to the femoral head, the signal intensity of the marrow cavity located distally to the fracture increased also markedly on the postcontrast images. The signal intensity of the femoral head, however, did not change on the postcontrast images and was lower than that of the marrow distal to the fracture or that of the unaffected side. We conclude that Gd-DTPA enhanced MR imaging may represent a unique noninvasive imaging modality for the assessment of femoral head perfusion after acute femoral neck fracture.

FLOW I

MODERATORS: R. D. WHITE, M.D., S. R. UNDERWOOD, M.D.

► **109** 10:45AM

BLOOD FLOW IN THE VICINITY OF THE CAROTID BIFURCATION

MD Cockman, FL Van Nice, and LW Jelinski
AT&T Bell Laboratories, Murray Hill NJ 07974

Using stroboscopically sampled micro-MRI images of the carotid arteries of eighty-gram rats, we have found a blood flow pattern "signature" that occurs at systole in the vicinity of the carotid bifurcation. This "signature" appears as three lobes of different intensity within the carotid and is sensitive to stenoses, providing a valuable marker for studying vascular damage.

EKG-gated spin-echo images at short TE (7.14 ms) of ~800 μm slices with true pixel sizes of 33 μm and 132 μm in the frequency- and phase-encode directions, respectively, were obtained in approximately six minutes. Phase-angle images were constructed from the spin-echo data and the transverse flow pattern throughout the entire heart cycle was visualized (see Figure). Flow through both carotid arteries was monitored simultaneously, showing that blood flow reaches the right carotid faster than the left, a phenomenon readily explained by the anatomy of blood supply from the heart. The phase-angle images show that the flow directions of the lobes of the "signature" change sign, indicating reverse flow pools near the carotid bifurcation. The appearance of the signature can be explained qualitatively as an impedance mismatch at the bifurcation. The appearance of the carotid flow "signature" changes dramatically in the presence of approximately 50% stenoses. The effects of flow through the right artery after occlusion of the left artery were also investigated.

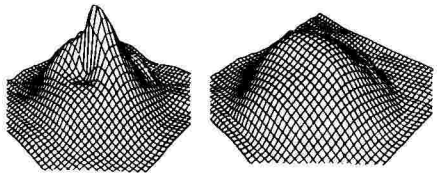

These results provide the first direct view of blood flow through arteries of sub-millimeter diameter, producing otherwise unavailable data for fluid dynamics modelling.

► **110** 10:57AM

Application of Rigorous Transport Theory to Flow/Motion in MRI

P R Moran, A D Elster
Wake Forest University, Bowman Gray School of Medicine

Bloch's MR Equations address explicitly only stationary magnetization behavior and evolution, for a subject. When local magnetization might be moving (in liquid flow or net tissue transport, in a medical MRI situation), however, the equations may be rigorously extended by Boltzman's Transport Equations to give the combined Bloch-Boltzman Equations. Surprisingly, for MRI applications, the corresponding rigorous solutions for magnitudes and spatially varying signal-phase, never were directly derived: published results have been borrowed from small-specimen contained sample nmr literature. Nevertheless, the rigorous forms of solution for the Bloch-Boltzman equations actually are quite simple to state and to apply. Three immediately important aspects provide novel insights and potentials for application in MR imaging with subjects possessing flow/motion: (1) The Phase-Response possesses an initial phase-bolus transport term, which can be a strong motion effect in extended subjects; it is not predicted from earlier approximate solutions. (2) Magnitude and Phase equations separate uniquely, in all cases, for all cycles and sequences: enormously simplified computation algorithms for accurate full-scan flow/motion modeling are possible for generalized MRI-modes. (3) Some "mysteries" frequently observed in clinical visual appearance of human subject blood vessels, for differing multi-slice staggering techniques, can be directly explained.

► **111** 11:09AM

MR BOLUS-TRACKING FLOW IMAGING: COMPARISON OF SEVERAL METHODS
KA Kraft, PP Fatouros, DY Fei
Dept. of Radiology, Medical College of Virginia, Richmond, VA

Several variations of the bolus-tracking technique for studying bulk fluid motion have been described, including 1) simple projection excitation of a plane orthogonal to the vessel orientation[1], 2) slice-selective imaging within the plane of the vessel with perpendicular saturation tagging[2], and 3) spatial premodulation of longitudinal magnetization to produce a sinusoidal intensity banding pattern throughout the image[3]. In this study we evaluated the above sequences using flow phantoms of varying configurations. Experiments were carried out using a 2.4 T Bruker Biospec and a 1.0 T Siemens imager. The objective of this work was to judge the utility of each sequence for depicting various ranges of fluid motion. Thus, a rational basis is established for applying such methods to flow measurements in vivo.

Method 1 has been found to accurately represent velocity profiles in tubes over a wide range of steady and nonsteady flow conditions. However, as a projection technique, the use of this method will be limited in vivo due to lack of anatomic information and the problems of background static tissue signal and overlapping vessels. Methods 2 and 3 involve selective excitation of a plane within which the vessel of interest lies, thereby avoiding problems of projection imaging while simultaneously revealing the regional anatomy. Our results indicate that method 2 is well suited for studying flow over a wide range of velocities. One disadvantage of this method is the inconvenience of tagging multiple points of the vessel simultaneously. Conversely, method 3 can readily depict flow patterns throughout a large continuous section of vessel. However, in images of high velocity flow, individual fluid velocity profiles are not clearly distinguished. This particular sequence, therefore, may be most useful for evaluating slow blood or cerebrospinal fluid motion.

Our studies using flow models indicate that the appropriate choice of a bolus-tracking method should be based on the expected range of fluid velocities. Care is required when quantitating flow directed obliquely with respect to the magnet gradient axes.

(1) K Shimizu et al., Radiology 1986; 159:195-199. (2) RR Edelman et al., Radiology 1989; 171:551-556. (3) L Axel and L Dougherty, Radiology 1989; 171:841-845.

► **112** 11:21AM

SHORT (TE3.5 msec) FIELD EVEN ECHO REPHASING SEQUENCES FOR IMPROVED BLOOD FLOW MEASUREMENT
D.N.Firmin, *G.L.Nayler, D.Pennell, P.Kilner and D.B.Longmore
National Heart and Chest Hospitals and *Picker International, London, U.K.

Field Even Echo Rephasing (FEER) type sequences have previously been developed and shown to accurately measure blood flow. There are, however, a number of limitations that can restrict the accuracy and reliability of the method; these normally become most apparent when more complex flow types are present such as those often found in the region of cardiovascular abnormalities. The limitations include signal loss due to phase dispersion, misregistration errors due to flow between the times of the three spatial encodings and quantification errors due to additional phase shifts introduced by orders of motion other than the one being imaged. The symmetrical gradient profiles utilised by the FEER sequence result in rephasing of all odd orders of motion whereas even motion orders still result in dephasing and contribute to signal loss. The effect of these even orders can be reduced by shortening the effective gradient durations. In this study the echo time of the FEER sequence was greatly shortened (down to 3.5 msec) to minimise the signal loss and reduce the effect of the other limitations, to some extent at the expense of the resolution, signal/noise ratio and the slice shape. The sequence was assessed in vitro using a stenosis phantom and in vivo on both normal subjects and patients. Comparisons were made with longer FEER sequences and shorter gradient echo sequences without the FEER gradient symmetry. As predicted by the theory, phantom experiments showed that the use of the short FEER sequence proved to be most effective in reducing signal loss. In patient studies the sequence has been used to advantage enabling velocity measurements through stenotic valves so that pressure gradients can be derived non-invasively. An additional advantage of the sequence is its suitability for fast repetition rates which enable measurements of acceleration or aortic pulse wave velocity in one acquisition period.

► 113 11:33AM

3D Flow Imaging with snapshot FLASH

David Norris[1], Dietmar Henrich[2], Dieter Leibfritz[1] and Axel Haase[3]
[1]Universität Bremen, [2]Bruker Medizintechnik, [3]Universität Würzburg, FRG.

The snapshot-FLASH experiment (1) is capable of delivering 128x64 element images with an imaging time of less than 250ms. We have previously investigated the use of this technique for projective flow imaging (2), and have now turned our attention to the rapid generation of 3D flow data sets. The procedure adopted was to selectively saturate a thin slice using a sinc-modulated 90^0 pulse, and subsequently to obtain a snapshot-FLASH image. The signal from stationary tissue is then strongly suppressed relative to that from flowing material. This experiment is then repeated n times for n different slice offsets giving a 128x64xn data set from the n contiguous slices. We have implemented this procedure on our Bruker 4.7T, 40cm Biospec imaging/spectroscopy system fitted with a 15cm gradient insert. Images of a human hand were obtained with n=64 slices, each slice having a thickness of 1mm. With ECG triggering the total imaging time is less than 1 minute. This technique should provide a robust method of studying flow, as the extremely short echo time of the snapshot-FLASH experiment (<3ms) makes it almost immune to motion induced phase changes, and also allows high velocity flow to be imaged.

(1) Haase A, Magn. Reson. Med. in Press.
(2) Norris D. G. et. al., Works in Progress, SMRM, Amsterdam 1989, p1125.

MONDAY a.m.

► 114 11:45AM

PHASE VELOCITY ENCODING OF LAMINAR AND TURBULENT FLOW IN A SMOOTH STENOSIS AND CURVED TUBE

J Oshinski*, C Biancheri*, DN Ku*, C Markou*, R Pettigrew#, H Engels+
*School of Mechanical Engineering, Georgia Institute of Technology, Atlanta, GA, 30332
#Emory University; +Philips Medical Systems

Magnetic resonance imaging using a gradient echo sequence and phase velocity encoding was used to generate two-dimensional velocity profiles in phantom models. Measurements were conducted on a Philips Medical Systems 0.5T imager using a head coil. Gyroscan Plus and Database Angiography (DBA) software were used to obtain and process the data. A steady flow recirculating system pumped water doped with maganese chloride through one-inch ID tubing to the models. Cross-sectional velocity profiles were obtained for several positions along a 180-degree curved one-inch tube model. Measurements were conducted for flows with Reynolds numbers ranging from from 500 to 9,000. Velocity profiles were also obtained for a 90% smooth stenosis model. Measurements were taken one diameter upstream of the stenosis, in the throat of the stenosis, and at 1.5, 3, and 5 diameters downstream of the stenosis. Flows with Reynolds numbers ranging from 500 to 4000 were measured.

The results indicate that velocity measurements using this technique can accurately measure spatially varying velocities, secondary flow, reverse flow, and limited unstable flow. The fully-developed laminar velocity profile upstream of the stenosis agreed to within 10% of theoretical profile. The maximum velocity measured was 242 cm/sec in the throat of the stenosis. For most flowrates the velocity at the throat of the stenosis agreed within 10% of the theoretical value. Velocity profiles obtained were smooth and continuous; however, some noise was seen near the wall at high flowrates. Velocity profiles for turbulent flow were obtained in limited cases. Turbulence intensity appeared to be an important cause in the loss of coherent phase data in disturbed flows. Comparison of MRI with laser doppler anenometry (LDA) velocity profiles from similar models showed good agreement on a point-by- point basis. The phase velocity encoding technique shows excellent promise as a quantitative velocimeter for hemodynamic studies and in the detection of vascular stenoses.

► **115** 11:57AM

SEQUENTIAL INVERSION RECOVERY SNAPSHOT– FLASH

U. Böttcher, D. Norris, D. Leibfritz
Universität Bremen, FB2, NW2,Leobenerstr. 2800 Bremen 33

In NMR imaging several parameters can be made the basis for obtaining image contrast between different tissues. Spin-lattice relaxation time is one parameter for tissue characterization. Fast gradient switching times make it possible to measure several projection steps after one inversion pulse with the Snapshot-FLASH method (1).

The experiments were performed on a BRUKER Biospec system with a 4.7T (40cm) magnet. We used a small gradient system with an inner diameter of 15cm and a homogeneous resonator with an inner diameter of 7.5cm.

We employed a hyperbolic secant pulse for the inversion. After a variable recovery delay we started the gradient echo imaging sequence. The small gradient system we used allowed the realization of gradient switching times of the order of 400 μs. We used a Gauss-pulse with a duration of three milliseconds to have a sufficantly thin slice for good resolution. The total duration of one phase encoding step was 11.7 milliseconds. After one inversion pulse 16 projection steps were obtained in 190 milliseconds. After a relaxation delay the measurement was continued to take the next 16 projections. Repeating this procedure allowed the measurements of enough phase encoding steps for the resolution desired. With a recovery delay of 5 seconds between the detection of 16 projection steps, it was possible to get an 256x256 image in less than one and a half minutes.

T1 weighted images were obtained from phantoms and the head of a rat, showing a good contrast between tissues with different T1 relaxation times.

1) Haase, A., J. Magn. Reson., in press

► **116** 12:09PM

REALTIME INTERACTIVE CONTROL OF THE OBLIQUE ANGLE IN MR FLUOROSCOPY

RC Wright, F Farzaneh, *JK Maier, RC Grimm, SJ Riederer, RL Ehman
MR Laboratory, Mayo Clinic, Rochester, MN
*General Electric Medical Systems, Milwaukee, WI

We have previously demonstrated realtime MR data acquisition and reconstruction in the technique we call MR Fluoroscopy (1). Typically, data acquisition is performed continuously using a short TR/TE sequence (e.g. 6/4.5 msec) with the number of phase encoding views reduced (e.g. 96) compared to conventional imaging. Immediately after measurement, raw data is directed to an array processor, reconstructed, and displayed. The lag between the acquisition of any echo and its display is less than 200 msec. We report here on how we have recently incorporated realtime control of angulation into the fluoroscopic acquisition. Suppose one starts with an axial plane. At the outset of the fluoroscopic scan the observer sees the axial image sequence on the display. While viewing the realtime display, the observer can then enter a rotation angle at the MR operator's console, and within several hundred msec observe the fluoroscopic images corresponding to slices rotated by this angle. Present angular resolution is 10 degrees, and rotation can be about any axis. By iterating this process one can tune the angulation to the desired plane of section to be imaged. We describe the implementation of realtime oblique angulation control, and present in vivo MR fluoroscopic image sequences.

Ref:
Farzaneh F, et al. Radiology 171:545-549 (1988).

BRAIN I

MODERATORS: W. G. BRADLEY, Jr., M.D., Ph.D., J. L. CREASY, M.D.

► 117 10:45AM

ECHO-PLANAR MRI OF THE CNS

'MK Stehling, 'JL Firth, 'BS Worthington, RJ Ordidge and P Mansfield

Dep. of Physics and 'Neurosurgery and 'Academic Radiology, University of Nottingham, NG7 2RD, England; 'present address: USZ, Dep. Med. Radiologie, Zürich, Switzerland.

EPI provides MR images in, typically, 30 - 100 ms from a single FID, i.e. after a single spin-system preparation. Tissue parameters including proton density, T1, T2, chemical shift and flow can be encoded by an appropriate preparatory pulse sequence (spin system preparation module) such as SR, SE, IR, bipolar gradients, and then read-out with the EP image formation module in a fraction of a second, without any repetition. If this is repeated rapidly (up to 20 times/ sec.), the evolution of tissue parameters can be monitored dynamically.

We have imaged more than 50 patients with pathology of the CNS with EPI. Ultrafast multislice MBEST (5 planes/sec.) and single and multislice, multipoint inversion recovery (e.g. 6 planes, 6 TI's in approximately 1 minute) provides 3D data sets with T1 or T2 information in patients with intra- and extraaxial tumours and inflammatory lesions. T1 and T2 maps can be calculated from this data. CSF flow in normals and hydrocephalics and intracranial blood flow can be observed with MBEST time course studies and quantified with flow encoding. Time course studies with ultrafast IR-EPI immediately after the injection of Gd-DTPA provides dynamic morphological information of intracranial pathology (gliomas, meningiomas, acoustic neuromas, metastases) and allows qualitative perfusion assessment. We demonstrate how the speed and flexibility of EPI can be employed to obtain morphological and functional information on the CNS and how interactive operation of an EP scanner can be used to optimise imaging parameters such as tissue contrast in real-time with the potential for improved lesion detection confidence, examination efficiency and patient comfort.

► 118 10:57AM

MRI AND MR-ANGIOGRAPHY OF THE CAROTID ARTERY: VALIDATION WITH DSA

G Bongartz, W Krings, P Vassallo, E Rummeny, PE Peters

Dept. of Diagnostic Radiology, University of Muenster, FRG

Recent developments in MRI enable us to visualize blood flow in a fast and comprehensive way. The ability to detect arterial stenosis has been described previously. Flow effects like higher-order motion or slow flow cause problems in MRA due to signal variations which exaggerate the degree of stenosis or produces complete signal loss. Turbulences occur mainly at the site of an atherosclerotic plaque as well as at all arterial truncations. Therefore minimal atherosclerotic damage and physiological flow effects may not be differentiated since both lead to focal signal defects in MRA.

High resolution MR images perpendicular to the arterial axis allow visualization of the arterial wall and atherosclerotic plaques in vivo. The combination of MRI (perpendicular to the carotid bifurcation) and projective MRA enables a differentiation between arterial wall change and flow effects (turbulences).

In this study, the results of 1. MRA (time of flight - method) 2. DSA (arterial) 3. MRI (perpendicular) of the carotid arteries in 70 patients with clinically suspected stenosis were compared. The first group of 5 patients were used as a training phase for the readers, in which the results of all modalities were directly compared. In the remaining patients the DSA films and the MR images were read independently by 3 radiologists.

We found an excellent correlation between DSA and MRA as regards the presence or absence of carotid stenosis in app. 90%. The degree of stenosis was overestimated in more than 35% (predominantly in the first 40 patients). The combination of MRA and MRI (perpendicular) provided precise assessment of the degree of arterial stenosis. Furthermore, it was possible to differentiate between various plaque structures, such as calcified plaques and infiltrative atheroma.

We conclude that a reliable assessment of the carotid arteries and the degree of stenosis can be achieved by the combination of MRA and MRI.

► **119** 11:09AM

MR-ANGIOGRAPHY: RESULTS IN 16 PATIENTS WITH CONFIRMED ANEURYSMS OF THE INTRACRANIAL ARTERIES.

S. Felber, W. Judmaier, F. Aichner, G. Birbamer
University of Innsbruck, Department of Magnetic Resonance

3D-MR-Angiography just recently introduced, is rapidly developing towards routine clinical application. Interpretation of MRA requires dedicated knowledge considering phase- and inflow effects. Pitfalls may also arise from signal loss due to susceptibility changes, if gradient echo sequences are used.
In order to estimate the confidence of MRA in intracranial aneurysms, the MRA results of 16 patients were compared to conventional X-Ray angiography.

MRA was performed on a 1.5 T Magnetom with a circular polarized head coil in all cases. For MRA a motion compensated 3D-FISP sequence was used. Axial orientation of the 3D-volume provides signal enhancement of vessels, depending on inflow effects, additional gradients compensate for constant velocity signal void. Small voxels and minimal TEś of 7ms are required for adaequate vessel enhancement and spatial resolution. In 14 patients the homogenity of the static magnetic field was optimized by shimming on the linear gradients (H_2O line-width: 14-18Hz). X-Ray AG was performed via transfemoral catheter-technique using nonionic contrast agents.

MRA demonstrated 15(16) angiographically confirmed aneurysms. One posterior communicating artery aneurysm which was less than 3 mm in diameter was not detected on MRA. In 3 cases MRA provided additional information to X-Ray angiography.

On 2 occasions arbitrary reformatted projectional images from MRA were superior to conventional AGś in localisation of the aneurysm, in another case MRA showed an additional aneurysm, not seen on X-Ray AG.

7 aneurysms of our series were clinically asymptomatic and detected by MRA during a routine brain MR study. MRA presently will not replace conventional AG, but can serve as a noninvasive screening tool and has the potential to offer additional diagnostic information in some of the patients.

► **120** 11:21AM

Time of flight magnetic resonance angiography using a new radiofrequency spoiled gradient echo 3D pulse sequence

Philip W. Chao, M.D., Felix Wehrli, PhD, John Listerud, PhD.

Magnetic resonance angiography (MRA) is a promising new technique but is limited by turbulent flow and other sources of dephasing which lead to signal losses. We performed MRA using a new 3D spoiled gradient echo technique with short echo delays times (5 ms) using a commercially available pulse sequence. The radio-frequency spoiled gradient echo pulse sequence was originally designed for thin section 3D contiguous images, but with the appropriate parameters is capable of excellent quality magnetic resonance angiography with imaging times as short as 3 minutes. In addition, this pulse sequence also does not have the central image artifact which occurs with gradient spoiled gradient echo images. We attempted to optimize imaging parameters and to examine the ability of this pulse sequence to visualize aneurysms.

We utilized a GE 1.5 T ® Signa, with version 4.0 hardware and software. For MRA the two key features are the ability to have short echo delay times (as short as 5 ms) by allowing only partial sampling of the echo and a radio-frequency spoiled gradient echo pulse sequence (SPGR ® GE (Milwaukee, WI)) which can be acquired using either 3DFT or 2DFT techniques.

We assessed the optimal flip angle by comparing the signal intensity of the right internal carotid bifurcation minus white matter signal intensity when we altered only the flip angle from 15° to 60°. Signal intensity was also compared to non-spoiled gradient echo images using the same imaging parameters varying the flip angle from 10° to 40°.

Optimal imaging parameters were TR40 ms, TE6 ms, flip angle 35°, 1mm contiguous slice thickness, 28 slices, which generates an axial data set with 28 contiguous slices. The axial plane of section was the optimal plane for visualization of flow. The dataset can then be either collapsed into a single plane or projected using a maximum pixel intensity ray projection technique. It is important to limit the projections to the area around the circle of willis and in some instances to the internal carotid artery on one side in order to reduce vessel overlap. This allowed the detection of smaller aneurysms.

Eight normal volunteers were scanned. Five cases of known aneurysms (7 total) on conventional angiography were compared to their appearance on SPGR MRA . All aneurysms (ranging in size from 2mm to 9mm) were seen on SPGR MRA. Turbulence caused dephasing of spins which obscured the aneurysm neck in 2 of 5 cases. Loss of signal was seen within the aneurysm in all 5 cases, presumably due to turbulence and dephasing of spins. Slight displacement of the flow signal in the artery from the outline of the artery was noted. The spin saturation effect obscured flowing spins distally in the imaging slab.

SPGR MRA allows the clinician to perform MRA without special research pulse sequences. This is a significant milestone in MRA and its potential future applications.

► **121** 11:33AM

THE VALUE OF PROTON SPECTROSCOPY FOR THE DIAGNOSIS OF BRAIN TUMORS.

D.Ott, Th.Ernst, H.Friedburg, J.Hennig
Radiol.Klinik, University Freiburg, FRG

During the last year a number of groups have reported significant changes in proton spectra of brain tumors as compared with normal tissue. Based on these findings, it has been tentatively assumed, that proton spectroscopy is able to play a key role in differential tumor diagnosis. We have undertaken a study of more than 100 patients with different brain tumors. Tumor diagnosis was based on histology either of post–operative samples or by biopsy. As a volume selection method we used the PRESS–technique with echotimes te of 135 or 270 ms. The voxel size used varied from 3.4 ml to 27 ml depending on the size of the lesion. Spectroscopic examinations were accompanied by at least one T2–weighted imaging sequence (Multislice–multiecho and/or RARE). The total examination time for imaging and spectroscopy was one hour.
Spectra from the normal brain contralateral to the tumor were acquired as reference. Tumor spectra showed a considerable variance, when different parts of large tumors were examined using small voxel sizes. The spectra of vital tumor tissue show increased choline and reduced creatine resonances at 3.2 and 3 ppm respectively. The occurence of signals in the methylene region of the spectrum (1.3 ppm), which can be attributed to lactate or lipids correlates well with parts of the tumor, which were judged to be necrotic from the imaging results. Although this general finding was found in all common tumors, spectra should considerable variance between patients with the same tumor and considerable overlap exists between spectra of different tumor types.
Our results strongly suggest, that proton spectroscopy gives information about the metabolic state of tumors. Differential diagnosis of tumors or the diagnosis of tumors vs. other lesions appears to be highly problematic. In at least one case examined so far, we could demonstrate, that the spectrum of a MS–plaque looks like a typical tumor spectrum. The relative intensity of the choline resomance compared to NAA can, however, be a usefull indicator for the grading of tumors.

► **122** 11:45AM

EVALUATION OF THE INTRACRANIAL VENOUS SYSTEM WITH THE THIN-SLICE OBLIQUE ACQUISITION SEQUENTIAL TECHNIQUE

JS Lewin(1), G Laub(2)
Department of Radiology, Case Western Reserve University, Cleveland, Ohio, USA (1), and Siemens Medical Systems, Erlangen, FRG (2)

The purpose of this study was to optimize a technique for visualization of the sub-ependymal veins and venous sinuses free from arterial overlap, with good spatial resolution, and with a short examination time.

Twenty volunteers were imaged using a new oblique 2D FLASH method with sequential acquisition of images rotated from 10 to 30 degrees from the sagittal toward the coronal plane, a 60 degree FA, 28 msec TR, 10–13 msec TE, 2–3 mm slice thickness, 256 by 256 matrix, velocity compensation, and a presaturation pulse over the carotid arteries. Examinations were performed on a 1.5 T system with a 10 mT/meter gradient capability and transmit/receive head coil. Total exam time varied from 6 to 10 minutes. Maximum intensity profile postprocessing was then performed.

The superior sagittal sinus (SSS), straight sinus, vein of galen, and internal cerebral veins were consistantly well visualized, with the thalamostriate veins, inferior sagittal sinus, and portions of the septal veins and Basal veins of Rosenthal well seen in most studies. Persistant small signal voids were noted at the junction of the Vein of Galen and straight sinus from turbulent flow.

Time–of–flight angiography of the midline venous structures performed in the sagittal plane, parallel to the primary direction of bloodflow, lacks adequate inflow enhancement, while coronal imaging of the entire SSS requires either thick slices with poor resolution or a prolonged imaging time. By rotating the imaging plane from the sagittal toward the coronal plane the magnitude of inflow is increased, proportional to the sine of the angle of rotation. At approximately 15 degrees of rotation the inflow from the midline venous system is adequate for inflow angiography, allowing a small number of slices to include the entire SSS and deep midline veins. The short imaging time, high spatial resolution, and high degree of consistancy suggest that this technique should be clinically useful in the evaluation of sinus thrombosis and other disorders of the intracranial venous system.

► **123** 11:57AM

Gd-DTPA-ENHANCED MR FOLLOW-UP OF INTRA-ARTERIAL (*ia*) ACNU CHEMOTHERAPY OF MALIGNANT GLIOMA (MG) AND CORRELATION WITH POSITRON EMISSION TOMOGRAPHY (PET) OF REGIONAL CEREBRAL GLUCOSE METABOLISM

N Roosen, T Kahn, KJ Langen, B Oeser, JCW Kiwit, M Bettag, WJ Bock, U Mödder, LE Feinendegen
Departments of Neurosurgery, Diagnostic Radiology & Nuclear Medicine, University Hospital, Düsseldorf, and Institute of Medicine, Nuclear Research Center, Jülich, Fed Rep Germany

Recent neuro-imaging developments appear very promising with regard to improved therapy follow-up of MG. The present report examines the potential value of *Gd*-MR imaging combined with PET of regional cerebral metabolic rate for glucose (rCMR*glc*) during *ia* chemotherapy of MG with the nitrosourea ACNU (nimustine).

Of 50 patients treated recently according to our *ia*ACNU management protocol (clinical review, see: Roosen et al: CANCER 1989, 64, in press) 8 individuals (WHO III: 3; WHO IV: 5) had combined *Gd*-MR and PET at various times after surgery (biopsy: 6; partial resection: 2). MR (21 examinations) was carried out with T_1-, ρ-, and T_2-weighted spin-echo pulse sequences at 0.35 T; *Gd*-enhanced T_1-weighted sequences were also performed. We compared rCMR*glc*-PET before and shortly after *ia*ACNU (14x2 examinations); 6x2 PET studies were obtained in untreated patients (*i.e.*, no prior radio- or chemotherapy), whereas 8x2 PET examinations were performed during later treatment courses. These data were correlated to MR and clinical course. The disease was scored as progressive (PD), stable (SD), or responsive (RD).

Correlation of MR with PET findings was good; additional MR information, *e.g.* presence of cysts and extent of peritumoral edema, proved very useful for PET interpretation. Based on MR and clinical course WHO IV-MG were PD (2), SD (2), or RD (1). PD was associated with increased rCMR*glc* on post-*ia*ACNU-PET in 1 patient, whereas no change was seen in the other PD case. The patient with RD demonstrated a decrease in rCMR*glc*. Results in SD cases were equivocal. Two WHO III-MG showed RD (one of these on histology only), and largely unchanged rCMR*glc* on post-*ia*ACNU-PET, whereas the PD tumor revealed a discrete rCMR*glc* decrease.

Chemotherapy of MG, especially *ia* chemotherapy, is controversial. Indeed, only a limited number of patients are responders. Furthermore, there is an inherent risk of complications. Therefore, early evaluation of tumor response to a particular therapy is an important goal. Our experience with combined *Gd*-MR and rCMR*glc*-PET follow-up supports the hypothesis that these studies might be helpful for early evaluation of the response of MG to *ia*ACNU.

► **124** 12:09PM

MR IMAGING OF THE PAROTID GLAND: PLAIN AND GD-DTPA STUDIES

Th.Vogl,MD; S.Dresel,MD; K.Mees,MD; D.Hahn,MD; J.Lissner,MD.
University of Munich, Department of Radiology
Marchioninistr. 15, 8000 Munich 70, West-Germany

In diagnosing lesions of the parotid gland ultrasound controlled aspiration cytology has so altered the mangagement that all diagnostic modalities must be examined in the light of this examination. MR with Gd-DTPA can be a new effective diagnostic method for lesions of the parotid gland. Our patient group of 65 patients consists 15 squamous cell carcinomas, 2 lymphomas, 3 adenoidcystic carcinomas, 10 adenomas, 20 patients with sjögrens disease, 5 inflammed parotid glands and 10 miscellaneous. Images were acquired in transverse and coronal orientation with long (TR=1600ms, TE=25/90ms) and short (TR=500ms, TE=25ms) spin-echo sequences. Five millimeter slice thickness was used. In 15 cases during and after Gd-DTPA application a very short sequence (TR=30ms, TE=13ms)with a flip angle of 30° was performed every minute over a period of at least eight minutes in order to measure the change in signal intensity over time. The signal intensity of the normal parotid gland was lower than fat and higher than muscle. The main duct was routinely seen with low to intermediate signal intensity. The main trunk of the facial nerve was found with intermediate signal intensity just lateral to the retromandibular vein or occasionally between the vein and the external carotid artery. After Gd-DTPA application in 42 patients with tumors the delineation as well as the differentiation of tumor masses and necrosis were better determined according to the higher enhancement in signal intensity of tumors compared with normal glandular tissue. In tumors showing slight contrast medium enhancement, Gd-DTPA proves to be not advantageous, because there is no contrast enhancement achieved between tumor and enhanced normal tissue. Inflammatory changes of the glands were best seen in T2-weighted images depending on the prolonged T2-relaxation times. Especially the sjögrens disease showed in T2-weighted images characteristic changes with inhomogeneous, pitted internal pattern. MR with Gd-DTPA has improved the diagnostic management of tumors of the salivary gland. Using T1- and T2-weighted sequences the real tumor extension can be differentiated from simultaneous processes like edema and inflammatory infiltrates. In inflammed parotid glands and sjögrens disease best results were reached with plain T2- and T1-weighted sequences. Application of Gd-DTPA in these patients is not needed.

SPECTROSCOPY III

MODERATORS: R. E. LENKINSKI, Ph.D., M. R. WILLCOTT, Ph.D.

► **125** 10:45AM

Integrated MRI/MRS Studies of Squamous Cell Carcinomas
RE Lenkinski, P Bloch, B Chance, M Maris K Vogele, RA Hendrix, and GW Mckenna
Departments of Radiology and Radiation Therapy and Otorhinolaryngology, University of Pennsylvania

Advanced head and neck tumors exhibit considerable variation in their signal appearance on MR images .We have found that the use of computed images which are pixel by pixel grey scale maps T2's provide a means for displaying this variation in a useful format. We have monitored the changes in the T2 values of these tumors as they are being treated by radiation therapy and have correlated these changes with alterations in their 31-P spectra.In interpreting these changes it is important to confirm that these spectra are obtained from well defined regions of tissues i.e. tumor vs. normal tissue. We have also measured the hemoglobin/deoxyhemoglobin concentration in these tumors by optical methods at locations guided by the MR images. We have observed changes in both the PME resonance and PCr/Pi ratio in these tumors. These changes have preceded any changes in volume by several days. The cahnges in the PCr/Pi ratio observed are suggestive of changes associated with reoxgenation of the tumor in the early part of therapy.

► **126** 10:57AM

Integrated MRI/MRS Studies of Acute Head Trauma
RE Lenkinski, M Rango,RI Grossman, T Gennarelli, W. Alves
Departments of Radiology and Neurosurgery, University of Pennsylvania

We have studied thirteen patients with acute injury with a mean interval from injury of 14+9 days. Seven patients were studied within 15 days and six patients within 15 to 30 days. The mean Glasgow Coma Score (GCS) was 7+3. Eight patients had a GCS of seven or lower. Follow up MRI/MRS examinations were carried out in eight of these cases.All of the patients were monitored in the magnet during the examination by an attending anesthesiologist. All of the MRI/MRS studies were performed on a 1.5 T clinical MR Signa scanner (General Electric Medical Systems, Waukesha WI) equipped with the standard spectroscopic research accessory. Dress localization was employed in the ^{31}P MRS portion of the study in eight of these cases. In the others we employed a 3D-CSI sequence for ^{31}P which yielded spectra from 4 cmx4 cmx4 cm voxels. In patients with large focal insults we found that the PCr/Pi ratio was reduced in the affected side of the brain. In some severe cases, there were little or no observable ATP resonances. Abnormal spectra were observed in two of the cases which were hyperventilated. These spectra exhibited a more normal appearance on follow up examinations when the patients were returned to unassisted ventilation. Our experience indicates that it is feasible to study patients with acute head injury with low GCS at short intervals from injury. We are currently extending our studies into the first 48 hours post trauma.

► **127** 11:09AM

QUANTITATION OF LACTATE LEVEL AND GLUCOSE UTILIZATION RATE IN HUMAN BRAIN GLIOMA BY ^{1}H LOCALIZED MRS AND FDG-PET

J.R. Alger, A. Bizzi, M.J. Fulham, B.X. DeSouza, S.W. Inscoe, J.L. Black, J.A. Frank, G. Di Chiro
Neuroimaging Section, NINDS, National Institutes of Health, and Georgetown University. Bethesda, Maryland

Localized ^{1}H-MRS and FDG-PET measurements are both fundamentally related to tissue metabolism. However, the measurements are unique with respect to one another. FDG-PET provides the rate of glucose utilization, while MRS provides a measure of the steady state level of a few metabolites. We have identified a lactate signal using localized 1H-MRS in seven cases of intracranial tumor and have obtained FDG-PET scans to obtain the glucose utilization rate in each of these cases. The quantitative evaluation of the absolute lactate level has been problematic, however reasonable estimates within 30% of its level can be made by comparison to signals of known intensity such as water or N-acetylaspartate in the contralateral hemisphere. Lactate concentrations in these cases were observed to be in the vicinity of 5 μmol/g. Glucose utilization rates measured by FDG-PET were hypometabolic (as low as 2 mg/ 100 g/min), as well as hypermetabolic (as high as 15 mg/100 g/min). If it is assumed that lactate is present in these brain tumors, because of blocked oxidative pyruvate metabolism due to relative hypoxia or to derangement of oxidative pathways (Warburg's hypothesis), then the PET results together with the MRS suggest the lactate pool is a very dynamic one which is turning over every few minutes. Thus the steady state lactate level depends as much on the capacity of the system that consumes it, either residual oxidation, or transport, as it does on the rate of its formation from glucose.

► **128** 11:21AM

LOCALIZED *IN VIVO* ^{31}P NMR STUDY OF METABOLITE GRADIENTS IN PORCINE KIDNEY

F. Parivar, P. T. Narasimhan, N. Farrow and B. D. Ross
Magnetic Resonance Spectroscopy Unit, Huntington Medical Research Institutes, Pasadena, CA

Using one-dimensional phase encode spectroscopy we have obtained localized ^{31}P NMR spectra of different regions of the intact porcine kidney with and without arterial occlusion, by inflation of a remote renal artery clamp. Glomular filtration rate (GFR) and fractional Na^+ reabsorption were simultaneously determined. The NMR spectrometer used was a GE CSI-II equipped with an Oxford Instruments 4.7 Tesla superconducting magnet and gradient coils. Pigs were anesthetized and a two-turn Helmholtz coil of 5 cm diameter was placed surgically around the kidney with a copper shield to prevent contamination from signals outside the kidney region. Sixteen-step phase encoding yielded spectra from six slices each of 5 mm thickness, identified with cortex, medulla and papilla by reference to MRI. Sixteen slice spectra of the kidney were obtained in ~ 35 mins, and the whole kidney spectra in < 5 mins.

Our results can be summarized as follows. In the control, ATP/Pi ratio for the cortex is greater than that for medulla. During hypofiltration (HF), when the GFR and Na^+ reabsorption are reduced 50%, an increase in the ATP/Pi ratio is seen in the whole kidney spectrum. This increase is visible in both cortex and medulla in the localized spectra. During hypoperfusion (HP), when GFR and Na^+ reabsorption are reduced to near zero, the ATP/Pi ratio is reduced 50% in the whole kidney spectrum. After nearly two hours of HF and HP (acute renal failure) the clamp was removed and ATP recovered to 75% of the control value. We postulate that 1) a cortico-medullary gradient of ATP exists in intact kidney, 2) reducing sodium reabsorption spares ATP in both cortex and medulla and, 3) limiting oxygen delivery, in the absence of sodium reabsorption, impairs ATP synthesis equally in the renal cortex and medulla. These results indicate heterogeneity in the renal metabolic response to hypoxia, and suggests the need for independent MRS examinations of cortex and medulla in studies of acute renal failure.

► **129** 11:33AM

IN-VIVO 13C-NMR OF LABELED DDP IN THE RAT.
HJ Muller[1], D Lanens[2], CJ Mulder[1], R Dommisse[2], J Lugtenburg[1], M Spanoghe[2], TJ De Cock Buning[1], FL Van de Vyver[2].
1.University of Leiden, The Netherlands. 2.University of Antwerpen, Belgium.

While the use of 13C-in vivo NMR spectroscopy for the study of labeled naturally occuring substances has been reported repeatedly, this is the first study of a 13C labeled xenobiotic product: 1-(ortho-chlorophenyl)-1-(para-chlorophenyl)-2,2-dichloropropane (DDP); labeled at C3.
An Oxford Biospec (1.9 T) and a Bruker MSL-400 (9.4 T) were used. At 1.9T an inverse gated decoupling sequence was used in combination with a Waltz 16 decoupling scheme and a home-built, double-tuned circular surface coil (25 mm ø). At 9.4 T the same sequence was used with broad-band decoupling and an adapted Bruker double-tuned coil (10 mm ø).
Female wistar rats (200 g) were injected intraperitoneally (ip) with 100 mg labeled DDP dissolved in a mixture of DMSO and sesame oil.
Spectra of liver, abdomen and head were obtained before and at regular intervals up to 14 days after the injection. Urine and faeces were examined with gc/ms and NMR. Isolated organs (2 rats) were examined by high resolution NMR.
The signal intensity of DDP over liver and abdominal fat varied over time. No DDP was observed in spectra from the head. In agreement with farmacokinetics no DDP metabolites were detected.
After injection of 40 mg DDP ip, the signal was still detected with good SNR.
Conclusion. The data demonstrate the possibility of detecting 13C labeled xenobiotics in the living rat by 13C-NMR. In the future, the localization of the sensitive volume will be improved.

MONDAY a.m.

► **130** 11:45AM

IN VIVO METABOLISM OF L-ALANINE USING ^{15}N NMR OF RAT-TISSUE EXTRACTS
N. Farrow, F. Parivar, K. Kanamori and B. D. Ross
MR Spectroscopy Unit, Huntington Medical Research Insts.; Calif. Inst. Technology, Pasadena, CA

We have recently employed (1) ^{15}N NMR to study (*in vivo*) cerebral ammonia metabolism in rats. Using an ^{15}N-labelled amino-acid (L-alanine) offers a more physiological means of elevating blood ammonia, by exceeding the capacity for hepatic urea synthesis (2).

Infusion of 1000 µmoles ^{15}N-L-alanine i-v over 30 mins into five 24-hour fasted rats was monitored by blood and urine samples, followed by freeze clamping of liver, kidney, muscle and brain. Urea synthesis was increased, and excess ^{15}N NH_4^+ detected in the urine. Hepatic and renal ^{15}N NMR spectra (Bruker AM 500 spectrometer; NA ~ 8000) showed the effects of transamination and deamination of alanine, as well as increased glutamine and urea. In muscle (not shown) glutamate and glutamine synthesis were observed and ^{15}N alanine was present.

In contrast, in brain no ^{15}N alanine, γ-glutamine or ammonia, and only traces of aspartate and glutamate were detected.

These findings contrast with the effect of direct infusion of ^{15}N H_4Cl and reflect limited cerebral uptake of L-alanine (3). In HE, it is likely that free ammonia, rather than an amino-acid, is the precursor of excess cerebral glutamine.

REFERENCES

1. Farrow N, Kanamori K, Raijman L and Ross B. *Proc. of the 8th annual meeting of the Society of Magnetic Resonance in Medicine, Works-in-Progress* 1989; p. 1017.
2. Kay JDS, Seakins JWT, Geiseler DG and Hjelm M. *Clin Sci* 1986; 70:31-38.
3. Oldendorff WH. *Research Methods in Neurochemistry* 1981; 5:91-112.

► **131** 11:57AM

^{19}F NMR SPECTROSCOPY OF ANTIPSYCHOTIC DRUGS IN VIVO IN HUMANS

RA Komoroski*, JEO Newton**, C Karson**, D Cardwell*, J Sprigg*
*Departments of Radiology and Pathology, University of Arkansas for Medical Sciences, and **VA Medical Center, Little Rock, AR 72205

The clinical efficacy of antipsychotic drugs is well established, but there is a great deal of individual variation in clinical response in patients given similar dosages. One possibility is that differences in pharmacokinetics are responsible for this variation. A number of antipsychotic drugs contain fluorine as an intrinsic part of their molecular structure. We have detected the neuroleptic drug trifluoperazine (TFP) in the brain and calf muscle of a patient suffering from schizoaffective disorder and receiving 120 mg/day orally. No metabolites were resolved. The concentration of the drug was estimated by comparison of the in vivo ^{19}F signal at about -61 ppm to that from 1 L of 0.055 mM trifluoperazine in 2% aqueous agarose. A small vial of 12 mM 2,2,2-(trifluoroethyl)-p-toluene sulfonate in $CDCl_3$ was incorporated into the rf coil housing as an area normalization standard. We estimate the total concentration of TFP and its fluorinated metabolites at 0.024-0.030 mM in brain. The level in muscle was similar. The ^{19}F signal from the rear of the head was three times stronger than that from the frontal region, which we attribute to contributions from drug and/or metabolites in muscle and fat at the rear of the head.

► **132** 12:09PM

In Vivo NMR Spectroscopy of the Human Prostate

M.D. Schnall, Y. Imai, B. Lenkinski, H. Pollack and H. Kressel
Department of Radiology University of Pennsylvania

The normal human prostate gland contains up to 60 mM citrate. Several investigators have utilized 13C NMR spectroscopy to study citrate levels in benign and malignant prostatic tissues. Early results have shown that the citrate levels in malignant prostatic tumors is significantly less than those in normal prostate or benign prostatic hyperplasia (BPH). These results suggest that the ability of NMR to detect citrate may be helpful in distinguishing benign from malignant disease in the prostate. Unfortunately, due to its low sensitivity and natural aboundance, localized 13C NMR is difficult to perform in vivo. We have been investigating the feasibility of using 1H NMR spectroscopy to detect citrate levels in vivo.

Endorectal surface coil water suppressed 1H NMR spectra were obtained from human volunteers. A volume selective stimulated echo (STEAM) pulse sequence was used. A selective presaturation pulse was used for water suppresion. A TR of 4 sec. and TE of 50 msec were used. Spectra taken from 21 cm3 and 8 cm3 voxels were obtained in less than 8 minutes. The citrate resonance is clearly seen at 2.6 ppm. Resonances from creatine and choline are also identified at 3.0 and 3.3 ppm respectively. High resolution spectra from an extract of freshly excised human prostate tissue were also obtained to confirm the above assignments. Assignment of the remainder of the high resolution spectrum is ongoing.

These results demonstrate the feasibility of using 1H NMR to detect prostatic citrate levels in vivo. The use of an endorectal surface coil is important to provide the high sensitivity that is required. Studies of normal and abnormal prostates are required to determain potential clinical impact.

MOTION SUPPRESSION/CORRECTION

MODERATORS: S. J. RIEDERER, Ph.D., L. P. CLARK, Ph.D.

► 133 10:45AM

MOTION CORRECTION USING IMAGE ECHO DATA IN MRI

JP Felmlee, RL Ehman, HW Korin, SJ Riederer
MR Laboratory, Mayo Clinic and Foundation, Rochester, MN 55905

Many MR scans prove to be diagnostically useless because of gross patient motion during image data acquisition. This study evaluated a method which would permit a retrospective correction for motion along the readout direction for standard studies degraded by motion irrespective of the type of scan used. This correction alone could salvage many clinical exams and has the advantage of requiring no unusual scanning procedures.

This method is similar to one previously described which uses interleaved "navigator" echoes to measure displacements, but in this case the one-dimensional Fourier transformed image data itself is used to provide tracking of the motion which occurred during the scan. Thus, standard pulse sequences can be used.

Phantom and volunteer studies were conducted to mimic the gross patient motion which can occur during imaging of the head and extremities. The once Fourier transformed image echo data and an edge detection algorithm were used to determine object position. The image echo data reliably tracked an object's motion, given that the object remained within the field of view. In fact, the results were similar to the motion measurement conducted using an echo without phase encoding (corr. coef. = 0.91). Comparison of the uncorrected images with those corrected using image echo data shows a dramatic improvement in sharpness and decrease in artifact in the corrected images.

► 134 10:57AM

SSFP TECHNIQUE WITH ZEROTH MOMENT NULLED FOR INSENSITIVITY TO MOTION

ML Wood[a], Y Zur[b], and LJ Neuringer[b]
[a]Tufts University and New England Medical Center [b]Francis Bitter National Magnet Laboratory, MIT

A steady state free precession (SSFP) imaging technique has been developed that maintains a steady state even in the presence of motion. All three gradients are balanced to give them a vanishing time integral, or zeroth moment, over each TR interval. This condition alone would cause images to have bands depending on the homogeneity of the magnetic field. Other SSFP techniques avoid these bands by leaving the frequency encoding or slice selection gradients unbalanced. However, motion along an unbalanced gradient inhibits SSFP, because it changes the amount of precession during each TR interval(1,2). Instead, the proposed technique decomposes the steady state transverse magnetization into a Fourier series in which each term has unique phase characteristics. Each term corresponds to a distinct echo, which can be isolated by combining data from separate acquisitions that alter the phase of each echo differently. The phase can be altered either by using RF pulses of different phase or preferably, by imparting an additional phase shift directly through the frequency synthesizer. Typically, six acquisitions of data are collected to isolate the six most intense echoes and produce an independent image from each one. The additional phase shifts for the six acquisitions are 0, 60, 120, 180, 240, and 300 degrees. The shortest TR possible (22 ms) and a flip angle that elicits a strong signal from CSF (ie. 60 degrees) are used. The top and bottom images on the right compare the SSFP technique to a similar one with an unbalanced frequency encoding gradient. The SSFP technique appears advantageous, because it preserved the intensity of CSF in spite of extensive motion in the cervical spine.

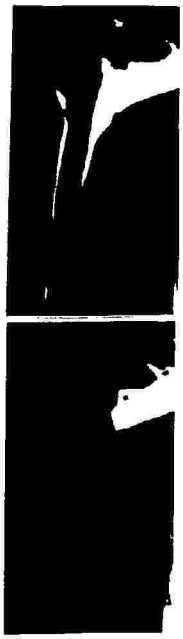

1. PA Wielopolski and EM Haacke: Book of Abstracts SMRM, 1989, 846.
2. M Deimling and G Laub: Book of Abstracts SMRM, 1989, 842.

► **135** 11:09AM

IMAGE UNSHARPNESS DUE TO RESPIRATORY MOTION: QUANTITATIVE STUDY OF ORGAN KINEMATICS IN THE UPPER ABDOMEN USING NAVIGATOR ECHOES

RL Ehman, JP Felmlee, HW Korin, SJ Riederer
Mayo Clinic and Foundation, Rochester, MN 55905

In spite of the fact that respiratory motion is the major limiting factor in MR examinations of the upper abdomen, little quantitative information is available about the kinematics of visceral motion during respiration. This knowledge would be especially relevant to the application of adaptive correction techniques [1] which have the capacity to reduce image unsharpness if motion is global rather than chaotic in nature.

The objective of this study was to quantitatively determine the kinematics of respiratory motion of upper abdominal visceral structures of special clinical interest (liver, pancreas, spleen, and kidneys) in volunteers. Specific goals were to measure craniocaudal and transverse motion, and to determine the extent to which respiratory motion is global (correlated) rather than chaotic.

The method utilized spin echoes derived from spatially localized lines of tissue which are defined by the intersection of orthogonal slice-selective 90 and 180 degree RF pulses. Frequency encoding along each line provided a means of tracking the view to view motion of tissue interfaces. The sequences used in this study permitted concurrent acquisition of line projections along longitudinal and transverse axes in the same acquisition. In regions where suitable tissue interfaces were unavailable, saturation tags were used to provide fiducial detail.

Analysis of the projection data obtained in a series of 8 volunteers indicates that the craniocaudal motion of upper abdominal structures is much greater than the transverse motion, by an average factor of 6.6. The small transverse motions tend to be uncorrelated across the width of the abdomen. In contrast, the relatively large craniocaudal motions are highly correlated from place to place in the upper abdomen and they are primarily translational in nature rather than compressive or dilative.

The results indicate that the major source of motion unsharpness in conventional upper abdominal MR imaging is due to respiratory craniocaudal translation. Straightforward methods for adaptively correcting such translational motion in coronal and sagittal images can therefore be expected to reduce the unsharpness of these mobile structures by 80% or more. Preliminary tests of the adaptive correction technique confirm this conclusion by demonstrating clinically useful improvements in upper abdominal image quality.

[1] Ehman RL, Felmlee JP. Radiology 173:255;1989.

► **136** 11:21AM

OPTIMAL GRADIENT WAVEFORMS FOR MOTION ARTIFACT SUPPRESSION

OP Simonetti, JL Duerk, GC Hurst
MetroHealth Medical Center and Case Western Reserve University, Cleveland, OH

Gradient moment nulling is a technique used to compensate for the dephasing and subsequent artifacts caused by intraview motion. Modifications of the gradient waveform, usually in the form of additional lobes, are made in an attempt to completely rephase transverse magnetization at the echo. The amplitudes of these additional lobes are normally determined by linear algebra techniques. A superior method of gradient waveform design based on nonlinear constrained optimization will be shown in this work. This method employs a priori knowledge of the motion of concern and characteristics of the gradient coil system to generate waveforms with not only reduced motion sensitivity, but minimized power, RMS current, and slew rate as well. The result is greater insensitivity to specific physiological motions, an increase in maximum number of slices, and reduced eddy current effects.

The constrained optimization problem involves minimizing an objective function of one or more variables subject to restrictions defined by a set of constraint functions. The desired gradient is to be optimal in the sense of producing an echo which has the least amount of motion induced dephasing. This can be expressed by a least-squares objective function which characterizes the deviation of the moments of the gradient waveform from those desired. Known characteristics of the motion of concern are incorporated as weighting factors. Additional terms can be employed to express power, RMS current, and slew rate as factors to be minimized. The shape, amplitude, and duration of this optimal waveform are constrained to lie within the limits imposed by the gradient amplifiers and desired echo time. By defining some finite set of parameters which completely describes the waveform and expressing the objective and constraint functions in terms of these parameters, we have formalized the optimization problem. The values of the parameters which minimize the objective function subject to the known constraints can be estimated using standard nonlinear constrained optimization algorithms.

Using polynomial functions to define those portions of the gradient waveform used for moment nulling, the polynomial coefficients become the parameter set to be estimated. The moments of the waveform, and hence, the objective function, are easily expressed in terms of these parameters. The endpoints of the polynomial sections are fixed to meet those gradient sections which are constant and predetermined by FOV, slice thickness, and other image characteristics. Estimation of polynomial coefficients which minimize the objective function subject to endpoint constraints and gradient amplifier limits yields a smoothly varying waveform with the desired imaging and refocussing characteristics.

► **137** 11:33AM

OPTIMIZATION OF GRADIENT MOMENT NULLING FOR MOTION INSENSITIVITY IN SSFP

Y Zur[a], ML Wood[b], and LJ Neuringer[a]
[a]Francis Bitter National Magnet Laboratory, MIT [b]Tufts University and New England Medical Center

Motion can inhibit steady state free precession (SSFP), so that tissues, such as CSF, become much less intense than expected. The reduction of intensity depends on the configuration of magnetic field gradient pulses. The effects of motion along the readout and phase encode gradients in SSFP techniques were analyzed theoretically to determine the extent of gradient moment nulling required to preserve SSFP for motion of constant velocity, acceleration, or jerk. Images of the cervical spine of human patients confirmed the theoretical predictions. Results of the analysis include the following: The zeroth moment (area) of the readout gradient pulses must vanish over each TR interval, to preserve SSFP for motion of constant velocity. Otherwise, even motion as slow as one mm/s can inhibit SSFP. If there is acceleration, both the zeroth and first moments must vanish over TR. The steady state is comparatively insensitive to motion along the phase encode gradients, provided that the total area of the gradient pulses vanishes over TR. The extent to which motion along the phase encode gradient disrupts SSFP depends directly on the increment of the gradient, rather than the actual gradient strength. Regardless of the type of motion or its direction, the most important requirement is that the area under the gradients be zero. The problem is that magnetic field inhomogeneities would produce artifactual bands in the images. However, preliminary results have been reported showing that multiple sets of data can be combined to eliminate these bands(1). Eddy currents and other imperfections make the area under the gradients nonzero. These imperfections and also diffusion cause less dephasing if TR is shorter. Therefore, the shortest possible TR and simplest configuration of gradient pulses are recommended.

1. Y Zur, ML Wood, and L Neuringer: Works in Progress SMRM, 1989, 1128.

MONDAY a.m.

► **138** 11:45AM

AN ADAPTIVE CORRECTION METHOD FOR 3D THORACOABDOMINAL MRI

HW Korin, JP Felmlee, RL Ehman, SJ Riederer, F Farzaneh
MR Laboratory, Mayo Clinic and Foundation, Rochester, MN 55905

3DFT volumetric imaging offers many advantages over 2D multi-slice imaging, chiefly those of higher resolution in the slice select direction and fully contiguous slices. However, it suffers greatly from motion artifacts for which no definitive compensation method has been proposed. The purpose of this study was to apply a recently developed adaptive motion correction technique which has produced excellent results in 2D imaging to the task of 3D imaging of the thorax and abdomen.

Although the externally visible motion in respiration is the expansion and contraction of the abdominal wall, the major organs tend to move cranio-caudally about 2 cm in normal tidal breathing. This means that in 2DFT imaging many structures move completely in and out of the individual slices with each breath. In 3D volumetric imaging however, they will remain within the selected volume, thus making a correction possible. The pulse sequence consists of a standard 3D gradient recalled echo sequence with interleaved, non phase encoded "navigator" (NAV) echoes. For the NAV echo, a sagittal slice through the right diaphragm was selected and read out along z. These NAV echoes provide a clear measurement of the position of the abdominal organs for each image echo and thus permit a retrospective correction of the image data for the view-to-view phase shifts generated by the motion. Flow compensation was used to correct intraview phase shifts. A restricted excitation slab along z addressed problems caused by signal wrap-around due to poor slab profile and the motion itself.

Phantom results have been excellent and validate the theory of the adaptive correction technique. Further progress with *in vivo* results has been very promising, showing among other things hepatic vessels and structures in the spleen which were invisible in the uncorrected images.

Ref.: RL Ehman and JP Felmlee, Radiology **173**: 255, 1989
HW Korin, F Farzaneh, RC Wright and SJ Riederer, Mag. Res. Med **12**: 99, 1989

► **139** 11:57AM

Correcting Motion Artifacts Via A Fast, Iterative, POCS Procedure
R. Steagall, S. Amartur, E.M. Haacke
Case Western Reserve University, Dept. of Radiology and Physics, Cleveland, OH 44106

Motion artifacts have long been the bane of body and cardiac imaging. With the development of gradient compensation schemes for motion between echoes, the remaining artifacts often caused by periodic motion between phase encoding steps become coherent. As a constraint, we choose a model to represent the motion with only a few degrees of freedom. Further constraints are also applied when possible to ensure reasonably rapid convergence. Specifically, the operation is defined via the equation:

$$f_k = f_{k-1} + B(L_p f_o - ML_o f_{k-1})$$

where f_o is the original ghosted image, Lo and Lp are constraint operators, M is the motion model operator, B is a relaxation parameter, and f_k is the kth iterated image.

Several types of motion (such as translational, dilational, and rotational) relevant to abdominal and cardiac imaging are discussed. Sensitivity to model parameters is also considered. Initial results on scaling and translational models for a 20% amplitude deviation show a reduction in ghosts to less than 5% and a significant improvement in resolution.

► **140** 12:09PM

USE OF SUPERPARAMAGNETIC CONTRAST MEDIA FOR FLOW SIGNAL SUPPRESSION
JL Duerk[1] , RE Tarver[2], TJ Ryan[2]
(1) MetroHealth Medical Center & CWRU, Cleveland (2) Indiana U. Medical Center, Indianapolis

Magnetic resonance imaging is prone to artifacts arising from tissue motion during the imaging pulse sequence. Respiratory and cardiac motion, along with flow are the most common sources of motion artifact. While gating techniques may be effective in reducing or eliminating artifacts from respiratory and cardiac motion, they are not as effective in eliminating sources of artifact arising from the hemodynamic variation of flowing material. Spatial pre-saturation techniques using RF pulses as a means of reducing signal from flowing blood prior to entering the imaging volume has been shown to produce significant reductions in flow artifacts. We propose an attractive alternative method for eliminating the signal from flowing blood by using superparamagnetic contrast media.

This work describes the use and effect of two superparamagnetic contrast materials (AMI-25, and Ultrasmall Superparamagnetic Contrast: Advanced Magnetics, Inc.) in canines undergoing cardiac gated MRI. Conventional T1 and T2 weighted short axis images of the heart and liver were obtained following myocardial infarction, both before and after administration of contrast. A 1mg Fe/kg dose of contrast media was used in six canines. No other techniques for flow artifact suppression were studied or employed. Images obtained before contrast were compared to those obtained serially afterward to assess efficacy in reducing both flow artifacts, and signal from slowly moving blood.

Significant improvements in image quality as a result of flow suppression were observed in scans obtained immediately after administration of contrast. Clearance of the contrast material by the liver limited the time interval for effective signal suppression. The relative advantages of this technique include ease of use, not having to place RF saturation regions along different axes adjacent to the imaging volume, not encountering SAR restrictions, and greater robustness by eliminating signal from flowing blood in MRI regardless of the direction of travel prior to entering the imaging volume. This is an attractive technique for reducing blood flow related artifacts in MR imaging.

PERFUSION/DIFFUSION

MODERATORS: D. J. LeBIHAN, M.D., Ph.D., T. J. BRADY, M.D.

► **141** 15:57PM

DETECTION OF SMALL PERFUSION CHANGES IN A TISSUE MODEL USING MRI SEQUENCES

DR Pickens, RR Price, DB Puffer, CH Lorenz, D Jolgren, J Creasy, CL Partain, AE James, Jr.
Department of Radiology and Radiological Sciences, Vanderbilt University

Development of imaging methods sensitive to diffusion and perfusion using magnetic resonance techniques is receiving increasing attention. We have extended MRI perfusion/diffusion methods described by Le Bihan et al.* by developing an interleaved acquisition sequence that produces a reference image and 8 images with graded sensitivity to perfusion and diffusion (gradient factors from 1.25 to 742 sec/mm2). We have used this sequence to evaluate the sensitivity of the technique to small changes in perfusion in an excised dog kidney. Canulae were placed in the renal artery, renal vein, and the ureter. A pumping system capable of producing variable flow rates as low as 16 ml/min was used to pump 0.9% saline solution through the kidney during the study. The flow rate was measured by timed flow from the renal vein into a graduated cylinder. Apparent diffusion coefficient (ADC) values from regions of interest in the renal cortex and medulla were plotted against gradient factor. Intensity verses gradient factor curves were characteristically biexponential, indicating the presence of both diffusion and perfusion. In the absence of perfusion, single exponential diffusion-dependent curves were obtained at the gradient factors used. Changes in flow as small as 8-10 ml/min produced readily separated results, showing the sensitivity of the method. Similar results were obtained using several excised kidneys, demonstrating the reproducibility of the technique.

*Le Bihan et al. Radiology 1988; 168:497-505

► **142** 16:09PM

DYNAMIC MRI OF BRAIN PERFUSION USING Gd-DTPA ENHANCED EPI

R. Turner, N. Patronas, D. Le Bihan
Biomed. Eng. Instr. Branch and Diagn. Radiology Dept., NIH, Bethesda, MD 20892.

The feasibility of Gd-DTPA real-time studies of brain perfusion with Echo-Planar Imaging (EPI) has recently been shown. The purpose of this study was to assess the relative merits of inversion-recovery, spin-echo and gradient-echo based EPI sequences in the evaluation of perfusion and blood-brain barrier abnormalities.
Patients with selected brain tumors were first examined with conventional imaging techniques to locate the tumor. Two types of EPI sequences were then applied. One used a spin-echo refocussing scheme compatible with built-in inversion-recovery capability, the other a gradient-echo refocussing scheme. Patients were injected simultaneously with the beginning of data acquisition (0.1mmol/kg body weight). Data acquisition was continued during and after injection for about 50 seconds. Two different kinds of effect were seen. Using the spin-echo (TE=85ms) and gradient-echo (TE=35ms) EPI sequences a transitory decrease of the signal intensity in normal gray matter was observed about 20 s after injection. This decrease has been ascribed to susceptibility effects due to local field gradients induced by the presence of Gd-DTPA in the capillaries, that decrease $T2^*$. Therefore, this initial part of the dynamic curve might reflect the blood transit time in the tissue that can be used to quantify blood flow. By contrast, using the inversion-recovery EPI sequence, an increase in signal intensity has been previously observed. This increased intensity may be ascribed to relaxivity effects that will decrease T1, and will depend on the number of water molecules involved in paramagnetic relaxation, i.e. in close contact with the Gd-DTPA complexes. This increase was significant and remained for a long time only when the blood-brain-barrier was disrupted, so that a significant amount of Gd-DTPA was in interstitial tissue. We suggest that the dynamic study of Gd-DTPA uptake using different types of EPI sequences can be used to assess separately blood perfusion and blood-brain barrier integrity.

► **143** 16:21PM

Perfusion-Diffusion Measurements on a 9L-Glioma Model at 4.7 T
SS Rajan, D LeBihan, L Rosa, J Francisco, M Carvlin
Dept. of Radiology, Georgetown Univ. Hospital, Washington D.C. 20007

Imaging techniques to obtain perfusion-diffusion images have recently been described. However, only few studies in animal models have been reported. We have implemented an imaging technique and a slab-scan technique on a 4.7 Tesla MR instrument, equipped with 1.8 G/cm gradients. This technique was used to study a rat brain tumor (i.c.) model (9L-Glioma). The 9L-Glioma cell suspension was stereotactically injected into the brains of Fischer 344 rats. The cells were initially grown in culture and a suspension of 4.0 μl was injected into the parietal lobe. The animals were examined between days 12 to 21 following implantation. The animals were anesthetized with a cocktail of ketamine (80 mg/Kg) and xylazine (12 mg/Kg) respectively. A standard spin echo imaging sequence was modified to include a pair of symmetric diffusion gradients (before and after the 180 degree RF pulse). Multislice images were obtained for three values of diffusion gradient (0, 0.6, and 1.5 G/cm). In the slab scan technique, the second slice-selection (during 180 degree RF pulse) was carried out in the second direction and the readout gradient (third gradient) was used to yield a line of data along the third direction. The co-ordinates for the second slice selection was obtained from a T2 weighted image. The following imaging parameters were used: TR/TE-2.5/0.080 s, 256x256 data matrix, FOV of 4x4 cm. Ten values of diffusion gradients were used (0 to 1.8 G/cm). Apparent diffusion coefficient (ADC) measurements were made by examining the signal from a region-of-interest as a function of gradient strength. The techniques were validated by making diffusion co-efficient measurements on phantoms of water and acetone. The ADC values of tumor, cortex and edema were found to be 1.22, 0.46 and 1.91 respectively. The slab scan technique uses two slice-selections and thus obviates the need for phase encoding. The shorter experiment times allows the use of more diffusion gradient values and thereby separation of perfusion and diffusion components. These two techniques are being used to characterize microcirculation changes during untreated tumor progression and regression after therapy.

► **144** 16:33PM

NEW CONSIDERATIONS IN THE MEASUREMENT OF PERFUSIVE FLOW BY NMR†
Q.S. Xiang and O. Nalcioglu
Department of Radiological Sciences, Division of Physics & Engineering, University of California-Irvine

Perfusive flow may cause NMR signal attenuation as a result of spin dephasing. This effect provides an opportunity to study the characteristics of the flow system. For a quantitative analysis and measurement, a straight-tube model of perfusion has been developed in refs.[1,2]. A basic assumption in this model is that the flow system consists of many straight capillary tubes in which flow takes place. Although the moving spins can make turns at the end of each capillary tube, the effects of turning of spins have not been well analyzed and are usually ignored. In this work, we analyzed the effects of turning of spins. First, the life-time (defined as the time passed before a spin makes a turn) distribution of the spins is calculated from the distributions of spin velocity and capillary tube length. Then the probability of a spin to make a given number of turns at echo time TE is obtained. These results can offer some interesting statistical features of the flow system and can be used to predict the behavior of signal intensity as a function of capillary tube length, flow velocity, applied gradient strength, echo time TE, etc. under different situations.

Experimental results, from a perfusion flow phantom which consisted of a container filled with glass beads and with water flowing through, were compared with the theoretical prediction. The observed discrepancy between the experimental results and the theoretical predictions according to the model given in refs.[1,2] reveals the weakness of the straight-tube model. Specifically, it appears that the curvature of the capillary channels should be taken into account in modeling the perfusive flow.

A new model which is much simpler but considers the curvature of each flow channel is developed. The spin motion projected in the direction of applied field gradient is assumed to be a simple harmonic oscillation superimposed on a drift translational motion. The relative phases of the oscillation for different spins may also be different and are assumed to be evenly distributed, the frequency and amplitude of the oscillation are determined by the channel size and the flow velocity. The behavior of the NMR signal intensity calculated from such a model agrees with the preliminary experimental results surprisingly well in spite of of the simplicity of the model. Further experiments and improvements of the theory are being carried out and will be reported later.

1. C.B. Ahn, et al., Med. Phys., **14**, 43 (1987).
2. D. Le Bihan, et al., Radiology, **168**, 497 (1988).

†Work supported in part by PHS Grant CA45229 awarded by the NCI, DHHS.

► **145** 16:45PM

Quantitative Perfusion/Diffusion Measurement In Vivo
TL Chenevert, JG Pipe, DM Williams, JA Brunberg
Department of Radiology, University of Michigan Medical Center

Reliable quantification of tissue perfusion and diffusion coefficients is severely compromised by bulk tissue motion phase shifts. Cardiac gating for brain perfusion/diffusion MRI often does not adequately reproduce all phase errors leading to residual ghost artefact. Signal averaging reduces ghosts but does not restore signal; consequently, quantification is invalid. We have investigated two approaches for quantification accuracy improvement: (a) phase correction algorithm in which motion insensitive data is used to correct motion sensitive, but phase corrupt data; (b) 2D localization via selective rf pulses such that data may be combined in a phase–insensitive manner to produce quantitative 1D perfusion and diffusion images of the tissue of interest. Application of these methods have significantly reduced sensitivity to undesired motions. Measured values in the normal human brain are approximately 0.7–1.2 x 10^{-5} cm^2/sec diffusion and 2–8% perfusion fraction. Perfusion and diffusion of human calf muscle was also measured in a time course experiment of (a) 0–6min normal flow; (b) 6–12min low flow due to pressure cuff on the thigh; (c) 12–18min reflow by release of the cuff. Measured perfusion fraction demonstrates clear flow differences in the three periods, whereas diffusion remains constant as anticipated.

► **146** 16:57PM

A TECHNICAL ASSESSMENT OF MICROSCOPIC IMAGING AT 2.0 T
AW Anderson, SK Holland, JH Zhong, BB Frederick*, and JC Gore
Department of Diagnostic Radiology, Yale School of Medicine
*Department of Biophysics, University of California, Berkeley

The magnetic field gradients produced by standard geometry Golay and Maxwell pair coils scale with the reciprocal of the enclosed cylinder's cross-sectional area. By winding such a set of X, Y, and Z coils on a 2.5 cm radius cylinder, we have obtained high-performance gradient coils in a compact insert for our GE CSI 2.0 T magnet. The coils can be driven by the CSI system through conventional gradient power amplifiers. They produce gradients as high as 80 gauss/cm with rise times under 100 microseconds and negligible eddy currents. The important design criteria and performance specifications of this inexpensive, homemade gradient set have been established.

We have used the gradient set and various miniature RF coils to image small objects with microscopic resolution. Using a 3D spin warp sequence with long acquisition times we have obtained images of a capillary tube phantom with an in-plane resolution of 7.8 microns and a slice thickness of 63 microns. Tissue samples and small biological structures have also been imaged with this technique with image volume elements as small as 10x10x125 microns. We have explored the advantages of different pulse sequences and imaging strategies in microscopy at 2.0 T and have established the trade-offs between imaging time, resolution and SNR for the methods we have implemented. The effects of susceptibilty variations and molecular diffusion on image resolution are also being quantified.

► **147** 17:09PM

A PHYSIOLOGICAL MRI: OXYGENATION LEVEL SENSITIVE CONTRAST IN RAT BRAIN IMAGES AT HIGH FIELDS.

Seiji Ogawa and Tso-Ming Lee
AT&T Bell Laboratories, Murray Hill, NJ 07974

Water MR images obtained at high magnetic fields (7T and 8.4T) with high spatial resolution (100μm x 100μm x 500μm) reflect via their image contrast some physiological events occurring in brain tissue. Numerous dark lines which enhance the contrast appear in the image when the blood oxygenation level becomes low. These lines represent blood vessels of various sizes, many of which are as small as 50μm in diameter. This contrast is observable in gradient echo images but not in spin echo images (a susceptibility effect due to paramagnetic deoxyhemoglobin). With this sensitivity to the blood oxygenation level in small blood vessels, the contrast can be used to monitor the activity of aerobic metabolism at various parts of the brain with high spatial resolution. This potential is demonstrated in the following experiments. When the state of global anesthesia in a rat is varied by different anesthetizing reagents or their dosages, the pattern of the image contrast changes. With EEG signals reflecting very low brain activity, the image contrast is low and indicates a low level of oxygen consumption (e.g. in a rat breathing oxygen with pentobarbital anesthetization). In a condition of hypoglycemia induced by insulin injection, the image contrast starts to diminish when the glucose level reaches around 40mg/100ml.

PELVIS

MODERATORS: S. McCARTHY, M.D., Ph.D., C. P. SEMBA, M.D.

► **148** 15:45PM

THE STIMULATED MENSTRUAL CYCLE: APPEARANCE ON M.R.I.

CL Janus[1], B Bateman[2], EE de Lange[1]
Dept. of Radiology[1] and Dept. of OB Gyn[2], University of Virginia

This project was undertaken to study the appearance on magnetic resonance imaging (MRI) of the uterus and ovaries of women taking medication to induce ovulation.

Magnetic resonance scans of the pelvis and endovaginal pelvic sonograms were obtained on approximately days 4, 8, 12, 16, 20 and 24 of the menstrual cycle of eight volunteers who were being treated for infertility with Clomid or Pergonal. Hormonal blood samples were obtained to document ovulation. Width of the endometrium and junctional zone showed an accelerated period of growth during days 8 - 16 and slower rates of growth from days 4 - 8 and 16 - 24. The number, size and appearance of developing ovarian follicles and the appearance and size of dominant follicles was recorded for each patient.

This study shows that the growth pattern of the endometrium of women taking ovulation-inducing medications is similar to that of women during non-stimulated cycles. These medications do not appear to alter the timing and rate of development of the endometrium in relation to ovulation. A different pattern was noted for the junctional zone, however, when compared to an earlier study of women with normal cycles who were not taking these medications.

Further understanding of the effects of ovulation-inducing medications could potentially help in selecting patients suitable for this type of treatment and in evaluating response to therapy.

MONDAY p.m.

► **149** 15:57PM

MRI OF JUXTA-UTERINE MASSES: CLINICAL APPLICATION IN 25 PATIENTS

S Aubel, P Wozney, R Edwards

University of Pittsburgh, Department of Radiology, Pittsburgh NMR Institute and the University of Alabama, Department of Obstetrics and Gynecology

The clinical utility of MRI in the evaluation of gynecologic masses was investigated in 25 patients. In each patient the final pathologic diagnosis was quantitatively correlated with the diagnostic impressions from pelvic examination, ultrasound and MRI.

All patients were evaluated on a 1.5 T General Electric Signa system with both short TR and long TR sequences. Five patients were also evaluated with Magnevist (Gd-DTPA). The pathologic diagnoses were: 11 benign ovarian masses, 9 uterine masses (5 benign, 3 malignant, 1 infection) and 5 adnexal masses (2 endometriomas, 2 cysts, 1 abscess).

Five levels of increasing diagnostic specificity were established: site of origin, consistency (cystic/solid), extent and size, degree of complexity, and diagnostic impression. The results from each study were then compared to the final pathologic diagnosis as shown below.

	Correlation with Final Pathologic Diagnosis (%)				
Examination	Origin	Consistency	Extent	Complexity	Diagnosis
Pelvic	56	60	50	16	26
Ultrasound	68	76	80	64	44
MRI	93	96	96	93	87

In two patients ultrasound failed to identify ovarian masses, and in two other patients fluid-filled bowel was mistaken for a mass. In one pregnant patient MRI provided the information necessary to avoid surgery, and in another patient MRI correctly diagnosed infection, despite the impression of malignancy at surgery. This study suggests that MRI provides information to alter or obviate surgery in selected cases.

► **150** 16:09PM

MRI COMPARED TO CT IN THE DIAGNOSIS OF RESIDUAL TUMOR FOR RETREATMENT STAGING OF OVARIAN CARCINOMA

MC Fishman-Javitt (1), JL Lovecchio (2), HL Stein (2)
G. W. Univ. Medical Center (1), North Shore Univ. Hospital (2)

Because of the limitations of physical examination in detecting early recurrence of ovarian carcinoma following primary treatment, cross sectional imaging has become an important adjunct preceding second look laparotomy. When confirmed by biopsy, recurrent tumor suspected by either physical examination or by cross sectional imaging drastically alters patient management. Twenty-four patients who underwent second look laparotomy, all had pelvic MRI scans performed on a 0.6 Tesla superconducting magnet with both T1 weighted (TE 32 TR 525) and T2 weighted (TE 60 TR 2000) 2D FT pulse sequences in the axial, sagittal, and coronal projections. Twenty patients had fourth generation contrast enhanced CT scans of the abdomen and pelvis. Scans were performed within three weeks preceding surgery. Findings were compared to surgical pathology. Nine patients had positive histology and fifteen had no evidence of tumor. MRI results had 5 true positive, 4 false positive, 4 false negative, and 11 true negative cases (sensitivity 56%, specificity 73%). CT results had 4 true positive, 4 false positive, 4 false negative, and 8 true negative cases (sensitivity 50%, specificity 73%). Although both CT and MRI were relatively insensitive and relatively nonspecific at detecting residual tumor, both modalities were more sensitive and more specific than physical examination alone (sensitivity 44%, specificity 66%). These findings suggest no clear-cut advantage of either MRI or CT, but that cross-sectional imaging is of value preceding second look laparotomy for ovarian carcinoma.

► **151** 16:21PM

PROSTATIC MRI TECHNIQUES AND PERIPROSTATIC VENOUS PLEXUS

PY Poon, RM Henkelman, MJ Bronskill, RW McCallum
St. Michael's Hospital and Ontario Cancer Institute, University of Toronto

When the prostate gland is examined by magnetic resonance (MR) imaging, many technical factors have to be organized in order to produce the highest quality images. Also the total examination time must be well tolerated by patients and represents an optimal clinical use of an MR facility.

Using a superconducting magnet operating at 1.5 T, we examined the prostate of normal volunteers. We investigated the individual technical variables one by one. For example, we observed that the signal to noise ratio (SNR) improved by a factor of 2 when a pair of surface coils substituted the standard body coil, i.e. a 12 cm circular coil in front of and a 30 cm rectangular coil behind the symphysis pubis. Fat suppression technique eliminated aliasing and improved the SNR. From our experiment, the optimal techniques for prostatic MRI were dual surface coils, fat suppression, SE 2000/30,60 ms using multislice and multiecho pulse sequences, field of view of 34 cm, two averages, 128 x 256 matrix and slice thickness of 5 mm with a 1.5 mm gap. The data acquisition time was 8.5 minutes for each plane. Both axial and coronal images were needed to completely study the prostate. The image time of 15 minutes for two planes should be well tolerated by patients.

We observed a high signal intensity rim around the prostate when SE 2000/60 pulse sequences were used to image the prostate. We hypothesized that the rim represented the periprostatic venous plexus (PVP). We injected gadolinium-DTPA intravenously and observed a further increase of signal in the rim even when the repetition time was reduced to 500 ms. This fully established the true identity of the rim as the PVP.

► **152** 16:33PM

MAGNETIC RESONANCE IMAGING IN THE DETECTION OF PROSTATE CANCER

[1]RF Brem, [1]CM Tempany, [1]A Yang, [2] HB Carter, [3]JI Epstein, [2]PC Walsh, [1]EA Zerhouni.

[1]Dept. of Radiology, [2]Dept. of Urology, [3]Dept. of Pathology, Johns Hopkins Medical Institutions, Baltimore, MD.

To evaluate the ability of magnetic resonance imaging (MRI) to detect clinically unsuspected prostate cancer we studied the pathologic specimens of 53 patients with a palpable prostate cancer who underwent MRI prior to radical retropubic prostatectomy (RRP). All patients had an MRI with a 1.5 T GE Signa using T1 (TE 20 TR 600) and T2 (TE 20/80 TR 2500) weighted sequences in both axial and sagittal planes prior to RRP and step sectioning of the surgical specimen. Pathological exam revealed no tumor in the contralateral prostatic lobe in 31/53 cases (58%) and an unsuspected contralateral lobe cancer in 22/53 cases (42%). MRI successfully detected 21 of 22 unsuspected prostate cancers for a sensitivity of 95% and correctly excluded cancer in 15 of 31 lobes where cancer was absent for a specificity of 48%. In this population with a high prevalence of unsuspected cancers the positive predictive value (PPV) and negative predictive value (NPV) for MRI was 57% and 94%, respectively. However, if the prevalence of unsuspected cancer was 10% instead of 42% it can be calculated that if the MRI was positive only 16% of patients would actually have cancer (PPV) and if the MRI was negative cancer would be correctly excluded 98% of the time (NPV). Therefore, although MRI has a high false positive rate, it can exclude the presence of prostate cancer with a high degree of accuracy.

MONDAY p.m.

► **153** 16:45PM

COMPARISON OF MRI, ULTRASOUND AND THE CLINICAL EXAM IN THE STAGING OF ADENOCARCINOMA OF THE PROSTATE

M. L. Schiebler[1], B. Keefe[1], C. A. Mittelstaedt[1], J. Mohler[2], S. McSherry[2], G. Dent[3], W. H. McCartney[1]

Radiology[1], Surgery[2], and Pathology[3], University of North Carolina at Chapel Hill

PURPOSE: To evaluate the accuracy of MR imaging, endorectal ultrasound and the rectal exam in the staging of adenocarcinoma of the prostate.

MATERIALS AND METHODS: Seventeen patients with biopsy proven adenocarcinoma of the prostate had endorectal prostatic ultrasound and MRI performed prior to retropubic prostatectomies. Pathologic evaluation of the tumor location, size, and microscopic analysis of capsule involvement was made with dedicated histopathologic sectioning of the fixed gland. Comparison was made between the clinical and imaging findings and what stage was found at histopathology.

RESULTS: MRI correctly staged (12/17) 71% of the patients, while ultrasound correctly staged (10/17) 66%. The clinical staging, however, was only (5/14) 36% accurate. The primary errors for both MRI and ultrasound were related to under staging microscopic invasion of either the seminal vesicles and/or the capsule. In (8/17) 47% of the patients the imaging findings of tumor location and size matched the palpable nodule. All of these cases were discrete nodules less than 2.0 cm in size on MRI in a well-defined peripheral zone (PZ). The staging accuracy for these eight was (75%).

DISCUSSION: When prostatic carcinoma nodules are small (<2.0 cm) and deform a normal sized PZ they are easily palpated and imaged. Even with these well-defined nodules, however, our staging accuracy by either MRI or US was only 75% with respect to the critical factor of whether or not the true prostate capsule had been involved. A potentially curative resection of adenocarcinoma of the prostate should not be denied to patients with possible capsule involvement on the basis of imaging findings alone.

► **154** 16:57PM

SCROTAL MRI, REVIEW OF 125 PATIENTS

CB Semba, MA Trambert, RF Mattrey
Department of Radiology, University of California, San Diego; UCSD/AMI MRI Institute

131 scrotal MR examinations were performed on 125 patients between 1985 and 1989, to evaluate scrotal pathology. The patient age ranged from 3 days old to 76 years old (mean of 36 years). The patients presented a variety of intra and extratesticular pathologies, ranging from possible mass lesions to infections or acute or chronic pain. Ultrasound was performed in approximately 50% of the cases prior to the MR examination. The MR studies were evaluated for clinical diagnosis, as well as depiction of normal scrotal structures. Clinical and\or surgical follow-up was available on most of the cases. All MR exams were performed on a GE 1.5 tesla Signa system using a 5 inch surface coil.

MR has higher sensitivity than ultrasound for infection, but similar sensitivity for scrotal abnormalities. However, due to tissue characterization capabilities MR appears to have greater specificity than does ultrasound. The ultrasound diagnosis and therapeutic path was altered by the MR examination interpretation in nearly 10% of patients. For example: there was 100% accuracy in differentiating epididymitis from torsion in the subacute setting. There was a 92% accuracy in determining seminomatous from nonseminomatous testicular tumors. The one error made in the 13 cases was interpretive.

Ten cases done before and after Gadolinium-DTPA suggest that this intravenous contrast material adds further specificity when evaluating scrotal pathology, and may allow for shorter examination time.

MR of the scrotum contributes significant diagnostic data to the sonogram, adding specificity and an easier anatomic display to the referring physician.

► **155** 17:09PM

MRI CAN DISTINGUISH SEMINOMATOUS FROM NONSEMINOMATOUS TUMORS

JO Johnson, NE Budorick, RF Mattrey
Department of Radiology, University of California, San Diego;UCSD/AMI MRI Institute

Seminomatous and nonseminomatous testicular neoplasms require a different surgical treatment approach. The ability to distinguish these two lessions preoperatively may aid in patient management.

We have studied the utility of MRI to distinguish seminomatous from nonseminomatous tumors in fourteen patients. Signal intensity, homogeneity, and appearance were assessed. MRI diagnoses were compared to pathologic diagnoses in all patients. Nonseminomatous lesions were heterogenous in signal intensity and typically contained internal hemorrhage. Most assumed signals as bright as testis. Seminomatous lesions were more homogenous in signal intensity and were darker than testis. One lesion was a 3 mm embryonal cell carcinoma with areas of hemorrhage and necrosis that could not be characterized because of limitations in spatial resolution. Of the 13 lesions that could be characterized, MRI correctly predicted the histological type prior to surgery in 12. The single error occurred in a patient with pure seminoma that was properly diagnosed on MRI. However, a central focus of hemorrhage was incorrectly interpreted as a nonseminomatous island. This error is potentially avoidable, since nonseminomatous elements are typically microscopic and multiple rather than a single focus. In addition, hemorrhage is an atypical event in seminomas.

In this small series, MRI distinguished seminomatous from nonseminomatous lesions in 12 of 13 cases, or 92%. This may be useful in planning surgical treatment strategies of these two neoplasms.

BASIC NMR

MODERATORS: S. R. THOMAS, Ph.D., M. A. FOSTER, Ph.D.

► **156** 15:45PM

Comparision of in vivo and in vitro NMR Dispersion Curves

MA Foster and JE Rimmington
Department of Medical Physics, University of Aberdeen, Scotland, UK.

The shape of tissue NMR dispersion curves depends critically on the state of bound water within the cell. We have measured curves both for humans in vivo and for rat in vitro to look for changes in bound water immediately after death. Six point proton dispersion curves were obtained for humans using 12 fixed field imagers sited throughout the UK and operating at frequencies between 1.7 and 64MHz. T1 and T2 measurements were made on predominantly white or grey brain, liver, spleen and thigh muscle. A test object was made of agarose and several concentrations of manganese chloride. By comparing results from the imager with those from a Bruker CXP100 relaxation spectrometer operating at the imaging frequencies, calibration curves were made to correct the imager readings. The spectrometer was also used to measure T1 and T2 for in vitro rat samples at 37C.

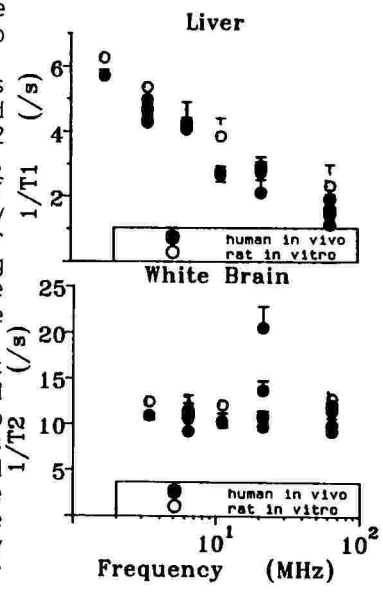

For T1 the in vivo and in vitro results were almost indistinguishable except for liver where the results agreed at low frequencies but the in vitro dispersion curve was too shallow. This is due to a rapid physiological change in this tissue on death rather than a species difference. Brain and spleen samples have monoexponetial T2 values. For these samples the in vivo and in vitro results were again in close agreement with the in vitro relaxation rates lying slightly higher than the in vivo results. This reflects the greater sensitivity of T2 to changes in cell micro-environment.

► **157** 15:57PM

QUANTIFICATION OF THE INTRINSIC MAGNETIC FIELD INHOMOGENEITY OF TRABECULAR BONE

JC Ford, FW Wehrli, DA Gusnard
Hospital of the University of Pennsylvania, Philadelphia, PA

The hypointensity of trabecular bone on gradient-echo images has been accounted to intrinsic magnetic field inhomogeneities, presumably caused by magnetic susceptibility differentials between the trabeculae and the marrow contents (1, 2). During the normal aging process as well as in diseases such as osteoporosis, the density of trabeculae decreases, which should lessen these intrinsic nonuniformities. Quantitating the effect entails a measurement of T2*, which is complicated by chemical shift-induced amplitude modulation (3), which can be accomplished by multicomponent analysis of the ROI interferogram (2).

Since this method (2) is demanding as far as data collection and analysis is concerned, we have evaluated the use of single-exponential fitting, ignoring the modulation. A useful model for testing this approach is the femur where bone of different degrees of trabeculation is found within the same anatomic entity (1). The results, plotted (semilog) in the Figure for a normal 31-year old volunteer give rise to the following observations: (i) The decay rates increase from diaphysis to metaphysis and epiphysis; (ii) a modulation with a period of approximately 4.5 msec is present; (iii) the behavior for the diaphysis closely tracks the one seen for subcutaneous tissue, in line with the absence of trabeculation in diaphyseal marrow. Since the fat-suppressed image of femoral bone was found to be virtually devoid of a water signal, the modulation must be due to different spectral components within fat, as shown in Ref. 3. A three-component analysis afforded T2* values for the major component within 10% of the ones derived from single-exponential analysis. In order to make the protocol clinically practical, a gradient echo pulse sequence was designed that permits automatic stepping through a predetermined array of TE's.

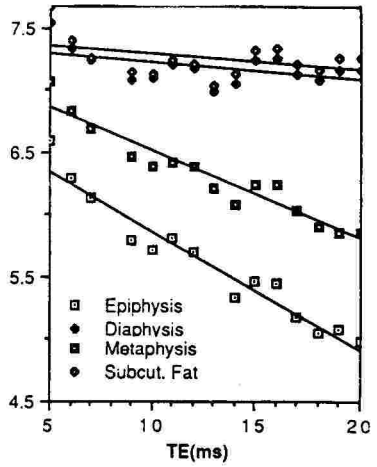

1. Sebag GH, Moore SG, SMRM 1989; 2. Wehrli et al, SMRM 89; 3. Wehrli FW, Perkins DG, Shimakawa A, Roberts F. Magn Res Imaging 5: 157-158.

► **158** 16:09PM

MAGNETIZATION TRANSFER CONTRAST AFFECTS ORDINARY MULTISLICE IMAGING

WT Dixon, H Engels, M Sardashti, M Castillo
Emory University Radiology Department, Frederik Philips Research Center, Philips Medical Systems, Atlanta GA 30322

Wolff and Balaban (1) have discovered that off resonant RF power reduces tissue magnetization but does not affect simple solutions. They call this large effect magnetization transfer contrast (MTC). Others (2) added long, off resonant pulses to a standard imaging sequence, producing MTC weighted images. RF used for extra slices in multislice imaging is "off resonant." Does MTC affect ordinary multislice images?

Comparing perfectly standard, TR=1s, 2 echo, multislice images with 1, 3, and 11 6mm slices on 24mm centers we see 15-20% muscle signal loss resulting from the extra 10 slices. Solution results and the effect of nonadjacent slices exclude slice overlap as a cause; we attribute the loss to MTC. These losses can ruin T1 and fat fraction measurements and affect image contrast.

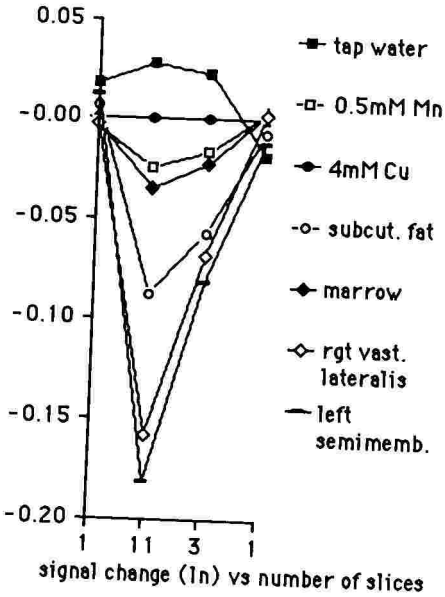

1 SD Wolff, RS Balaban. Mag Res Med 10, 135 (1989).
2 DAC Kelley et al. Soc Mag Res Med 1989 Abstract Book p. 1036 (WIP).

► **159** 16:21PM

IMPROVED IDENTIFICATION OF NORMAL AND ABNORMAL PARAMAGNETIC ENHANCEMENT PATTERNS BY CHEMICAL SHIFT IMAGING

J Simon, D Rubinstein, J Stears, R Pacini, L Ketonen, J Szumowski
Magnetic Resonance Imaging, University of Colorado Health Sciences Center

The detection of paramagnetic contrast enhancement using Tl-weighted spin echo sequences is limited in lipid rich regions by the strong lipid signal which may be isointense with enhanced lesions. Paramagnetic enhancement combined with chemical shift imaging optimized for lipid suppression (PEACH-imaging) results in an image dominated by regions of enhancement rather than normal lipid.[1] The PEACH approach can be used to determine normal enhancement patterns in the orbit, skull base, and spine.

Normal enhancement patterns were determined in presumed non-pathologic lipid rich regions in patients referred for MRI of the head and spine. Images were obtained by conventional technique (Tl-weighted spin echo) and compared to paired studies using hybrid lipid suppression (frequency selective pulse + chopper fat suppression) at high field (1.5 T). Normal enhancement patterns obviated by the chemical shift method were searched for and evaluated at low field (0.35 T) using conventional technique.

Although in the majority of cases large areas of pathologic enhancement were easily detected using the conventional technique, the chemical shift approach revealed more subtle abnormal and normal regions of enhancement. These included enhancement in abnormal tissue interspersed with normal lipid (e.g. a subfraction of scar cases), and normal enhancement surrounded by a large volume of normal lipid (e.g. nerve root ganglion, extraocular muscles).

Application of this knowledge of the normal anatomic enhancement patterns should improve interpretation of normal and abnormal MRI studies.

[1]Simon JH and Szumowski J. Chemical shift imaging with paramagnetic contrast material enhancement for improved lesion depiction. Radiology 1989; 171:539-543.

► **160** 16:33PM

19-F IMAGING ASSESSMENT OF CEREBRAL BLOOD FLOW

JA Helpern, CA Branch, JR Ewing, KMA Welch
Department of Neurology, Henry Ford Hospital, Detroit, MI 48202

The development of an atraumatic, nonradioactive imaging assessment of cerebral blood flow (CBF) in man would be of great clinical utility. Toward this goal, we have developed high-speed NMR imaging of 19-F labeled gasses, administered *via* inhalation, in cat brain. Cats were anesthetized, intubated, mechanically ventilated, and placed inside a 1.9 T magnet. A modified Helmholtz coil, tunable to both 1-H (80.3MHz) and 19-F (75.5MHz), was placed around the head of the cat. An imaging program written to obtain 1280 gradient refocussed echo images over a 36 minute period from a single slice was employed. Images were signal averaged in blocks of 40, resulting in a total of 32 one minute (67s) images. Imaging parameters were: TE = 2.23ms, TR = 102ms, matrix = 16X16, FOV = 16cm, and slice thickness = 2cm, resulting in a voxel volume of 2.0cc. The imaging protocol consisted of the collection of 5 images in the absence of fluorinated gas (for baseline determination), 12 images during which time the animal was administered 25% O2 and 75% trifluromethane, and 15 images collected during washout. The entire protocol was performed without interruption of the imaging program. The resulting 19-F images demonstrate the uptake and clearance of the 19-F labeled gas. Voxels from brain and extracranial tissue (muscle) were identified using corresponding 1-H images. The signal intensity of these voxels in the 19-F images were used together with our measurement of the partition coefficient and input function (the concentration of trifluoromethane measured in the expired air by means of an anesthetic gas monitor) to measure regional CBF, using a one-compartment maximum likelihood analysis (see Figure). CBF measured in the cat brain as described above was 50 ml/100gm-min and compares well with published values for this anesthetic model. This report represents the first application of NMR imaging in conjunction with the use of an indicator dilution technique to measure regional CBF.

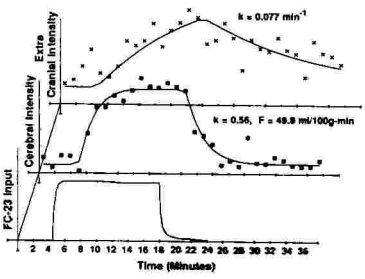

► **161** 16:45PM

CARBON-13 IMAGING OF SMALL ANIMALS IN VIVO

N.Iriguchi, O.Takizawa, S.Chu+, S.Morishita*, M.Sumi*, Y.Sakamoto*,
R.Nishimura*, A.Kojima* and M.Takahashi*
Siemens-Asahi, SISCO+ and Unversity of Kumamoto*

C-13 imaging is a potential means for investigations of metabolic pathways in living systems. C-13, naturally 1.1% abundant,has MR sensitivity and molar concentration of 1.6% and roughly 0.1% respectively of those of protons in living systems. For C-13 enhanced MR researech, small animal MR is important.

Using a horizontal bore 7 Tesla 18.3 cm system SIS 300/183, we obtained C-13 images of small animals in vivo. Figure 1 shows a C-13 image of a hamster head in 64 encoding SE 42/27 accumulated 4096 times.

Fig.1

With field strength signal intensity becomes high at a rate more than that of noise caused by the sample loss.

► **162** 16:57PM

THE USE OF OXYGEN-17 WATER IN MONITORING EXPERIMENTAL CEREBRAL ISCHEMIA.

AL Hopkins[1], EM Haacke[2], WD Lust[3], PA Wielopolski[2], RG Barr[4], and CB Bratton[5].
(1) Depts. of Anatomy and Radiology, (2) Dept. of Radiology, (3) Division of Neurosurgery, (4) Dept. of Biochemistry, Case Western Reserve University and University Hospitals, Cleveland, OH 44106. (5) Dept. of Physics, Cleveland State University, Cleveland, OH 44115.

When perfusion fluid or blood is enriched with oxygen-17 water ($H_2{}^{17}O$), the T_2 of the perfused organs and tissues is lowered due to the spin-coupling between the ^{17}O and the protons exchanging with it. Since this stable isotope is apparently biochemically interchangeable with ordinary ^{16}O, its relatively weak effect on proton T_2 can be compensated for by increasing concentration without toxic effects. For the first time the T_2 image intensity effect has been used to follow the the ischemia resulting from ligation of the common carotid artery. The injection of $H_2{}^{17}O$ produces a rapid and long lasting decrease in T_2 image intensity in the normally perfused cerebral hemisphere and eye. In contrast, the intensity of the ischemic structures remains high.

Unilateral common carotid artery ligation was carried out on anesthetized Mongolian gerbils and those animals showing marked neurological symptoms on recovery from surgical anesthesia were reanesthetized for imaging. Half-Fourier imaging was done with the orbital coil of a Siemens 1.5T Magnetom using a TR of 4.0s and a TE of 90ms. Due to the rapid development of edema it is possible to distinguish, on the basis of the increased signal amplitude, the ischemic hemisphere within at least the second hour after ligation. The i.p. injection of about 1% (b.w.) of $H_2{}^{17}O$ leads to as much as a 50% fall in intensity in the normally perfused areas. The greatest change is seen in the vitreous humor of the eye. Due in part to residual collateral circulation there is also approximately a 10% decrease in intensity in the ischemic tissues. These intensity changes are also observed in areas of the ischemic hemisphere in which there is no edema or other prior evidence of ischemia before the injection of $H_2{}^{17}O$.

► **163** 17:09PM

SIMULTANEOUS MULTISLICE NMR IMAGING OF F-19*

H. K. Lee, O. Nalcioglu, R. Buxton and D. Long**
Department of Radiological Sciences, Division of Physics & Engineering, University of California-Irvine

The fluorinated blood substitute perfluoroctylbromide is an interesting contrast agent due to its insignificant toxicity and potential in studying vascular perfusion[1]. However, there are several difficulties in F-19 NMR imaging. One among them is the fact that the fluorinated blood substitutes exhibit complex multi-peaked spectra[2,3]. For instance, in the case of PFOB at 1.5T, the first two peaks are separated by 1.05KHz while another group of closely spaced peaks occur at a frequency which is 2KHz lower. These multiple peaks cause chemical shift artifacts along the readout direction and hence create blurred images. To make things even worse, in 2D imaging when we apply a slice selection gradient during the selective 90° rf pulse, undesired slices are also excited due to multiple peaks. A possible solution to this latter problem is to apply a stronger selection gradient to minimize the effect of chemical shifts in the slice thickness direction. Unfortunately, this approach does not seem to work for a compound like PFOB which has a great amount of peak separation, namely 17ppm for the two highest peaks.

In the current presentation a new technique is proposed to solve this problem. The essence of the new method is the utilization of the two highest spectral peaks to excite different multislices simultaneously in a controlled fashion with or without a slice gap. By collecting two sets of multislice images for the in-phase and out-phase images, each slice can be retrieved after addition and subtraction as done in the conventional Dixon method[4]. The new method also improves the signal-to-noise ratio per unit scan time.

We will present experimental results obtained with phantoms demonstrating the capabilities of the new technique.

References
1. D. M. Long et al. Invest. Radiol. **15**, 242(1980).
2. P. M. Joseph et al, JCAT **9**,1012(1985).
3 S. Thomas , Proc. SPIE **626**, 7(1986).
4. W. T. Dixon, Radiology **153**, 189(1984).

* Work supported in part by grant CA45229 awarded by the National Cancer Institute, DHHS.
** Department of Radiology, University of California-San Diego.

CONTRAST I

MODERATORS: G. L. WOLF, M.D., W. A. MURPHY, M.D.

► 164 15:45PM

Theoretical Considerations for the Design of Targeted MR Contrast Agents

Evan Unger, M.D.
University of Arizona, Department of Radiology, Tucson, Arizona

Paramagnetic MR contrast agents based on complexes of gadolinium are non-specific agents and their use outside of the CNS has been disappointing. However, because these agents cause enhancement in the micromolar range, there are possibilities for designing targeted MR contrast agents. Superparamagnetic contrast agents cause enhancement much stronger than the paramagnetics opening further possibilities. Some important points regarding targeted MR contrast agents may be summarized as follows. 1) It is not possible to use monoclonal antibodies as MR contrast agents with direct attachment of gadolinium complex to the antibody. By first preforming a skeleton of polymer and coupling this to the antibody with the paramagnetic complexes this increases the relaxivity and the amount of gadolinium, but still is impractical as an MR contrast agent. 2) Macromolecules can be used with paramagnetic complexes as blood pool contrast agents but consideration to their design must include provision to prevent decomplexation of paramagnetic ions. 3) Liposomes can be labelled with paramagnetics or used effectively to entrap paramagnetic ion and target blood pool, RES and hepatocytes. 4) There are a number of different possible designs for superparamagnetic contrast agents and by making the particles as small as possible and incorporation with certain molecules or artificial membranes, a degreee of targeting can be achieved. 5) Despite their limitations, targeted MR contrast agents have great potential to increase the role of MR in body imaging.

MONDAY p.m.

► 165 15:57PM

Gd-DPTA-Dextran as a Versatile New MRI Contrast Agent

K.C. Li[†], F.E. Armitage[†], R.G. Quisling[†], C. Mladinich[†], D.E. Richardson[‡]
Department of Radiology[†] and Department of Chemistry[‡], University of Florida
Gainesville, Florida.

In order to modify the biodistribution of Gd-DPTA, we synthesized a series of Gd-DPTA based complexes that are bound via ester linkage to various molecular weight polysaccharides (9.4k, 40.2k, 70.8k, 487k). Synthetic procedures were developed to produce esterified polysaccharides with no detectable crosslinking. T1 measurements were obtained at 100 MHz for concentrations ranging between 1.0 to 5.0 mM for each of the new compounds and Magnevist. The in vitro experiments showed that the relaxivities (1/T1) of the Gd-DPTA-Dextran solutions were not significantly different from each other, but were significantly higher than that of Magnevist. In vivo experiments were performed in 6 rabbits using a 1.5 T GE Signa imager and the 70.8k Gd-DPTA-Dextran, which has a molecular weight approximating that of albumin. Pre-contrast images were obtained using SE 300/20 pulse sequence. A dose of 0.1mM Gd/kg was then injected at a rate of 2 ml/min intraveneously into each rabbit. Post contrast scans of the head and abdomen were obtained at 5 to 10 minute intervals up to a maximum of 60-90 minutes. The in vivo experiment demonstrated persistent enhancement of the blood pool for over 90 minutes, slow renal and biliary excretion, no penetration of the blood brain barrier and sustained enhancement of the abdominal viscera. We conclude that the biodistribution of the 70.8k Gd-DPTA-Dextran is similar to the albumin labeled compound and very different from Magnevist. No toxic effects were observed for the macromolecular complexes evaluated thus far. It is likely that alteration of the size of the dextran will result in different biodistributions which may have a variety of research and clinical applications.

► **166** 16:09PM

ORAL MAGNETIC PARTICLES AS A CONTRAST AGENT FOR ABDOMINAL AND PELVIC DISEASES.
Peter A. Rinck[1], Olaug Smevik[1], Audun Øksendal[2]
MR Center, Medical Section, University of Trondheim N-7006 Trondheim (1)
Nycomed A/S, R&D Division, N-0401 OSLO 4, Norway (2)

A superparamagnetic oral MRI contrast agent has been developed by Nycomed AS, Norway. The active component of the agent consists of magnetic iron oxide particles (20%) imbedded in monodisperse polymer particles as a carrier matrix (size 3.5 µm). The magnetic particles create inhomogeneities in the local magnetic field consequently shortening T_2-relaxation and thus inducing a signal loss in the bowel.In a clinical phase II study the contrast agent has been used in two different protocols: (a) Examination of patients with cancer testis after the ingestion of the agent at 0.5 and 1.5 T; (b) Examination of patients with pelvic and lower abdomen diseases before and after ingestion of the agent at 1.5 T.
The contrast agent was effective at T_1-, T_2- and proton density weighted spin echo sequences with doses of 0.25 or 0.5 g/l. The agent did not create artifacts in addition to the already existing (i.e. motion, respiratory, flow and chemical shift) with the concentrations used.
Generally, there was a good differentiation of the contrast-filled bowel in the abdomen and the pelvis. This made it more easy to distinguish between normal and pathological tissues and to get a better delineation of tumors. In particular the differentiation of the distal wall of the uterus in the pelvis, the delineation of the bowel versus lymph node metastases in the abdomen and the exclusion of abdominal tumors versus e.g. faeces, was helpful in a number of patients. The contrast medium was well tolerated.
In conclusion, the use of negative oral contrast agents can improve the diagnostic value of abdominal and pelvic MRI and is rather helpful in some diagnostic questions.

► **167** 16:21PM

GADOLINIUM-DTPA-ENHANCED DYNAMIC MRI IN RENAL TRANSPLANTS
C Dewey, B Schnackenburg, B Wenig, M Lüning, K Sydow, W Blank, S Deveaux, G Timm, M Koch, J Haustein
Humboldt University (Charité), Institute of Diagnostic Radiology, GDR

Purpose: It is the purpose of the present study to evaluate renal transplant function by means of dynamic contrast-enhanced MRI.

Methods and patients: 35 MRI studies of renal transplanted patients were performed in 15 patients with normal function and 20 with histologically proven chronic rejections (1.5 T Gyroscan S15, 17 cm surface coil). Dynamic MRI was performed with GE sequences FFE 27/13, $\alpha = 50^{\circ}$, 30-sequential for 4.5 S-images and bolus application of Gd-DTPA (0.1 mmol/kg b.w.). Dynamic signal behaviour in cortex (peak-time, peak-value, slope of decrease of SI), medulla (value at peak-time in cortex, slope of increase of SI) and urinary bladder was evaluated.

Results: No difference in cortex peak-time of SI was found between patients with normal or impaired renal function. Scintigraphically proven GFR correlated significantly with signal values in the medulla ($p < 0.05$ for value at peak-time in cortex, slope of increase of SI). No side effects were observed or reported after administration of Gd-DTPA in patients with impaired renal function. Serum creatinine ranged up to 4 mg/ dl.

Conclusion: The kinetic SI-profiles reflect the functional status of transplant perfusion and the glomerular filtration rate.

► **168** 16:33PM

RENAL TOLERANCE OF GD-DTPA - A RETROSPECTIVE EVALUATION OF 1,171 PATIENTS

J. Haustein, HP Niendorf, T. Louton
Schering AG, Berlin/Bergkamen, Clinical Research Diagnostics, FRG

Purpose: To assess the renal tolerance of gadopentetate dimeglumine by evaluating serum creatinine values in patients with normal (< 113 µmol/L), slightly impaired (113 - 124 µmol/L), and severely impaired (> 124 µmol/L) renal function.

Methods: Serum creatinine data from European phase III studies conducted between 1985 and 1987 in which 1,171 patients were evaluated retrospectively. Serum creatinine was measured at baseline and at 24 hours post injection of 0.1 or 0.2 mmol/kg b.w. of gadopentetate dimeglumine.

Results: For each group, the median, mean and SD showed no relevant changes over time. The median value of the difference (24-hour value minus baseline value) was zero or negative. No side effects were seen or reported during 24 hours observation period.

Conclusion: The data from this retrospective evaluation indicate that gadopentetate dimeglumine shows good renal tolerance in patients with or without pre-existing impairment of renal function.

group	serum creatinine [mikromol/L]			n =	median	mean	SD
1	(normal)	< 113	baseline	1060	79.56	82.22	14.00
			24 hours		81.33	84.72	17.75
2	(slightly impaired)	113 - 124	baseline	69	114.92	117.58	3.99
			24 hours		114.92	114.11	17.96
3	(severely impaired)	> 124	baseline	42	141.44	152.81	45.31
			24 hours		139.23	141.48	54.93

MONDAY p.m.

► **169** 16:45PM

The Use of GD-DTPA For Renal Tumor Detection: Time Dependent Effects in Animial and Man

L. Teschmacher, MA Trambert, BD Coley, KG Baker, RM Mitten, RF Mattrey
Department of Radiology, University of California, San Diego, UCSD/AMI MRI Institute

MR imaging is becoming a commonly used technique in the evaluation of abdominal disorders, particularly in patients with renal cell carcinoma where MR stages the extent of disease more accurately than does CT. The potential use of MRI with Gd-DTPA, a relatively new paramagnetic intravenous contrast agent, in assessing the integrity of the kidney needs to be assessed. While the general pharmacokinetic data of Gd-DTPA parallels that of water-soluble agents used with CT, the relative difference in wash-in and wash-out rates of these contrast agents in renal tumors and normal kidneys is not known.

The purpose of this study was to establish and compare the time curves for enhancement of VX-2 carcinoma and normal kidney on CT and MR images after IV injection of Renografin-76 (R-76) and Gd-DTPA.

VX-2 tumor was induced in 10 New Zealand white rabbits via direct injection of tumor cells into the upper pole of the right kidney. Following 18-21 days, rabbits were imaged in the coronal plane using a GE 9800 CT scanner with R-76 (2.2cc/kg). Immediately thereafter, coronal images were obtained with a GE 1.5 Tesla Signa MR system using 0.1 mM/kg of Gd-DTPA. The imaging studies were performed both before and at multiple time points after contrast out to 60 minutes. CT was performed prior to MR, as it was found that Gd-DTPA significantly interferes with CT signal intensity of normal renal parenchyma whereas R-76 does not affect MR signals. Rabbits were then frozen and sliced for anatomic correlation. Tumor and normal kidney signals on MR and CT images were examined using region of interest analysis.

Similar human data from MR and CT were obtained to assess the time-dependent enhancement of tumor versus normal renal parenchyma in human tumors. Data analysis showed that both agents increase the contrast between tumor and normal kidney. While tissue contrast between tumor and kidney was poor before contrast injection, the percent change in tissue contrast was greater for CT.

► **170** 16:57PM

FERROSOMES: TUMOR DETECTION BY SELECTIVE ENHANCEMENT OF PERITUMORAL MACROPHAGES

G. Patrizio, DD Stark, G. Elizondo, C. Fretz, CGS Eley*, JT Ferrucci

Department of Radiology, Massachusetts General Hospital - * Vestar, Inc.

Liposomes [small unilamellar vesicles (SUVs)] previously shown to concentrate in neoplastic tissue, were loaded with 11 nm size superparamagnetic iron oxide crystals. "Ferrosomes" having a mean size of 80 nm were prepared as a colloidal suspension (Vestar Inc.) containing 5 mg lipid/ml (distearoylphosphtidylcholine, cholesterol and behenic acid [2:1:0.6 mol ratio]) and 15 mM iron. Fischer 344 or ACI/N rats implanted subcutaneously with adenocarcinoma (R3230) or hepatoma (H-4-11-E), were imaged at 0.6 T before, and 5 and 24 hours after intravenous injection of ferrosomes, 50 µmol Fe/kg. After ferrosome injection T1 weighed GE (126/18/60; TR/TE/FA) T2 weighted SE (1500/40,80) and GE (146/22/10°) images showed a ring of decreased signal intensity at the periphery of tumors, which remained unchanged from 5 to 24 hours. The tumor itself was unaffected. Histologic examination (Prussian blue stain) revealed the presence of stainable iron in macrophages located between tumor and surrounding subcutaneous adipose tissue. Control studies with unencapsulated iron oxide showed no tumor uptake. Blood samples showed the intravascular $t_{1/2}$ for ferrosomes to be 5 hours, compared to 10 minutes to unencapsulated iron oxide crystals. These results suggest that liposome encapsulation prolongs the vascular half life of iron oxide particles and furthermore, leads to particle uptake by macrophages located at the periphery of tumors.

► **171** 17:09PM

EFFECT OF SUPERPARAMAGNETIC IRON OXIDE CONCENTRATION AND MAGNETIC FIELD STRENGTH ON LIVER-LESION MR IMAGE CONTRAST

DI Thickman, RE Hendrick, KA Jerjian, C Schanker
Department of Radiology, University of Colorado Health Sciences Center

Superparamagnetic iron oxide (AMI-25, Advanced Magnetics, Inc.) is a promising MR contrast agent for improving detectability of liver lesions. However, some toxicity has occurred with intravenous doses above 30 umoles/kg. This study was performed to assess the enhancement of liver-lesion contrast using low levels of iron oxides at four different imaging magnetic field strengths. Fifteen Fisher 344 rats had adenocarcinoma percutaneously inserted into the liver. Iron oxide concentrations of 0 (control group), 2.5, 5, 10, and 20 umoles/kg were given intravenously to 3 rats in each concentration group. Rats were killed one hour after injection of iron oxide. Imaging of all rats was performed at 0.15T using SE 500/30 and SE 2000/45-90 with 7.5mm slice thicknesses, and at 0.35T, 0.5T, and 1.5T using SE 500/40 and SE 2000/40-80 with 5mm slice thicknesses. Signal differences between tumor and liver were standardized to signals from tumor, liver, muscle, and a distilled water phantom. These standardized signal differences showed increasing values with increasing iron oxide concentrations at all field strengths, although the gain from 0 to 10 umoles/kg far exceeded the gain from 10 to 20 umoles/kg concentrations. The greatest percentage contrast gain between 0 and 20 umoles/kg iron oxide occurred at 0.35 and 0.5T. At 0.15T iron oxide produced smaller gains in tumor-liver contrast. At 1.5T, greater tumor contrast existed prior to administration of iron oxides, so iron oxide provided less benefit. Low dose iron oxide (10 umoles/kg) provided excellent lesion contrast at field strengths from 0.15 to 1.5T. In fact, at doses near 20 umoles/kg the tumor-liver contrast was the same using 0.35, 0.5, and 1.5T units for all pulse sequences.

BRAIN II

MODERATORS: R. M. KESSLER, M.D., J. L. SHERMAN, M.D.

► **172** 15:45PM

IMAGING CEREBRAL AVMs BY MRA: BENEFIT OF GD-DTPA

JL Creasy, TC Kerner, RC Dawson, RM Kessler
Department of Radiology, Vanderbilt University Medical Center

Cerebral arterial vascular malformation (AVMs) can be imaged by magnetic resonance, cut film and digital subtraction angiography. However, only MR angiography offers the advantages of viewing the data from any projection following single acquisition, and of precisely localizing abnormal vessels three-dimensionally by analyzing the data sets slice by slice. We have also investigated the added benefits of the administration of gadolinium in the visualization of components of these lesions.

Eight patients were studied with routine MR imaging, as well as MR angiography sequences. Several patients received MR angiograms both prior to and following the administration of gadolinium DTPA. MRI pulse sequences were performed with the three-dimensional FISP sequence with flow compensating gradients to enhance vascular contents, utilizing a flip angle of 20°, TR 40 msec and a TE of 8 msec, 64 partitions and single acquisition. Slice thicknesses range from 1-2½ mm. Once acquired, each of the 64 slices is reconstructed and projection angiogram images are created using a maximum intensity ray projection algorithm from any arbitrary angle through the 3-D data set.

In all cases the MR angiogram demonstrates normal large intercranial vessels. Using gadolinium allows the visualization of additional, small normal arteries and veins, and large vessels with slower flow.

MRA has potential usefulness as a screening modality in the evaluations of cerebral AVMs as a precise 3-D localizer of abnormal vessels. The addition of gadolinium to the regimen allows visualization of both smaller vessels and vessels with slower internal flow.

► **173** 15:57PM

GADOLINIUM ENHANCEMENT OF INTRACRANIAL LESIONS ON SPIN DENSITY AND T2 WEIGHTED IMAGES

FW Wessbecher, KR Maravilla, RW Dalley
Department of Radiology, University of Washington

While many pathologic entities in the brain are best demonstrated on gadolinium DTPA (Gd) enhanced T1 weighted images, spin density and T2 weighted images remain essential to identify nonenhancing abnormalities with increased water content, including low grade tumors, areas of edema, infarction and demyelination. However, little attention has been directed to the relative advantages or disadvantages of combining Gd with long TR pulse sequences. In view of this, we have undertaken a study comparing pre and post Gd spin density and T2 weighted images.

Axial T1 weighted (TR = 600/TE = 20), spin density, and T2 weighted images (TR = 2700/TE = 30-80) were obtained on a 1.5 Tesla Signa scanner both pre and post Gd and directly compared. To date, 15 patients with enhancing intracranial lesions have been analyzed; 9 patients with recurrent astrocytoma, 3 patients with metastatic disease, one patient with a sphenoid wing meningioma, one patient with a pineal germinoma and one patient with a venous angioma.

Comparison of nonenhanced spin density and T2 weighted images with post Gd spin density and T2 weighted images revealed better differentiation of enhancing lesions from adjacent edema (9 of 15 patients) and hemorrhage (1 of 15 patients) on the post contrast studies. Similarly, enhancing tumor could be distinguished from postoperative changes in 5 of 9 cases with tumor recurrence. This difference was much more marked on spin density images compared with T2 weighted images probably due to greater residual T1 effects on the long TR/short TE images. In comparison with enhanced T1 weighted images, no new lesions were demonstrated on enhanced spin density or T2 weighted images. Two of 18 lesions which demonstrated clear enhancement on T1 weighted images were not discernible from adjacent edema on enhanced spin density or T2 weighted images. Importantly however, no lesions were obscured on the post Gd compared with the pre Gd long TR studies and no T2 shortening effects were seen that might be misinterpreted as hemosiderin. Our findings confirm that enhanced spin density and T2 weighted images alone cannot replace enhanced T1 weighted images. However, in the majority of cases conspicuity between enhancing and nonenhancing pathology on spin density and T2 weighted images is greatly improved on the post Gd sequences and no information is obscured by gadolinium. Thus we conclude that in order to optimize conspicuity the preferred Gd imaging protocol would be to obtain the long TR images after, rather than before, the administration of gadolinium.

► 174 16:09PM

GD-DTPA ENHANCED MR IMAGING OF INTRACRANIAL VASCULAR LESIONS

H HENKES, W SCHOERNER, R BITTNER, P SCHUBEUS, T HEIM, R FELIX
Dep. of Radiology, University Clinic Rudolf Virchow/Charlottenburg
Freie Universität Berlin

Purpose: At present, Gd-DTPA as a paramagnetic contrast agent for MR imaging has been primarily used to delineate brain lesions characterized by disruption of the blood-brain barrier (BBB). Experience concerning the use of Gd-DTPA in cerebrovascular disease is limited. In the present study, we determined the diagnostic value of Gd-DTPA enhanced MR imaging in cerebrovascular malformations as well as other intracranial vascular disorders without disruption of BBB.
Materials & Methods: Imaging studies were retrospectively evaluated in 12 patients. Five patients had arteriovenous malformations (AVM), 4 had (partially thrombosed) aneurysms. Three patients (children) suffered from Sturge-Weber disease. Unenhanced and contrast enhanced CT scans (3 rd generation scanners) were available in all patients. MR examinations were performed on a 0.5 T superconductive system. T2-weighted images (WI) (SE 1600/30,70) as well as unenhanced and Gd-DTPA enhanced T1-weighted images (FLASH, 315/14, θ=90°) were generated.
Results: AVM: T2-WI's were *inferior* to unenhanced and contrast enhanced CT scans (CT/C) in detecting arteriovenous malformations in 3/5 patients and *equivalent* in 2/5 patients. Gd-DTPA enhanced T1-WI's were *inferior* to CT/C in 2/5 patients, *equivalent* in 2/5 patients and *superior* to CT/C in 1/5 patients. In all patients with AVMs, Gd-DTPA enhanced T1-WI's were diagnostically more accurate than T2-WI's. In 4/5 cases, CT/C and Gd-DTPA enhanced T1-WI demonstrated the typical pattern of serpiginous enhancing lesions. Feeding and/or draining vessels near the skull were very clearly demonstrated by CT/C as well as Gd-DTPA enhanced MR imaging in 2 patients. Aneurysms: T2-WI's were inferior to unenhanced and contrast enhanced CT. Focal contrast enhancement was observed in all patients on CT/C and on Gd-DTPA enhanced T1-WI. Gd-DTPA enhanced T1-WI's were not superior to CT/C in any of the patients. Sturge-Weber disease: T2-WI's did not demonstrate pathologic vascular structures in all patients. In comparison, the diagnosis was not possible in 2 of the 3 patients on unenhanced CT. On unenhanced T1-WI's, no epi- or subcortical signal void was observed. Gd-DTPA enhanced T1-WI's were the most accurate method in detecting leptomeningeal angiomatosis. The degree of contrast enhancement was greater and the extension of pathologic vascular structures was more pronounced on Gd-DTPA enhanced T1-WI than on CT/C.
Conclusion: In the detection of AVMs and cerebral vascular aneurysms, Gd-DTPA T1-WI's are superior to unenhanced T1-WI and superior to T2-WI. Sensitivity and findings are comparable to CT/C. In Sturge-Weber disease, T2-WI's are not diagnostic. Gyral calcification and contrast enhancement are typical CT findings. Gd-DTPA enhanced T1-WI's, however, appear to be best suited for the detection of leptomeningeal angiomatosis.

► 175 16:21PM

A CLINICAL TRIAL OF GADOLINIUM–DTPA–BIS–(METHYLAMIDE)

AM Aisen*, G Kaplan*, and SR Aravapalli**
*The University of Michigan and **The University of Syracuse

We investigated the safety and efficacy of gadolinium diethylenetriaminepentaacetic acid bis–(methylamide) (Gd–DTPA–BMA), a proprietary, nonionic gadolinium chelate (Salutar, Inc., Sunnyvale, Calif). Thirty patients were selected from individuals referred for MRI with a known or suspected diagnosis of a space occupying lesion of or adjacent to the central nervous system, for whom it was judged that contrast enhancement might increase diagnostic yield. There were 17 men and 13 women, ages ranged from 19 to 84 years (mean 49). Scans were performed of the brain, pituitary, acoustic nerves, and/or foramen magnum in 20 subjects, of the spine in 9, and of the skull base in one patient. Scans were ordered for a variety of reasons, broadly categorized as follows (with some overlap): rule out suspected tumor or mass lesion (9); follow–up of CNS tumor (6); evaluation of disk or other impingement on spinal cord, including postoperative patients (5); rule–out metastases (3); rule–out pituitary adenoma (3); rule–out acoustic neuroma (2); follow–up of abscess (1); evaluate extent of head and neck tumor (1). The contrast agent was administered in a dose of 0.1 mmol/kg, except for one 123 kg man who received .074 mmol/kg. All but one patient received T1– and T2–weighted pre and T1–weighted post infusion studies appropriate to their clinical situation; the remaining patient only had T1–weighted images.

All but one patient had brief neurologic examinations before and after the study; none showed any changes. There were no major adverse reactions, and only a few minor reactions felt likely to be due to contrast administration: one patient had mild, transient dizziness, and 3 patients had minor redness, swelling or bruises at the injection site. There were no significant changes in vital signs resulting from contrast administration. Hematologic and biochemical blood tests were performed in all but one patient (who only had post–study labs); there were few significant changes. Two patients had moderate increases in serum gamma glutamyltransferase, and several patients had changes in serum iron levels. The relationship of these changes to the agent is not known. One patient had a dramatic increase in platelets, which was normal on retest, and may have been laboratory error.

The scans were reviewed, and the utility of the agent subjectively evaluated by 2 experienced radiologists. In 6 subjects, contrast administration was of major diagnostic help, either revealing lesions not apparent without enhancement, or providing important lesion characterization. In 7 patients this was true to a moderate degree, and in 2 subjects the agent was of minor help. In 12 patients the lack of abnormal enhancement patterns was important in excluding pathology (e.g., pituitary adenoma or acoustic neuroma). In 3 of our patients the agent offered no significant help. We conclude that in this limited series Gd–DTPA–BMA proved a safe and useful agent for evaluation of the CNS and surrounding structures with MRI.

► **176** 16:33PM

GADOLINIUM-DTPA ENHANCED MR IMAGING OF CRANIAL NERVE PATHOLOGY
OB Boyko, WJ Meisler
Department of Radiology, Duke University Medical Center

We reviewed the T1-weighted MR findings in 220 pediatric/adult MR studies in patients who received 0.1 mmol/per kg of IV gadolinium-DTPA. Routine T1 and T2- weighted spin echo images were obtained at 1.5 Tesla prior to contrast administration. Post contrast T1-weighted images were acquired using a 5 or 3 mm slice thickness with a 2.5 or 1 mm interslice gap. In our series 36 patients had enhancement referrable to cranial nerve pathology, forming the study group for our presentation. In 17 cases conspicuity of lesion pathology was improved with gadolinium-DTPA over noncontrast T1 and T2-weighted images (CN II-neuritis (2), retinoblastoma, meningioma (2), leptomeningeal tumor spread (2); CN III, IV, V, VI-pituitary adenoma (2); CN V inflammation or tumor (2); CN VII/VIII-acoustic neuroma (6), leptomeningeal tumor spread (2).

In our series cranial nerves normally did not show gadolinium-DPTA enhancement but pitfalls in interpretation can occur because of enhancement of normal anatomic structures (choroid plexus, hypoglossal canal) or pseudomasses resulting from accentuation of phase misencoding of flowing blood by the shortened T1 of blood. Significantly in 12 cases lack of cranial nerve enhancement provided important clinical information excluding pathologic involvement of cranial nerves.

Gadolinium-DTPA is a valuable adjunct to routine spin echo imaging in the elucidation and demonstration of cranial nerve pathology.

► **177** 16:45PM

CLINICAL EFFICACY OF GD HP-DO3A, A NON-IONIC GADOLINIUM CRYPTELATE
VM Runge, DY Gelblum, MI Pacetti, FJ Carolan, GG Heard.
Tufts University and the University of Kentucky Magnetic Resonance Imaging and Spectrocopy Center

Gd HP-DO3A (SQ 32,692, Squibb Diagnostics) was evaluated as an intravenous MR contrast agent in Phase II clinical trials in adult patients with known intracranial neoplastic disease.

To date, 13 patients have been studied at 1.0 T with dosages of 0.05 to 0.3 mmol/kg Gd HP-DO3A in this ongoing clinical investigation. Mean age was 51±18 years, with 5 males and 8 females. Diagnoses for 11 patients in whom final pathology is now available from surgical specimens included astrocytoma (4), glioblastoma (2), metastases (2), meningioma (1), eosinophilic granuloma (1), and desmoplastic medulloblastoma (1). T1 and T2 weighted images were acquired pre-contrast, with post-contrast T1 weighted images obtained immediately, 30, and 60 min. after injection.

For the 12 lesions that demonstrated substantial enhancement, the increase in signal intensity immediately post-contrast correlated with dosage despite the varied pathology (enhancement{dose}: 38±19%{0.05}, 100±6%{0.1}, 136±18%{0.2}, 144±56%{0.3}). Greater enhancement of normal muscle and gray matter was also noted with higher contrast dosage when comparing 0.05 vs 0.3 mmol/kg (muscle: 33±4% vs 47±8%, gray matter: 3±2% vs 8±5%). The post-contrast exam provided significant additional diagnostic information in 12 of 13 cases. The T1 relaxivity in vivo (a measurement which is concentration independent) of Gd HP-DO3A is approximately equal to that of Gd DTPA.

Gd HP-DO3A offers four advantages over Gd DTPA for the study of intracranial neoplastic disease. This new agent is non-ionic, inert to chemical substitution by copper or zinc ions, does not cause biochemical abnormalities (in our limited experience), and can be administered at dosages up to 0.3 mmol/kg (three times the FDA approved dose for Gd DTPA).

► **178** 16:57PM

PHASE II CLINICAL TRIAL OF GD HP-DO3A: IMPROVED SAFETY PROFILE AND IMAGING POTENTIAL

FJ Carolan, GG Heard, MI Pacetti, DY Gelblum, SM Wolpert, VM Runge
Division of MRI, Tufts/New England Medical Center

The biochemical changes and enhancement characteristics associated with Gd DTPA (Berlex Laboratories, NJ) and Gd HP-DO3A (SQ32,692 Squibb Diagnostics, NJ) were compared using data from Phase II clinical trials.

Twelve patients (age: range 20-71, mean 49 years) with known intracranial pathology were given Gd HP-DO3A at dosages from 0.05 to 0.3 mmol/kg. Results were compared with 30 patients (age: range 24-86, mean 51 years) receiving 0.1 mmol/kg Gd DTPA in a previous Phase II investigation. 12-lead EKG, CBC, SMA-20, PT/PTT, serum iron and urinalysis were analyzed immediately prior to, and at 2, 4, 8, 24, and 48 hours following administration of the contrast agents.

11 of 28 and 9 of 30 patients demonstrated an abnormally high serum iron and total bilirubin, respectively, within 48 hours after administration of Gd DTPA, with a mean rise in serum iron of 610% and total bilirubin of 95% for all patients studied. No significant changes in serum iron, total bilirubin or other laboratory parameters were observed after administration of Gd HP-DO3A. No apparent clinical side effects were observed with either agent. Enhancement of brain lesions was comparable at equimolar doses for both agents.

The lack of biochemical changes with Gd HP-DO3A, a non-ionic agent, despite administration of up to 0.3 mmol/kg, implies greater tolerance than that for Gd DTPA at 0.1 mmol/kg. Dosages up to 0.3 mmol/kg can safely be administered, allowing potentially increased diagnostic application, particularly outside the brain. Specific potential applications for increased dosages of Gd HP-DO3A include the diagnosis of hepatic metastases and evaluation of myocardial ischemia.

► **179** 17:09PM

BRAIN METASTASES: T2-WEIGHTED VS GD-DTPA ENHANCED MR IMAGING

N Hosten, W Schörner, P Schubeus, R Felix
Dpt. Radiology, UKRV/Charlottenburg, FU Berlin

Differentiation of metastatic and vascular lesions by plain and contrast enhanced MRI was studied.
Retrospectively, MR images of 30 patients with cerebral metastases proven by histology or repeated exams were analyzed. T2-WI (SE, TR 1600 ms, TE 70 msec) and GD-DTPA enhanced T1-WI (GE, TR 315 ms, TE 14 msec) were available in all patients. All studies were performed on a 0.5 T Magnetom.
Lesions seen on T2-WI were divided into small and large (< or > than 1 cm) and structured and unstructured. Percentage of contrast enhancement in these four groups was then determined.
Plain T2-WI and Gd-DTPA enhanced images identified a total of 194 and 265 lesions resp. T2-WI missed lesions that were located at grey/white matter border, were hidden in edema of larger lesions or close to bone. Small, unstructured white matter lesions were found in 9 patients. 29/87 lesions, which are generally considered vascular showed marked enhancement and were classified metastatic. 53/55 large, unstructured and all 37 structured lesions did enhance. On T2-WI size and detection of a structured nature, representing edema, tumor and possible necrosis thus thus appear to be the most important sign of a malignant genesis.
We conclude that application of GD-DTPA encreases both sensitivity and specificity of MR imaging when cerebral metastases are suspected. Especially small, unstructured white matter lesions were demonstated to be metastatic in 30% of all lesions by breakdown of blood brain barrier.

IMAGING I: FAST

MODERATORS: F. W. WEHRLI, Ph.D., J. L. DUERK, Ph.D.

► **201** 10:30AM

CARDIAC STUDIES USING SUBSECOND FLASH MRI

D Chien, KD Merboldt, H Bruhn, ML Gyngell, W Hänicke, J Frahm.
Max-Planck-Institut für biophysikalische Chemie, Göttingen, FRG

In applying the FLASH sequence with very short repetition times (4-5 ms) and echo times (2-3 ms), images of the beating heart have been obtained within a single cardiac cycle without averaging. A data matrix of 64 x 128 pixels yields measuring times of about 300 ms that approach echo planar imaging, but with a conventional gradient system. Using a 2.0-T Siemens Magnetom this technique produces images which show distinct phases of the cardiac cycle without motion artifacts. Cardiac triggering allows the acquisition to be freely positioned within the cardiac cycle, and enables a cine display of heart functions from diastole and systole using images from different heartbeats. Since no averaging is required, this technique allows imaging of patients with cardiac arrhythmia. For a clear assessment of myocardial wall thickening and heart valve movement, two slice selective pre-saturation pulses are applied before the image acquisition to null out the blood signal. This results in excellent delineation of myocardial structures. In addition, oblique, single scans of the heart allow comparative studies of myocardial wall functions between individuals, particularly along the long axis and short axis of the left ventricle. This may significantly enhance functional studies of the human heart.

TUESDAY a.m.

► **202** 10:42AM

RAPID SPIN ECHO (RASE) IMAGING OF THE ABDOMEN & PELVIS: QUALITATIVE COMPARISON WITH MULTIACQUISITION SPIN ECHO SEQUENCES

SA Mirowitz, JKT Lee, JJ Brown, JP Heiken, SS Eilenberg
Magnetic Resonance Imaging, Mallinckrodt Institute of Radiology

A new method (RASE), in which a series of 11 images is obtained during a single suspended respiration was compared subjectively by three experienced MR readers to standard multiacquisition T1-weighted spin echo sequences. A total of 84 examinations in 18 patients were evaluated blindly in terms of severity of artifacts in phase-encoding direction, edge sharpness and overall image quality. Phase encoding artifacts were judged to be absent or mild in 92% of RASE examinations vs 35% of standard spin echo. Edges were sharp or only mildly blurred in 91% of RASE examinations vs 49% of standard spin echo. Overall image quality was excellent to good in 85% of RASE vs 45% of standard spin echo. These results indicate that, in addition to a marked reduction in imaging time, the RASE technique allows for considerable improvement in image quality.

► **203** 10:54AM

ECHO-VOLUMAR IMAGING

[1]M. K. Stehling, R. J. Ordidge and P. Mansfield

Department of Physics, University of Nottingham, NG7 2RD, England, UK; [1]present address: USZ, Dep. Med. Radiologie, Zürich, Switzerland.

To sample the 3D k-space representation of a 3D object in a single continuous trajectory, two orthogonal rapidly repolarised magnetic gradient fields (MGF) are required. The third MGF can be of constant sign. An oscillating ky-subspace trajectory can be formed by driving our whole-body double-actively shielded transverse gradient coils (100 μH inductance) with a 4 kHz rectangular waveform (≤300 V, ≤800 A, slew rate ≤0.1 mT/mμs) to yield trapizoidal oscillating MGFs. In 64 ms, 256 y-gradient-echos can be formed from a single FID, positive and negative gradient echos representing a line of corresponding sign in ky-subspace. A constant phase encoding gradient spaces the ky-subspace trajectory out into a zig-zag shaped kx-ky-plane. Modulation of the y-gradient echo train by a 250 Hz oscillating x-MGF corresponds to a folding of the kx-ky-plane in the shape of a concertina and yields 16 kz-planes. With a sampling frequency of 128 kHz (≡ frequency bandwith) this yields a three-dimensional 16 * 16 * 32 pixel matrix after modulus Fourier transformation. Thus, theoretically, a 3D image can be generated from a single FID in 64 msec. However, the alternating directionality of alternate kz-planes (formed as positive or negative x-gradient echoes, respectively), in the presence of T2-decay of the FID, necessitatess the acquisition of two data sets with opposite x-gradient starting phases. Splicing of these data sets yields two new data sets containing kz-planes of positive or negative directionality only.

We have obtained two-shot 64 ms modulus Echo-Volumar (EVI) images of phantoms and the complete human head (from vertex to spinal cord). The resolution on the 16^3 pixel head images is approximately 1 cm^3 and clear discrimination of cortex, basal ganglia, ventricles and cerebellum is obtained. 32 x 16 x 16 pixel EVI images of the complete thorax provide coarse delineation of mediastinal structures, lung fields and thoracic wall.

We present the first two-shot (modulus) EVI images based on 16^3 and 32 x 16 x 16 matrices to demonstrate the feasibility of near-instantaneous three-dimensional image acquisition and discuss necessary improvements in gradient driver and coil technology required for improved EVI image quality. The potential of this new technique is illustrated with the first EVI images of biological samples.

► **204** 11:06AM

RATIONALE FOR USING CONTRAST-ENHANCED FAST MRI

D. Le Bihan, P.Choyke, J. Frank, R. Turner
Diagn. Radiology Dept. and Biomed. Eng. Instr. Branch, NIH, Bethesda, MD 20892.

Paramagnetic compounds are now widely used for contrast-enhanced MRI. The dependence of signal and contrast in contrast-enhanced MR images upon acquisition parameters and paramagnetic compound concentrations for the conventional spin-echo based sequences has been well studied and characterized. However, such contrast prediction is far more complicated when using fast imaging sequences (FLASH, FISP, GRASS...) based on Steady-State Free Precession (SSFP) schemes. The use of low flip angles results in more complex effects on T1 and T2. Refocussing from gradient echoes makes SSFP sequences very sensitive to susceptibility effects. On the other hand, the feasibility of real-time studies of kidney and brain perfusion with Steady-State Free Precession (SSFP) using paramagnetic compounds such as Gd-DTPA or Dy-DTPA has recently been shown. The purpose of this study was to design a simulation tool in order to optimize acquisition parameters. We present software developed on a personal computer which simulates contrast and/or signal map for several types of contrast-enhanced SSFP sequences. The program generates a high-resolution three-dimensional color display of contrast and/or signal intensity versus user-chosen biologic (T1, T2), physical (relaxivity, susceptibility) or pulse (TR,TE,flip angle) parameters. This program was tested using a phantom made of a series of polyacrylamide gels doped with various concentrations of paramagnetic compounds. The agreement between the experimental data and the theoretical predictions given by the simulation was excellent. The program was then used to optimize sequence design and pulse parameters in order to enhance separately relaxivity effects and susceptibility effects. The results were applied in studies involving animals and patients. Examples of applications include optimization of SSFP sequences for dynamic renal function studies, detection of blood brain barrier disruption due to brain tumors and evaluation of cerebral perfusion for function mapping.

► **205** 11:18AM

Contrast Capabilities and Artifact Assessment of the RARE Sequence

R.V. Mulkern, S.T.S. Wong, C.S. Winalski, F.A. Jolesz
Brigham and Women's Hospital, Boston, MA 02115

Methods for decreasing overall patient scan times in MRI include the use of gradient recalled (GR) echo techniques (EPI, FLASH, GRASS, etc). A decrease in available tissue contrast is often accepted when fast GR methods are compared to standard spin echo sequences. An alternative to fast GR techniques involves individually phase encoding a large number of RF refocussed echoes within a single echo train (Hennig et al, Magn. Reson. Med. 3:823;1986). The technique has been termed the RARE sequence (Rapid Acquisition Relaxation Enhanced) and has been used to generate images with tissue contrast similar to that of long TE, long TR, spin-echo sequences in a matter of seconds. We have explored the contrast capabilities available from a 128 echo, 10 ms echo separation, version of the RARE sequence. Studies were performed at 1.5T with in vivo human brain and knee images and rabbit brain images. The effective TE was altered by a) relocating the zero-phase encode echo in a linear phase array and b) reshuffling the collection of phase encodes between positive and negative values for odd and even echoes. Significant T_2 contrast and s/n manipulation were obtained with both methods. The ability to incorporate T_1 contrast into the RARE sequence was tested by a) reducing the TR to its minimum value of 1500 ms in a four signal average data collection scheme (total image time = 6 s) and b) placing a 180° inversion pulse prior to the RARE sequence to "null" out selected tissues. The latter method proved most effective for producing significant T_1 contrast, including CSF nulling. We demonstrate that the T_2 dependent blurring artifact in the phase encode direction may be redirected to the slice encode direction in 3d-FT RARE sequences, thereby removing the artifact from individual "slices". We conclude that the RARE sequence has the potential to decrease patient scan time while maintaining many of the contrast capabilities associated with standard spin-echo methods.

TUESDAY a.m.

► **206** 11:30AM

T1 IMAGES DERIVED FROM RAPIDLY ACQUIRED GRADIENT-ECHO DATA

SA Bobman, FW Wehrli, DM Yousem
Department of Radiology, Hospital of the University of Pennsylvania, Philadelphia, Pennsylvania

Several methods are commonly employed for source data acquisition for computation of T1 images. Typically, the pulse sequences of the acquisition utilize multiple repetition or inversion times to exploit differences in longitudinal recovery. Since both short and long interpulse times must be obtained, the total scan time is relatively lengthy. The purpose of this work is to determine if difference in flip angles rather than interpulse times can be used to accurately derive calculated images of T1 in a relatively short time.

Limited flip-angle imaging is typically implemented with gradient-recalled echoes to prevent the inversion of the longitudinal magnetization that would occur with a 180-degree RF pulse. Short repetition times allow the development of steady state free precession, especially for large flip angles. This causes an increased signal in stationary spins having long T2 values, which complicates the mathematical determination of T1. However, by using a pulse sequence which dephases (i.e. "spoils") the residual transverse magnetization, it is simpler to linearize the equation describing signal behavior; the magnitude of T1 becomes a function only of the signals and flip angles.

Accordingly, an interleaved multi-planar version of gradient-echo imaging was chosen to acquire the source images, as it was expected that the various imaging gradients from adjacent slices would dephase the residual transverse magnetization. Additionally, an RF-spoiled, volume-acquired implementation of gradient-echo imaging was also used. Several separate data acquisitions were performed with identical TR (500 msec.) and TE (5 msec.), but with varying angles of nutation. For each slice, images acquired with relatively small flip angles were individually paired with those of a 90-degree flip angle to produce T1 images; by using only two source images per slice, no linear regression need be performed, so each image can be computed in approximately one second on a Sun-4 workstation.

Phantom and clinical results will be presented. Both the noise levels and accuracy of the observed T1 values appear dependent on the choice of the smaller flip angle. The T1 estimates appear shorter than those predicted by methods employing conventional pulse sequences, such as spin echo. Nonetheless, calculated T1 images with low noise can be derived, despite the relatively short acquisition time. Sources of error will be discussed.

► **207** 11:42AM

MEMMoRI: MULTI-ECHO, MUTLI-MOMENT REFOCUSSED IMAGING
JL Duerk, OP Simonetti, GC Hurst
MetroHealth Medical Center & Case Western Reserve University, Cleveland, OH

The design of gradient waveforms used for motion compensation involves determining functions which meet imaging conditions, and also have zero valued time moments (sensitivity to derivatives of position) by the echo time. This work describes a theoretical basis for simplified design of Multi-Echo, Multi-Moment Refocussed Imaging (MEMMoRI) gradient waveforms.

Expansion of the gradient moment integral for a time shifted waveform shows that refocussed moments are independent of the time origin. For multi-echo sequences with $TE_n = TE_1 + (n-1)*(TE_2-TE_1)$, n = 2 to N, the TE_n images can be obtained from repeated waveform units as shown in the figure below. All echo images will have identical nulled moments if the repeated gradient waveform unit has zero valued moments. Further, non-refocussed moments can be shown to be a weighted sum of all equal and lower moments of an unshifted gradient waveform starting at the origin. Examples in liver imaging confirm the predicted insensitivity to motion in all echoes in comparsion to identical non-refocussed multi-echo sequences.

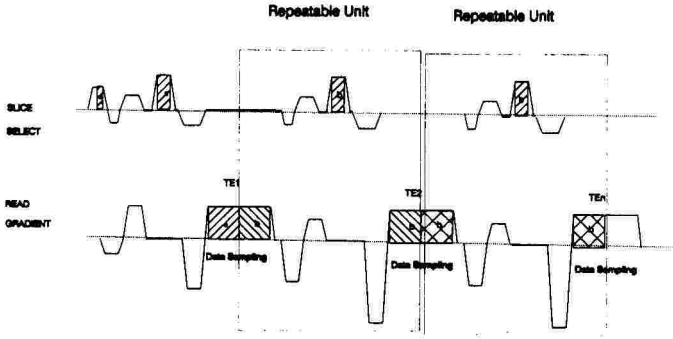

TE1 and TE2 are the first and second echo times, n is any echo number, and N refers to the total number of echoes.

► **208** 11:54AM

"SNAPSHOT - FLASH" IMAGING OF THE LIVER
EE de Lange, JP Mugler III, SB Gay, CL Janus, JR Brookeman
Dept. of Radiology, University of Virginia Medical Center, Charlottesville, Virginia

Since respiration artifacts are a significant problem in MR Imaging of the upper abdomen using common spin-echo (SE) techniques, there exists a need for an appropriate method with which high quality MR Images can be obtained during breath holding. The recently introduced "snapshot-FLASH" technique enables T_1- or T_2-weighted images to be obtained in less than one second (1).

We have implemented this technique on our standard 1.5 Tesla whole body MR Imager (Magnetom 63SP, Siemens Medical Systems Iselin, NJ) to evaluate patients with liver lesions. Images are obtained with a repetition time (TR) of 5-6 milliseconds and echo time (TE) of 3.3 milliseconds. Employing a 128 x 128 data matrix, images are acquired in 650 - 750 milliseconds, with a minimum field-of-view of 260 mm. Inversion or driven equilibrium preparation pulses were used to generate T_1 or T_2 contrast, respectively (2).

In a preliminary study of normal volunteers, we found that using inversion preparation pulses provide excellent T_1 contrast between liver and spleen comparable to the standard short TR/TE SE sequences at low field strength. This potentially enables the snapshot-FLASH technique to be a highly suitable sequence for liver screening without image degradation from respiratory artifacts.

We have evaluated patients with liver pathology such as metastases and hemangiomas employing the snapshot-FLASH sequences. Standard SE T_1- and T_2-weighted sequences were obtained for comparison. In addition, we have explored the potential role of other preparation pulses to provide T_2 contrast for characterization of liver lesions.

1. Haase A, Matthaei D, Norris D, Leibfritz D, 8th SMRM, 1989; 364.
2. Kiefer B, Deimling M, Finelli D, 8th SMRM, 1989; 367.

MRA I

MODERATORS: P. J. KELLER, Ph.D., D. G. NISHIMURA, Ph.D.

► **209** 10:30AM

A NEW APPROACH TO 2D INFLOW-REFRESHMENT ANGIOGRAPHY

T Matsuda, M Doyle, GM Pohost
Cardiovascular NMR Laboratory, University of Alabama at Birmingham

INTRODUCTION Described is a new 2D inflow-refreshment angiographic sequence (STREAM, Suppressed Tissue with REfreshment Angiographic Method). It maintains angiographic clarity, while yielding reduced artifacts related to motion and pulsation.
SAMPLING STRATEGY In conventional 2D inflow-refreshment angiography each slice is fully sampled before advancing to the next. For STREAM the sampling strategy is altered to that of conventional multi slice imaging: i.e. for each phase encoding step *all slices* are sampled. In this situation the TR is substantially prolonged which results in loss of *intrinsic* static suppression. Thus an *active* suppression strategy has been adopted.
ACTIVE STATIC SUPPRESSION To suppress static tissue, we introduced a wide presaturation slab, typically ten times the slice thickness, positioned just ahead of the selected slice. Upon each application of the sequence, the slab presaturates a number of slices distal to the selected slice. As the slab advances, static tissue ahead of the selected slice receives multiple presaturation pulses. Four or five such pulses are sufficient to established a low steady state signal from static tissue which is maintained for all subsequent slices.
ADVANTAGES OF STREAM 1) The sampling strategy results in virtual elimination of significant artifact. 2) Static suppression and slice excitation are performed by separate RF pulses, thus the flip angle for each can be separately optimized.
EXPERIMENTAL METHOD STREAM was used to obtain angiograms of the abdominal aorta in three normal volunteers using a Philips Gyroscan (1.5T), TR 3 sec for 64 slices, TE 16 msec, slice thickness 2.5 mm, matrix 128^2, total acquisition time less than 7 min.
RESULTS No dominant artifacts due to internal motion or blood pulsation are seen in angiograms obtained with STREAM. The overall flow/static contrast is comparable to that of conventional 2D inflow angiograms.
CONCLUSIONS STREAM allows acquisition of high quality angiograms, accompanied by significant artifact reduction without extending the acquisition time. Additionally, static signal suppression is dissociated from slice excitation and does not rely on a short TR. Removal of the short TR constraint allows ECG triggering to be incorporated.

TUESDAY a.m.

► **210** 10:42AM

REALTIME MR PROJECTION ANGIOGRAPHY

DG Brown, RC Wright, SJ Riederer, CR Jack, RL Ehman
MR Lab, Mayo Clinic, Rochester, MN 55902 USA

Current MR Angiography methods require lengthy data acquisition, reconstruction, reformatting, and projection times. The method presented here provides substantial reduction of data acquisition time, and total elimination of reconstruction and image processing delays. We use a set of contiguous 2DFT GRASS images, TR/TE/flip angle of 51/16/45 degrees, with the phase and frequency axes placed so that the desired projection is formed along the phase encoding (PE) direction. Resolution in the projection image is principally determined by the frequency encoding resolution in the axial images. The PE resolution, and hence the scan time, can thus be reduced with negligible effect on the projection image. If the PE resolution is reduced too far, however, signal averaging within the pixel causes a loss of contrast in the maximum pixel projection. When the carotid bifurcation is imaged with a 16 cm field of view, a comparison between 256 and 32 PE's per image shows negligible loss of contrast in the projection image, but a considerable loss is seen when only 24 PE's per image are used. Measuring only 32 views per image instead of 256 can provide an eight-fold savings in scan time with little effect on the projection image. The placement of the phase axis obviates the need for image reformatting and eases the task of projection. With our realtime reconstruction hardware we reconstruct each slice and project it into one line of the final angiogram in less than 400 msec. These steps are performed during data acquisition for the following slice, effectively eliminating all image processing time.

► **211** 10:54AM

ABDOMINAL MR ANGIOGRAPHY: ADAPTIVE CORRECTION OF RESPIRATORY MOTION USING NAVIGATOR ECHOES

JP Felmlee, RL Ehman, HW Korin, SJ Riederer, D Brown
MR Laboratory, Mayo Clinic and Foundation, Rochester, MN, 55905

Time of flight MR angiography of the upper abdomen is currently limited by the problem of respiratory motion. The most successful technique to date has utilized multiple breath-hold acquisitions of single slice gradient echo images, with subsequent ray-tracing reprojection of the image data set to yield a projection angiogram. The multiple breath-holds of 10 to 15 sec required for this procedure are tiring and in some cases impossible for sick patients. Furthermore, inconsistencies in respiratory inflation often lead to misregistrations in the data set, causing degraded angiograms. To date, 3DFT and nonbreath-hold multiplanar time-of-flight methods have not been feasible due to the problem of respiratory motion.

The objective of this study was to apply adaptive techniques using interleaved "navigator" echoes to correct (1) breath-hold MR angiography acquisitions that are degraded by inconsistent inflation and (2) 3DFT and multiplanar time-of-flight MR angiographic acquisitions of the upper abdomen that are degraded by respiratory motion.

We incorporated an additional echo into the three MR angiography sequences listed in the previous paragraph. In all cases, this navigator echo was derived from a sagittal slice intersecting the right hemidiaphragm, whereas the image echo was from a coronal plane or from a volume slab in the case of the 3DFT sequence. The navigator echo was not phase encoded, except in the case of the breath-hold sequence.

In each case, the navigator echo data were processed to extract the craniocaudal position of the diaphragm at each time in the acquisition. These data were used to adaptively correct the image data for craniocaudal displacements prior to ray tracing, in a manner previously described [1].

The results indicate that in volunteer and patient studies, breath-hold data sets that are degraded by inconsistent inflation can be corrected to yield angiograms that are markedly improved compared with uncorrected images. In some cases, the extent of misregistration artifact in the original images was not appreciated until the corrected images were generated. Application of the adaptive correction technique to nonbreath-hold 3DFT and multiplanar 2D angiographic acquisitions yielded promising results, with visualization of vascular structures that are completely invisible due to respiratory motion in the uncorrected angiograms.

[1] Ehman RL, Felmlee JP. Radiology 173:255;1989.

► **212** 11:06AM

MR ANGIOGRAPHY IN PELVIC AND ABDOMINAL VENOUS OCCLUSION.

Y Yuasa, M Endo, A Tanimoto, S Momoshima, H Shiga, K Hiramatsu, CL Dumoulin*, S Souza*
Keio University, Tokyo, Japan, GE Research & Development Center, Schenectady*

<METHODS AND MATERIALS> All MR studies were performed on a SIGNA system (General Electric, 1.5 Tesla). 2D phase contrast and 2D time-of-flight technique were used for MR angiography (MRA) evaluation. In 2D time-of-flight MRA, 36 to 120 axial 5mm thick contiguous slices with TR/TE 22/13msec, 30 degrees flip angle were made, followed by reformation by maximum intensity profile. Conventional venography was also performed before or after MRA, and was compared with MRA. MRA was performed in 16 cases (deep vein thrombosis, 12 cases; postoperative follow-up, 2 cases; liver tumor, 2 cases).

<RESULTS> Normal venous structures were clearly demonstrated by both phase contrast and time-of-flight techniques, and occlusive venous lesions were easily identified. Collateral venous channels were also detected.

<DISCUSSION> Phase contrast and time-of-flight are the two major well established MRA techniques. In the detection of abdominal and pelvic venous occlusive diseases, both techniques proved to be effective. The phase contrast method is easier to use (breath-holding is unnecessary, and additional image processing is not required). The time-of-flight technique is more useful to analyze vascular structures three-dimensionally. One of the major disadvantage of 2D phase contrast MRA was overlapping of the arteries and veins. Multi-view-angle acquisition of phase contrast MRA might be helpful, but this requires a much longer acquisition time. In 2D time-of-flight MRA, repeated breath-holding was a major problem since the level of breath-holding should be constant throughout the study. Another problem of this method was limited anisotropic spatial resolution of the reformatted images, and thinner slice should be used to get better resolution. In conclusion, both techniques are useful and complementary in their roles in diagnosis of vascular pathology in the abdomen and pelvic cavity.

► **213** 11:18AM

Optimization of Imaging Parameters in Fast LFA Angiography

TA Tasciyan, SJ Riederer*, RJ Herfkens**

Thomas Jefferson University Hospital, Mayo Clinic*, Cedar-Sinai Medical Center**

Various MR angiographic techniques exist that delineate vessels either through the use of flow-induced phase shifts or utilizing signal variations resulting from the influx or efflux of tagged spins. The technique we have worked on, Fast LFA Angiography, delineates the blood vessel using the phase induced signal differences from flowing blood during systole and diastole. With this technique, we consistently observed that for a given subject the quality of the angiographic image could degrade considerably when the TR or the flip angle was changed, all other parameters kept constant. This change could be as small as 10 ms in ΔTR or 10^0 in Δflip angle. It was also observed that the optimal TR and flip angle changed with the artery. So, we simulated the Bloch equations for moving spins to gain insight into the effects of repetition time and flip angle, to possibly optimize these imaging parameters. The initial simulations were carried out for the pulsatile flow patterns encountered in the common carotid and the popliteal arteries, for TR's of 22, 33, and 55 ms and flip angles of 15^0, 30^0, and 45^0.

Several differences were observed in the simulated magnetization patterns of the popliteal and carotid arteries. Specifically, the simulation results revealed that the signal in the popliteal artery was determined by spins that had already reached steady-state; whereas the signal in the carotid was mainly determined by the magnetization of incoming fresh spins. The simulations further suggested that among the repetition time and flip angle cases studied, the best choice for the popliteal would be a TR of 33 ms, a flip angle of 15^0; the best imaging strategy for the carotid would not include the 15^0 flip angle. The angiographic images confirmed the simulation results. However, based on these results a general guideline can not be provided for all angiographic techniques. In fact, the simulations suggest that the optimal parameters not only depend on the pulsatile flow pattern displayed within the artery, but also depend on the particular technique used.

TUESDAY a.m.

► **214** 11:30AM

MR ANGIOGRAPHY: EXPERIENCE WITH 116 STUDIES

PM Colletti, MR Terk, C-S Zee, GP Teitelbaum, H Kim, PW Ralls, WD Boswell, H Simon

USC School of Medicine, Department of Radiology

We describe our experience using MR angiography in 94 patients and 22 normal volunteers.

Inflow MR angiography using a 2D field echo TR 36-50, TE 13-18, TIP angle 45-90° with selective presaturation and 3D reformatting was performed on 20 volunteers (2 brain, 13 carotid, 4 extremities, 3 abdomen) and 86 patients (36 brain, 19 carotid, 13 extremity, 24 abdomen).

Normal and abnormal vessels are demonstrated including cerebral aneurysm, AVM, and tumor; carotid stenosis and arteritis, renal artery stenosis, IVC tumor, extremity tumor and trauma.

Inflow MR angiography may demonstrate vascular lesions in the head, neck, body, and extremities.

MR pelvic venogram compressed view and anterior view left iliac vein occluded by tumor

► **215** 11:42AM

MR Angiography in the portal system: early clinical results.

Finn JP (1), Edelman RR (2), Kane R (1), Longmaid HE (1), Dunwoody W (1), Jenkins R (1), Mattle H (1,2).
New England Deaconess Hospital, Boston MA 02215(1), Beth Israel Hospital, Boston MA 02215(2).

Introduction. Abnormalities of the portal venous system may complicate a wide variety of liver diseases, and detection of such abnormalities may fundamentally influence treatment and prognosis . Current non-invasive techniques for imaging the portal system have drawbacks; ultrasound (US) is limited by patient habitus and spin-echo MR imaging is complicated by motion artifacts and the unpredictable effects of flow on the image. These problems can be overcome by acquiring single-slice, flow-compensated gradient-echo images during breath-holding and post-processing these to form projection angiograms (1). Graphic information on flow direction and velocity can be derived by presaturation bolus tracking (2).
Methods. We have applied projection MR angiography in 11 patients with liver disease and suspected portal hypertension. Single-slice gradient-echo images were acquired in multiple planes with repetition time/flip angle/echo time = 30ms/30deg/10ms. Presaturation bolus tracking of the portal system was applied in 8 patients. Post-processing was performed using a maximum intensity projection technic. The MR studies were performed on a 1.5T (3 patients) or 1T (8 patients) imaging system (Siemens Medical Systems, Erlangen, FRG). Correlative imaging with US, CT or contrast angiography was available in all patients.
Results. When compared to US, MR angiography provided additional clinical information on portal status in 6 patients with liver disease. Unsuspected spleno-renal shunts were shown in 2, unsuspected reversal of flow in the main portal vein in 1, and additional collateral vessels in 3 patients. Normal portal flow was shown in 1 patient, decreased flow in 2, absent flow in 2, and reversed flow in 2. Branch occlusion of the left portal vein with normal flow velocity in the right portal vein was shown in 1 patient . In all patients studied, the MR angiography findings were corroborated by US, CT, contrast angiography or surgery.
Conclusion. MR angiography offers clear advantages over other modalities for imaging the anatomy of the portal venous system and collateral vessels, and for the study of flow abnormalities. MR has the potential to be the method of choice for the study of the portal venous system in patients with portal hypertension.
References. 1. Edelman RR et al. AJR 1989; 153, 755-760.
2. Edelman RR et al. Radiology 1989; 171, 551-556.

► **216** 11:54AM

ECG TRIGGERED INFLOW-REFRESHMENT ANGIOGRAPHY

M Doyle, T Matsuda, GM Pohost
Cardiovascular NMR Laboratory, University of Alabama at Birmingham

INTRODUCTION We have developed a new approach to 2D inflow-refreshment angiography (STREAM, Suppressed Tissue with REfreshment Angiographic Method) which allows ECG triggering. Previously, conventional inflow techniques could not be triggered due to their short TR dependance. A number of triggering strategies are presented, none of which substantially increase acquisition time. All results were obtained on a Philips Gyroscan (1.5T, 1m bore).
STREAM SEQUENCE A set of planes are sampled in a manner analogous to conventional multi slice imaging, i.e. rather than separately sampling each slice, *each K-space line* is sampled for the *set of slices*. For a set of 64 slices, sampling of one K-space line requires about three seconds. Thus approximately three cardiac cycles are spanned for each acquisition series. Static tissue suppression is achieved by application of a separate RF pulse. The typical acquisition time is 7 minutes, however angiograms have been acquired within 2 minutes by employing a phase encoding reduction scheme.
CONVENTIONAL ECG TRIGGERING The combination of the STREAM acquisition strategy and ECG triggering results in individual slices being acquired at one phase of the cardiac cycle. However, the complete set of slices are distributed over three cardiac cycles. Thus the projection of the set of slices results in angiograms depicting the pulsatile blood flow pattern. This is manifested, as one looks along the vessels, as cyclic increases and decreases in signal intensity, resulting in the appearance (in this three cycle acquisition time) of three bright regions, each representing systole.
CINE ANGIOGRAPHY It is possible to obtain cine angiograms by multiple application of conventionally triggered STREAM with suitable trigger delays. This could become clinically feasible when combined with reduced phase encoding. Developments may allow STREAM to acquire line scan projections, thus permitting ultra fast cine angiography.
PROGRESSIVE TRIGGERING To generate an angiogram with uniform vessel intensity the triggering position was gradually stepped through the cardiac cycle for successive sampling sets. When the trigger position reached the end of the cycle it was reset and repeated the sweep. We have found that 8 sweeps through the cardiac cycle produces uniform vessel intensity in angiograms.
CONCLUSIONS STREAM allows ECG triggering without substantially increasing the acquisition time. It can be used to perform cine angiography, demonstrating the pulsatile nature of arterial flow. Alternatively, triggering can be employed to ensure uniform intensity of blood vessels. Further development should allow rapid acquisition of cine angiograms.

COMBINED CORRELATIVE IMAGING

MODERATORS: D. N. LEVIN, M.D., Ph.D., J. C. WEINREB, M.D.

► 217 10:30AM

ROC ANALYSIS OF HIGH-FIELD MR IMAGING VERSUS CT FOR THE DETECTION OF FOCAL HEPATIC LESIONS

E Rummeny, K Wernecke, G Bongartz, S Saini[1], W Wiesmann, J Fervers, PE Peters

Departments of Radiology, University of Muenster, D-4400 Muenster (FRG) and Massachusetts General Hospital[1], Boston, MA 02114

To compare the diagnostic performance of high field MR imaging and computed tomography (CT) in the detection of focal hepatic lesions we studied the receiver operating characteristics (ROCs) of MR images, unenhanced CT images and enhanced CT images.

The sample included a total of 900 images: 450 whithout disease and 450 with disease. Images were obtained from 31 patients with proven primary cancer (11 colorectal, 10 gastric, 4 pancreatic, 4 esophageal carcinoma, 2 carcinoid tumors). All patients underwent laparotomy. The presence or absence of lesions was based upon intraoperative sonography and intraoperative or pathological findings. MR-images were obtained at 1.5 T (Magnetom, Siemens). T1-weighted (T1W) images were acquired as presaturated spin echo images (SE 800/15/4) and as breatholding Flash 60 images (FL 100/6/60°). T2-weighted (T2W) images were obtained with presaturated SE SE 800/70/4 and 2000/70/2 pulse sequences. CT images were obtained before, during and 4 to 5 hours after bolus injection of 60 g of iodine using a 3rd generation CT scanner.

All five radiologists achieved significantly ($p<.05$) better results with the SE 2000/70 and FL 100/6/60° sequences as compared to the T1W SE 800/15/4 images and unenhanced CT images. Comparisons among MR pulse sequences and enhanced CT images showed a significant ($p<.05$) superiority of the SE 2000/70 over the bolus enhanced CT images. Mean A_z (area under the curve) was .96±.006 for the SE 2000/70, 0.92±.02 for the FL 60 and .91±.05 for the bolus enhanced CT images .91±.05.

We conclude that T2W SE 2000/70 images obtained at 1.5 T are significantly superior to T1W SE 800/15 MR images and bolus enhanced CT images for the detection of hepatic metastases. Furthermore this analysis indicates that T1W FL 60 MR images and contrast enhanced CT images offer comparable performance for this purpose.

► 218 10:42AM

HM-PAO SPECT AND GD-DTPA ENHANCED MR IN CNS-MANIFESTATIONS OF AIDS

H Henkes, M Cordes, J Hunger, R Jochens, T Heim, R Felix

Dep. of Radiology, University Clinic Rudolf Virchow/Charlottenburg; Freie Universitat Berlin

Purpose: Although CT and MR imaging have demonstrated a high sensitivity in detecting brain lesions, determination of the etiology causing the lesion is still poor. However, specificity is crucial for prognosis and therapy in patients with acquired immunodeficiency syndrome, suffering from various opportunistic CNS infections as well as tumorous lesions of the brain. Lesions with multiple etiologic factors that occur simultaneously in the same patient further complicate diagnostic and therapeutic decisions. The aim of the present study was to determine the diagnostic value of HM-PAO SPECT in patients with intracranial AIDS manifestations, which had been confirmed by MR. In addition, the incidence, the localization as well as the degree of altered brain perfusion in AIDS-patients with clinical symptoms of CNS disease and a normal MR examination were investigated.

Materials & Methods: Twenty male patients (age median; 38 years) with proved HIV-1 infection, CDC IV, were examined. Clinical and/or histologic diagnoses were toxoplasmosis (10x), lymphoma (3x), meningitis (2x), and HIV-encephalitis (5x). SPECT examinations were performed using a rotating gamma camera after i.v. application of 555 MBq99mTc-HM-PAO. Axial, coronal and sagittal slices were generated. MR studies (0.5 T Magnetom) were performed using T2-weighted images (SE 1600/30,70) and unenhanced as well as Gd-DTPA enhanced T1-weighted sequences (FLASH 315/14, $\alpha=90°$).

Results: MR imaging demonstrated 38 lesions in 10 patients with cerebral toxoplasmosis. SPECT detected focally altered brain perfusion in all patients. Twenty-eight of the 38 toxoplasmotic lesions showed hypoperfusion, 10 lesions were hyperperfused, 3 patients of this group had multiple perfusion deficits. In one patient with cerebral lymphoma, the lesion was hyperperfused, in the others they showed hypoperfusion. In one patient with meningitis - as demonstrated by MR - perfusion was reduced in adjacent brain tissue. One patient with meningeal tuberculosis showed focal hyperfusion. In 3 patients with HIV-encephalitis and normal MR, SPECT dectected multiple perfusion deficits.

Conclusion: The sensitivity of SPECT in detecting focal lesions is inferior to MR. At present, SPECT does not provide differentiation between toxoplasmosis and lymphoma. However, SPECT demonstrates altered brain perfusion in areas larger than the corresponding focal lesion detected by MR imaging. SPECT appears thus potentially useful in AIDS-patients with symptomatic brain disease and a normal MR who may have altered brain perfusion. HM-PAO SPECT is a helpful diagnostic method complementary to CT and MR imaging in patients with AIDS-related brain disease.

TUESDAY a.m.

► **219** 10:54AM

INTRACRANIAL MENINGIOMAS: HOW FREQUENT ARE CHARACTERISTIC FINDINGS IN MRI AND CT ?

P Schubeus, W Schörner, C Rottacker, B Sander, R Felix

Department of Radiology, UKRV Charlottenburg, FU Berlin, West Germany

MRI has been regarded to be inferior to CT in the diagnosis of intracranial meningiomas by some investigators. In order to asses the value of MRI in this question plain and enhanced MRI and CT examinations were reviewed with respect to the frequency of characteristic findings in both imaging techniques.

All 43 cases were examined prior to any surgery and were proven by histology. MRI examinations were performed at 0.5 T (Magnetom, Siemens). All studies included plain T1-weighted (SE 400/30 or FLASH 315/14, 90), proton density-weighted (SE 1600/30) and T2-weighted images (SE 1600/70 or 90), as well as T1-weighted images after administration of 0.1 mmol Gd-DTPA/kg body weight (Magnevist, Schering). Slice thickness usually was 10 mm. CT examinations always consisted of plain and enhanced scans. Slice thickness was 8 mm in most cases.

MRI proved to be superior to CT in visualizing the extraaxial tumor location (31 vs. 20), the dural tumor base (42 vs. 33), a tumor capsule (28 vs. 7) and a meningeal enhancement adjacent to the tumor (19 vs. 1). Advantages of MRI over CT could be contributed to multiplanar imaging, reduced artifacts and superior contrast between meningeal structures, grey matter and white matter in MRI. MRI was inferior to CT in visualizing calcifications (2 vs. 12) and in demonstrating a typical signal intensity of the tumor as compared to a typical tumor density in CT examinations (32 vs. 39). Both methods showed equivalent results in demonstrating mass effects (38 vs. 37), hyperostosis (5 vs. 3), even tumor contours (42 vs. 42) and a homogeneous contrast enhancement (34 vs. 33).

In conclusion, there is no general superiority of MRI or CT in the diagnosis of intracranial meningiomas. However, both imaging techniques are of different value in demonstrating certain characteristic features of meningiomas.

► **220** 11:06AM

EVALUATION OF THE POST-OPERATIVE ASCENDING AORTA; A COMPARISON OF MR AND CT

JC Weinreb, R Libes, D Naidich, D McCauley, AC Galloway, SB Colvin, A Litt
Department of Radiology and Division of Cardiothoracic Surgery, New York University Medical Center

Surgical management of aneurysms of the ascending aorta and aortic arch involves prosthetic replacement of the ascending aorta and often replacement of the aortic valve. Post-operative complications are often asymptomatic. We used MRI and CT to study 30 asymptomatic patients with a history of surgery of the ascending aorta and aortic arch in order to (1)determine the normal appearance on MR of the post-operative thoracic aorta (2) the frequency of late complications of aorta surgery,and (3) the comparative value of MR and CT for follow-up of these patients.

MR was performed at 0.5T (Philips S5 Gyroscan) with EKG gating. Axial SE T1-weighted sections and oblique sagittal SE T1-weighted sections were obtained in all cases. 26 patients were also studied with axial GRE sequences which were viewed in cine mode (8-16 frames per section). CT was performed using standard dynamic bolus technique. 3 patients had non-contrast CT due to known contrast sensitivity. The MR and CT were evaluated independently for surgical complications including flow in false channels, aneurysm, disection, and pseudoaneurysm. The normal appearance of the post-operatrive aorta was assessed and compared.

26% had flow in a false channel. 20% had dissections including 3 in the ascending aorta. Two patients had pseudoaneuyrsms in the region of the prior surgery. In general, MR and CT depicted these complications equally. On CT the graft prosthesis could occasionally be delineated. This was not possible on MR. Oblique sagittal images did not add any additonal information to the axial images. GRE cine imaging depicted 1 dissection and one patent false channel that were not apparent on the SE images alone.

► **221** 11:18AM

CHEST-WALL INVASION IN MRI: A COMPARISON WITH CT AND SURGICAL FINDINGS

R.Ch. Bittner, Schorner W., Henkes H., Weiss T., Loddenkemper R.*,
Kaiser D.*, Felix R.
Department of Radiology, University Clinic Rudolf Virchow/Ch., FU Berlin, FRG
* Lung Clinic Heckeshorn, Berlin, FRG

Preoperative assessment of tumor extent is crucial for surgical planning in patients with intrathoracic malignancies and suspected chest-wall invasion. The present study compares the diagnostic value of MRI in the detection of chest-wall invasion with CT and surgical findings. 21 patients with histologically proved pleura related masses were studied with MRI and CT. All patients underwent surgery. MR imaging was performed with a 0.5 T superconductive system (Magnetom, Siemens). All patients were examined with ECG-gated T1-weighted (T1-WI) and T2-weighted (T2-WI) spin echo (SE) sequences (T1-WI: TR=600-1000 msec, TE=22/30 msec, T2-WI: TR=1000-2000 msec, TE=90/115 msec). Additionally, in 10/21 patients a T1-WI ungated multislice gradient echo (GRE) sequence (TR=310-460 msec, TE=12-14 msec, 0=90°) was performed. In 5/10 patients, this sequence was repeated after i.v. administration of Gadolinium (Gd)-DTPA (o.1 mmol/kg body weight).
Surgery confirmed chest-wall invasion in 19/21 patients. Tumor invasion of the chest-wall was visible on CT in 14/19 patients. Characteristic MRI patterns of tumor invasion were high signal intensity (SI) lesions within the chest-wall and/or the pleura of all 19 patients on SE T2-WI and Gd-DTPA enhanced GRE T1-WI. The GRE sequence could replace ECG-gated SE T1-weighted sequence in chest-wall imaging. However, tumor and adjacent muscle tissue were difficult to differentiate with both techniques. High SI pleural lesions, found in 5/21 patients, appeared not to be specific for tumor invasion. Histology confirmed pleural tumor invasion in 3/5 patients, pleural inflammation in 2 patients had a similar appearance. The value of Gd-DTPA can not yet be determined. Gd-DTPA enhanced GRE images may replace time consuming SE T2-WI in the detection of chest-wall invasion.

TUESDAY a.m.

► **222** 11:30AM

MRI in the evaluation of congenital heart disease of newborns : review of our experience in 62 patients.

B. KASTLER , A. LIVOLSI, Ph. GERMAIN, W. GU, D. WILLARD, A. WACKENHEIM
University hospital STRASBOURG FRANCE

Our aim was to prove feasibility and to find new applications for cardiac MRI in a newborn population.

Patients : 62 patients (age ranging from 2 to 33 days) with various congenital heart disease were included in the study. 9 patients were controlled post operatively (Senning, Blalock-Taussig, Switch).

Imaging technique : Images were acquired on a 0.5 Tesla MR-Max Imager with ECG-gated single echo spin echo sequences (TE - 26 ms - TR = approx 350 ms). Slice thickness was 3 to 5 mm, multiple contiguous slices were acquired in three imaging planes (5 to 7 mm run). 2D echocardiography was performed prior to MRI in all patients.

Results

- Pre-operatively MRI was most contributive in the assessement of abnormalities of the greal vessels, conotruncunal region of the heart, pulmonary venous returns, and small ventricular septum defects.
- Post-operatively MRI demonstrated complementary information to 2 DE in all 8 patients.
  1) depicting completely the Senning correction
  2) clearly visualizing the patency of the proximal segment of the reinserted coronary arteries in the switched aorta
  3) appreciating the size and patency of the pallative shunts and of the main and brand pulmonary arteries in the Blalock procedures.

From this study we conclude that MRI is a valable imaging modality in CHD in newborns whenever there is a need for more information than echocardiography can provide.

► 223 11:42AM

Gadolinium DTPA Enhanced MRI in Patients with Acoustic Neuromas in Comparison with CT

T Heim, W Schörner, H Henkes , R CH Bittner, P Schubeus, R Felix
Dep. of Radiology, University Clinic Rudolf Virchow/Cha, FU Berlin, FRG

Purpose: It is wellknown that CT fails to demonstrate small neuromas because of bone artifacts in the cerebello-pontine angle. In the present study we compared the diagnostic sensitivity of Gd-enhanced MRI with enhanced CT.
Materials&Methods: Thirty patients with histologically proven acoustic neuromas were studied before and after contrast administration (Gd-DTPA 0.1 mmol/kg) in comparison with CT. MR examination were performed on a 0.5 T superconductive system. All patients were examined with T1- weighted (T1- WI) spin echo sequences (SE TR= 400 msec, TE= 30msec) or multislice gradient sequences (FLASH TR= 315 msec ; TE= 14 msec, flip angle 90) and 29 patients with T2- weighted (T2- WI) spin- echo sequences (SE TR= 1600 msec, TE= 70- 120 msec). Unenhanced and contrast enhanced CT scan were available in 25 patients.
Results: Unenhanced CT detected four lesions in 13 patients (30,7%), enhanced CT 21 lesions in 25 Patients (84 %). Unenhanced T1- WI MR revealed 24 lesions in 30 patients (80 %), T2-WI 20 lesions in 29 patients (68 %). After application of Gd-DTPA we found 30 lesions in 30 patients (100 %).
Conclusion: These results indicate that contrast - enhanced MR is superior over CT for routine purposes in most cases with acoustic

► 224 11:54AM

MRI COMPARED TO CT IN THE DIAGNOSIS OF RECURRENT OVARIAN CARCINOMA

MC Fishman-Javitt (1), JL Lovecchio (2), HL Stein (2)
G. W. Univ. Medical Center (1), North Shore Univ. Hospital (2)

There is little or no data regarding the efficacy of MRI in the detection of recurrent ovarian carcinoma. If the extent of disease could be accurately assessed preoperatively, then surgical approach and or biopsy procedures can be tailored in order to plan appropriate therapy. Eighteen patients who underwent laparotomy for suspected recurrence remote from the time of primary diagnosis (not for second look laparotomy) had advanced disease at the time of the initial diagnosis. All had MRI scans performed on a 0.6 Tesla superconducting magnet with both T1 weighted (TE 32 TR 525) and T2 weighted (TE 60 TR 2000) 2D FT pulse sequences in the axial, sagittal, and coronal projections. Seventeen patients had fourth generation contrast enhanced CT scans of the abdomen and pelvis. Most scans were performed within one month preceding surgery, and all but one were within three months prior. There were 17 patients with surgically proved recurrence. MRI and CT findings were compared to surgical pathology in the detection of involvement of the true pelvis (uterus, broad ligament, vagina, rectum), ascites, metastases to the omentum, serosa, mesentery, lymph nodes, abdominal wall, bowel, liver, and distant sites (e.g., - pleura). The overall agreement of MRI with surgical results was 55%, and for CT was 76%. Thus, in the evaluation of recurrent ovarian carcinoma for extent of disease, CT was superior to MRI.

SPINE I

MODERATORS: M. T. MODIC, M.D., E. R. McVEIGH, Ph.D.

► **225** 10:30AM

MRI OF SPINAL CORD AND CSF MOTION WITH SPATIAL MODULATION OF MAGNETIZATION

LM Levy, BD Bolsten Jr, E McVeigh, RN Bryan
Department of Radiology, Johns Hopkins Hospital, Baltimore, MD

This study examines the usefulness of spatial modulation of magnetization for imaging the pulsatile motion of the spinal cord and cerebrospinal fluid, with comparison to presaturation tagging and phase-contrast imaging techniques.

Imaging was performed by spatially modulating the amount of magnetization prior to imaging. A uniform series of stripes was created by using nonselective radiofrequency pulses with binomial amplitudes, separated by field gradient pulses (1). Velocity measurements were calibrated with phantom studies, and MR examinations were performed on a number of subjects.

Images were obtained in less than 2 minutes, displaying both the magnitude and direction of motion. Flow patterns of CSF were easily observed in various portions of the spinal canal. Serial images of the cervical spinal cord obtained during the cardiac cycle demonstrated deflections of the stripes within the cord and correlated with measurements based on spin echo phase images and presaturation tagging (2). In addition, internal deformation within the cord were observed, demonstrating the effect of differential and shear forces across the cord. In comparison to presaturation tagging, SPAMM permitted much greater speed in stripe placement, and allowed rapid placement of much larger series of stripes over the field of view, thereby providing improved temporal resolution and increased spatial information.

MRI with spatial modulation of magnetization can provide useful information, efficiently and noninvasively, for the evaluation of diseases restricting cord motion or affecting the CSF circulation.

(1) Axel L, et al: Radiology 1989; 172:349-350.
(2) Levy LM, et al: Radiology 1988; 169:773-778.

TUESDAY a.m.

► **226** 10:42AM

THE VALUE OF GADOLINIUM ENHANCED MRI OF THE C-SPINE IN DEGENERATIVE DISEASE

MR Dadsetan, C Bazan, H Ahmadi, JR Jinkins

Neuroradiology Section, The University of Texas Health Science Center at San Antonio

INTRODUCTION: To evaluate the value of Gadopentetate Dimeglumine (GD) enhancement in the MRI diagnosis of degenerative disease of the C-spine, a retrospective study was undertaken.

MATERIALS AND METHODS: Sixty axial examinations of the cervical spine were evaluated in subjects with acquisitions consisting of either: 1) T1 weighted spin echo images without GD; 2) T1 weighted spin echo images with GD; or 3) gradient recalled echoes. All imaging was performed with a 1.5 Tesla GE clinical unit.

RESULTS: Contrast and/or spatial resolution were superior in the T1 weighted GD enhanced acquisitions as compared to the images obtained in the other two groups of subjects.

DISCUSSION: The difficulties of attaining both high spatial and high contrast resolution on one single axial imaging sequence of the C-spine are largely overcome with the addition of GD to T1 weighted spin echo images. This is believed to be due to the high spatial resolution inherent in T1 images combined with the enhancement of the epidural venous plexus and perhaps other normal anatomic structures within the neural foramina allowing superior visualization. In many circumstances this imaging protocol may negate the necessity of additional time consuming axial acquisitions in the evaluation of degenerative disease of the C-spine.

► **227** 10:54AM

SERIAL GADOLINIUM ENHANCED MR IN MULTIPLE SCLEROSIS OF THE SPINAL CORD

MA Mikhael
Evanston Hospital, McGaw Medical Center of Northwestern University, Evanston, IL

Out of 29 cases studied with MR for suspected multiple sclerosis (MS) of spinal cord, 15 cases showed MS plaques confirming the clinical diagnosis. Nine of the 15 positive MR cases showed enhanced MS plaques indicating active disease. MR studies were performed in 1.5 T magnet. A pre-enhanced series (SE: TR 600-2000 ms, TE 20-70 ms) and a post-enhanced series (SE: TR 600 ms, TE 20 ms) were obtained for all cases. If the post-gadolinium study showed enhanced plaques, serial enhanced MR studies were obtained every 4 weeks for follow-up and correlation with medical treatment.

For confirmation of the clinical diagnosis of multiple sclerosis, T2-weighted images for the spinal cord can visualize both the acute and the old chronic plaques. For the differentiation of the old plaques from the active acute plaques that require aggressive medical treatment, it was important to obtain post-gadolinium enhanced MR (TR 600 ms, TE 20 ms). Active acute plaques show enhancement after 20 cc of gadolinium-DTPA injected intravenously.

Serial enhanced MR showed the active plaque to lose gradually its clear delineated margins and high-intensity signal after the fourth week and to lose completely the enhancement after 6-8 weeks. The segment of the spinal cord that shows the enhanced plaques is usually swollen, and the swelling lags behind the loss of the enhancement of the plaques. In 2-4 months the spinal cord returns to its normal dimensions and active plaques disappear to be visualized only on T2-weighted images as chronic plaques.

From our series, enhancement of the active plaques further stress the fact that the blood-brain barrier is disturbed in active multiple sclerosis lesions. The gadolinium is a useful marker for new and clinically active lesions and should be used to follow-up the efficiency of the medical treatment. In our series, correlation between the symptomatology and the enhancement showed clear correlation with the clinical findings. The disappearance of enhancement slightly lags behind clinical improvement.

► **228** 11:06AM

HALF FOURIER SPIN ECHO IMAGING IN ROUTINE CLINICAL BRAIN AND CERVICAL SPINE PROTOCOLS

F.A. Jolesz, R.B. Schwartz, G.T. LeClercq, D.A. Feinberg, R. Kikinis, M.D. Ainslie
Dept. of Radiology, Harvard Medical School and Brigham & Women's Hosp., Boston, MA

We have implemented Half Fourier (HF) spin echo imaging in the routine clinical protocols for MR imaging of brain and cervical spine. After application to over 500 cases, we have found HF imaging to offer several important advantages:

1) Significant reduction of imaging time is achieved without sacrificing contrast or spatial resolution. With uncooperative patients, sufficiently T2 weighted multi-slice data sets were obtained within 3 minutes, combining HF data synthesis with zero filling.

2) Long TR imaging is available. By increasing TR to 4 sec, we obtained brain and spine images with a significant increase in contrast-to-noise ratio in heavily T2 weighted images acquired within 8 minutes. The improved CSF-tissue contrast resulted in a "myelographic" appearance especially useful in cervical spine studies.

3) More slices can be acquired without a significant time penalty. HF imaging offers two ways to get more slices: by increasing TR, proportionally more slices can be acquired; or alternatively, by using a shorter TR, two interleaved acquisitions can be obtained. The large number of slices available in long TR sequences has been particularly useful in head and neck imaging, where images of the brain, base of the skull, and neck have been collected within the same acquisition. Interleaved acquisitions have been utilized for zero-gap imaging and have been processed for computerized 3D rendering. While a single long TR acquisition also provides sufficient slices for zero-gap imaging, there is significant cross-talk with non-rectangular slice profiles. Using rectangular slice profiles prevented this cross-talk, but gradient moment nulling was not possible, and is necessary for HF imaging which is sensitive to motion and phase errors.

In conclusion, we recommend the routine use of HF imaging. This technique provides the examiner freedom to manipulate imaging time, spatial resolution, and volume imaged to fit the clinical requirements, without adversely affecting the ability to demonstrate pathology.

► **229** 11:18AM

EARLY DIAGNOSIS OF EXPERIMENTAL INTERVERTEBRAL DISC INFECTION BY MRI WITH HISTOPATHOLOGIC CORRELATION

MR Dadsetan, RF Kilcoyne, J Pullium, JR Jinkins
University of Texas Health Science Center at San Antonio

In clinical studies of spinal infection, MRI is very useful in making the diagnosis of chronic diskitis. Very little is known concerning when the acute phase of the MRI signal becomes abnormal. In order to study this time sequence, we injected the lumbar intervertebral discs in 7 rabbits with a staphlococcal aureus suspension. Seven discs in 3 rabbits were injected with saline as a control. Forty-eight hours later, sagittal MRI of the lumbar spine was performed utilizing T_1 and T_2 weighted spin echo pulse sequences without GD-DTPA and axial and sagittal T_1 weighted spin echo images with intravenous GD-DTPA injection. For comparison, 67 Ga was injected at the start of the study in all infected and control rabbits and a radionuclide scan was performed 48 hours later. All rabbits were sacrificed at 48 hours after innoculation and the disc, endplates, and spinal canal were examined histopathologically. The results shows that none of the controls had evidence of diskitis by MRI, gallium scan, or histopathological evaluation. On the other hand, all infected discs had an abnormal MRI signal and abnormal histopathologic changes but normal 67-Ga scans. The MRI showed abnormal signal on T_2 weighted images with a decrease in height of the disc space. Pathologic changes in the infected disc included the presence of bacteria without evidence of polymorphonuclear cells, disruption of the anulus fibrosus, herniation of the nucleus pulposus and tissue necrosis. No fibrotic changes nor abnormal vascularization were seen. No epidural involvement was observed. The absence of these findings seems to explain the lack of gadolinium enhancement. This study reveals the limitations and value of MRI early in the course of acute disc infection.

► **230** 11:30AM

WHY ARE DISCS UNUSUALLY BRIGHT IN FIELD-ECHO IMAGES OF THE SPINE?

JP Mugler III, JR Brookeman
Dept. of Radiology and Biomedical Engr., University of Virginia, Charlottesville VA

It is well known that the contrast behavior of field-echo (FE) sequences often differs substantially from that of traditional spin-echo (SE) sequences. Much research effort has been dedicated to providing accurate theoretical models and experimental verification of the characteristics of the short TR field-echo sequences such as FAST, FISP, FLASH, GRASS, etc. Field-echo sequences with longer TRs are also useful in a clinical setting, although less effort has been devoted to describing their specific properties. We have found FE sequences with TRs of 300-600ms and flip angles of 5-90° to be particularly useful in imaging the spine. However, we observed that the FE sequences yield a substantially increased disc/vertebral body contrast-to-noise ratio (CNR) compared to SE sequences, even when the timing parameters (TR,TE) are the same as the SE sequence and the flip angle is 90°. Given a relatively long TR and a flip angle of 90°, one would predict the FE contrast behavior to be very similar to that for a SE sequence with equivalent timing parameters, except of course for any chemical shift and static field inhomogeneity effects. Using comparable 2D sagittal FE (TR/TE 500/15, 90°) and SE (TR/TE 500/15) sequences on a volunteer, we measured a 65% decrease in the bone marrow signal and a 130% increase in the disc signal, leading to a change in the CNR from -15 for the SE to +28 for the FE. Imaging was performed on a 1.5 Tesla Magnetom 63SP (Siemens Medical Systems, Iselin, NJ). Recently, part of this disc/vertebral body contrast anomaly was explained by the work of Wehrli et al [1]. They found that the signal loss in the vertebral body results from the combined effects of the trabeculation of the bone and chemical shift modulation of the signal. It is important to note however that not only does the bone marrow signal decrease markedly in the FE image, but the disc signal may also increase substantially.

Based on results from a numerical simulation of the Bloch equations, we propose the following explanation for the increased signal in the disc. The actual excitation profile used in the FE sequence results in a substantial signal increase for tissues with T1s of approximately 1 second or longer as compared to the response of either a FE sequence with an ideal excitation profile or a standard SE sequence. This net signal increase occurs due a relative signal enhancement toward the edges of the slice, where the flip angle is at or near the Ernst angle for the given conditions. In a SE sequence, the 180° pulse serves to change the Ernst angle to its supplement [2]. For a nominal 90° pulse, the flip angle is nowhere greater than 90°, and so this signal enhancement toward the edges of the slice does not occur. Simulation and experimental results were in good agreement, both predicting an increase in the disc signal by approximately a factor of 2. The signal enhancement toward the slice edges for FE sequences was demonstrated by Young et al[3] some time ago, but its ramifications in routine clinical imaging have not previously been widely recognized.

1. FW Wehrli, JC Ford, DA Gusnard, J Listerud, 8th SMRM, 217 (1989). 2. TJ Provost, RE Hendrick, 4th SMRI, 105, (1986).
3. IR Young, DJ Bryant, JA Payne, *Magn Reson Med*, 2, 355 (1985).

► **231** 11:42AM

31-Phosphorus MR Spectroscopy of Head and Neck Tumors *In Vivo*

Thomas Vogl[1], M.D.
Ferdinand Peer[1], Victor Reiman[2], Claudia Rennschmid[2], Josef Lissner[1]

[1]Dept. of Radiology, Univ. of Munich; [2]Dept. of Head & Neck Surgery,Univ. of Munich

Non-invasive preoperative differentiation of benign hypertrophy and malignant tumors can be useful for appropriate therapy planning. Wheras magnetic resonance imaging is characterized by high sensitivity but low specifity, MR spectroscopy is supposed to offer further information about the histology of the tissue. For evaluating the value of this method 35 patients with head and neck masses underwent comparative investigation by means of magnetic resonance imaging (MRI) and 31-phosphorus magnetic resonance spectroscopy (MRS). The examinations were made before therapy and in 7 cases during radio- and chemotherapy.

The images where obtained on a 1.0 Tesla whole-body scanner by application of the paramagnetic contrast-medium Gadolinium-DTPA. Gd-DTPA proved as useful for evaluating the metabolic state of the lesions.

In-vivo spectroscopy was done at 1.5 Tesla, using the ISIS-technique for deep-lying tumors and a 50mm surface coil for superficial masses. The evaluation of the spectra was made by a least square-fit-procedure, which determined chemical shift, T2 relaxation time and relative area of the peaks usually found in a 31-p in-vivo spectrum.

Spectroscopy revealed significant increased concentrations of phosphomonoester, phosphodiester and inorganic phosphorus in the lesion, whereas the concentration of the phosphocreatine was lower in comparison to muscle tissue. In nearly all masses, pH showed a slight alcaline shift. The variability of the spectra within patient groups of similar histology was higher than within lesions of the same metabolic state. Existence of necrotic regions detected by MRI was marked by an increase of inorganic phosphorus in the spectrum. Masses with anamnestic evaluated high growing rate were spectroscopical charactarized by raised concentrations of phosphomonoester. Even though there is no correlation between histology and spectra visible, it is possible to evaluate vascularisation and metabolic state of tissue by 31-p-spectroscopy. These preliminary results suggest that 31-p-MRS may be useful for the detection of tumor growth, individual therapy planning and therapy control.

► **232** 11:54AM

MRI SPECTRUM OF THE HEAD AND NECK MANIFESTATIONS OF AIDS

C.H.Flowers, M.F.Mafee,B.Raofi, B.Lum
Magnetic Resonance Center, University Of Illinois College of Medicine

The MRI of 50 patients with Acquired Immune Deficiency Syndrome(AIDS) and AIDS-related COMPLEX (ARC) were reviewed for evaluation of encephalopathy. Cerebral atrophy was observed in 36%, cerebellar atrophy in 38%, and brainstem atrophy in 13%. Focal demyelination was observed in 27%, while diffuse demyelination was observed in 15%. Toxoplasmosis was observed in 13%, and primary central nervous system lymphoma was observed in 6%. Cryptococcal meningitis was observed in 4%, and mycobacterium tuberculosis was observed in 2% of our patients. Lymphoid hypertrophy was recognized in 23% of our patients, meanwhile sinusitis was demonstrated in 15% of our study group. Two cases of cerebral infarction were observed in our patient population. In our study,no patients exhibited demyelinating changes of the corpus callosum and junctional "U" fibers. These fibers were involved only by toxoplasmoid abscesses or primary central nervous system lymphoma. Another interesting observation was the predominant involvement of the subinsular and peritrigonal areas with demyelination.

SPECTROSCOPY IV

MODERATORS: H. C. CHARLES, Ph.D., P. A. NARAYANA, Ph.D.

► **233** 10:30AM

MR STUDY OF MUSCULAR AND REPRODUCTIVE FUNCTIONS IN DANINE MUSCULAR DYSTROPHY

CT Burt, J Kornegay NJH Sharp, L Kwock, S VanCamp

NIEHS, Rsch. Triangle, UNC Dept. Radiology, Chapel Hill, Dept. Comp. Animal & Special Species, Col. Vet. Medicine, NC State Univ., Raleigh, North Carolina

There is a need for an appropriate animal model of human muscular dystrophy on which therapies can be tested. One new model developed at the College of Vet. Medicine, NCSU is a line of dogs containing a hereditary muscular dystrophy. With this model we felt MR would give important information of the etiology and symptomatology of the disease. To do this, ^{31}P analysis of intact semen samples at 8.8T and evaluation of both ^{1}H and ^{31}P NMR of PCA extracts of diseased and normal muscle. out studies included MRI and MRS of the affected muscle using a 1.5T Gyroscan MR imager,

The results of these examinations present both similarities and some contrasts with the human disease. The MRS shows elevated inorganic phosphate and somewhat decreased PCr/ATP levels. There is, however, no increased pH. There is also some indication of increased intensity in the phosphodiester region. The proton images of the diseased muscle have a mottled appearance which is presumably due to deposition of fatty and fibrous connective tissue. The phosphorus extracts confirm the in vivo study with all metabolites decreased by about 2/3's on a muscle wet weight basis undoubtedly due to the increased fatty infiltration. The proton spectra show principal resonances due to taurine, creatine, and choline. There are also noticeable signals arising from adenosine nucleotides, carnosine, and anserine. The main finding is that carnosine and anserine are dramatically reduced in the diseased muscle. This is also reported to be the case in Duchenne muscular dystrophy and, therefore, one can conclude that the diminution of dipeptides may be the most convenient marker from a MRS standpoint to monitor the disease.

The semen samples also showed abnormalities involving the concentration of glycerol-phosphorylcholine. This is of interest because it is one of the first demonstrations that reproductive function can also be involved in the disease process.

► **234** 10:42AM

TRANSRECTAL MULTINUCLEAR MAGNETIC RESONANCE SPECTROSCOPY FOR THE CHARACTERIZATION OF NORMAL AND MALIGNANT PROSTATES *IN VIVO*.

J. Kurhanewicz, M.A. Thomas, P. Jajodia, T.L. James, M.W. Weiner, P. Narayan.
VA Medical Center/UCSF, San Francisco CA 94121.

We have recently described the construction and safe use of a transrectal probe for clinical spectroscopy of the prostate. The object of this study was to determine differences in citrate levels using transrectal ^{1}H MR spectroscopy and differences in phosphorylated metabolites using transrectal ^{31}P MR spectroscopy between normal, hyperplastic and malignant prostates. Water suppressed ^{1}H MRS spectra in four malignant and three normal prostates were obtained using our transrectal coil and a binomial (1331,2662) spin echo sequence on a Philips Gyroscan 2T MRI/MRS whole body system. The spectra of healthy prostates showed an intense resonance from the methylene protons of citrate at 2.5 ppm, confirming the presence of high concentrations of citrate in the normal prostate. ^{31}P MR spectra were obtained for 15 individuals with normal (N=5), hyperplastic (N=4) and malignant (N=6) prostates. Normal prostates had PCr/ATP ratios of 1.2 ± 0.2, PME/ATP ratios of 1.1 ± 0.1 and PME/PCr ratios of 0.9 ± 0.1. Malignant prostates had PCr/ATP ratios that were lower (0.7 ± 0.1) than that of normal prostates ($p<0.02$) or prostates with benign hyperplasia (1.1 ± 0.1, $p<0.01$). Malignant prostates had PME/ATP ratios (1.8 ± 0.2) that were higher than that of normal prostates ($p<0.02$). Using the PME/PCr ratio, it was possible to metabolically differentiate malignant prostates (2.7 ± 0.3) from normal prostates ($p<0.001$). Additionally there was no overlap between the PME/PCr ratios of individual normal and malignant prostates. These studies demonstrate that multinuclear MR spectroscopy (^{31}P, ^{1}H) can characterize metabolic differences between normal, benign and malignant prostates.

TUESDAY a.m.

► **235** 10:54AM

QUANTITATIVE MRI AND ^{31}P-MAGNETIC RESONANCE SPECTROSCOPY STUDIES OF DERMATOMYOSITIS.
JH Park, J Vansant, NG Kumar, SJ Gibbs, M Penner, CL Partain, AE James
Department of Radiology, Vanderbilt Medical School and Siemens Medical Systems, Inc.

MRI and ^{31}P-magnetic resonance spectroscopy (MRS) were used to examine five patients with dermatomyositis in order to add a new, quantitative dimension to the classical modalities for the diagnosis and evaluation of inflammatory muscle diseases. T1 and T2 weighted images of the thigh as well as the absolute T1 and T2 values for different muscle groups were acquired with a 1.5 T Siemens Magnetom. ^{31}P spectra of the quadricep muscles were obtained during rest, exercise, and recovery using an 8.0 cm surface coil, TR = 3000, and 64 acquisitions. T2 weighted images of the patients' thighs showed increased signal intensity predominately in the vastus lateralis and vastus medialis with less involvement of other muscle groups. T1 and T2 values of the vastus lateralis were significantly elevated with values as high as 2250 and 65 msec, respectively. The T1 and T2 values ± SE in five normal subjects were 1351 ± 39 and 37 ± 0.7, respectively. MRI abnormalities of the patients demonstrated focal and inhomogeneous distribution of muscle involvement rather than a generalized pattern. ^{31}P spectra showed elevated P_i/PCr ratios (0.28 - 0.30) in the resting muscles of the two most severely debilitated patients (normal range, 0.13 - 0.17). During exercise at 25% maximum voluntary contractile force, all patients had elevated P_i/PCr ratios (0.45 - 0.75) as compared to normal subjects (0.25 - 0.40). The T1 and T2 values as well as the P_i/PCr ratios correlated with symptomatology.

In conclusion, non-invasive MRI and MRS hold promise as combined technologies for improved localization for surgical biopsies, quantitative evaluation of the disease processes, and long term follow-up of therapeutic regimes for inflammatory myopathies.

► **236** 11:06AM

ERROR ANALYSIS OF THE FITTING OF MR RELAXATION DATA: THE DOUBLE EXPONENTIAL FIT
SJ Gibbs, RM Willcott, RR Price, CL Partain, AE James, Jr.
Department of Radiology and Radiological Sciences, Vanderbilt University

Determination of MR relaxation time requires a procedure that produces an array of signal intensities as functions of repetition time (TR) for T1, or echo time (TE) for T2. Curve-fitting procedures are then employed, using models appropriate to the data. It is generally accepted that the model for a 1-component system (e.g., water) is a simple exponential. For biological systems, the model is the sum of n exponentials, where n is unknown. Several investigators have published results of simplifying assumptions in which n is assumed to be a small number, generally 2. While a single exponential may provide a rather poor fit and the resulting relaxation time cannot be meaningfully applied to a complex biological system, it is reproducible by a variety of curve-fitting methods. Clearly, increasing the number of exponential terms improves the fit to the data as measured by Chi square or some similar parameter. However, with limited, noisy data, it also increases the uncertainty in all parameters estimated. Further, the applicability to complex biological systems of relaxation times estimated by a dual exponential expression is little, if any, better than that determined by a single exponential. Examples are presented to demonstrate that the sense of security conveyed by a small value of Chi square may not be justified.

► **237** 11:18AM

NON-LINEAR LEAST SQUARES FITTING OF IN VIVO ^{31}P NMR DATA

PB Barker[1] and S Sibisi[2]
[1]Johns Hopkins Hospital, Baltimore, MD 21205, [2]Cambridge University, United Kingdom

In vivo ^{31}P NMR spectra usually have one or more of the following characteristics; low signal-to-noise ratios, overlapping peaks, and undulating baselines. Each of these features makes the measurement of peak area difficult. The traditional method of manual curve fitting in the frequency domain may be both inaccurate and irreproducable under these conditions, and is certainly a time-consuming process. This presentation concerns the use of direct Non-Linear Least Squares (NLLS) fitting of the FID as a means of analyzing ^{31}P NMR spectra in an automated fashion. Time-domain fitting is especially appropriate in the case of spatial localization pulse sequences such as "DRESS" or Chemical Shift Imaging which involve delayed data acquisition.

NLLS involves the iterative, two-step minimization of the difference (χ^2) between the model equation (consisting of a sum of exponentially decaying oscillators) and the experimental FID. In the linear step, phases and amplitudes are fit whilst the decay times and frequencies are held fixed. In the non-linear step, the frequencies and decay times are fit using a Levenberg-Marquardt algorithm. Starting values, which are required for the linewidth and frequency parameters, can be obtained from the normal Fourier Transform of the FID. In comparison to Linear Prediction Singular Value Decomposition (LPSVD, 1), NLLS appears to be more stable under conditions of low signal-to-noise (2). This is primarily due to the ability of NLLS to incorporate prior knowledge about any spectral parameters (phase, frequency, linewidth, number of peaks, etc..) into the model. Examples of the use of NLLS will be shown using spectra recorded from the human brain on a General Electric 1.5T Signa spectrometer.

(1) H Barkhuijsen, R de Beer, WMMJ Bovee and D van Ormondt, *Journal of Magnetic Resonance*, **61**, 465 (1985)
(2) S. Sibisi, unpublished results

TUESDAY a.m.

► **238** 11:30AM

SHORT ECHO T2 WEIGHTED 31P CSI: APPLICATIONS TO IN-VIVO PHOSPHORUS IMAGING

S Posse, F Lazeyras, N Herschkowitz, W Aue, and HC Charles*
NMR Unit of the Medical Faculty, Universitat Bern, Bern, Switzerland
*Dept. of Radiology, Duke University Medical Center, Durham, NC, USA

Localized phosphorus spectroscopy is generally accomplished using FID's rather than spin echoes (SE) due to the shorter T2's of some of the phosphorus metabolites. We have investigated the possible advantages of T2 weighted spectra, using localized short SE sequences on a phantom (10 mM PCr, 10 mM ATP, 1 mM Pi) and in-vivo. Planar spin echo (SE) CSI was accomplished using both selective excitation (TEmin = 2.8 ms) and saturation (TEmin= 2.0 ms).

Figures 1a,b show data (phantom) from selective saturation FID and SE sequences respectively with similar S/N for the FID and short SE (TE=2 ms) sequence. The decreased β-ATP S/N is attributed to off-resonance effects of the 800 us refocussing pulse, otherwise the data are comparable. Examples of human brain spectra under similar conditions to the phantom (FID and 2.4 ms SE) are shown in Figure 2a and 2b. Again the data are similar although no baseline artifact is evident in the uncorrected SE data and the Pi is slightly better resolved. Figure 3 shows a T2 study on the phantom (TE = 2 ms -116 ms) and Figure 4 shows a similar study on human brain (TE = 2.8 ms - 116 ms). The PDE region shows the most rapid decrease in S/N with respect to TE.

Short SE (TE < 3ms) acquisitions for 31P spectroscopy are technically feasible with fast stable gradient systems with little degradation in S/N. Potential uses of such short SE sequences include 1) Simple removal of baseline artifacts in the chemical shift dimension, 2) Simplified automatic phase correction of spectra, 3) Better resolution of Pi for pH measurements in brain where broad PDE components may obscure acidic shifts, 4) Measurement of T2 for various metabolites, and 5) SE editing in muscle spectroscopy to resolve the NAD region.

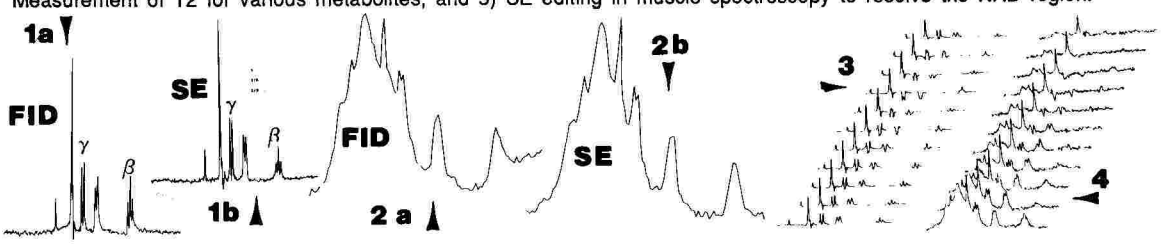

► **239** 11:42AM

^{31}P and ^{1}H MRS Studies of Deep White Matter Lesions

D. Sappey-Marinier, B. Hubesch, R. Deicken, G. Fein, C. Van Dyke, and M.W. Weiner

Magnetic Resonance Unit and Psychiatry Service at VA Medical Center
University of California, San Francisco

The goal of these experiments was to characterize changes of phosphate and proton metabolites in patients with Deep White Matter Lesions (DWMLs) of unknown etiology.

Methods: Ten subjects with DWMLs and ten elderly controls with no observable lesions were examined on a whole body 2T Philips Gyroscan MRI/MRS system. The volumes of interest (100 ml for ^{31}P and 30 ml for ^{1}H) were selected to encompass white matter in the hemisphere with the most extensive lesion, as measured on a multislice T2-weighted image. ^{31}P spectra were obtained in 20 min (640 scans, TR=2 sec) using an improved ISIS sequence for spatial localization. ^{1}H spectra were acquired using a modified ISIS localization sequence with outer volume suppression pulses. Water suppression was achieved by incorporating semi-selective 11-TE-22 (TE=100 msec) spin-echo and DANTE presaturation pulses into the ISIS sequence.

Results: In phosphorus, PDE and ATP concentrations and the ATP/Pi ratio were significantly decreased while PME, Pi and PCr were unchanged. By contrast, the proton metabolite (NAA, Cr, Cho) ratios were not changed from control.

Conclusion: The decrease in phospholipid breakdown products (PDE) detected by ^{31}P MRS in patients with DWMLs suggest altered phospholipid metabolism. Furthermore, reduced ATP concentration and ATP/Pi ratio may reflect an ischemic basis. However, the normal pattern of ^{1}H metabolites in DWMLs is consistent with the benign clinical status of these patients.

► **240** 11:54AM

OPTIMIZATION OF VOLUME SELECTED MR IMAGING FOR LOCALIZED PROTON SPECTROSCOPY

WR Riddle, MR Willcott, RR Price, DR Pickens, CL Partain, AE James
Department of Radiology and Radiological Sciences, Vanderbilt University

Determining the location of a volume of interest in water suppressed proton spectroscopy using stimulated echoes (STEAM) is often difficult. We have developed a companion imaging sequence for locating the selected spectroscopic volume. The sequence generates images from echoes resulting from three orthogonal selective radiofrequency pulses. Volumes of interest with the general shape of rectangular parallelopiped are selected by defining the envelopes for the three radiofrequency pulses in the presence of constant gradients. Images can be made using the stimulated echo or either of the two spin echoes that result from the sequence. High resolution (resoluton greater than 0.5 mm) images of spectroscopic volumes have been obtained using phantoms and verified with conventional imaging techniques. Development of the sequence, optimization of image quality, and methods for selecting the volume of interest will be demonstrated.

CARDIAC

MODERATORS: C. B. HIGGINS, M.D., W. J. MacINTYRE, Ph.D.

► **241** 15:45PM

DYNAMIC 3D MAPPING OF LEFT VENTRICULAR CONTRACTION

EA Zerhouni[a], ER McVeigh[a], J Prince[b], B Bolster[c], G Hill[b], M Guttman[c], S Bouton[a], J Lima[d], J Weiss[d].
Departments of Radiology (a); Electrical Engineering (b); Biomedical Engineering (c); Cardiology (d); The Johns Hopkins University.

Myocardial ischemia is a local phenomenon that produces abnormalities in segmental wall function. The detection of ischemic heart disease has been hampered by limitations in conventional imaging methods. Specifically, the inability to track individual points in the myocardium as a function of time does not allow the quantification of regional asynchrony during contraction.

We have developed a tissue tagging MRI technique to map the temporal patterns of strain in the entire left ventricle with a time resolution of 25ms. We have also developed image analysis software to reconstruct a model of the contracting left ventricle from the MRI data.

This tissue tagging pulse sequence is a hybrid of three motion tracking techniques. In-plane motion is tracked using a star pattern of striped tags. The-through plane motion is measured in one of two ways: 1) using velocity encoding in the slice selection direction, or 2) imaging the translation of parallel tags in long axis images that contain parallel tags at the positions of the short axis slices. Using this data, the motion and deformation of 8 to 12 segments in each slice of the left ventricle is reconstructed. A 3D model of the beating heart is reconstructed and displayed using rendering software on a TAAC1 accelerator. This method allows regional analysis of myocardial strain previously unavailable.

TUESDAY p.m.

► **242** 15:57PM

MAGNETIC RESONANCE IMAGING OF REVERSIBLE MYOCARDIAL ISCHAEMIA USING DIPYRIDAMOLE

DJ PENNELL, SR UNDERWOOD, PJ ELL, RH SWANTON, JM WALKER, DB LONGMORE
THE NATIONAL HEART AND MIDDLESEX HOSPITALS, LONDON, ENGLAND

Limitation of space and motion artefact make MR imaging during dynamic exercise difficult. Pharmacological stress with dipyridamole, a coronary artery vasodilator, is used as an alternative to exercise for thallium scanning. This study examines the feasibility of using dipyridamole to detect ischaemia during MR imaging.

Forty patients with a history of angina and an abnormal exercise electrocardiogram were studied by thallium myocardial perfusion tomography and MR wall motion imaging using a cine gradient refocussed sequence with velocity compensation (FEER) with a TE of 14ms. Images were obtained in the horizontal and vertical long axis and short axis planes before and after pharmacological stress with 0.56mg/kg dipyridamole intravenously over 4 minutes. The myocardium was divided into 9 segments for direct comparison of perfusion with wall motion. Segments were assessed visually into grades; normal, hypokinesis or reduced perfusion, akinesis or very reduced perfusion.

Reversible deterioration of at least one grade in segmental wall motion occurred in 24 (60%), and reversible thallium perfusion defects occurred in 36 (90%) of the patients. The site of wall motion change was invariably associated with a reversible thallium defect. Thallium defects of greater than 2 segments were always associated with wall motion deterioration but most single segment thallium defects went undetected by MRI. There was a significant correlation between detection of wall motion abnormality and the angiographic severity of coronary artery disease. There were no signicant differences in ventricular volume or ejection fraction changes following dipyridamole between the groups with and without detectable reversible wall motion changes but there was a significant reduction in the signal intensity of the abnormally moving segments when compared to the normal segments in each patient after normalisation to fat signal. In 9 cases the change was apparent visually and it was maximal in the subendocardial region.

We conclude that MR imaging of reversible wall motion abnormalities in patients with coronary artery disease is feasible during pharmacological stress with dipyridamole and may be associated with MR signal reduction. The failure to demonstrate wall motion abnormalities in all cases of reversible thallium defects may be due to the small size of the defect or the ability of dipyridamole to cause perfusion defects in the absence of myocardial ischaemia.

► **243** 16:09PM

MRI OF AORTIC COARCTATION: CLINICAL UTILITY IN PATIENT MANAGEMENT

P Wozney, E Cotten, JA Ettedgui

University of Pittsburgh, Departments of Diagnostic Radiology, Pediatric Cardiology and the Pittsburgh NMR Institute

The clinical impact of MRI in the diagnosis and therapy of coarctation of the thoracic aorta was evaluated in 24 patient studies during a 15 month period ending in June 1989. As a result of this investigation, the routine management of coarctation has been altered. In the uncomplicated case, cardiac catheterization has been eliminated, reducing cost, morbidity and mortality.

MRI studies were ECG-gated, and performed on a 1.5 T General Electric Signa system. Short TR series were performed in all 24 cases, and in 21 cases (88%) gradient-echo cine-MRI series were also performed. Patient age range was 4 weeks to 23 years. Indications for MRI were: evaluate native coarctation prior to surgery (12 patients), assess for restenosis following surgery (7), evaluate for aneurysm formation following balloon angioplasty (3), and evaluate dilated aorta for dissection (2).

MRI was correlated with cardiac cineangiography, echocardiography and surgery. MRI was comparable to cineangiography in 5 cases, and in another 16 cases MRI obviated the necessity for angiography. In all patients MRI provided anatomic definition superior to echocardiography. In 4 patients MRI was vital in establishing the diagnosis. These included a four-week-old respirator-dependent infant who could not be catheterized due to a lack of venous access, a patient with an aneurysm following balloon dilatation, and a patient with mild aortic regurgitation initially overlooked with echocardiography. Cine-MRI was valuable in establishing the hemodynamic significance of coarctation, confirming a small intimal flap, and identifying subtle aortic regurgitation.

► **244** 16:21PM

AUTOMATED DETECTION OF LEFT VENTRICULAR BORDERS IN GATED CARDIAC MAGNETIC RESONANCE IMAGES: EXPERIMENTAL AND CLINICAL STUDIES

SR Fleagle, DR Thedens, TD Scholz, JC Ehrhardt, DJ Skorton
The University of Iowa College of Medicine, Iowa City, IA

Nuclear magnetic resonance (MR) imaging of the heart permits accurate and precise delineation of cardiac anatomy, but quantitation of chamber volume and mass has previously required manual tracing of cardiac borders. To reduce the analysis time and subjectivity of manual tracing of left ventricular endocardial (ENDO) and epicardial (EPI) borders from MR images, we developed an automated border detection method, based on graph searching principles. We tested the program on 147 short-axis spin-echo images obtained from 13 excised animal hearts and on 39 short-axis spin-echo images from 11 normal human volunteers. We compared computer-derived borders to observer tracings and computer-derived LV mass to actual mass.

Results: With an analysis time of less than 30 seconds per image, the program found borders on all of the in vivo images. Three ex vivo images were excluded, two because the program failed to find a complete border and one due to ambiguous morphology caused by poor slice selection. One of the program failures and the ambiguous image were the most basal images and thus mass could not be computed. This resulted in calculation of 11 masses and 144 EPI borders. Additionally, 14 images were below the ENDO apex, so only 130 images were analyzed for ENDO borders. Computer-derived LV mass in excised hearts correlated highly with actual mass ($r=0.99$, $y=0.99x+5.8$ gm, SEE=4.8, N=11). Computer-derived ENDO and EPI areas correlated with observer-traced areas in vivo and ex vivo:

Computer vs. Observer Areas (cm^2)

Border	n	r	Regression Equation
Animal ENDO	130	0.97	$y = 0.90x + 0.31$
Animal EPI	144	0.99	$y = 1.02x - 0.11$
Human ENDO	39	0.92	$y = 1.04x - 0.63$
Human EPI	39	0.90	$y = 0.81x + 6.29$

Conclusion: This new method of automated border detection accurately derives data on LV geometry from MR images and may be clinically useful.

► **245** 16:33PM

TWO DIMENSIONAL ANALYSIS OF HEART WALL MOTION MRI

L. Axel
Dept. of Radiology, Hospital of the University of Pennsylvania

Conventional cardiac MRI permits only analysis of wall thickness and bulk regional displacement. Magnetically tagging the myocardium to produce a pattern of stripes at a specific phase of the cardiac cycle permits following the motion of the tagged myocardium in subsequent cardiac phases by the corresponding displacement of the stripes. Diplacement of a single stripe does not reveal the component of motion along the stripe. However, the components of the motion within the plane of the image can be defined in two dimensions by tracking the motion of the intersection points of a grid of such tagging stripes. This motion is a combination of rigid body motion (translation and rotation) and deformation (or strain); the strain is more directly related to the regional contractile properties of the myocardium. If the motion within the triangle defined by three adjacent intersection points is homogenous, we can decompose the net motion of the three points into the equivalent rigid body motion and deformation of the triangle. The strain tensor which describes the deformation of this triangle has two principal strains (eigenvectors), which are independent of the particular orientation of the tagging grid. We can now generate a new quantitative display, with the strain eigenvectors overlaid on the original heart images. While this analysis can be carried out "by hand", interactive analysis programs are necessary for practical application.

TUESDAY p.m.

► **246** 16:45PM

STRIPED TAGS (STAG) FOR MEASURING MYOCARDIAL DEFORMATION

ER McVeigh, B Bolster, EA Zerhouni
Department of Radiology, The Johns Hopkins Medical Institutions

To measure the deformation of the myocardium during contraction, a set of internal markers must be used. Two MRI methods have been proposed to place markers in the myocardium by perturbing the magnetization in a well-defined pattern and then imaging the deformation of the pattern as a function of time. The first method (1) uses slice-selective inversion pulses to create a star pattern; the second method (2) spatially modulates the magnetization (SPAMM) using a sequence of hard pulses and gradients to form a two-dimensional rectangular grid of dark lines. The star pattern follows the morphology of the left ventricle, but the deformation measurements are inherently one-dimensional. The SPAMM method gives two-dimensional information over the entire field of view but the grid pattern does not match the morphology of the ventricle and the resolution of the grid is limited by interference effects at the intersection points of the grid lines.

We have developed a hybrid technique that produces a star pattern of striped tags (STAG) to exploit the advantages of both methods. The pattern is created as follows: each 180° RF pulse that is used to produce an inversion tag (two points of the star) is split into two 90° pulses. A short time between the two 90° pulses is used to modulate the magnetization as a function of position along the tag line. The sequence of the two 90° pulses is made self-refocusing so that there is no phase shift in the magnetization as a function of the direction perpendicular to the tag line. This sequence is repeated with different tag selection gradients to create multiple striped tag lines at different angles. STAG allows noninvasive measurement of the transmural dependence of myocardial strain with unprecedented resolution.

1. EA Zerhouni et al. *Radiology*, 169, 59, (1988)
2. L.Axel, L Dougherty, *Radiology*, 171, 841, (1989)

► **247** 16:57PM

Analysis of First Pass Perfusion with Magnetic Resonance Imaging: Initia Clinical Experience

Dennis J. Atkinson (1,2), Robert Edelman (1), Deborah Burstein (1)
Department of Radiology, Beth Israel Hospital (1) Boston MA, and Siemens Medical Systems (2), Iselin NJ

Magnetic resonance can show cardiac morphology and function, but evaluation of cardiac perfusion has been difficult. The need for cardiac gating limits the free selection of repetition time (TR) and prolongs the acquisition time. We have overcome this problem by implementing an ultrafast scanning technique that produces strongly T1-weighted images.

Methods and Materials: The method consists of a 180° inversion pulse followed by a very rapid gradient-echo acquisition (repetition time <4 ms). Acquisition time is on the order of 50 - 100 ms, permitting assessment of first-pass dynamics of a contrast agent through the heart. The method was applied in an isolated perfused rat heart model and in four healthy human subjects.

Results: Gadolinium-DTPA in the perfused heart model produced strong contrast between perfused and non-perfused regions. In humans, first-pass images showed transit of the contrast agent bolus through the cardiac chambers. There was peak three-fold enhancement of the left ventricular myocardium approximately 15 sec after administration of the contrast agent bolus, with prolonged wash-out due to retention of the agent within the interstitium.

Conclusion: First-pass studies of cardiac perfusion are feasible in an occlusive infarct model and in human subjects. These studies can be performed on a conventional whole-body imaging system using standard hardware.

► **248** 17:09PM

GLOBAL AND REGIONAL RIGHT VENTRICULAR FUNCTION IN ARRHYTHMOGENIC RIGHT VENTRICULAR DYSPLASIA STUDIED BY MAGNETIC RESONANCE IMAGING.

SR Underwood, ED Burman, E Rowlands, RH Mohiaddin, RSO Rees, DB Longmore
National Heart & Chest Hospitals, London, UK

Arrhythmogenic right ventricular dysplasia is thought to be a form of cardiomyopathy in which ventricular arrhythmias of right ventricular origin are associated with structural abnormalities of the right ventricle. The diagnosis should be considered in any patient presenting with a right ventricular arrhythmia, but it can be difficult to confirm because of the problems of assessing right ventricular structure and function. We have investigated the potential of magnetic resonance for assessing both global and regional abnormalities in these patients, comparing the findings with echocardiography and X-ray ventriculography.

Ten patients (7M, 3F; mean age 29, range 13-41) were scanned using a Picker International 0.5 Tesla machine. Other investigations included X-ray ventriculography in 6 with endomyocardial biopsy in 1, electrophysiological studies in 9, echocardiography in 9, and radionuclide ventriculography in 4. End diastolic and end systolic right and left ventricular volumes were measured from spin echo images in contiguous transverse planes, and cine gradient echo imaging was performed in oblique planes to assess regional wall motion and thinning. Magnetic resonance showed abnormal areas of thinning and hypokinesis in 8 patients, principally affecting the anterior wall and outflow tract. Four had abnormalities of global function and reduced ejection fraction. Two patients with normal echocardiograms had abnormal magnetic resonance scans, as did 2 patients with normal X-ray ventriculography. The right ventricular wall was too thin for a reliable estimate of fatty infiltration, which is a common histological finding in these patients. Magnetic resonance showed abnormal left ventricular function in 3 patients in addition to the right ventricular abnormalites. In 1 patient, no abnormality was found.

Magnetic resonance imaging, therefore, can demonstrate abnormalities of global and regional right ventricular function in patients with arrythmogenic right ventricular dysplasia, and it is more sensitive than echocardiography and X-ray ventriculography.

IMAGE PROCESSING

MODERATORS: M. L. WOOD, Ph.D., R. F. JOHNSON, Ph.D.

► 249 15:45PM

STATISTICAL SEGMENTATION AND REGION GROWING METHODS FOR IMPROVING MR ANGIOGRAMS

P. M. Margosian

MRI Division, Picker International, Highland Heights, OH

Current methods for making MR Angiograms relay on acquisition methods that make images in which the blood vessels are the brightest objects. One robust approach is to acquire many thin slices, then make a series of maximum amplitude projection images which can provide a three dimensional appreciation of blood vessel spatial relationships (1). Visibility of blood vessels is improved by suppressing "background" pixels, either by sequence methods (2) or by postprocessing (3). Postprocessing methods have the advantage of minimizing patient examination time.

A method for increasing blood vessel contrast, which segments blood vessels by use of both statistical and region growing concepts, works as follows:

(a) Divide the current image and its two nearest neighbors into 3D subregions (typical size 16x16x3); form the regional histograms. Retain only pixels from the top few percent of the histogram (or the upper lobe if the histogram is bimodal) that also lie in the slice.

(b) For each remaining pixel, require that at least two neighboring pixels (in a 3x3x3 local volume) have "similar" intensities, otherwise zero the pixel.

(c) Omit pixels in the bottom 20% of the intensity range (background).

(d) Finally, make maximum amplitude projections from what remains.

The effect of various threshold criteria on visibility of blood vessels will be illustrated with a variety of images. The results are pictures with bright blood vessels on a dark or translucent background.

References:

(1) Laub, G., Mueller, E., et. al., Proc SMRM, p876, 1988
(2) Dumoulin, C., Souza, S., Proc SMRM, p725, 1988.
(3) Laub, G., Rossnick, S., et. al., Proc SMRM, p508, 1986.

TUESDAY p.m.

► 250 15:57PM

THE MAXIMUM INTENSITY PROJECTION AS A SEGMENTATION TOOL

KS Denison, CH Wood, PM Margosian
MR Division, Picker International, Inc., Highland Heights, Ohio 44143

The maximum intensity projection (MIP) technique has been used in MR angiography to generate three dimensional views of vasculature. MIP is a technique where parallel rays are cast through a volume from a given viewing angle and the maximum intensity along each ray chosen for display. The result is a projection of the brightest voxels only onto the output image plane. When coupled with acquisition techniques designed to make flowing material hyperintense, these projections selectively enhance the blood vessels. By computing projections from several viewing angles a smoothly rotating display of the vasculature can be made.

The MIP technique provides a good degree of selective enhancement of blood versus static tissue. However, some static tissue remains which may interfere with an accurate reading of the projection images. To reduce further the remaining static tissue, the MIP technique has been adapated and used as a segmentation technique. During the computation of the projections, a count is kept for each voxel in the original volume. The count is incremented each time the voxel is selected as the maximum along a ray. After computing several projections, the voxels are segmented by thresholding based on the count. Those with a high count are most likely blood while those with low counts are most likely static tissue.

The output from this technique is a new volume containing very few signal containing voxels. Angiographic projections are computed from this new volume. The resulting projections demonstrate suppressed static tissue which lowers the potential for obstruction of the vasculature.

► **251** 16:09PM

BAYESIAN IMAGE PROCESSING OF MR IMAGES

X Hu, VE Johnson*, WH Wong*, C-T Chen
Department of Radiology and Department of Statistics*
The University of Chicago

In the past few years, image processing techniques based on Bayesian models have received considerable attention. In our earlier work, we developed a novel Bayesian approach which was applied primarily to positron emission tomography image processing and reconstruction. In this paper, we describe how the technique has been modified to process MR images in order to improve image quality and reduce artifacts. Results of its application to MR images will be presented.

In the Bayesian model used, the probability density of an image conditioned on the observed data (i.e. its posterior density) is the product of its likelihood, which is the product of normal likelihoods of each pixel in the case of MRI, with a prior density. Gibbs priors, with line processes to model boundaries, were utilized. The specific form of prior is chosen by assuming that the image is smooth everywhere except across the boundaries. This prior has the effect of smoothing the image without blurring the sharp edges. From a statistical point of view, image processing under this formalism is to estimate the image according to its posterior densities. By using an iterative procedure, we obtain an estimate of the average image under this density. We have applied this technique to phantom and human images and promising results were obtained. Specifically, processed images with reduced noise and no degradation of resolution were produced with the technique. It is obvious from these preliminary studies that this technique can be useful for processing MR images, especially those with low signal-to-noise ratio.

► **252** 16:21PM

DETECTABILITY OF OPPOSITE POLARITY LESIONS IN MR MAGNITUDE IMAGES

SC Moore, MF Kijewski*
Worcester Polytechnic Institute, Worcester, MA, *Harvard Medical School, Boston, MA

The common practice of displaying the magnitude of the complex magnetization in each image pixel distorts not only the expected signal, but also the expected noise (1). This effect is most pronounced in regions of an MR image where each pixel's "true" signal magnitude is comparable to or less than the noise. Because low signals occur in clinical MRI both naturally (from tissues with short T2 or long T1) and artificially (from some contrast agents), it is important to understand the detailed implications for human observer performance under these conditions. In most medical imaging modalities, the detectability of a lesion is independent of its "polarity" (sign of its contrast). For MR magnitude images, a dual-polarity detection study should, therefore, serve as a sensitive test of the effects of the nonstationary noise signals in low-signal regions.

The ROC curves shown in the figure were generated by applying a lesion-matched filter (crosscorrelator) to 96 image sets for each polarity. This filter provides a "decision variable" which is predictive of human observer performance in detection tasks. The magnitude calculation significantly decreased the detectability of negative-polarity lesions (compared to the positive-polarity lesions) by decreasing the matched filter signal-to-noise ratio. It is also important to note that the negative-polarity ROC curve is quite skewed, implying that the standard deviations of the lesion-present and lesion-absent distributions are unequal. A human observer ROC study demonstrated a comparably skewed ROC curve for the negative-polarity lesions.

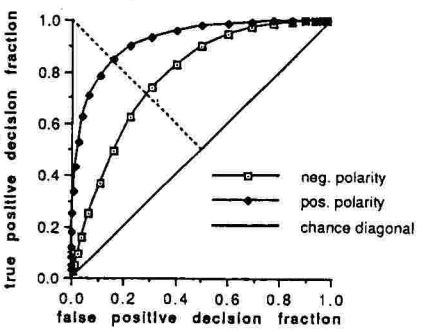

[1]Henkelman RM, Med. Phys. 12: 232-233, 1985.

► **253** 16:33PM

Parametric Imaging: Overcoming the Gibbs Artifact

Z.-P. Liang* and E. M. Haacke+
*BMRL and NCSA, UIUC, Urbana, IL; +CWRU, Cleveland, OH.

In Fourier MR imaging, it is often desirable to reduce the number of phase encoding measurements so as to reduce the imaging data acquisition time. However, this will cause Gibbs ringing in the reconstructed images, as evidenced near regions of high contrast. In this presentation, we propose a new parametric modelling method to overcome this problem. With this method, an image to be reconstructed is modeled by a parametrized generalized series. We will show that by properly building the basis functions using a priori function (for example, localized polynomials) weighted complex exponentials, an image can be very effectively represented in this model and thus the Gibbs artifact can be removed or significantly reduced. In addition, this new model has an advantage over the existing ones (for example, the LPA model by Liang and Haacke and the ARMA model by Smith et al) for improving image resolution and signal-to-noise ratio since the basis functions may be better chosen. Such models will eventually provide an optimal solution for overcoming the Gibbs artifact and improving signal-to-noise. This should prove particularly useful for handling very short data sets such as the case in 3D Fourier imaging.

TUESDAY p.m.

► **254** 16:45PM

HALF SCAN APPLICATIONS FOR MR IMAGING

M Terk, P. Colletti, H. Simon
LAC/USC Imaging Sciences Center

Halfscan technque has been demonstrated to be useful in the uncooperative patient where motion artifact is a problem. In this paper we analyzed our experience with such patients and have examined additional applications of half scan technique as applied to clinical imaging at 1.5 T with a Philips Gyroscan S15.

We have compared a series of phantom as well as clinical images obrtained with techniques utilizing Halfscan to those obtained with conventional imaging. The use of Halfscan enabled repetition times to be used beyond those typically employed. Half Scan technique was also used with other techniques typically felt to be too long in most clinical settings; these included: Inversion Recovery, 3D acquisitions, SPIR, Increased number of signal averages and use with MR angiography. Among the most promising applications was the use of Halfscan in abdominal imaging with increased number of signal averages. This sequence alllows for reduction of motion artifact with compensation for reduced signal to noise to doubling the number of signal averages.

Since June of 1989 we have examined 69 patients with Halfscan so far. Of these, the majority (N=61) have employed half scan to reduce motion artifact. Of these it is estimated that the Halfscan technique allowed for a diagnostic examination where none would be possible in 70% of the cases. Five cases were obtained in conjumnction with other techniques and comparison with conventional scans is available. The result of these studies indicate that the Halfscan technique can be utilized to improve image quality in the situation ofordered noise such as respiration when used in conjunction with an increase of the number of signal averages. We have also demonstrated the possibility of prolonging the TR to examine systems with long Tl relaxation times.

► **255** 16:57PM

PIXEL-BY-PIXEL DECOMPOSITION OF IN VIVO TRANSVERSE DECAY CURVES

T. Sandor, R.V. Mulkern, Z. Goldberg, A. Bleier, J. Tieman, F.A. Jolesz
Brigham and Women's Hospital
Boston, MA 02115

Image data sets of human brain have been generated with high field (1.5T) 128 echo CPMG imaging sequences using standard 2d-FT imaging methods. Data sets consisted of 128 magnitude calculated images reconstructed on 128X128 matrices. Echo spacings of 10 ms were employed. We have shown that (a) the sequences provide sampling of regional tissue transverse decay curves (TDC's) suitable for biexponential decomposition (eg, white matter, grey matter, white matter lesions, CSF), and (b) T2 values calculated with the imaging methods are in agreement with T2 data obtained with spectroscopic methods in simple phantoms. When the seed values for the non-linear fitting procedure are known, the biexponential decomposition of a single TDC on a Microvax II requires 20-30 seconds. This amounts to nearly 70 hours of computer time considering that, on average, the whole brain area contains up to 10,000 pixels. Clinical acceptability demands a dramatic reduction of the time of computation. To achieve this, the algorithm has been transported to a SUN 3/260 computer equipped with four array processors that can provide 20Mflops top speed each with double precision capability. In addition, an automated seed finding algorithm has been developed and incorporated. As final results, the computations provide four images: two images representing the amplitudes of the respective biexponential terms and two images corresponding to the short and long relaxation times. With these techniques, the speed with which pixel-by-pixel biexponential decompositions of CPMG image data sets proceeds at a rate of over 100 times faster than that performed currently on the Microvax. These speeds are required for testing the potential of biexponential TDC decompositions in terms of improving tissue specificity in a clinical environment.

► **256** 17:09PM

THREE-DIMENSIONAL MODELING OF AN ABDOMINAL AORTA PHANTOM FROM TWO MR IMAGES

JW Peifer*, DN Ku*, H Engels+, R Pettigrew#
School of Mechanical Engineering, Georgia Institute of Technology, Atlanta, GA 30332
+Philips Medical Systems; #Emory University

An approach is being investigated for creating three-dimensional computer models of vascular structures based on MR images from a limited number of projective views. The modeling approach exploits the fact that blood vessels form a tree-like structure of connected branches and organizes the three-dimensional (3D) vascular geometry into a format which facilitates quantitative evaluation. For example, the severity and extent of a stenosis could be compared to mean vessel diameter. Vascular structures are modeled as a collection of connected circular frusta. Three-dimensional geometry is found by identifying the same vessel features (centers, edges, and bifurcation points) in different views and backprojecting to the 3D solution. The views should be chosen to optimize visualization of the region of interest, and future plans are to extend the approach to optimize view selection for each of the branches in the arterial structure. Preliminary results have been generated by manually digitizing arterial features from just two views of a glass phantom of the abdominal aorta and seven branches scanned on a 1.5 Tesla Philips system at Emory University. Single slice (100 mm thick) spin echo magnitude images were acquired for coronal and sagittal views. The diameters of the vessels in the glass model were measured with calipers and compared with the computed diameters of the backprojected model. Vessel diameters measured in the glass model vary from 5.9 to 25.4 mm and differ from the diameters of the backprojected model by an average of 0.72 mm and by a maximum of 1.82 mm. From this 3D computer model, quantitative vessel diameter, length, and position are available for any subset of the vascular structure. Statistical evaluation of these quantities can also be performed to summarize branch characteristics. The model can be enlarged or shrunk, and critical branches can be isolated individually without image noise. Visualization is enhanced by displaying shaded renderings of the computer model from different perspectives or in cine loops. The advantages of this approach over tomographic reconstruction are that fewer scans are required and quantitative evaluation is facilitated by the data organization in the computer model. Future plans include optimizing view selection based upon arterial geometry and automating feature extraction.

JOINTS

MODERATORS: T. A. POWERS, M.D., E. E. KIM, M.D.

► **257** 15:45PM

MRI OF RHEUMATOID ARTHRITIS: ASSESMENT WITH GD-DTPA ENHANCED FAST IMAGING

Gerhard Adam, Franz Fenke, Klaus Bohndorf, Rolf W. Günther
Department of Diagnostic Radilogy, University of Technology, Aachen FRG

MRI has shown to be usefull in evaluation of rheumatoid arthritis. Nevertheless until now it was difficult or even impossible to differentiate between pannus formation and synovial fluid or the swollen synovium. Therefore we evaluated the use of Gd-DTPA enhanced MRI in diagnosis of rheumatoid knee joint arthritis. Examinations were performed on a 1.5 T imager using a knee coil with emit and receive capability. After a coronal scout view T1 weighted images (TR= 0.6 sec, TE= 22 msec) were obtained. Subsequently T2* weighted images were obtained using a FISP 3D sequence (a=40°, TR= 0.03 sec, TE= 13 msec). Finally T1 weighted gradient echo imaging was performed using a FLASH 2D sequence (a=70°, TR= 0.04 sec, TE= 10 msec) before and after intavenous application of Gd-DTPA. We examined 18 patients with rheumatoid arthritis and for control 8 patients with osteoarthritis. Previously all patients were examined clinically and with plain film radiography.
Medullary bone signal abnormalities were well delineated on precontrast T1 weighted SE sequences, while cartilage, ligamental and other soft tissue pathology and joint effusions were better visible on T2* and T1 weighted nonenhanced gradient echo scans. For more specific diagnosis of subcortical and articular pathology, including differentiation of cysts, synovitis, effusion and pannus, Gd-DTPA enhanced MRI was superior to plain scans and provided excellent delineation of the - even not swollen - synovium from pannus and other abnormalities. In osteoarthritic joints no or little signal increase occured while synovium of rheumatoid arthritic joints showed an high enhancement.
Gd-DTPA enhanced MRI is necessary and conclusice in assesment of rheumatoid arthritis.

TUESDAY p.m.

► **258** 15:57PM

MRI OF SHOULDER INJURIES IN PROFESSIONAL BASEBALL PLAYERS

JL Torres, DL Burk, P Marone, DG Mitchell, MD Rifkin, D Karasick
Thomas Jefferson University Hospital, Philadelphia, PA

MRI of the shoulder in professional baseball players with shoulder complaints or injuries offers a noninvasive, precise approach that is useful in defining the distribution and extent of a wide spectrum of exercise-related injuries ranging from stress injuries to complete rotator cuff tears. MRI exams of the shoulder were performed on 10 professional baseball players with throwing injuries. The studies were correlated with plain radiographs in all cases, arthrography in 2 players, and surgery in 5 players.

MR exams were performed with a 1.5 Tesla unit using a 4 inch loop gap resonator coil or a custom anterior 5 inch coil. Spin echo 600/20 axial localizer scans were followed by coronal oblique 2000/40/80 and 600/25 sequences. Sagittal SE 2000/40/80 images were then obtained for players with suspected rotator cuff injuries and axial SE 2000/20/80 images for players with suspected instability. Scans were performed using a 14 cm FOV, 2 signal averages, 128 x 256 matrix, 5 mm slice thickness, 1 mm interslice gap, and respiratory compensation to reduce motion artifacts. These patients provided a unique technical challenge, as most weighed at least 200 pounds and had broad shoulders.

Chronic trauma due to throwing produces a characteristic avulsion injury at the distal insertion of the supraspinatus muscle. In seven of these players, small cuff tears at the distal insertion, presumably caused by avulsion injury, were visualized prospectively on MRI. Five were confirmed at surgery and surgery is pending in two players. Arthrographic confirmation of tears was obtained in the first two players and plain films demonstrated bony defects at the greater tuberosity in all cases. In addition to rotator cuff disease, one player had severe posterior instability with posterior capsular thickening. One player with unusual axillary pain had a latissimus dorsi tear which healed with rest. In conclusion, MRI is a valuable noninvasive technique for evaluating the shoulder in athletes who are at risk for career-threatening injuries.

► **259** 16:09PM

Evaluation of rotator cuff disease and glenohumeral instability with MR imaging. Correlation with arthroscopy and arthrotomy in a large population of patients.
Michael B. Zlatkin M.D., Joseph P. Ianotti M.D. PhD., John L Esterhai M.D. Murray K. Dalinka M.D., Herbert Y. Kressel M.D., Kurt Spindler M.D.
Departments of Radiology and Orthopedics, Hospital of the University of Pennsylvania.

The diagnostic performance of Magnetic Resonance Imaging (MR imaging) in the diagnosis of rotator cuff disease and glenohumeral instability was evaluated in one hundred and six patients. Correlation with arthroscopy or arthrotomy or both was obtained in all patients. All studies were performed on a GE 1.5T scanner. A 5 inch surface coil pair was utilized in the majority of patients. A prototype single loop 7 inch anterior shoulder coil was utilized in 15 patients. Two separate protocols were utilized. For the rotator cuff coronal oblique spin echo (SE) short TR/TE and long TR/TE were emphasized. For the evaluation of glenohumeral instability axial short TR/TE images and/or gradient echo images with a large flip angle (70 degrees) as well as axial long TR/TE were emphasized.

The sensitivity and specificity of MR imaging in differentiating a complete tear from an intact tendon was 100% and 95% respectively. MR imaging consistently predicted the size of the rotator cuff tear. Atrophy of the supraspinatus muscle was highly correlated with the size of the complete chronic rotator cuff tear. The sensitivity and specificity of MR imaging in differentiating tendonitis from cuff degeneration/partial tear was 82% and 85% respectively and differentiating a normal tendon from tendonitis consistent with the impingement syndrome was 93% and 87% respectively.

In the evaluation of shoulder instability MRI also performed well. Hill -Sachs lesions were identified in 12/39 patients in this population and were confirmed arthroscopically. The sensitivity and specificity of MR imaging in the diagnosis of labral tears associated with glenohumeral instability was 88% and 86% respectively. MRI could visualize the capsule and glenohumeral ligaments well. Type II and III capsule insertions were highly correlated with recurrent glenohumeral dislocation. We conclude that MR imaging performs well in evaluating the spectrum of pathologic changes in rotator cuff disease and glenohumeral instability.

► **260** 16:21PM

MRI OF THE KNEE: CORRELATION OF RADIAL SCANS WITH SAGITTAL AND CORONAL SCANS
Robert C. Hewes, M. D. , Ted Miller, M. D.

Kettering Medical Center

Traditional MRI scans of the knee have been performed using Spin Echo T1 images in the sagittal and coronal plane. However, to optimally visualize the entire meniscus, radial scans centered on each condyle were developed. We use a fast scanning (GRASS) to optimally enhance the meniscal pathology. We now have done 100 cases where both radial fast scans and sagittal and coronal T1 weighted images were obtained of the knee joint. We evaluate the accuracy of diagnosis by seeking follow-up including surgical and clinical evaluation. We independently correlated the findings on the coronal, sagittal, and radial scans to determine accuracy by each scanning parameter and also the scan sequence that was most definitive of the abnormality. We will also present preliminary data of 3DFT MRI of the knee, correlated with the radial, coronal, and sagittal scans, as well. The scanning parameters to perform 3DFT scans comparable to direct radial fast scans will be discussed.

We find that the radial scans provide more complete evaluation of the meniscus and with the GRASS scans, the contrast is better to define meniscal pathology. 3DFT evaluation of the knee allows single scan acquisition in a timely manner and reconstruction as necessary in any desired plane.

► **261** 16:33PM

THE USE OF STRESS MRI VIEWS OF THE PATELLOFEMORAL JOINT TO EVALUATE PATELLAR ALIGNMENT

FG Shellock, J Mink, A Deutsch, G Slimp, J Fox, J Machek, J Dolinar
Cedars-Sinai Medical Center, Los Angeles, California

Instability of the patellofemoral joint may not be appreciated without the application of a loading force. Therefore, a special device was used to apply force to simulate weight-bearing during MRI in order to evaluate patellar alignment. A prototype device (MEDRAD, Pittsburgh) was used to apply loading forces ranging from 100 to 220±5lbs (depending on the subject's body weight) with the knees flexed at 20±5 degrees. T1-weighted axial images were obtained through both knees while the subject applied static isometric muscular force for 34 seconds. Eight normal subjects (16 joints) and 16 patients (26 symptomatic joints) clinically suspected of having patellar malalignment were evaluated. Normal subjects had patellae that were congruent with the femoral trochlear grooves. Of the 26 symptomatic joints studied, the stress view MRI study demonstrated the following: 10-lateral subluxation, 1- lateral tilt, 14-medial subluxation, 1-normal alignment. Stress MRI views also identified abnormal alignment in 4 asymptomatic joints. These data indicate that stress MRI views are potentially useful for identifying patellar malalignment.

► **262** 16:45PM

INVESTIGATION OF THE DISTAL INTERPHALANGEAL JOINT UNDER FLEXION

T.A. Carpenter, L.D. Hall, R.J. Hodgson.
Herchel Smith Laboratory for Medicinal Chemistry, University of Cambridge

The distal interphalangeal (dip) joint is susceptible to osteoarthritis. Investigation of the cartilage by magnetic resonance imaging is therefore of interest to assess its state during the course of the disease. Experiments were performed on unaffected dip joints in an attempt to assess the validity of such measurements. The behaviour of MR images of the cartilage was also examined at different angles of flexion of the joint.

Images were obtained using the standard spin echo protocol. Chemical shift selection was used to assess chemical shift artifact. Most of the work was at a field strength of 2T but controls were performed at 0.6T and fingers were aligned both along and perpendicular to the main magnetic field; these precautions were taken to try and identify susceptibility artifacts. Experiments were performed with two widely different types of probe, both of which were characterised before use to check for unexpected rf effects. Experiments were performed on normal healthy volunteers. Images were made at various angles of flexion, usually in the sagittal plane, although coronal planes were used. Various experimental parameters were used; most experiments used those chosen for maximal contrast.

The signal intensity across the cartilage was found to vary considerably. No explanation for this could be found in terms of susceptibility-, rf- or chemical shift-artifacts. The variation appeared to change consistantly depending on the angle of flexion of the joint. Such a change in the image upon flexion may be useful in assessing the state of the cartilage, as the behaviour might be expected to be modified in damaged tissue.

► **263** 16:57PM

HIGH RESOLUTION MRI OF THE ANKLE: PATHOLOGIC CONDITIONS

R Kier, S McCarthy, M Dietz, S Rudicel
Dept of Diagnostic Radiology, Yale University Medical School

Magnetic resonance imaging of the ankle is a new application that remains relatively unexplored. High anatomic resolution is required to depict the many small structures which can become involved in pathological processes.

Sixty patients with ankle pain or injury and inconclusive or negative radiographs have been studied with high resolution technique: A 17 cm standard linear transmit/receive coil operating at 1.5 T (GE Signa) yielding 3 mm slices with in plane resolution of 0.5 mm in three orthogonal planes. Both T1- and T2-weighted images are obtained, with a total study time of 40 minutes.

Pathologic conditions diagnosed prospectively include osteochondritis dessicans of the talus (12 cases), achilles tendonitis (4), plantar fasciitis (4), partial and complete achilles tendon tears (3), pre-achilles bursitis (2), cortical stress fractures (3), trabecular fractures (3), tarsal coalition (2), osteoid osteoma (1), hemangioma (1), and peroneal tendonitis (1).

We conclude that high resolution MRI of the ankle provides unique information allowing diagnosis of a variety of pathologic conditions not discernable with other techniques.

► **264** 17:09PM

SPONTANEOUS OSTEONECROSIS OF THE KNEE: UNENHANCED AND GD-DTPA ENHANCED MR IMAGING

Philipp Lang, Gunther Schwetlick, Michael Mauz, Alexander Kirgis, Roland Felix, Harry K. Genant
Dept. of Radiology, University Clinic Rudolf Virchow/Charlottenburg, Free University Berlin, Dept. of Orthopaedic Surgery, Oskar-Helene-Heim, Free University Berlin, Dept. of Radiology, University of California San Francisco

Spontaneous osteonecrosis of the knee is a rare disorder that may cause severe pain and progressive disability. The diagnosis is difficult since findings on conventional radiographs are subtle. Scintigraphy, on the contrary, lacks specificity, while arthroscopy is often negative.

We studied 7 patients with clinico-radiographically suspected spontaneous osteonecrosis of the knee prospectively with MR imaging (0.5T Siemens Magnetom, 1.5T GE Signa; *T1-WI:* SE: TR=400-500 msec, TE=20-30msec; GRE: TR=315msec, TE=14msec, $\theta=90^0$; *T2-WI:* SE:TR=1600-2500 msec, TE=90-240 msec). Four patients were also examined after i.v. administration of 0.1mmol/kg body weight Gd-DTPA (Magnevist, Schering, Berlin, Fed. Rep. of Germany) (*T1-WI:* GRE: TR=315msec, TE=14msec, $\theta=90^0$). MR imaging findings were correlated to conventional radiographs and scintigraphy (7 pts.) as well as histology (3 pts.).

Scintigraphically, increased radionuclide uptake was observed in 6 patients. T1-weighted MR images showed areas of decreased signal intensity in the medial (4 pts.) or lateral (3 pts.) femoral condyle. T2-WI demonstrated a uniform increase in signal intensity in 4 patients; in the other 3, signal increase was only observed in the periphery of the lesion. After i.v. administration of Gd-DTPA, contrast enhancement was demonstrated either in the periphery (2 pts.) or throughout the entire lesion (2 pts.). The areas with signal intensity increase on T2-WI and contrast enhancement after Gd-DTPA corresponded histologically to repair tissue and capillaries that were infiltrating the necrotic zone. We conclude that MR imaging is a sensitive and specific method in the diagnosis of spontaneous osteonecrosis of the knee. Demonstration of active repair tissue typical for osteonecrosis with use of T2-WI allows differentiation from degenerative arthritis of the knee. Gd-DTPA enhanced T1-WI MR imaging may replace unenhanced T2-WI in the patient who can not tolerate prolonged imaging.

BRAIN III

MODERATORS: G. BYDDER, M.B., Ch.B., K. R. MARAVILLA, M.D.

► **265** 15:45PM

SEVERE ANAPHYLACTOID REACTION AFTER IV GD DTPA

KL Weiss, HS Jhaveri
Department of Radiology, Albert Einstein College of Medicine

Serious contrast reactions following the IV administration of Gd-DTPA (Magnevist) although extremely rare, can occur. As yet, there has been no published case of a severe anaphylactoid reaction to Gd-DTPA.

After obtaining informed consent, 20 cc Gd-DTPA was infused slowly in an obese female to confirm and better characterize an apparent small extradural extramedullary cervical lesion. Her medical history was notable for asthma as well as an episode of respiratory distress following IV administration of an iodinated contrast agent for CT. The patient was removed from the scanner approximately six minutes post infusion complaining of mild facial and throat swelling, pruritus and difficulty breathing. Over the next five to ten minutes she became progressively short of breath with increasing hoarseness and labored speech until almost inaudible. Oxygen was administered by mask and 3 cc epinephrine 1:10,000 infused IV slowly with good response. Patient was transferred by EMS to the nearby ER where initial exam was notable for an edematous uvula and tongue obscuring visualization of the upper airway. Solucortef, subcutaneous epinephrine, vasonephrine, benadryl and humidified oxygen were administered. Subsequently, she was transferred to the ICU where further reduction in tongue and uvula edema were demonstrated allowing visualization of an edematous vallecula. Although speech had progressively improved, she was still noted to have a "hot-potato voice". Solucortef, benadryl and humidified oxygen were continued with further clinical improvement resulting in full resolution of her angioneurotic edema by her discharge two days later.

Although quite rare, radiologists must be aware of and be prepared for a potentially life-threatening anaphylactoid reaction following Gd-DTPA infusion. If the patient has a strong allergic history including prior contrast reaction, it may be prudent to raise the threshold for performing a Gd-DTPA study and also consideration should be given to premedication.

TUESDAY p.m.

► **266** 15:57PM

SIGNIFICANCE OF FULLY RELAXED ^{31}P-MRS OF BRAIN AND LIVER DISEASES

S. Naruse, Y. Horikawa, C. Tanaka, T. Higuchi, T. Ebisu, S. Ueda
Department of Neurosurgery, Kyoto Prefectural University of Medicine
and Meiji College of Oriental Medicine

Clinical ^{31}P-MRS are usually measured with 2 or 3 sec repetition time (Tr), which is too short to wait for full recovery of T_1 relaxation in each metabolite. Consequently, these spectra would not always represent real ones. Therefore, we measured the fully-relaxed spectra from the normal and various diseases in the brain and the liver with 15 sec Tr, and compared those data with ordinary 2 sec Tr spectra.

Total 158 examinations were done on 32 normal volunteers and 73 cases covering brain tumors, cerebral infarction, dementia, epilepsy, liver tumors, liver cirrhosis and hepatitis. Localized ^{31}P-MRS were obtained using ISIS method with a 1.5 T whole-body MRI/S machine (Gyroscan S15, Philips). Two spectra with different Tr values, 2 sec and 15 sec, were obtained in each examination. The VOI varied from 27 ml to 147 ml. The peak integrals of spectra were calculated by the curve-fitting program working on a SUN 3 work station.

Spectal patterns vary depending on the organs and diseases when the Tr is changed from 2 sec to 15 sec. In the normal adult brain, an increase of PCr is more prominent than any other peak on 15 sec-Tr spectra, while in the neonatal brain and brain tumors, the increase of PME is most prominent. On the 15 sec Tr spectra of liver tumors, the PDE peak increased in the hemangioma and the PME peak increased in the hepatocellular carcinoma compared to the normal liver. Similar changes occur in other diseases with degenerative or regenerative abnormalities. These changes come from the difference in T_1 value of each metabolite in each disease, that implies the changes of mobile condition of metabolites. Judging from our results that the changes occur predominantly on PME and PDE which relate to phospholipid metabolism, it is suggested that the fraction of freely-mobile precurssor of cell membrane increases in many diseases and immature tissue such as neonatal brain.

So far as using the short repetition time, the important data concerning the mobility of metabolite could not be detected. We should carefully take accout of relaxation times of each metabolite in ^{31}P-MRS analysis.

► **267** 16:09PM

Fundamental study of intravoxel incoherent motion imaging with three orthogonal gradients method

T. Ebisu, S. Naruse, Y. Horikawa, C. Tanaka, T. Higuchi, S. Ueda, K. Shimizu, N. Nishimura, S. Okamura, Y. Hashimoto
Department of Neurosurgery, Kyoto Prefectural University of Medicine; Department of Neurosurgery, Meiji College of Oriental Medicine; and Medical System Divisions, Shimadzu Corporation

Intravoxel incoherent motion (IVIM)imaging has recently been reported using additional gradient pulses in one way direction. However, in vivo molecules display microscopic random motions in three dimensional direction. Therefore, we have developed a magnetic resonance (MR) method to IVIM imaging by using gradient pulses in three orthogonal directions.

Phantoms containing water and acetone, normal volunteers and patients with cerebral infarction, brain edema and brain tumor were examined. MRI was performed at 1.0 T (SMT-100, Shimadzu Corp., Japan) with cardiac gating spin echo sequences, with or without additional IVIM gradients on the readout axis or three orthogonal axes. TE was 140 msec.

Three orthogonal gradients method was useful to demonstrate the difference of apparent diffusion coefficient (ADC) more clearly because of totally larger attenuation value (b value). The lesion of brain tumor, brain edema and infarction were demonstrated clearly according to difference of ADC value and moreover, resolving edema was also detected because of its lower ADC value. IVIM imaging will become useful clinically in future if the problem of artifacts of motion and eddy current are overcome.

► **268** 16:21PM

IMAGE-GUIDED LOCALIZED PROTON AND PHOSPHORUS MRS OF INTRACRANIAL TUMORS - A USEFUL DIAGNOSTIC TOOL ?

W. Heindel, J. Bunke, W. Steinbrich, G. Friedmann
Department of Radiology - University of Cologne Medical School, D - 5000 Köln 41, West Germany

Complementary to morphological studies by magnetic resonance imaging (MRI), localized *in vivo* NMR spectroscopy (MRS) opens the way to a biochemical characterization of brain tumors. This study was designed to evaluate the diagnostic usefulness of image-selected proton and phosphorous MRS in patients suffering from intracranial tumors.

A 1.5 T whole body MR system (Philips, Gyroscan S15) operating at 64 MHz for ^{1}H and 25.9 MHz for ^{31}P was used. ^{1}H MRI preceded spectroscopy in order to judge the tumor macroscopically and to define the volume of interest (VOI) within the lesion. Volume selection to obtain water-suppressed ^{1}H spectra was achieved by a spatially selective 90^{0}-180^{0}-180^{0} spin echo sequence. Typical spin echo times were 272 (or 136) ms, repetition time 2s. For ^{31}P a modification of the "Image-Selected in Vivo Spectroscopy (ISIS)" - sequence utilizing adiabatic inversion and excitation pulses was used (repetition time 3s).

In primary intracranial tumors ^{31}P MRS demonstrated in particular reduced phosphodiesters (PDE), but also reduced phosphocreatine (PCr) signals and normal or alkaline pH values. ^{1}H spectra revealed an increased Cho/(P)Cr ratio, while N-Acetyl Aspartate (NAA) was reduced or absent. In contrast with an oligodendroglioma, most astrocytomas and glioblastomas showed increased levels of lactate. In some tumors, calculation of tissue pH from ^{31}P indicated an alkaline environment, though lactic acid was demonstrated by ^{1}H. Similar observations in animal studies have been interpreted as evidence for an active regulation of intracellular pH.

Spectra from meningiomas demonstrated the most obvious differences: In ^{31}P the PCr peak decreased below the level of ATP, the phosphodiester signal was reduced and tumor pH was often within the alkaline range. In ^{1}H neither NAA nor (P)Cr were detected in one patient, while the Cho/(P)Cr -ratio was increased in another patient. In both cases a duplett at 1.47 ppm was observed, which could be assigned to the amino acid alanine.

In conclusion, the results of this clinical study show that localized ^{31}P MRS and ^{1}H MRS reveal complementary metabolic information on human brain tumors, which might improve the diagnostic specificity of MRI.

► **269** 16:33PM

PRELIMINARY RESULTS OF in vivo P-31 MRS IN ALZHEIMER'S DISEASE
Y Mashima, H Yamada, M Ichinose, M Tanno, K Nagasawa* and S Naruse**
Tokyo Metropolitan Geriatric Hospital, YMS*, Kyoto Pref. Univ. of Med.**

Recent in vitro P-31 MRS(magnetic resonance spectroscopy) demonstrated increased level of PME(phosphomonoesters) and/or PDE(phosphodiesters) in Alzheimer's disease. Reported reuslts ,however,are still controversial. No in vivo MRS study has disclosed , so far, any characteristic MRS pattern in this disease.

In the present paper brain in vivo P-31 MRS study was conducted in Alzheimer's disease as well as in normal controls using a surface coil and non-localized SPECREC techniques. MRS data were obtained with two different repetition times, TR=1 sec. and TR=15 sec. Areas of beta-ATP and PME or PDE were measured. Ratios of PME/beta-ATP at TR of 1 sec. and at TR of 15 sec. were compared each other.

PME/beta-ATP ratio was not increased in Alzheimer's disease(0.41) compared with normal controls(0.69) at short repetition time(TR=1 sec.). However the peak of PME was more enhanced in Alzheimer's disease at long repitition time(TR=15sec.). Ratios of PME/beta-ATP at TR=15sec. were 2.99 in Alzheimer's disease(n= 2) and 0.78 in normal controls(n= 3).

These results may suggest the presence of factors making T1 relaxation time of PME prolong and possible alteration of metabolism of phosphoglicerides and phospholipids in Alzheimer's disease. From preliminary results the P-31 MRS finding might become an in vivo marker of Alzheimer's disease.

TUESDAY p.m.

► **270** 16:45PM

OPTIMIZATION AND CLINICAL EVALUATION OF 3-D TIME-OF-FLIGHT ANGIOGRAPHY IN CONGENITAL VASCULAR MALFORMATIONS OF THE BRAIN
G. MARCHAL, H. BOSMANS, L. VAN FRAEYENHOVEN, G. WILMS, P. VAN HECKE, C. PLETS, A.L. BAERT
Department of Radiology, University Hospitals K.U. Leuven

During the last 8 months the clinical value of 3-D Time-of-Flight (TOF) MR angiography has been prospectively evaluated in 26 patients with congenital intracranial vascular lesions, 13 arteriovenous malformations (AVM) and 13 venous angiomas (VA). All were studied with a 1,5 Tesla Siemens Magnetom with either a FLASH or FISP 3-D sequence with velocity rephasing in the slice select and frequency encoding directions (TR/TE=40/10msec, angle=20°).

In the initial phase of the study the entire region of interest was imaged with one single large acquisition volume (60 - 120 mm slab). Later on, the angiograms were obtained with adjacent but slightly overlapping thin 30 mm 3-D slabs. This last technique clearly improved the vascular detail. Gadolinium-DTPA was given IV in 17 patients and a dose of 0,1 mmol/kg. Gadolinium slightly improved the visualization of the veins but not of the arteries. MR angiograms were compared with the available conventional angiograms and MR studies. In AVMs the topography of the nidus was equally well appreciated on the MR as on the conventional angiograms. However, in 5 of 15 patients the hyperdynamic afferent arteries were incompletely shown because of incomplete rephasing. In 3 patients the venous drainage also was incompletely visualized. Compared to the conventional MR studies, MR angiography offered the same detection rate but a better anatomic insight.

12 of the 13 VAs could also be identified. Detailed imaging necessitated however Gadolinium injection and thin slab acquisition.

► **271** 16:57PM

Varied MR Appearance of Autism: Report on Fifty Pediatric Patients Having the Full Autistic Syndrome

MA Nowell, DB Hackney, A Muraki, M Coleman
MR Imaging of Prince George's County, Greenbelt, Maryland

To date, attempts to characterize the MR findings in autistic patients have been based upon either a very small study population or upon an older, adult study group. This study of 52 pediatric patients was undertaken to determine whether distinct morphologic changes are seen in children and therefore that the abnormalities are developmental in nature or are found more consistently in adult patients and thereby represent later sequelae to the autistic state.

Fifty-two autism patients ranging in age from two to eighteen years were imaged on a 0.5 Tesla (Picker) system using T1W, T2W spin echo and short tau IR (STIR) techniques. All patients were diagnosed as having the full autistic syndrome, were followed at the Center for Autism Research in Washington, D.C., and were not maintained on chronic sedation. The following morphologic characteristics of the brain were evaluated: ventricular size, brain asymmetry, amygdala size, fourth ventricular size, midsagittal vermian height and vermian shape.

No statistically significant correlation was found to exist between the morphologic findings and clinical presentation, course or laboratory analyses. The reported MR findings did not present a characteristic pattern capable of predicting either the presence or severity of autism in pediatric patients.

Insofar as the constellation of MR findings in this group of fifty pediatric patients was highly variable we advise caution in the interpretation of MR images of autism patients. Autism is a heterogeneous disease entity with multiple clinical subgroups and does not present with a uniformly consistent radiologic picture.

► **272** 17:09PM

Pediatric CNS- imaging:Clinical correlation of focal white matter abnormalities on MRI

Franz Ebner,M.D., Roland Einspieler,M.D.Michael Millner,M.D., and Erwin Justich,M.D.
Karl Franzens University,Departments of Radiology and Pediatrics
A-8036 Graz,Austria

Focal abnormalities of signal intensity in the brain white matter are a frequent finding in MR imaging in elderly patients(1-4).The prevalence and clinical significance of focal white matter abnormalities in the age groups from 0 to 18 years are less clear(5-7).In the time period from I/87 to I/89 624 consecutive patients beneath the age of 18 years were referred to brain MR in order to evaluate various neurologic deficits.Sex-ratio:349 were male (55,9%) and 275 were female(44,1%).Children who presented with delayed myelinisation or hypoxic periventricular leukomalacia were not included in the present study.Imaging was performed using a 1.5 T superconductive magnet system (Gyroscan S 15 / Philips Company).Inversion recovery and spin echo pulse sequences with very long TR/TE´s (3500/100,150 msec) in infants were employed.When ever possible imaging was performed without any sedation.Mild sedation was achieved by chloral-hydrate,50-80 mg/kg body weight.In some cases general anaesthesia was performed with a premedication of Pethidin-hydrochloride,1 mg/kg,Promethacine,1mg/kg, and 0.01 mg Atropine/kg.General anaesthesia used minimal dosage NO_2,(5 l), O_2 (2,5 l) and 0.4% Halothane.Monitoring in everycase was enabled by ECG and pulse oxymetry. In infancy (age 0 to 2 years) 2 / 81 patients(2,5%) exhibited focal brain white matter abnormalities(WMA). In childhood between 3 and 9 years 8 / 179 children had focal WMA (4,5%).The most frequent etiology in this group was encephalitis (n=4):measles,herpes,haemophilus,candida albicans. In group III (age 10 to 14 years) 17 / 162 children (10,5%) had focal WMA, six of them were proved clinically to suffer from multiple sclerosis(MS).All of them had,according to Poser´s classification,clinical definite or laboratory supported definite MS. In 5 children the presence of WMA was associated with clinically long standing partial or generalized epilepsy. In adolescence from 15 to 18 years 26 / 202 patients demonstrated brain WMA on MR (12,9%).Again multiple sclerosis was the most frequent etiology. Clinical correlation of focal WMA: Metabolic disorders(n=8), tuberous sclerosis(n=1), delayed myelination(n=2), partial epilepsy(n=4), generalized epilepsy(n=5), encephalitis(n=5), miliar tuberculosis(n=1), multiple sclerosis(n=17), histiocitosis X(n=2), apnoe syndromes(n=5), trauma(n=3), methotrexate therapy(n=3).

CONTRAST II

MODERATORS: E. C. UNGER, M.D., D. C. THICKMAN, M.D.

► **301** 10:42AM

DYNAMIC MRI OF TUMOR WITH GADOLINIUM-DTPA

Y Mashima, H Yamada, M Ichinose, M Tanno, H Watanabe* and S Naruse**
Tokyo Metropolitan Geriatric Hospital, YMS* and Kyoto Pref. Univ. of Med.**

In order to evaluate clinical usefulness of dynamic MRI for the diagnosis of tumor, following studies were conducted utilizing a superconducting MRI system(GE, SIGNA; 1.5 T, performance type) in eleven patients including 3 patients with brain tumor, 3with liver tumor, 2 with pancreas tumor, 2 with kidney tumor and one with adrenal tumor.

Dynemic MR images were obtained using GRASS(gradient recalled acquisition in the steady state), in which following parameters were selected: TR=25-100 ms, TE=12-15 ms, Flip angles=30-60 degrees. The scan time of one image is about 6 seconds. Pre-scan was made only once before taking a pre-contrast image to determine transmitter and receiver attenuations. With the same attenuation values, thereafter, 10 images were successively obtained after intravenous bolus injection of Gadolinium-DTPA(0.1 mmol/kg). Thus, we are able to obtaine TICs(time-intensity-curves) from ROVs, set on tumor and surrounding regions. Findings obtained from dynamic study were compared with images using other pulse sequences(T2 weighted, T1 weighted proton density and enhanced t1 weighted).

These dynamic MR images revealed clearly the vascular perfousion(hyper- and hypo-) & tumors. Variety of structure of tumors were distinctly observed on these images. The TICs of tumor showed similar vascular pattern to time density curves on X-ray CT.

From these results, dynamic MRI with Gadolinium-DTPA in concluded to be a useful study for the diagnosis of both tumor morphologh and vascularities.

► **302** 10:54AM

Ytterbium-diethylenetriamine Pentaacetic Acid (Yb-DTPA) as a Novel Contrast Agent in Magnetic Resonance Imaging (MRI).

Susanta K. Sarkar, Robert E. Rycyna, Robert E. Lenkinski* and Lewis B. Kinter
Smith Kline & French Labs, 709 Swedeland Road, King of Prussia, PA 19406 and
*Dept. of Radiology, Univ. of Pennsylvania, Philadelphia, PA 19101.

Recently it has been reported (1) that the contrast generated in the MR image with the administration of Gd-DTPA is not only due to the dipole-dipole interaction but also arises from the differences in susceptibility between the capillaries containing the contrast agent and the surrounding tissue. Therefore, it would be desirable to have contrast agents which work with one or the other mechanism.

In order to separate effects due to T_1 relaxation and susceptibility differences, we chose a lanthanide, Yb-DTPA, which has negligible T_1 relaxivity. However Yb-DTPA has substantial molar susceptibility. We have studied the effects of Yb-DTPA on rat kidney images and find that susceptibility induced spin dephasing is responsible for the signal intensity decrease observed in T_2 weighted images. As expected, this decrease in intensity is more pronounced in gradient recalled echo images.

Figure 1 shows a plot of the ratio of intensities, obtained from gardient recalled echo images, of rat papilla to muscle as a function of time, following administration of Yb-DTPA. Results will be presented to monitor renal function using this "renal clearance curve" obtained by Yb-DTPA enhanced fast imaging.

References:
1. A. Villringer, et al., Magn. Reson. Med. 6, 154, 1988.

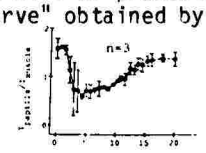

Time (min) after injection of Yb-DTPA

Fig 1. Ratio of intensities of Rat Papilla to Muscle obtained from Yb-DTPA Enhanced Gradient Recalled Echo Images.

► **303** 11:06AM

Contrast-Enhanced MRI of Reversible Ischemic Injury in Rat Brain using Iron-Dextran

KP Aicher, ME Moseley, BL Engelstad, and DL White
Contrast Media Laboratory, Department of Radiology, University of California, San Francisco

A problem in the application of contrast agents to imaging of ischemic tissue is that the flow restriction is often not complete, allowing the agent to equilibrate in both ischemic and normal regions and obscure the difference between them. Contrast agents whose effects are based on flow or perfusion, rather than on concentration alone, potentially could alleviate this problem.

Iron-dextran has been used as a long-lived, paramagnetic intravascular contrast agent to provide additional structural detail in the T2-weighted MRI of normal rat brain [1]. About one-half of the overall intensity change was attributed to flow (or perfusion) effects, apparently arising from magnetic susceptibility changes. This work has been extended to a model [2] of reversible ischemia in the rat brain.

Imaging was performed on a GE CSI-II 2 Tesla Imager with self-shielding gradient coils. Diffusion images [3] were first obtained to confirm ischemia in the right hemisphere [2]. Pre- and post-contrast (1.0 mmole Fe/kg Imferon™ iron-dextran) T2-weighted spin-echo images (TR 2800; TE 100) then were obtained. After reflow, additional sets of T2-weighted and diffusion images were obtained.

As reported [3], diffusion MRI revealed injuries as hyperintense areas that were not apparent on ordinary T2-weighted images ($SI_{inj.}/SI_{un\text{-}inj.}$ = 1.22 ± 0.02 and 1.05 ± 0.04, resp.). After administration of Iron-dextran, ischemic regions were visible as relatively hyperintense regions ($SI_{inj.}/SI_{un\text{-}inj.}$ = 1.20 ± 0.05). Upon reflow, the intensity of the injured hemisphere decreased ($SI_{inj.}/SI_{un\text{-}inj.}$ = 1.09 ± 0.04). Euthanasia without reflow caused the relative hyperintensity of the injured region to decrease ($SI_{inj.}/SI_{un\text{-}inj.}$ = 1.10 ± 0.04), indicating that flow effects were operative.

These results suggest that a combination of flow-sensitive contrast agents and pulse sequences can aid in the assessment of ischemia. It is likely that this technique can be made more sensitive by the use of long-lived superparamagnetic contrast agents.

1. DL White, et al., Soc. Magn. Reson. Med. 8th Ann. Meeting Abstr., p809 (1989).
2. EZ Longa, et al. *Stroke* 1989;**20**;84-91.
3. J Mintorovitch, et al., Soc. Magn. Reson. Med. 8th Ann. Meeting Abstr., p1002 (1989).

► **304** 11:18AM

EFFICACY OF PHOSPHONATE-MODIFIED GdDTPA AS TARGETED MRI CONTRAST AGENT.

I. K. Adzamli, M. Blau
Radiology Department, Harvard Medical School, Brigham & Women's Hospital, Boston; and Department of Radiology, Univ. of Mass. Medical Center, Worcester, MA.

Paramagnetic complexes of bifunctional ligands of the type DTPA--Link--Diphosphonate are under development in our laboratories for use as MRI contrast agents in the detection of infarcts, ischaemia and other incidences of soft-tissue calcification.

To demonstrate the usefulness of this class of agents, T1-weighted spin echo images were acquired of two different experimental lesions in rats with and without the contrast agent. The agent used in this assessment is GdDTPA modified by 1-hydroxy-3-aminopropyl-1,1-diphosphonate coupled to one of the carboxylates. Control sets of rats GdDTPA or no agent. Lesions were I: Myocardial infarcts induced by subcutaneous injection of isoproterenol, 100mg/kg, 24hrs prior to the intravenous injection of contrast agent, 200umol/kg; II: Ischaemia was induced in skeletal muscle by application of a torniquet to restrict blood flow to the hind leg for 3hrs and then released 24hrs prior to injection of contrast agent, 200umol/kg. A period of 3hrs elapsed before imaging to allow unlocalized agents to clear from the system. MR parameters were TR = 520ms, TE = 20ms, 2mm-thick slices, 12 acquisitions. Radiolabels were used to determine the duration of target localization.

Images (to be shown) of sections through infarcted rat heart show contrast between infarcted and normal tisse at 3hrs with modified contrast agents which was not evident in the two sets of controls. Similarly, retention of the modified agent in ischaemic tissue was demonstrated on images. The experiments using radiolabels detected the modified agent at target tissues for up to 6 weeks. Current work is aimed at shortening target retention.

The modified complexes serve as target-specific contrast agents and are effective in delineating the targeted lesions long after GdDTPA has cleared. The need to quickly image in the presence of declining concentrations of GdDTPA no longer exist with this targeted agent. It will also be useful in clearly delineating infarct size, since one can afford to wait for zero background.

► **305** 11:30AM

Influence of GdDTPA on Regional Transverse Decay Curves (TDC's) in Perfused Rabbit Kidneys

R.V. Mulkern, M.E. Stromski, H. Brady, S. Gullans, F.A. Jolesz
Brigham and Women's Hospital, Boston, MA 02115

The multiexponential behaviour of TDC's in tissue is now well established. The precise nature of TDC components, however, remains poorly understood. By coupling a physical model of water exchange with biexponential TDC's, a fuller understanding of TDC components may be obtained. In this study, we have applied a recently developed 128 echo imaging sequence to study the effects of GdDTPA on regional TDC's in perfused rabbit kidneys. Kidneys from white New Zealand rabbits (n=4) were perfused with Krebs-Henseleit solution and imaged on a 1.9T, 30 cm magnet. Clear differentiation between inner medulla, outer medulla, and cortex was provided by the images. TDC's from voxels within all three tissue types were extracted and fit to biexponential functions, yielding two "apparent" relaxation rates and volume fractions. The fraction of the quickly decaying component was observed to decrease from cortex to inner medulla. The addition of 0.5 mM GdDTPA to the perfusate caused an increase of this volume fraction and moderate increases in the two relaxation rates. A two-site exchange model (Zimmerman and Britton, J. Phys. Chem. **61**:1328;1957) was used to estimate "real" water volume fractions and exchange rates between these fractions from the NMR data. Calculations were based on the assumption that the perfusate T_2 represented the smaller of the two relaxation times in the **absence** of water exchange. A typical set of results obtained from the data analysis is provided. The "real" water volume fraction of the fast relaxing component g, and the water exchange rate from this fraction k, are shown before and after GdDTPA addition.

	Pre-GdDTPA		**0.5 mM GdDTPA**	
	g	k (Hz)	g	k (Hz)
Cortex	0.88 ± 0.02	0.21 ± 0.02	0.94 ± 0.02	0.04 ± 0.02
Outer Medulla	0.81 ± 0.04	0.44 ± 0.10	0.86 ± 0.02	0.17 ± 0.07
Inner Medulla	0.71 ± 0.03	0.69 ± 0.14	0.87 ± 0.04	0.06 ± 0.03

Within the assumptions of the model, GdDTPA appears to lower the water exchange rates from compartment g. These results demonstrate the feasibility of testing models of water exchange in tissue with TDC's obtained from **imaging** techniques.

► **306** 11:42AM

WEDNESDAY a.m.

ARTIFACTS AND CONTRAST AGENTS

T.BACH-GANSMO A.ERICSSON A.HEMMINGSSON
UPPSALA AKADEMISKA HOSPITAL, UPPSALA, SWEDEN

Paramagnetic contrast agent used in regions prone to motion may be an additional source of noise, reducing the quality of the examination. Susceptibility induced artifacts created by negative contrast agents are concentration dependant and may be avoided.

The occurence of artifacts originated by moving contrast agents have been studied in vitro.

The positive contrast agent, $CuNo_3$, gave heavy artifacts of high and low signal intensity . Particularly the occurence of low signal artifacts is interesting.
High concentrations of magnetite (1mg Fe/ml) gave ghost artifacts from the region adjacent of the contrast agent, both of high and low signal intensity. Intermediate concentrations of magnetite (0,2 mg Fe/ml) gave rise to diffuse banding of the original image, whereas low concentrations (0,1 mg/ml) gave no artifacts. This concentration is however high enough to create a total signal void.

The other aspect is that when the moving structure is out of the imaging plane, the positive contrast agent did not induce artifacts. Susceptibility induced artifacts where however apparent with high concentration magnetite, even when they were moving outside the slice selected.

► **307** 11:54AM

GADOLINIUM-DTPA POLYLYSINE : A PROMISING AGENT FOR MR-ANGIOGRAPHY

GJ Marchal, H. Bosmans, P. Van Hecke, P. Aerts, P. Vanhoenacker, A.L. Baert and U. Speck*
Depart. of Radiology, Univ. Hospitals K.U. Leuven, Belgium and Schering AG*, Berlin, FRG

Flow in high resistance peripheral vessels such as in the lower limbs, is characterized by a short period of positive flow during systoly and almost no flow during diastoly.

Hence 3-D time-of-flight sequences for MR angiography are only successful when applied in a plane perpendicular to the vessel course. On the contrary, when applied in a plane parallel to the vessel, this method suffers from the rapid saturation of the inflowing spins. A solution to this problem is the application of successive thin 2-D slices perpendicular to the vessel, however at the expense of an increased acquisition time.

Another approach is to selectively enhance the T1 relaxation rate of the blood to prevent saturation. Although Gadolinium-DTPA somewhat improves visualization of the veins in brain angiograms, its efficacy is hampered by its rapid extravascular diffusion.

Gadolinium-DTPA Polylysine is a new Gadolinium derivate with blood pooling capability. Used at doses between 0,02 and 0,08 mmol/kg it produced excellent time-of-flight angiograms in the rabbit. Images were acquired with a 3-D FISP sequence, with TR/TE = 40/10 msec, angle 20°, acquisition volume 200 x 200 x 60 mm^3 and 64 partitions. Submillimeter arteries and veins were visualized over the entire length of the posterior limbs.

If on-going studies confirm the low toxicity of this new agent, Gadolinium-DTPA polylysine could offer a totally new approach to MR angiography.

CINE/DYNAMIC MRI

MODERATORS: L. AXEL, M.D., Ph.D., M. SILVER, Ph.D.

► **308** 10:30AM

MR TRANS-MITRAL VALVE AND PULMONARY VENOUS FLOW MEASUREMENT

RH Mohiaddin, M Amanuma, DB Longmore
The National Heart & Chest Hospitals, London UK

Left ventricular diastolic dysfunction is now recognised as a significant cause of cardiac symptoms even in patients with apparently normal systolic ventricular function. Trans-mitral and pulmonary venous flow are important indexes in the evaluation of diastolic function. Cardiovascular magnetic resonance imaging is a totally noninvasive technique and provide excellent anatomical images as well as valuable functional information. The aim of this work is to measure trans-mitral blood flow velocity, pulmonary venous flow velocity and the volume of pulmonary venous flow in 20 healthy volunteers. A Picker International Vista MR2055 machine operating at 0.5T was used. Velocity mapping was performed using the Field Even Echo Rephasing sequence (FEER) with and without velocity compensation to measure trans-mitral valve and right lower pulmonary venous flow velocity profiles in an oblique plane parallel to the horizontal long axis of the heart. The sequence was repeated 31 times per cardiac cycle with a 1 msec gating delay and a repeat time covering the entire ventricular systole, ventricular diastole and atrial systole. Using the same technique quantitative blood flow measurements were made in a planes perpendicular to the right (RLPV) and left (LLPV) lower pulmonary veins. Flow (ml/sec) was calculated from cross sectional area (cm^2) and mean velocity (cm/sec). Normal diastolic trans-mitral flow shows two positive peaks, one during early ventricular diastole and the other during atrial contraction. Peak mitral flow velocity in early diastole was (68±12) cm/sec, and in atrial systole (39±10) cm/sec. The ratio of peak mitral flow velocity in early diastole to that at atrial contraction was (1.9±0.6). Pulmonary venous flow showed two positive peaks, one during ventricular systole and another in diastole. A small back flow during atrial systole was noticed. Peak systolic velocity in the RLPA was (41.3±11) cm/sec, Peak diastolic velocity was (36.0±10) cm/sec, peak back flow velocity was (12±2) cm/sec. The mean flow index were (13.0±3.8) ml/sec/ m^2 and (11.9±2.6) ml/sec/m^2 in the RLPV and LLPV respectively. Cine magnetic resonance blood flow imaging provides a non-invasive technique for assessing trans-mitral and pulmonary venous haemodynamic which is of importance in the study of diastolic function of the left ventricle. The clinical use of this technique is promising.

► **309** 10:42AM

Renal artery stenosis: evaluation by magnetic resonance arteriography and quantification of renal venous flow

Robert R. Edelman (1), Ducksoo Kim (1), Henri Hoogewoud (2), Heinrich Mattle (1,3), Craig Kent (4), Dennis Atkinson (5). From (1) the Department of Radiology, Beth Israel Hospital, Boston, MA, (2) Hôpital Cantonal, Fribourg, Switzerland, (3) the Department of Radiology, New England Deaconess Hospital, Boston, MA, (4) Deptartment of Surgery, Beth Israel Hospital, Boston, MA, and (5) Siemens Medical Systems, Iselin, NJ

Introduction: Renal artery stenosis is a significant etiology of systemic hypertension. Currently, no noninvasive method is entirely satisfactory for the diagnosis of this condition. We have studied the feasibility of using MR angiography and flow quantitation to detect and characterize renal artery stenosis in a group of 25 patients, and correlated the results with conventional angiography. In additional subjects renal flow was assessed by measuring flow through the renal veins.

Methods and subjects: A series of breath-hold, two-dimensional flow-compensated gradient-echo images are obtained in multiple planes, spanning the kidneys and aorta. The images are processed with a maximum intensity projection algorithm to create projection images. The individual images and MR angiograms were assessed without knowledge of the clinical history or results of conventional angiography. Studies were graded for presence and severity of renal artery stenosis, number of renal arteries, and aortic plaque. Flow through the renal veins was computed by using a bolus tracking method for quantifying flow velocities; cross-sectional area was measured on oblique flow-compensated gradient-echo images.

Results: There was good correlation between MR angiography and conventional angiography. Normal subjects showed contiguous bright signal in the renal arteries. Renal artery stenosis was indicated by vessel narrowing and/or focal or diffuse signal voids. Renal artery stenosis of moderate or severe degree was correctly graded by MR in all subjects. Renal artery stenosis was overgraded in 4 of 55 renal arteries. The number of renal arteries was correctly determined in all subjects. Renal flow measurements were rapid and could be obtained consistently. Correlation of flow measurements with severity of renal artery stenosis, serum creatinine levels and other patient parameters will be presented.

Conclusion: In this preliminary study, MR angiography was an accurate means for the noninvasive evaluation of renal artery stenosis. Renal flow measurements can also be obtained. MR has the potential to be a useful diagnostic tool in the work-up of renovascular hypertension and other pathologies involving the renal arteries.

► **310** 10:54AM

GRADIENT ECHO MAGNETIC RESONANCE AORTOGRAPHY: INITIAL CLINICAL EXPERIENCE IN TWENTY-NINE PATIENTS

Peter Lanzer, M.D., Gary Gross, M.D., Susan Mulligan, M.D. Gerald Pohost, M.D.
University of Alabama, Birmingham, AL.

To assess the clinical potentials of gradient echo magnetic resonance aortography (MRA) 29 symptomatic males were evaluated (mean age 60.9 $\pm$7 years) with peripheral vascular disease documented by x-ray aortography (A). In each patient aortograms were assessed to determine clinical management and the severity of aortic lesions using calipers. A identified the need for forty-eight revascularization interventions (RI) and MRA identified fifty-one RI. A and MRA agreed on forty-three interventions, three and six RI respectively, were identified either by A or MRA, and two RI were different between methods. Based on A and MRA, identical clinical management was suggested in twenty patients.

The correlation coefficient between the severity of lesions estimated by A and MRA was r = 0.71 for all 415 paired measurements and ranged between r = 0.10 and r = 0.92 in subsets of specific vascular segments.

The results indicate that gradient echo magnetic resonance angiogrpahy provides clinical information similar to A in approximately two-thirds of patients with peripheral vascular disease considered for revascularization. The variable definition of the severity of stenoses is responsible for the differences in clinical interpretation between the two angiographic methods. More extensive experience is needed to better characterize the observed differences and to determine the clinical value of this evolving imaging technology.

► **311** 11:06AM

CLINICAL ASSESSMENT OF STENOSES USING SHORT ECHO CINE MR VELOCITY MAPPING

PJ Kilner, DN Firmin, RSO Rees, RH Mohiaddin, DJ Pennell, SR Underwood, DB Longmore
National Heart and Chest Hospitals, London, England.

We used very short echo time (TE=6ms and TE=3.6ms) Field Even Echo Rephasing (FEER) sequences for phase shift cine velocity mapping of post stenotic jet velocities in a total of 23 patients. Diagnoses were: Stenosed valved conduit to pulmonary artery (11), arterial anastomosis after single lung transplant (8), coarctation of aorta (3) and mitral stenosis (1).

Peak jet velocities up to 3.8m/sec were recorded. In 19 of the 23 cases signal was obtained and velocity measured in the jet core region, with only the most turbulent para- and post-jet regions suffering signal loss. Signal loss prevented jet velocity measurement in in only four patients, two with coarctation and two with stenosed conduits. In these cases accurate alignment of the image plane through the jet core was in question. Peak pressure gradient estimates were made from MR velocity measurements by applying the modified Bernoulli equation. For four of the significantly stenosed pulmonary conduit cases, corresponding catheter or echo Doppler gradient estimates are available, as follows: MR 27 - D 30, MR 57 - C 54, MR 40 - D 45, MR 34 -D 27 (D=Doppler, C=catheter, estimated or recorded pressure gradients in mms Hg).

We conclude that use of sequences with very short echo time has largely surmounted the problem of signal loss which, up to now, has prevented MR jet velocity measurement. This has considerable potential importance as a non invasive means for assessment of stenoses at locations inaccessible to ultrasound, but inaccuracies due to malalignment, signal loss and partial volume effects must be recognised and avoided.

► **312** 11:18AM

MR MORPHOLOGICAL AND FLOW IMAGING IN PERIPHERAL VASCULAR DISEASE
RH Mohiaddin, C Sampson, Firmin DN, Underwood SR, Longmore DB
The National Heart & Chest Hospitals, London UK

Atherosclerosis is a chronic, progressive and widespread disorder and as there is a discomfort and risk of complications with invasive procedures, it was only natural that alternative, non-invasive methods should be developed. The disease produces problems by either reducing blood flow due to the development of a high grade of stenosis and total occlusion or the release of emboli from ulcerated plaques. Clinical symptoms occur when the reduction in blood flow is greater than the compensatory vasodilatation of distal arterioles. Techniques for detecting atheroma depend either on imaging the diseased vessels or on assessing the effect of stenosis on pressure and flow. Magnetic resonance imaging (MRI) is a totally non-invasive technique and has been used to identify atherosclerotic plaques and assess their effect on blood flow and blood flow velocity. The aorto-iliac region of 10 normal subjects and 13 patients with documented peripheral vascular disease has been studied. For the anatomical study multi-section spin- echo (TE 40ms) images were acquired in a transaxial as well as oblique planes covering the infrarenal abdominal aorta and the common iliac arteries. In all the studies a slice thickness of 5mm was used. The resulting images were compared with the a corresponding radiological angiogram. The velocity map technique was used to measure velocity profiles in an oblique plane containing the abdominal aorta, the right and the left iliac arteries. Using the same technique quantitative blood flow measurements were made in the abdominal aorta, 3cm above the bifurcation, and in the right and left iliac arteries 3cm below the bifurcation). Flow was calculated from each sequence by:

$$\text{Flow (ml/sec)} = \text{Area (cm}^2\text{)} \times \text{mean velocity (cm/sec)}$$

MR vascular imaging shares other tomographic techniques the disadvantage of interrupted display of vessels with tortuous course. To address this problem a multi-offsets velocity mapping technique was used to acquire flow data in planes predominantly parallel to the three vessels in 4 normal subjects and then by generating a single maximised image from the stack of imaged acquired a complete functional angiogram based on flow signal can generated.
Magnetic resonance imaging (MRI) has become an important imaging modality for the aorta and large vessels. Because MRI signal is absent from flowing blood in the vascular system, high natural contrast exists between the lumen and the vessel wall, providing an optimal situation for the delineation of vascular anatomy and atherosclerotic plaque. Blood flowing into a stenosed region must, being incompressible, undergo acceleration with the mean velocity increase being proportional to reduction in the cross sectional area. Measurement of the peak velocity through a stenosis can be then used to measure pressure gradient.

► **313** 11:30AM

MR PULMONARY ANGIOGRAPHY
TM Grist, JR Macfall, CE Spritzer, DS Sallee, HD Sostman
Department of Radiology, Duke University Medical Center, Durham, NC

WEDNESDAY a.m.

Noninvasive evaluation of the pulmonary vasculature is currently limited to studies of pulmonary perfusion using radioisotopes. Pulmonary vascular anatomy may only directly be visualized using transcardiac catheterization and injection of contrast. The objective of this work is to develop techniques for noninvasive imaging of the pulmonary vasculature using MRI.

All studies were performed using a 1.5T MR scanner (GE Signa) equipped with shielded gradient coils. MR pulmonary angiograms may be formed by acquiring sequential 2DFT gradient recalled echo images and subsequently reprojecting the data set in the desired plane. The effects of image acquisition parameters as well as display options were studied in 10 normal volunteers. In addition, the sequence was evaluated in selected patients with pulmonary vascular abnormalities. Three categories of image acquisition parameters were varied, including options which influence flow related enhancement (FRE), parameters which alter spin dephasing, and variations in the acquisition time or breatholding requirements. In order to study the effects of FRE, we varied the Tr (22-50ms), flip angle (15-90°), slice thickness (3.0-50.0 mm), and acquisition plane orientation. Spin phase effects were analyzed by varying the Te (3-9 ms), flow compensation gradients, and voxel size (5.1-86 mm^3). Display options were studied by altering the projection angle, algorithm (maximum pixel intensity, integrated pixel intensity, sum) and by editing the input data.

High quality images were obtained by collapsing a series of coronal images into a coronal plane using analgorithm which selects the maximum pixel intensity along a "ray" through the slices. Misregistration artifacts related to breatholding were minimized and patient tolerance improved by using a short Tr (22 ms), thicker slices (up to 10mm) and 1 NEX. Adverse spin phase effects were reduced by using small flip angles and short Te (3.0ms) echoes without flow compensation. Angiograms showing segmental pulmonary vascular anatomy may be formed in 1 minute using six 10 second breatholds. Smaller branches of pulmonary vessels may be visualized by acquiring thinner slices and extending the acquisition time. In summary, we describe a technique which shows remarkable potential as a noninvasive means of studying pulmonary vascular anatomy

► **314** 11:42AM

EVALUATION OF THORACIC VENOUS OBSTRUCTION WITH MRI

ME Hansen, CE Spritzer, HD Sostman
MRI Section, Duke University Medical Center, Durham, North Carolina

Thirty-five patients with suspected thoracic venous obstruction and/or thrombosis underwent magnetic resonance imaging (MRI) using a 1.5 T superconducting system. Fast imaging (GRASS: TR 33, TE 13, 60° flip angle) and dynamic (cine GRASS) sequences were used in addition to spin echo T1 and T2 weighted) techniques. MR studies were retrospectively evaluated for presence, nature, and level of venous abnormality and presence of collateral venous channels. Pulse sequences and image planes were compared in terms of diagnostic content for three anatomic regions containing a) superior vena cava (SVC), b) internal (IJV) and external (EJV) jugular veins, and c) axillary (AXV), subclavian (SCV), and brachiocephalic (BCV) veins. MR results were correlated with CT (24 cases), contrast venography (15), ultrasonography (2), surgery (4), and autopsy (1). Low flip angle techniques in the axial plane were best for evaluation of the SVC and neck veins. Shoulder region veins were also best assessed with low flip angle sequences, but both axial and sagittal planes were necessary. Overall sensitivity and specificity of MRI were 97% and 96% respectively, with regional values of 100% and 100% for SVC, 100% and 50% for IJV and EJV, and 89% and 100% for AXV, SCV, and BCV. Interpretive errors were caused by non-occlusive clot, slow flow, and artifact due to metallic devices. MRI's noninvasive nature and multiplanar capability make it attractive for evaluation of thoracic veins. Accuracy can be optimized by use of flow sensitive techniques.

► **315** 11:54AM

CINE MRI ASSESSMENT OF THE INFERIOR VENA CAVA: NORMAL AND ABNORMAL FLOW PATTERNS

M. L. Schiebler[1], M. A. Mauro[1], J. Mohler[2], S. McSherry[2], W. H. McCartney[1]
Departments of Radiology,[1] and Surgery[2]
University of North Carolina at Chapel Hill

PURPOSE: To evaluate normal and abnormal flow patterns in the inferior vena cava (IVC) with cine MRI in normal volunteers and in patients with suspected IVC pathology.

MATERIALS AND METHODS: Twenty individuals had cine MRI performed on their IVC's in the axial plane with a 1.5T Philips magnet. Thirteen patients had suspected pathology involving the IVC and had intra-operative confirmation of their intraluminal disease and seven were normal volunteers. The cine pulse sequence consisted of a cardiac-gated, fast-field echo technique with 8-12 cardiac phases per slice and a 50 ° flip angle. Either one or four total levels were acquired per experiment. Routine axial spin-echo pulse sequences of TR 600/TE 20 and TR 2400-3000/TE 20 and 100 with parallel pre-saturation pulses outside of the imaging volume were also employed.

RESULTS: Cine MRI was accurate in demonstrating a normal IVC in 16/19 cases. There were three false positive cases related to flow artifacts; two were at the level of the renal vein confluens and one case was related to turbulence at the eustachian valve at the entrance to the right atrium. Cine MRI correctly showed total occlusion of the IVC with collateral formation in one case.

DISCUSSION: This is one of the first studies of the normal and abnormal cine MRI appearance of the IVC. This small series suggests that cine MRI should be used as an adjunct to routine pre-saturated spin-echo images in the analysis of intraluminal disease of the IVC because of the frequency of flow-related artifacts that may be potentially interpreted as true intraluminal masses or thrombi.

BRAIN IV

MODERATORS: J. S. ROSS, M.D., T. L. CHENEVERT, Ph.D.

► **316** 10:30AM

HIGH RESOLUTION 64 MSEC INSTANT IMAGES OF THE HEAD

RM Weisskoff, J Dalcanton, MS Cohen
Advanced NMR Systems, Inc, Woburn, MA

Instant (or echo-planar) imaging has succeeded in providing dramatically improved temporal resolution in MR images, often at the expense of spatial resolution and signal-to-noise. We present here a technique that doubles the spatial resolution of single-shot images without sacrificing sub-second temporal resolution. We created 128x256 1.5mm resolution images of the human head with a readout time of 64 msec. These images were produced using a single RF excitation on our GE 1.5T scanner retrofitted with Advanced NMR's Instant Scan technology, including our own gradient, RF, data acquisition, processing and display systems.

Our "standard" acquisition is 32 msec long, covering k-space to produce approximately 3mm isotropic resolution. However, in the head, the transverse relaxation times are sufficiently long that we can double the acquisition period to acquire twice as many phase-encoded lines, thus doubling the resolution in that dimension. In addition, we offset the acquisition in the read direction so that it covers only the positive half of k-space. We construct the negative half by conjugate synthesis.

While we have produced high resolution images in the body previously [1], that resolution was achieved by tiling k-space with four independent instant data sets, producing a complete image in 10-20 seconds. Using our new technique, we have produced multi-slice T2-weighted images covering the entire brain in 2 to 4 seconds with resolution approaching the motion-compromised effective resolution typically seen in a similar conventional MR set. Because of its extremely good temporal resolution, this technique also can be used to monitor both the passage of contrast agents in real time.

[1] RR Rzedzian, Society for Magnetic Resonance in Medicine, WIP 51, 1987.

► **317** 10:42AM

INFLAMMATORY PROCESSES OF CORTICAL GRAY MATTER: HISTOLOGIC CORRELATION OF MRI FINDINGS

OB Boyko, SR Alston, PC Burger
Department of Radiology, Duke University Medical Center

MR imaging has proven very useful in delineating inflammatory processes of cerebral white matter. We reviewed the MR findings in six patients who had pathologically proven inflammatory processes localized primarily to the cortical gray matter. Five patients had Creutzfeld-Jakob disease (C-J; subacute spongiform encephalopathy) and one patient chronic encephalitis (Rasmussen's syndrome). In addition a specimen MR of a C-J case from the neuropathology museum was obtained. MRI scans were performed at 1.5 T using T1 and T2-weighted spin echo pulse sequences.

All MRI scans demonstrated normal white matter signal intensity. Cortical gray matter signal was definitely abnormal in one case (C-J), equivocal in two (C-J and chronic encephalitis) and normal in three cases (C-J). T2-weighted images best demonstrated the abnormal bright signal of the cortical gray matter (long T2) and this correlated with histologic findings of severe spongiform change (vacuoles within the neuropil). Cortical gray matter was markedly thinned in only one case (chronic encephalitis). Specimen MRI in a case of C-J also demonstrated abnormal cortical gray matter T2 signal.

In six cases where CT was available, MR was more sensitive than CT in detecting cortical gray matter abnormalities.

MRI can be a useful adjunct in the evaluation of patients with suspected pathology delimited to the cortical gray matter. Due to the different histologic architecture and thus "water environment" of the gray matter versus the white matter, further adaptations of pulse sequences may be helpful to improve the sensitivity of MRI in the evaluation of cortical gray matter disease processes.

► **318** 10:54AM

QUANTITATION OF BRAIN ATROPHY BY MRI USING 3D GRADIENT ECHO SEQUENCES AND VOLUMETRIC POSTPROCESSING

G. Birbamer, A. Kampfl, S. Felber, G. Laub*, H. Ehrike*, F. Aichner
University of Innsbruck, Department of Magnetic Resonance
Siemens Medical Systems, Erlangen*

Estimation of regional and global substance loss of the central nervous system by means of distance ratios in CT and MRI do not allow absolute quantitation. 3D-MR-Imaging of the brain, using gradient echo sequences with isotropic resolution already enables reformatting of arbitrary orientations and would serve as an ideal basis for volumetric studies.

In order to separate brain tissue from CSF-spaces, a manually supported segmentation algoritm was implemented into a 1.5 T Magnetom (Siemens), which automatically calculates the volume of the selected tissue. Images for segmentations were 1.0 to 1.4 mm thin contiguous slices obtained by a 3D Flash sequence with a minimal TE of 5 ms. All examinations had been carried out on a 1.5 T Magnetom using a circular polarized head coil, after consent of the patient was obtained.

Volumetric calculation of the brain was performed in one anatomic specimen, 4 volunteers and 6 patients clinically presenting with dementia: Alzheimer disease (n = 2), spinocerebellar atrophy (n = 2), multiinfarct dementia (MID; n = 2). Using the new algoritm, exact calculation of the brain volume is possible and offers new insights into the diagnosis and progress of dementia.

► **319** 11:06AM

THE USE OF MRI-GUIDED INTERSTITIAL LASER SURGERY IN EXPERIMENTAL BRAIN TUMORS

N. Higuchi, M. El Azouzi, P.McL. Black, M.R. Moore, D. Hsu, F.A. Jolesz
Depts. of Radiology and Neurosurgery, Harvard Medical School and Brigham & Women's Hospital

We have previously shown that MRI can be used to control energy deposition during interstitial laser irradiation, and can discriminate reversible from irreversible signal change in affected tissue. We have studied the effects of laser power and energy level on lesion size and on the corresponding histologic appearance of the lesions in normal animal tissues (brain, liver, and muscle).

To prepare for future use in the treatment of human brain tumors, we applied this method to experimental prolactinomas produced by estrogen implant in Fischer 344 rats. An Nd:YAG laser was used with an optical fiber inserted into the tumor via a transfrontal approach. T1- and T2-weighted MR images were obtained before, during (T1-weighted only), and after laser irradiation, using spin echo sequences (500/20, 2000/80) on a 1.9 T MR imager.

It was possible to locate the tip of the fiber and to visualize the laser-induced changes in the brain on MR images. Before laser treatments, the tumor was isointense or hypointense (on T1- and T2-weighted images, respectively) compared with normal brain tissue. While T1-weighted images obtained during laser irradiation consistently showed a decrease of signal from the lesion, after laser irradiation both T1- and T2-weighted images presented a variety of appearances depending on the laser settings (2-15 watts, 100-200 joules, continuous or pulsed exposures) and the position of the fiber tip relative to specific anatomical structures. These changes were compared with the corresponding histology.

We conclude that MRI-guided interstitial laser surgery has very good potential as an alternative method for the treatment of brain tumors.

► **320** 11:18AM

Fast Scanning of the Brain at 0.5 Tesla

A. Darkazanli, M.Sc., P. Granstrom, M.D., E. Unger, M.D., J. Seeger, M.D., R. Carmody, M.D., A. Gmitro, Ph.D., T. Toshida, H. Suzuki
University of Arizona, Department of Radiology (AD, PG, EU, JS, RC, AG)
Toshiba Corporation (TY, HS)

This study was performed to evaluate the role of fast scanning sequences for MR imaging of the brain at 0.5 Tesla. The sequences, FLASH, FISP, ROAST (Resonant Offset Averaging with Steady State Free Precession) and CE-FAST were implemented and optimized for a 0.5 Tesla Toshiba MRT-50A scanner. The effect on image contrast of the parameters of 2D, 3D, flip angle, TR, TE and readout bandwidth were evaluated. Additionally, a pixel replacement algorithm was developed which was found to improve artifacts from magnetic susceptibility. Five normal volunteers were then scanned with each of these sequences and the signal intensities of gray and white matter, CSF and noise were measured and the contrast to noise for gray/white matter differentiation and CSF were calculated. After this, 5 patients with multiple sclerosis are evaluated to determine which sequences have the most contrast for detecting plaques.

We have the following conclusions: **1)** In all cases image quality is better with 3D than 2D. **2)** A bandwidth of 25 kHz works well with these sequences. **3)** FLASH has the best gray/white matter contrast of any of the sequences. While CE-FAST has brilliant contrast for CSF, the gray/white differentiation is poor with this sequence. **4)** FISP with fully balanced gradients is quite prone to susceptibility artifacts which can be compensated for by the use of the replacement algorithm or by using ROAST instead. In either cast, the gray/white differentiation is poor.

► **321** 11:30AM

Leukoencephalopathy in Cerebral Amyloid Angiopathy: Magnetic Resonance Imaging

D.J. Loes, M.D., J. Biller, M.D., W.T.C. Yuh, M.D., M.N. Hart, M.D., J. C. Godersky, M.D., H.P. Adams, Jr., M.D., S. P. Keefauver, M.D., and D. Tranel, Ph.D.
The University of Iowa Hospitals and Clinics, Iowa City, Iowa 52242

We reviewed the MR studies of four patients with biopsy-proven cerebral amyloid angiopathy (CAA).

All patients were imaged on a 0.5 Tesla superconducting magnet. Two patients who presented with dementia were imaged during their initial evaluation. One patient was studied acutely following a lobar intracerebral hemorrhage; one patient was imaged 2 years following surgical evacuation of a lobar hematoma.

MR findings included multifocal and/or diffuse white matter signal hyperintensities on T-2 weighted images, remote from areas of current or previous hemorrhage, in 3 of the 4 patients. The white matter signal abnormalities were most prevalent in the centrum semiovale and deep periventricular region, and spared the corpus callosum and internal capsule. The more diffuse and confluent white matter lesions were found in the two patients with dementia.

The white matter signal abnormalities may correspond to areas of ischemic demyelination; these pathologic findings have been previously described with CAA. In the appropriate clinical setting, we believe CAA should be considered in the differential diagnosis of white matter signal hyperintensities seen with MR.

► **322** 11:42AM

Projection venography of the brain using MR

H Mattle (1,2), RR Edelman (1), J Kleefield (1), HM Hoogewoud (3), D Atkinson (1,4). (1) Department of Radiology, Beth Israel Hospital, Boston, MA, (2) Department of Radiology, New England Deaconess Hospital, Boston, MA, (3) Hôpital Cantonal, Fribourg, Switzerland, and (4) Siemens Medical Systems, Iselin, NJ.

Projection venography (Edelman RR et al.) was used to study normal venous structures and venous pathology of the brain.
Methods: Twenty subjects who had recently undergone conventional cerebral angiography were studied. A series of overlapping, two-dimensional flow-compensated gradient-echo images were acquired in sagittal, coronal, and/or transverse planes. Presaturation was applied over the neck to eliminate signal from inflowing arterial spins. Scan variables were: TR/TE/flip angle/slice thickness/number of excitations = 30 msec/10 msec/30°/3-5 mm/1, matrix 192x256, FOV 23 cm. The images were post-processed with a maximum intensity projection algorithm to produce projection images along user-defined viewing angles. The MR venograms were then correlated with the conventional cerebral angiograms.
Results: The cerebral venous sinuses and veins such as the superior and inferior sagittal sinuses, lateral sinuses, sinus rectus, sphenoparietal, cavernous and inferior petrosal sinuses, basilar vein of Rosenthal, internal cerebral vein, thalamostriate veins and venous angle, sylvian veins, superficial middle cerebral veins and meningeal veins draining into the superior sagittal sinus were seen. The MR venograms reliably showed cerebral venous and superior sagittal sinus thrombosis, cerebral venous angiomas, and draining veins from arteriovenous malformations. In conjunction with bolus tracking techniques, the method can be used to determine the patency of veins or sinuses (eg, in patients with falx meningiomas).
Conclusion: MR venography reliably depicts the cerebral venous anatomy. It is complementary to conventional spin-echo methods for the assessment of pathology involving the cerebral veins and sinuses.
Ref.: Edelman RR et al. Radiology 1989; 172: 351-357.

► **323** 11:54AM

MRI EVALUATION OF CANINE HYDROCEPHALUS

V. Deo-Narine, T. Vullo, D. GOmez, R. Zipagan, J.P. Whalen and P.T. Cahill
The New York Hospital-Cornell University Medical College New York, N.Y.

With the induction of hydrocephalus compensatory mechanisms, such as transventricular absorption (TVA), help stabilize the CSF pressure at normal or elevated values. This study investigated the effects of ventricular compliance and TVA in chronic hydrocephalus using MRI and Gd-DTPA flow studies.

Hydrocephalus was surgically induced by injection of silastic into the basal cisterns of mongrel dogs. Pressure measurements were obtained every three days until a plateau generally 16 cm. of H20 above normal was achieved (3-5 weeks). Changes in ventricular volumes were evaluated by serial MRI studies on a 0.6T Teslacon MRI system using a slice thickness of 3 mm. and intraplanar resolution of 0.6 mm. By the use of angiocatheters introduced through burr holes, Gd-DTPA was perfused at a constant rate into one lateral ventricle while outflow was maintained from the other lateral ventricle. MR images were acquired every 3 minutes for up to 90 minutes of total perfusion time. Post perfusion MR scans were also obtained at 24, 48, and 72 hours at which time horseradish peroxidase (HRP) was perfused into the ventricles, and the brain fixed in situ for electron microscopy.

Increased signal due to Gd-DTPA inflow was measured in the periventricular (PV) region within one hour after the start of perfusion, was a maximum well beyond the PV after one day and decreased over the next two days. Electron microscopy showed that HRP also appeared in the PV extracellular space. In conclusion, TVA appears to be a major compensatory mechanism in chronic hydrocephalus.

MRA II

MODERATORS: V. HAUGHTON, M.D., T. VOGL, M.D.

► 324 10:30AM

"Black blood" angiography of the carotid bifurcation

Robert R. Edelman (1), Heinrich Mattle (1,2), Dennis J Atkinson (2,3), Jonathan Kleefield (1)
Department of Radiology, Beth Israel Hospital (1), Boston, MA, Department of Radiology, New England Deaconess Hospital (2), Boston, MA, and Siemens Medical Systems (3), Iselin, NJ

Recently, magnetic resonance methods have been developed for creating angiogram-like images of the carotid bifurcation, which portray the vasculature within a substantial thickness of the body. To date, these methods have employed flow-compensated gradient-echo sequences which make flowing spins appear bright. However, these "bright blood" angiograms may suffer from poor flow contrast when depicting a severe stenosis, due to turbulent flow distal to the lesion, or slow flow proximally. In order to overcome this problem, we have implemented several techniques for creating "black blood" angiograms, which are insensitive to the velocity or pattern of flow.

Methods: The goal is to produce a series of thin, contiguous sagittal slices in which blood appears dark, and is contrasted with muscle and fat, which appear brighter. The images are then postprocessed by using a "minimum intensity projection" (MIN) algorithm to create a series of angiogram-like images along user-selected projection angles. Three methods were compared in eight normal subjects and 12 patients with atherosclerotic lesions involving the carotid bifurcation: (1) 3D gradient-echo (GRE) with presaturation and dephasing; (2) thin-slice 2D spin-echo (SE) sequences using an optimized slice profile and presaturation; (3) ultra-fast short time inversion recovery (STIR) sequence; the inversion time is selected to null the signal from blood. Image acquisition times are in the order of 3 - 10 minutes.

Results: The 3D GRE sequences produced inadequate suppression of vascular signal. The SE sequence generally produced nearly complete signal voids from flowing spins, because of the combined effects of presaturation and wash-out between the 90^{o} and 180^{o} pulses. The angiograms accurately depicted carotid stenoses, and were less sensitive to flow turbulence than the "bright blood" sequences. However, a small focus of persistent signal was often seen in the carotid bulb, presumably related to recirculating flow. The ultrafast STIR sequence had a significant advantage in that signal from blood was nulled regardless of the velocity or pattern of flow. Black blood angiograms were comparable to bright blood angiograms in normal subjects and those with mild or moderate stenoses. Black blood angiograms were generally superior for depicting severe stenoses and ulcerations.

Conclusion: Black blood angiography is a useful, complementary tool to bright blood angiography for the study of the carotid bifurcation. The technique largely overcomes problems of flow turbulence and slow flow encountered with previously described angiographic methods.

► 325 10:42AM

MR ANGIOGRAPHY OF ANEURYSMS

EK Fram, PJ Keller, BP Drayer, JA Hodak, RA Flom, CR Bird, KD Williams, JM Zabramski, RF Spetzler
Barrow Neurological Institute, St. Joseph's Hospital and Medical Center, Phoenix, AZ 85013

WEDNESDAY a.m.

Detection and evaluation of aneurysms with conventional magnetic resonance (MR) imaging may be difficult as it requires one to mentally reconstruct vessels from a series of sections. Vascular loops and small aneurysms may be difficult or impossible to differentiate. We utilized MR angiography technique in an attempt to overcome these difficulties.

Among 50 patients who underwent cerebral MR angiograms, 9 angiographically proven aneurysms were present in 5 patients. MR angiography was performed using contiguous 1.5 mm spoiled GRASS images with TR = 50 or 100, TE = 10, a flip angle of 50 degrees, and flow compensation, with a total acquisition time of 10-12 minutes [1].

Post-processing software employing a maximum pixel intensity ray tracing technique was utilized to produce two-dimensional projections of the data in multiple projections. During post-processing, regions of the volume scanned could be isolated for inclusion in the angiographic projections. Using this process of mathematical dissection, any desired projection of any vessel could be produced without superimposition of other vessels.

The patent lumen of the aneurysm was detected in 8/9 aneurysms, even in the two giant aneurysms. However, one parasellar aneurysm was not visualized due to signal loss secondary to susceptibility artifact which resulted from the adjacent air-filled sphenoid sinus.

MR angiography differs significantly from conventional angiography. Disadvantages include the lower spatial resolution, dephasing due to complex flow, and susceptibility artifact from adjacent air/brain interfaces. We expect further improvements in image quality with further reduction in TE and pixel size.

Despite these limitations, MR angiography provides several potential advantages over conventional angiography in the imaging of aneurysms. The technique is rapid and noninvasive. It is possible retrospectively to produce any desired 2D-angiographic projection of the brain. If the artifacts described above can be eliminated, it will be possible to interactively dissect out a region of the cerebral vasculature and rotate the region to optimally visualize the aneurysm, its neck, and the surrounding vasculature. At this point, we feel that conventional angiography is required for detection and evaluation of aneurysms.

[1] Keller PJ, Drayer BP, Fram EK, Williams KD, Dumoulin CL, Souza SP. Radiology, Nov. 1989, In Press

► **326** 10:54AM

MR ANGIOGRAPHY OF CEREBRAL VENOUS OCCLUSIVE DISEASE

EK Fram, PJ Keller, BP Drayer, JA Hodak, RA Flom, CR Bird, KD Williams, JM Zabramski, RF Spetzler
Barrow Neurological Institute, St. Joseph's Hospital and Medical Center, Phoenix, AZ 85013

Magnetic resonance (MR) imaging is an excellent noninvasive technique for the evaluation of patients with suspected cerebral venous occlusive disease. MR can detect venous thrombosis, complications such as hemorrhagic cerebral infarction, as well as etiologies for venous occlusion, such as tumor or mastoid infection.

However, visualization of the cerebral venous drainage may at times be difficult when thrombosis involves only small venous structures. False positives can be caused by flow-related enhancement and false negatives can result from acute thrombosis in which acute thrombus in a vein may be relatively isointense with respect to brain.

MR angiography was performed in four patients with cerebral venous occlusive disease. Among the patients evaluated, thrombosed vessels included the superior sagittal sinus, the straight sinus, internal cerebral veins, transverse sinus, sigmoid sinus, and superficial cortical veins. MRI angiography was performed using contiguous 1.5 mm spoiled GRASS images with TR = 50 or 100, TE = 10, a flip angle of 50 degrees,and flow compensation, with a total acquisition time of 6-12 minutes [1]. Post-processing software employing a maximum pixel intensity ray tracing technique was utilized to produce two-dimensional projections of the data in multiple projections. Correlation between MR and conventional angiography was excellent.

MR angiography is a rapid noninvasive technique which provides excellent visualization of the intracerebral venous system. In most occluded vessels studied in this series, occlusion was more readily demonstrated on the MR angiograms than on conventional MR imaging, particularly in the two cases in which there was thrombosis of the anterior half of the superior sagittal sinus. Therefore MR angiography is a useful adjunct to conventional MR evaluation of the brain in patients with suspected cerebral venous occlusive disease.

1. Keller PJ, Drayer BP, Fram EK, Williams KD, Dumoulin CL, Souza SP. Radiology, Nov. 1989, In Press

► **327** 11:06AM

MRI AND MR-ANGIOGRAPHY OF THE CAROTID ARTERY: VALIDATION WITH DSA

G Bongartz, W Krings, P Vassallo, E Rummeny, PE Peters

Dept. of Diagnostic Radiology, University of Muenster, FRG

Recent developments in MRI enable us to visualize blood flow in a fast and comprehensive way. The ability to detect arterial stenosis has been described previously. Flow effects like higher-order motion or slow flow cause problems in MRA due to signal variations which exaggerate the degree of stenosis or produces complete signal loss. Turbulences occur mainly at the site of an atherosclerotic plaque as well as at all arterial truncations. Therefore minimal atherosclerotic damage and physiological flow effects may not be differentiated since both lead to focal signal defects in MRA.

High resolution MR images perpendicular to the arterial axis allow visualization of the arterial wall and atherosclerotic plaques in vivo. The combination of MRI (perpendicular to the carotid bifurcation) and projective MRA enables a differentiation between arterial wall change and flow effects (turbulences).

In this study, the results of 1. MRA (time of flight - method) 2. DSA (arterial) 3. MRI (perpendicular) of the carotid arteries in 70 patients with clinically suspected stenosis were compared. The first group of 5 patients were used as a training phase for the readers, in which the results of all modalities were directly compared. In the remaining patients the DSA films and the MR images were read independently by 3 radiologists.

We found an excellent correlation between DSA and MRA as regards the presence or absence of carotidl stenosis in app. 90%. The degree of stenosis was overestimated in more than 35% (predominantly in the first 40 patients). The combination of MRA and MRI (perpendicular) provided precise assessment of the degree of arterial stenosis. Furthermore, it was possible to differentiate between various plaque structures, such as calcified plaques and infiltrative atheroma.

We conclude that a reliable assessment of the carotid arteries and the degree of stenosis can be achieved by the combination of MRA and MRI.

► **328** 11:18AM

CSF Flow Dynamics by Cine-MR

RS Hinks (1), RM Quencer (2), MJD Post (2)
(1) Picker International, Highland Heights, Ohio, 44143
(2) University of Miami Radiology Dept., Miami, FL, 33136

The use of phase mapping methods allows the investigation of flow velocities in MR imaging (1). Using special flow-sensitized and flow-desensitized cine sequences, we have used this methodology to evaluate CSF flow dynamics in both the brain and spine. All studies were performed at 1.5 T on a standard clinical MR system using ECG or PPG gating for cardiac synchronization. A flow phantom was used to investigate the accuracy of the velocity measurements by comparison with a presaturation bolus tagging experiment.

In a series of volunteers and patients we noted:
1. All regions demonstrated both cranial and caudal flow as a function of the heart cycle.
2. There is a wide range of flow velocity profiles in the normal population.
3. Maximal flow rates typically occur in the cervical spine and at about 200 msec after the R-wave.
4. CSF flow in both the thoracic and lumbar regions peaks somewhat later in the heart cycle than in the C-spine and at a lower velocity.
5. Narrowing of the subarachnoid space leads to a local increases in CSF velocity and often turbulence.

(1) GL Nayler, DN Firmin, DB Longmore, J. Comput. Assist. Tomagr. 10, 715 (1986).
(2) RS Hinks, MJD Post, RM Quencer, Society of Magnetic Resonance in Medicine, Eighth Annual Meeting, Abstract #1034.

► **329** 11:30AM

WEDNESDAY a.m.

MEASURING ARTERIAL STIFFNESS BY STROBOSCOPIC NMR MICROSCOPY

LW Jelinski, MD Cockman, HK Tubbs, and RW Behling
AT&T Bell Laboratories, Murray Hill NJ 07974

The non-invasive measurement of vascular dynamics and elasticity is critical in understanding hemodynamic conditions of cardiovascular diseases. We report stroboscopic nuclear magnetic resonance images at 33 μm resolution of the carotid arteries of 80-gram rats. EKG-gated transverse images of the artery were obtained using a slice-selective 2D spin-echo imaging technique. The variation in arterial cross-sectional area was mapped out for the entire heart cycle. The cross sectional area of the carotid artery increased about 40% between diastole and systole, corresponding to a pressure increase of about 30 mm Hg. The dimensional changes were correlated with the absolute blood pressure to determine Young's modulus, a measure of arterial stiffness. The NMR-derived arterial stiffness (7×10^5 dynes/cm^2) was in excellent agreement with the value measured for the transverse modulus of an excised carotid artery (6.5×10^5 dynes/cm^2). The *local* effects of the vasoconstrictor, phenylephrine and the vasodilator, nitroprusside, were visualized directly. Although the blood pressure increased with phenylephrine, the drug had no direct effect on the stiffness of the arterial wall, whereas nitroprusside appeared to directly affect the arterial wall elasticity.

These results describe how arterial stiffness can be measured directly and non-invasively by MRI. They furthermore provide the first direct view of the dynamics of arteries of sub-millimeter diameter and suggest that animals as small as juvenile rodents will serve as valuable models for hemodynamic studies. Potential applications to humans will be discussed.

► **330** 11:42AM

MR IMAGING WITH GD-DTPA IN NASOPHARYNGEAL TUMORS

Th.Vogl,MD; S.Dresel,MD; G.Grevers,MD; K.Kang,MD; J.Lissner,MD.
University of Munich, Department of Radiology
Marchioninistr. 15, 8000 Munich 70, West-Germany

In this study the value of MR with Gd-DTPA in combination with plain T1- and T2-weighted images in evaluation of most common nasopharyngeal tumors is compared with CT scans and pathologic findings. 92 patients with different tumors had been examined. The most found lesions were squamous cell carcinomas, lymphoepithelial carcinomas and adenoid-cystic carcinomas. MR examinations were performed at 1.0T with a head coil in two or three slice orientations. Images were acquired with long (TR=1600ms, TE=25/90ms) and short (TR=500ms, TE=25ms) spin-echo sequences. Five or eight millimeter thick sections were made, depending on the extent of the tumor. The contrast-medium Gd-DTPA was injected in a dose of 0.1mmol/kg patients weight. CT scans were obtained on a Siemens Somatom DRH with four millimeter thick sections before and after application of contrast material. In delineating anatomical features, small muscles like levator and tensor veli palatini muscle and other structures like pharyngobasilar fascia were better identified after administration of Gd-DTPA. This was due to the slight increase in signal intensity after Gd-DTPA of the lymphoepithelial mucosa and of muscle fascias. In primary carcinomas of the nasopharynx MR with Gd-DTPA had been superior to CT in all cases. It was possible to see early involvement of the tissues surrounding the tumor as well as necrotic areas and vessels in the lesion. Discrete crossing of the midline by the tumor was also best demonstrated in the Gd-DTPA enhanced images. In secondary carcinomas of the maxillary sinuses growing into the nasopharynx CT was equal to MR. Small infiltrations of the bony walls of maxillary sinuses were better seen in CT, however the exact extension of the tumor was better judged in contrast-enhanced MR images. In T2-weighted sequences MR proved to be helpful in differentiating tumor masses in the maxillary sinuses from inflammatory changes fluid and cysts. MR with Gd-DTPA also allowed recognition of infiltration or involvement of the carotid artery and jugular vein well in coronal planes. Gd-DTPA enhanced MR in combination with plain T1- and T2-weighted sequences allows new diagnostic possibilities. CT scans should be done additionally, if there is any question about bony infiltrations.

► **331** 11:54AM

MR-imaging with Gadolinium-DTPA in carcinomas of tongue, oro- and hypopharynx

Roland Einspieler, M.D., Franz Ebner, M.D., Wilhelm Posawetz, M.D., Erwin Justich, M.D.
Karl Franzens University,Department of Radiology and ENT- department
A-8036 Graz,Austria

In a prospective study the value of intravenously administered gadolinium-diethylene-triamine pentaacetic acid (Gd-DTPA) in addition to noncontrast imaging in evaluating T- and N- stage of carcinomas of the upper digestive tract was analysed. Twenty four patients with primary diagnosis of squamous cell carcinomas of tongue, oro- and hypopharynx were examined by using magnetic resonance (MR) imaging. The contrast-agent Gd-DTPA was administered in a dosage of 0.2 mmol / kg in all patients. Eleven patients had surgery after examination; histopathological verification was performed in all tumours. Marked contrast enhancement produced by Gd-DTPA was observed in all carcinomas and in normal pharyngeal mucosa. The clinical T-stage of the tumours in comparison to surgical evaluation was diagnosed correctly with MRI in 9 patients, as opposed to the clinical stage (7/11) . The surgical N-stage showed a correlation with MRI in 8 of 11 patients, was overstaged in one and understaged in two patients; the clinical estimation (including ultrasound) of pathologically enlarged lymph nodes was correct in 7 patients, overstaged in 3, and understaged in one patient. In tumours stage T1 and T2 we found similar results in comparison to clinical examination including ultrasound; in tumours stage T3 and T4 the true tumour extension was better assessed by MRI particularly in tumours adjacent to the hypopharynx.

ABDOMEN

MODERATORS: H. Y. KRESSEL, M.D., E. A. ZERHOUNI, M.D.

► **332** 14:45PM

ECHO-PLANAR IMAGING OF THE LIVER AND UPPER GASTRO-INTESTINAL TRACT

'M.K. Stehling, 'D.F. Evans and P. Mansfield

Department of Physics and 'Surgery, University of Nottingham, NG7 2RD, England, UK
'present address: Departement Med. Radiologie, USZ, Zürich, Schweiz

Liver and upper GI tract are not readily accessible with conventional, 2D-FT MRI due to respiratory, cardiovascular and peristaltic motion. The ability of Echo-Planar Imaging (EPI) to produce MR images in a fraction of a second has overcome these problems. We have used the 128 ms EPI variant MBEST to image liver, gallbladder, stomach and the proximal gut. The images are based on 128 x 128 and 256 x 128 pixel matrices and provide resolution in the mm range. In addition to being fast, EPI provides almost free choice of T1 and T2 contrast. The former can be obtained with ultra-fast inversion recovery EPI in (TI + 128) ms, where TI is the inversion time. The latter with "shifted k-space scanning", an imaging procedure which exploits the reduced T2 weighting and increased S/N ratio obtainable when an asymmetrical gradient echo train envelope is generated, i.e. the main gradient echoes are made to occur earlier than halfway through the experiment. Contrast, resolution and region of interest can be altered interactively in real-time EPI scanning to obtain maximum anatomical detail, lesion conspicuity and detection confidence.

Snap-shot EPI images based on 256 x 128 pixel matrices were obtained on patients with focal and disseminated liver pathology to show the priciple and potential of interactive MRI. The effect of "shifted k-space sampling", now routinely used in EPI, on S/N ratio and resolution will be discussed. Fasting and fed motility patterns of the gastric antrum and proximal small intestine were measured in six volunteers for up to two hours in order to study the Migrating Motor Complex phases. Based on the EPI GI-tract movies, quantitative evaluation of peristaltic wave velocity and frequency was performed. Movies of induced gall bladder contraction were also obtained.

► **333** 14:57PM

STIR imaging of liver cirrhosis

Giovanna Patrizio PhD, Paolo Pavone MD, Casimiro Simonetti MD, Renato Pietroletti MD, Mario Simi MD, Roberto Passariello MD.

Short TI Inversion Recovery sequence (STIR) at the null point of healthy subjects liver parenchyma was performed to assess the usefulness of Magnetic Resonance Imaging (MRI) in detecting T1 alterations occurring in hepatic cirrhosis.
Fifteen patients with cirrhosis and fourteen normal volunteers were imaged at 0.5 T (Esatom 5000). T1 (260/20) and T2 (1600/30-70-120) Spin-Echo sequences were acquired . Subsequently, Inversion Recovery technique at the null point of normal liver was performed employing a TR of 800 msec, a TI of 136 msec, a TE of 30 msec and 4 number of signal averaging.
In a preliminary phase, IR parameters were chosen to null the SI of normal subjects liver parenchyma (SNR= 1.25 ± 1.10). In eleven cirrhotic patients imaged with the same sequence, an high signal intensity was detected in the liver. SNR valued, ranging from 4.5 to 9.8 according to the hepatic involvement, were analysed and related to laboratory data and bioptic findings. Five patients did not show any signal intensity alteration: minimal hepatic damage was found at laboratory data and biopsy.
The results of this study show that short TI inversion recovery is a promising technique in the detection and staging of hepatic cirrhosis by means of MR Imaging.

WEDNESDAY p.m.

► **334** 15:09PM

OPTIMIZING MR TECHNIQUE FOR DETECTING HEPATIC METASTASES AT HIGH FIELD

S Albert, NE Leeds
Department of Radiology, Beth Israel Medical Center, New York, NY

The increase in spin-lattice and spin-spin relaxation times (T_1 and T_2) of metastatic lesions in the liver as well as the increase in motion artifacts at high field, require further development of MRI techniques for imaging liver metastases at high field.
The purpose of the study is to optimize the MR pulse sequence for detecting liver metastases at a magnetic field strength of 1.5T.

The sensitivity of the following pulse sequences for detecting liver metastases was investigated: spin-echo(SE) T_1-weighted (SE300/20), SE T_2-weighted (SE2000/100), fast T_2-weighted gradient-echo (GE) (GE200/40/15°) and T_2-weighted inversion recovery (IR) (IR1000/100/60 and IR1300/130/80). The T_2-weighted IR technique is comprised of IR pulse sequences with relatively long echo times of 60 - 160ms. Comparatively short inversion times of 100 - 130ms were employed to allow a synergistic contribution to contrast of T_1 and T_2 and fat suppression. T_2-weighted GE images were obtained with small flip angle and relatively long echo times. The GE images were produced with a variant of the GRASS (Gradient Recalled Acquisition in the Steady State) pulse sequence. Respiratory compensation was utilized in conjunction with all pulse sequences.

Our results show that the T_2-weighted IR pulse sequences are more sensitive in detecting liver metastases at 1.5T than all other sequences used,and that the SE T_2-weighted pulse sequence is more sensitive than the T_2-weighted GE and SE T_1-weighted pulse sequences at this field strength.

► **335** 15:21PM

ORTHOTOPIC LIVER TRANSPLANTATION: MR IMAGING

Philipp Lang, Rudolf Steffen, Michael Mauz, Mathias Langer, Roland Bittner, Peter Neuhaus, and Roland Felix
Departments of Radiology and Surgery, University Clinic Rudolf Virchow, Charlottenburg, Free University Berlin, Fed. Rep. of Germany

Liver transplantation has become a life-saving therapeutic option in many patients with end-stage liver disease. In the present study, 21 patients who had undergone orthotopic liver transplantation were prospectively studied with MR imaging.

MR images were generated on an 0.5T superconductive system (Magnetom, Siemens, Erlangen, FRG). Axial T1-weighted MR images were acquired in gradient-echo mode (FLASH) with use of a TR of 306 msec, a TE of 14 msec, a flip angle of 900, and 4 excitations. Axial multiecho imaging was performed with a TR of 1600 msec, a TE of 30, 60, 90, and 120 msec, and 1 excitation.

A perivascular collar surrounding the portal vein and the inferior vena cava was demonstrated in all 21 patients. The perivascular collar demonstrated low signal intensity (SI) on the T1-weighted gradient-echo images and high SI on the multiecho images. In 16 of the 21 patients, the perivascular collar was also demonstrated around peripheral portal venous branches. A large perihilar fluid collection which appeared to be connected to the perivascular collar was observed in one patient. Laboratory analysis of the aspirated fluid demonstrated liver lymph. Two of the patients with follow-up MR had biopsy proved graft rejection. In both patients, the caliber of the intrahepatic vessels was markedly smaller at the time of rejection. Retrohepatic areas of high SI on both T1-weighted and multiecho images corresponding to postoperative hematoma were seen in 6 patients.

Impaired lymph drainage appears likely to be the cause of the perivascular collar since transplant surgery results in complete interruption of lymphatic vessels. The large lymphocele demonstrated in one of our patients appears to confirm impaired lymph drainage as a possible cause of the perivascular collar. In contrast to recent CT reports, however, a perivascular collar around peripheral portal branches does not appear to be a sign specific for rejection, since only two of our patients demonstrated clinical-laboratory and bioptic sign of rejection at the time of the MR. The smaller caliber of the hepatic vessels during rejection may be related to a decrease in total hepatic flow.

In conclusion, MR imaging represents a noninvasive method for the assessment of the liver allograft. A perivascular collar is a normal finding in the hepatic transplant. MR imaging is particularly useful in the distinction of blood from other extrahepatic fluid collections and may hold diagnostic potential in liver transplant rejection.

► **336** 15:33PM

EVALUATION OF PRESACRAL RECURRENCY OF COLORECTAL CARCINOMA

LANZA R., CAPRIO F., CERIONI M., CAROTTI L.
ISTITUTO RADIOLOGIA I.N.R.C.A. -ANCONA

Authors compare the findings at computed tomography (CT) and magnetic resonance imaging (MRI) in evaluation of the pelvis in patients after abdominoperineal resection for colorectal carcinoma.
MRI was performed in 48 patients with presacral recurrency on CT examination or when CT was unable to descrminate fibrosis from recurrent tumor.
The results were verified with findings at biopsy, surgical exploration or follow-up.
MRI correctly demonstrates absence of recurrence in 35 patients and a recurrent tumor in 11. It was indeterminate in two cases.
By characterizing T1 and T2 values, MRI has demonstrated a superior ability to distinguish malignancy from fibrosis and both from normal soft tissue of various relocated organs.
Recurrent tissues have prolonged T1 and T2 values, which give a low signal on T1 weighted images but medium-to high signal on T2-weighted images.
Postoperative and radiation fibrosis consistently displays low intensity signal both in T1 and T2 weighted images.
Posterirly relocated organs (expecially uterus and seminal vesicules) can be easily recognized by high contrast and multiplanar sections of MRI.

► **337** 15:45PM

CORRELATION OF POLYCYSTIC LIVER CYST CONTENTS AND T1 RELAXATION TIMES

PL Davis, DH Van Thiel

University of Pittsburgh, Departments of Radiology and Surgery, Pittsburgh NMR Institute

We have observed that the MRI intensity of cysts in polycystic liver disease can vary considerably on short TR/TE spin echo images in the same patient. We wanted to determine how the T1 relaxation time correlated with the contents of the cysts.

A total of 14 cysts were aspirated under MR guidance from 2 polycystic livers which had been removed during hepatic transplantation. The cysts were selected to cover the full range of MRI intensities observed on the short TR spin echo images. The T1 relaxation times were measured with a RADX desktop analyzer. The cyst contents were then sent for a variety of measurements including total protein, cholesterol, triglyceride, albumin, total bilirubin, osmolality, free hemoglobin, WBC, RBC, and platelets for either one or both livers.

Very good correlation ($R > .92$) was found between 1/T1 and triglyceride, albumin, and total bilirubin. Good correlation ($R > .85$) was found between 1/T1 and WBC, RBC, and platelets in the one liver for which these measurements were performed. Poor correlation was found between 1/T1 and osmolality.

In conclusion, the T1 relaxation time, and hence the MRI intensity, of a cyst in polycystic liver disease correlates well with some of the cyst contents but not with others.

► **338** 15:57PM

MRI appearance of obstructive jaundice: correlation with histopathology

Giovanna Patrizio PhD, Renato Pietroletti MD, Paolo Pavone MD, Giuseppe Calvisi MD, Terenzio Ventura MD, Mario Simi MD, Roberto Passariello MD.

To determine the MRI appearance of chronic jaundice we realized an animal model of extrahepatic bile duct obstruction comparing MR tissue characteristics and morphologic features with microscopic pathological findings of liver parenchyma.
Thirty-one Sprague Dawley rats weighting 300-400 gr. underwent biliary obstruction by means of the ligature of the choledocus. In vivo imaging was performed on an Esatom 5000 superconducting magnet operating at 0.5 T, before and 20 days after surgery. T1 weighted Spin-Echo images (TR 220 / TE 30) were obtained and analyzed by measuring the signal to noise ratio of liver parenchyma. Hematoxilin-eosin stained sections were taken through liver samples of all animals studied.
According to the signal intensity and histologic behaviour, three groups of animals could be distinguished after surgery: a) five rats showed the lowest increase of liver signal intensity, a normal choledocus and a low degree of ductular hyperplasia; b) a significant increase ($P < 0.05$) of SI was observed in 8 rats having an enlarged choledocus (7÷9 mm in diameter) and a high degree of liver parenchyma ductular hyperplasia; c) the remaining animals had an intermediate behaviour in terms of increased SI and hepatic involvement, but only half of them showed an enlarged choledocus. The results of this study demonstrate that the good correlation existing between the increased MR signal intensity and the physiopathological alterations of liver parenchyma after bile duct obstruction can give useful information in the MRI evaluation of hepatic damage occurring in chronic jaundice.

► **339** 16:09PM

EVALUATION OF HEMATOMA BY MRI IN FOLLOW-UP OF AORTO FEMORAL BY-PASS

Ernesto Di Cesare MD, Paolo Pavone MD, Paolo Di Renzi MD, Luca Marsili MD, Casimiro Simonetti MD, Nicola Foti MD, Roberto Passariello MD.

We selected a population of 20 patients with atherosclerotic disease, submitted to implantation of aorto-femoral by-pass graft. These patients were studied by MRI with T1 and T2 weighted sequences. Investigation was performed at 1 week, 1, 3 and 6 months after dacron implantation, to evaluate the normal evolution of hematoma and the potential development of complication. At the first week examination hematomas presented medium signal intensity in T1 weighted sequences and high signal intensity in T2 weighted sequences; after 1 month the amount of the hematoma was reduced and we found a decrease of signal intensity on T2 weighted sequences; progressive reduction of size and signal intensity in T2 weighted sequences was noted 3 months after surgery with complete disappearance at 6 months. Thus MRI was useful in this study in the evaluation of patency, morphology and identification of intraluminal thrombosis but also in the characterization of periprothesic by-pass hematoma and differentiation from flogistic complications.

MRA III

MODERATORS: R. I. PETTIGREW, M.D., D. J. PENNELL, M.D.

► **340** 14:45PM

PSEUDO-ANGIOGRAPHY BY T1 BASED DATA MANIPULATION

M. Doran, G.M. Bydder, I.R. Young
NMR Unit, Hammersmith Hospital, DuCane Road, LONDON W12 ORS U.K.

Angiographic methods based on time of flight (1) and phase differences (2) have been described. We have been evaluating methods dependent on exploiting T1 differences to show analogous results. These techniques do not exploit the motion of the blood, but the difference between its T1 and those of most normal tissues though they do not, therefore, usually work as well close to lesions, similar to those of blood in vivo. However, the approach does not need machine modifications, ensures that substantial time delays occur only when useful magnetisation lies along the Z axis and avoids the problems associated with balancing relaxation behaviour and the timings needed for the blood displacement. As an example of the approach, we will assume a situation where 4 tissues (A,B,C,D) are involved (D being blood in this example). Consider an inversion recovery excitation and data recovery given by the relationship $S=S_o(1+E_{R1}-2E_{I1})E_{E2}$ where $E_{R1} = \exp(-TR/T_1)$, $E_{R2}= \exp(-TE/T_2)$ and so on, from which a set of signals (S_A,S_B,S_C,S_D) is obtained. Other sets can be derived from a pair of saturation images (where the magnetisation is destroyed prior to recovery - so that the signals follow the relationship $S_1=S_o(1-E_{R1})E_{E2}$). Under these circumstances it is possible to adjust the precession angles at acquisition of the sequences so as to satisfy three relationships of the form $S_{A1}+S_{A2}+S_{A3} = 0$ (where S_{A1} is the signal of component A from experiment 1), and the signs are chosen depending on the actual sequence parameters, for A,B and C, while still leaving a useful level of signal from component D. In the leg, for example, which can be regarded as a three component system, a single inversion recovery (TR=600 msec,T1=142 msec) and saturation sequence (TR 100 msec, with flip angle at acquisition of 30^o), can be used to cancel fat and muscle, while leaving the blood signal. Because the grey matter time constant is closer to that of blood in the brain gives a less good relative signal. The use of inversion recovery tends to be slow, though sequences significantly faster than that used here can be designed.

(1) Laub G, Mueller et al, Proc. 7th Ann. Mtg. Soc. Magn. Reson. Med., San Francisco p876 (1988). (2) Dumoulin CL, Souza SP, Hart MR, Magn. Reson. Med., 5, 238 (1987).

► **341** 14:57PM

T2-ENHANCED TIME-OF-FLIGHT MAGNETIC RESONANCE ANGIOGRAPHY

G Laub(1), JS Lewin(2)
(1)Siemens AG, Medical Engineering, Erlangen, FRG, and (2)Department of Radiology, Case Western Reserve University, Cleveland, Ohio, USA

Time-of-flight effects (TOF) combined with volume acquisition techniques provide high resolution three-dimensional data sets which can be processed with non-linear algorithms to yield projection type MR angiograms.

There are two major issues related to TOF imaging: phase shift effects from the motion of spins along imaging gradients, and contrast between flowing blood and stationary tissues. Flow compensation techniques for reduction of phase dispersion from intra-voxel velocity variations in turbulent flow have generally used first order flow compensation and echo times as short as possible. However, successful compensation for turbulent flow can be achieved separate from the short TE, allowing for a wider range of relaxation effects and blood/tissue contrast. The purpose of this study is to examine the relaxation effects of varying TE and flip angle while keeping velocity compensation constant.

The effects of flow compensation gradients can be considered independent of echo time as long as the first moment remains zero and higher moments remain unchanged, allowing for the creation of variable TE flow compensated gradient echo sequences. Consistent flow compensation independent of echo time has been achieved with a new 3D FISP sequence with a TE from 7 to 40 msec, 20 cm FOV, 256 by 256 matrix, and 128 partition capability, allowing the acquisition of 0.8 mm isotropic voxels. This sequence has been applied to the carotid arteries and intracranial vessels, demonstrating improved blood/tissue contrast and better small-vessel delineation with longer echo times secondary to the slower T2* decay of blood compared to the surrounding tissues. Enhancement of susceptibility effects is also noted with prolonged echo times, limiting this technique in the region of the circle of Willis.

In summary, the TE in 3D gradient echo methods can be varied independent of flow compensation, allowing for a greater range of blood/tissue contrast than obtainable from the standard short TE techniques.

WEDNESDAY p.m.

► **342** 15:09PM

FAST IMAGING OF THE ABDOMINAL AORTA AND PERIPHERAL VASCULATURE

KM Link, P Margosian, W Sattin
Bowman Gray School of Medicine and Picker International

MRA of the abdominal aorta and peripheral vasculature was performed on a 1.5T system (Picker International, Highland Heights, Ohio) having a 12 mT/m gradient capacity. Images of the extremity were obtained in a linearly polarized split-top head coil. Examination of the vasculature was conducted with the following four sequences: a) 35-45/18 FAST 40°, b) 35-45/18 FAST 30°, c) 35-45/10 FAST 40°, d) 35-45/10 FAST 30°. The pulse sequences were performed both with and without MAST. Slice thickness was 5 mm with a slab thickness of 15 cm. FOV was 25-30 cm for the extremities and 35-40 cm for the abdominal aorta and pelvic vasculature. The imaging matrix was 256 x 256. Acquisition time varied from 7-12 minutes. 2-D images were obtained in the transaxial plane and reconstructed in the sagittal plane in a 3-D format. With this technique the steady state or stationary tissues are isointense. Time of flight enhancement causes increased signal from flowing blood so that subtraction techniques are not required. Slab thickness cannot be too big or there will be a loss of through plane flow enhancement. The 18 msec TE sequences with MAST produced the best images of both the abdominal aorta and peripheral vasculature in a study of volunteers less than 40 years of age and in patients being studied for another reason who were not known to have atherosclerotic disease. There is adequate visualization of the major visceral vessels including the renal arteries and veins. There is some difficulties with signal dropout in the iliac arteries because of the anterior-to-posterior and medial-tolateral course of these vessels. This was a similar problem in extremities. This is believed to be due to the fact that the vessels do not run parallel to the long axis of the body and are not perpendicular to the imaging plane. Offsetting the imaging plane appears to improve this problem. Although the exam has the disadvantage of being time consuming when examining the peripheral vasculature, especially the leg, it has obvious advantages when compared with traditional imaging modalities.

► **343** 15:21PM

NMR ANGIOGRAPHY BY ENHANCED QUASI-HALF-ECHO SEQUENCE*

Q. Guo and O. Nalcioglu
Department of Radiological Sciences, Division of Physics & Engineering, University of California-Irvine

The purpose of the current study was to investigate an imaging pulse sequence for combining the advantages of both gradient quasi-half-echo and flow-insensitive techniques. The imaging pulse sequence is shown in Fig.1. Here Gz and Gy are the usual selection and phase encoding gradients, respectively. The gradient waveform indicated by GX2 is the enhanced quasi-half-echo sequence which compensates both the velocity and acceleration effects at echo time. By adjusting the gradient waveform appropriately the duration of time τ could be shortened. It can also be shown that for short values of τ both the velocity and acceleration phases are approximately equal to zero and very small for higher orders for the quasi-half echo signal. Another waveform GX1 is used to generate a flow sensitive image. By interleaving GX1 and GX2 one can obtain two images simultaneously in which the first is sensitive to flow whereas the second is not. By taking the difference of the two one may obtain a flow image. It should also be noted that the T2 effect is the same in both images.

It is expected that as τ, the offset between quasi-half-echo data sampling and half-echo data sampling, becomes shorter a higher signal may be obtained from the flowing spins. On the other hand, as τ becomes shorter more blurring of the image occurs. Therefore, in order to reconstruct the quasi-half-echo images with a standard 2D Fourier transform, we have to choose a suitable value of τ both for image quality and flow insensitivity. The results obtained from a study using a phantom have shown that when τ was larger than 10% of the data sampling window the blurring of images was not serious. The flow phantom used in the current study was a funnel-shaped tube with a small entrance at the larger end. This shape causes a turbulent area around the entrance if the flow velocity is chosen appropriately. In the turbulent flow area the constant velocity compensation gradient pulse sequence can not rephase the signal of flow while the quasi-half-echo gradient pulse sequence does not cause too much signal loss with τ=0.8ms. The preliminary results on a human volunteer indicate that the clear carotid angiograms can be obtained showing the bifurcation even without any ECG gating.

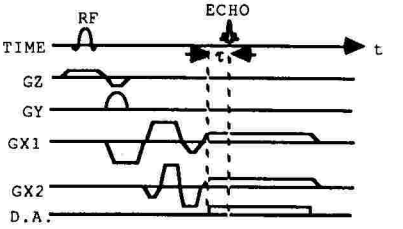

Figure 1. The imaging pulse sequence

* Work supported in part by PHS grant number CA45229 awarded by the NCI, DHHS.

► **344** 15:33PM

MR ANGIOGRAPHY USING PROJECTION-RECONSTRUCTION IMAGING

DG Nishimura, JM Pauly, A Macovski
Magnetic Resonance Systems Research Laboratory, Stanford University

In MR angiography, whether based on time-of-flight, phase, or relaxation effects, Fourier transform (FT) imaging with phase encoding gradient(s) dominates. The use of a phase-encoding gradient places limits on the minimum TE and creates a displacement artifact as the position along the phase-encoding axis is encoded at a different time than the position along the readout axis. This displacement artifact, while small in many situations, can become significant and misleading in such situations as bifurcations and curved vessels, especially in high-resolution images. To deal with these problems inherent in FT imaging, we have been studying the application of projection reconstruction (PR) imaging for MR angiography. Our approach to PR is to acquire FIDs, beginning the k-space sampling at the origin and assembling a set of radial "spokes" before reconstruction. The use of FID's minimizes both TE and flow-induced dephasing effects. We have incorporated this imaging sequence into both the selective inversion recovery (SIR) method and the 2D phase-contrast method, although it should be applicable to all methods. In conjunction with an asymmetric RF pulse, TE's under 1 ms are achievable with SIR and under 6 ms with the phase-contrast method (limited by the flow-encoding interval). In the phase-contrast method, the flow-encoding gradient can be either inverted between images or toggled on and off between images. In the latter case, one of the two images remains highly flow-compensated. Experimental results on phantoms and humans confirm the elimination of the phase encoding displacement artifact and reveal high-integrity flow signals. These results clearly demonstrate the potential for improved flow visualization with PR imaging.

► **345** 15:45PM

THIN SLICE MR ANGIOGRAPHY

D. Saloner, C.M. Anderson, and R.E. Lee
Department of Radiology, VA Medical Center, UC San Francisco

The concept of using multiple thin slices stacked in projection to obtain MR angiograms was first described by Gullberg et al. Recent results have shown the utility of this procedure for obtaining angiograms at a variety of sites in the body. The technique has been extremely effective in obtaining rapid sequential slices through the lower abdomen which otherwise produces poor angiographic images because of respiratory motion. We have investigated the variation of the signal intensity under different breathing regimens and have noted, particularly in venous flow, that there is significant blood flow variation and signal amplitude changes with heavy breathing. The single slice method typically takes less than 10 seconds per image and can be comfortably applied within a single breathhold. Techniques described to date typically stack multiple axial slices. We investigated the use of multiple thin slice imaging with coronal and sagittal acquisition. This is particularly useful in attempts to image the takeoff of the carotid and vertebral arteries from the aortic arch. Larger volume excitations presaturate the blood in the aortic arch resulting in low contrast angiograms. Thin single slice acquisitions were compared with 3D acquisitions using axial rf excitation and a coronal readout gradient. In single slice mode, the slice thickness was found to be critical. When the slice thickness was significantly larger than that of the vessel of interest, phase mixing within a voxel resulted in decreased contrast and resolution. 3D acquisition provided a reduced partition thickness. The positioning of the axial excitation slab was found to be critical in avoiding presaturation of the blood while in the arch.

► **346** 15:57PM

MINIMUM VOXEL AND MAXIMUM GRADIENT RE-PROJECTION FOR MR ANGIOGRAPHY
S. Napel, B. K. Rutt, S. Dunne
Robarts Research Inst., Univ. of Western Ontario, London, Ontario, CANADA

Conventional MR angiography (MRA) methods require the maximization of signal intensity in blood vessels with respect to surrounding tissue, and presents the resultant data in projection image format. These methods suffer from problems of signal loss in regions of complex blood flow, which may lead to false diagnosis of vessel narrowings. We have developed two alternatives to conventional MRA which rely instead on the minimization of signal from blood vessels, and are therefore insensitive to signal loss problems. Both methods require the acquisition of two- or three-dimensional images with flow voids within blood vessels, which can be accomplished using variations of spin echo imaging in combination with spatial presaturation techniques. Minimum voxel re-projection produces angiographic images of blood vessels from this data by extracting the minimum signal intensity along each ray traced through the three-dimensional volume. Maximum gradient re-projection enhances the detection of vessel boundaries by computing the maximum spatial gradient of signal intensities along the same rays. Preliminary results of implementing these two algorithms on a SUN 2/360 computer with TAAC-1 image processor, using conventional spin echo MR images show promise as an alternative to maximum voxel MRA. We will compare these two approaches with each other and with other MRA methods.

► **347** 16:09PM

FAST FOURIER PROJECTION FOR MR ANGIOGRAPHY
Shane Dunne, Sandy Napel, Brian Rutt
Robarts Research Inst., Univ. of Western Ontario, London, Ontario, CANADA

We present a new algorithm for fast projection of volumetric MR angiographic data, based on the projection-slice theorem of Fourier transform theory. This algorithm produces density-sum projections of volumetric MR data sets at any desired viewing angle, in times that are significantly shorter than conventional ray-tracing re-projection methods. For example, a 128 x 128 x 128 voxel data set can be re-projected onto a 128 x 128 pixel matrix in about one second, as opposed to about one minute for a conventional ray-tracing approach (times measured on a Sun 3/260 computer with a TAAC-1 accelerator). Lower resolution projections may be computed interactively (at rates of several times per second).

The method is based on extracting a 2D plane which intersects the origin of a 3D data block in Fourier space, followed by a 2D inverse FFT and magnitude calculation to produce the projected image. Although the 3D FFT required to initially convert real space data into the form required by this algorithm can be time-consuming (about three minutes for the data set and hardware described above), there are some important situations where the 3D FFT is not necessary. In particular, MR data is acquired directly into 2D or 3D Fourier space. In other cases, a single 3D FFT followed by multiple 2D inverse FFT's to produce projections at multiple view angles may be more efficient computationally than multiple ray-tracing steps.

We have developed a display tool based on the new algorithm which will be extremely useful for diagnostic viewing of MR Angiography because of its speed. This new high-speed re-projection method will also be very useful in combination with other processing and display techniques, including non-linear methods such as maximum voxel re-projection and shaded surface display, as a rapid method of orienting the final viewing angle prior to invoking the slower algorithm.

HARDWARE SYSTEMS & CHARACTERISTICS

MODERATORS: M. S. COHEN, M.D., J. C. GORE, Ph.D.

► **348** 14:45PM

FIELD MAPPING FOR SHIMMING MAGNETS USING A SPHERICAL RING PHANTOM AND OSCILLATING GRADIENTS

M.I. Hrovat, L.P. Panych
Dept. of Radiology, Harvard Medical School and Brigham & Women's Hosp., Boston, MA

Magnet shimming involves (1) B_o field sampling followed by (2) spherical harmonic analysis and (3) shim coil current adjustment. The above 3 steps are repeated until a desired field homogeneity is obtained. Iterating to a successful magnet shim depends on the ability to accurately sample the field. In the past, we have used a rig containing small probes to sample the field at appropriate points; however, the rig has a distorting effect on the field as well as requiring long acquisition times. An alternative technique proposed by Sekihara et al. achieves field sampling by imaging of a homogeneous phantom with B_o inhomogeneity calculated from two spin echo phase images with equal TEs but different T-180s.

We are investigating a new fast method for B_o field mapping which takes advantage of the fact that spherical harmonic expansion of the field only requires sampling on a spherical surface. We suggest following a circular trajectory in k-space by use of oscillating gradients as the appropriate sampling strategy since it both minimizes imaging time over a spherical surface and is compatible with the symmetry of the surface to be sampled. By using a ring phantom, oscillating gradients, and the spin echo sequence proposed by Sekihara et al. it is possible (with just 2 spin excitations) to sample the field along a circle in the x-y plane to any desired degree of angular resolution. Our phantom consists of a set of nine plastic disks, each containing a ring of sample (H_2O) at varying radii such that the sample rings form a spherical surface. Sampling of the field on each disk is achieved by slice selection followed by circular sampling in k-space. It is theoretically possible to fully sample the field for spherical harmonic analysis with as few as 18 excitations (2x number of disks). This differs from other phantom imaging techniques which are more time consuming since they require acquisition of full 2D data sets.

► **349** 14:57PM

AUTOMATIC REMOTE TUNING AND DECOUPLING INTERFACE FOR INTRACAVITY PROBES

GJ Misic and EJ Rhinehart
Medrad, Incorporated; Pittsburgh, Pennsylvania

Intracavity probes, especially those designed to be inexpensive, single use disposables, present unique problems in the electrical design of a tuning, matching, and decoupling network. The geometry of inflatable types, such as prostate and vaginal probes based on a balloon structure, is not sufficiently constant to allow high signal to noise ratio performance without tuning on an individual basis, following placement of the probe. The cost of high Q, non-magnetic components such as tuning capacitors, varactor diodes, and PIN diodes precludes their use on a disposable device.

To address these problems, an external interface device was developed which performs an automated tuning procedure. An integrated, high impedance FET preamplifier and a crossed diode decoupling network were used in the interface device. The compatible family of probes use a series resonant, Faraday shielded coil and a one-quarter wavelength (at 64 MHz) cable; the probe appears as a high impedance parallel resonant device at the interface box input port. Automatic tuning is accomplished by placing a parallel resonant circuit which includes a varactor diode across input port of the interface. The voltage to the varactor is adjusted by the internal circuitry to optimize the scalar value of S21 between an internal RF source and the probe.

The interface box was evaluated, both with phantom studies and under in-vivo conditions. The results were found to be superior to both fixed tuned probe systems and to the earlier design autotune device which did not include the FET preamplifier and used the S11 parameter for probe tuning optimization.

WEDNESDAY p.m.

► **350** 15:09PM

In Vivo RF-Field Mapping with Amplitude Modulated Pulses

R. Stollberger, M. Scheidegger*

Magnet Resonanz (MR), Universität Graz, Auenbruggerplatz 9, A-8036 Graz/LKH
*Inst. of Biomed. Engineering, ETH and Univ.Zürich, CH-8044 Zürich

In Vivo RF-Field Mapping with Amplitude Modulated Pulses

Due to RF-eddy and displacement currents, the distribution of the effective RF-field in vivo is of special interest. Particularly at high B0-fields (>= 1.5 T), the induced RF-currents provoke that the actual field deviates from the field of the empty coil, depending on the special geometrical and electrical conditions. Based on previous work (1), different methods for an accurate and comparatively fast determination of the RF-field in vivo were developed and compared by simultation and measurements. All the investigated methods (variation of the excitation pulse, evaluation of spin echo amplitudes, and evaluation of the ratio of the amplitudes of a stimulated echo and a primary spin echo) base on the proportionally between the flip angle and the B1-amplitude. Using an appropriate experimental design, errors due to the tissue parameters RHO, T1, T2 will be suppressed. The sensitivity distribution of the coil is canceled out by the calculation of the field. The latter is necessary if the RF-eddy currents are not negligible (2). The best results were obtained using a multiple slice sequence. The flip angle of the excitation pulse is varied in combination with that of a compensation pulse to suppress the effect of the T1 relaxation in the mapping. This sequence allows to determine the RF-field distribution in 15 slices with a matrix size of 128x256 in 4.3 min.

1. R. Stollberger, P. Wach, G. Mc Kinnon et al., Proc. 7th Annual Meeting (Works in Progress p 106), SMRM 1988
2. R. Stollberger, P. Wach, Proc. 8th Annual Meeting, 1174, SMRM 1989

► **351** 15:21PM

EddyFID: An NMR method for Eddy Current Analysis and Pre-Emphasis Calibration

R. Scott Hinks
Picker International, Highland Heights, Ohio, 44143

Imperfect gradient response due to eddy currents represents a serious problem for MR imaging. Classical methods of characterizing eddy currents have depended on measuring and integrating changing magnetic fields by means of a gradient search coil. Various problems with this methodology (including DC drift, sensitivity to motion, signal to noise, and spatial averaging) led to our development of an NMR-based method of measuring gradient step response. As illustrated in Figure 1, a long, constant gradient pulse (about 3 seconds) is first applied. The NMR signal of a small, short T1 sample is then monitored by acquiring FID signals very rapidly after the gradient is switched off. The frequency of each FID is computed by a least squares fit of phase vs. time. Normalizing this data to the frequency of an FID acquired with the gradient ON then gives an direct measure of the step response of the gradients, and hence, the eddy currents. This method reproducibly measures both short and long time constant eddy currents to 0.1%.

Gradient pre-emphasis may then be calibrated by computing the gradient waveform required to achieve the desired step function and mapping it to a series of exponential terms.

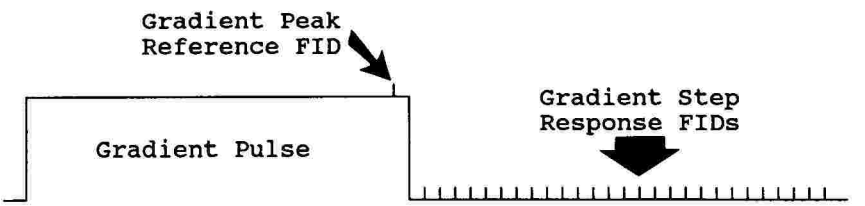

Figure 1

► **352** 15:33PM

A HIGH PERFORMANCE QUADRATURE LUMBAR SPINE COIL FOR 1.5 TESLA

GJ Misic, MA Weinstein*, and DK Manley
Medrad, Inc., and Cleveland Clinic Foundation*

In order to gain added signal to noise ratio performance under clinical imaging conditions, a lumbar and thoracic spine coil was developed exploiting quadrature polarization technology. The coil was designed to achieve several goals, including an effective penetration depth of 12 to 14 centimeters, a uniform field of view of 25 to 30 centimeters in the sagittal plane, and sufficient signal to noise ratio performance to allow high resolution axial imaging with a field of view as small as 16 centimeters. Since the direction of the circular polarization of the NMR signal is dependent on the direction of the B0 magnetic field, a means was required to allow field selection of the field polarization of the coil.

The final coil design consists of a single loop coil and a two loop coil in the pattern of a flattened saddle coil, the former having a sensitivity to vertically polarized RF, and the latter to horizontally polarized RF at the depth of the region of interest. A simple 90 degree phase shift network operating at an impedance of 100 ohms is used to combine the two 100 ohms outputs of the two coils to drive a single 50 ohm preamplifier. The output cable to the preamplifier is selectively connected to the appropriate coil-network junction to obtain proper coil polarization sense.

The final coil design was evaluated both by comparison phantom and in-vivo studies. The improvement in signal to noise ratio was sufficient to allow equivalent quality images to be obtained with one half the number of excitations, cutting imaging time in half.

► **353** 15:45PM

HYPERTHERMIA MONITORED BY MRI: AN INTEGRATED DEVICE

D. Le Bihan, J. Delannoy, Ching-nien Chen, R. Turner, R.L. Levin.
Diagn. Radiology Dept. and Biomed. Eng. and Med. Branch, NIH, Bethesda, MD20892

Hyperthermia (HT) is being used as an adjunct treatment in cancer or chronic infection. It has recently been shown that MRI can be used during HT sessions to map in real time the key HT parameters of temperature and blood flow. MR spectroscopy can also be used to monitor changes in metabolism. In order to use MRI to monitor hyperthermia (HT), we have built a single functional unit that includes, concentrically from outside to inside: (a) a modified Mini Annular Phased Array (MAPA) designed for the HT treatment of limb tumors using rf; (b) a MRI rf coil geometrically and electrically compatible with the HT system, used for transmitting and receiving; (c) a high performance magnetic field gradient coil. This unit lies on the mobile patient support of the MRI unit and can be quickly removed from the magnet bore, so that the MRI scanner can be easily switched from the HT to the conventional configuration and vice-versa. This combined device was optimized for a 1.5T (64 MHz) MRI unit (Signa, GE).

The new MAPA consists of a cylindrical array of four pair of dipole elements which are activated in phase and with equal amplitude so that their electric fields constructively interfere along the central axis to maximize the power deposition there. Cross-talk between the HT system working at 168 MHz and the MR coil (64MHz) was minimized by several rf filters and switches. The gradient coil (25cm i.d.) has a low inductance that allows larger gradient strengths to be reached (>40mT/m) with shorter rise times (<100us) than with conventional coils, of value for temperature imaging using diffusion measurements. This gradient coil is driven by the usual MR system amplifiers.

The unit was tested using a cylindrical phantom containing a doped polyacrylamide gel. Heating was induced at the center of the phantom using a power level of 600 W for 30 minutes. Heating and imaging were performed using in a time-sharing process (500ms heating and 200ms recording for a 700ms repetition time). High resolution (128x256 pixels) temperature images were derived from diffusion MR images as recently described, showing the power deposition map (SAR) of the MAPA. The temperature determined from these MR images were within 0.2^{o}C of those measured from thermocouples placed inside the phantom.

► **354** 15:57PM

HIGH RESOLUTION IMAGING OF THE HUMAN EYE USING VERY SMALL SURFACE COILS

J.F. Schenck, S. Lerman*, A.G. Schechter**, S.P. Souza, C.L. Dumoulin, D.R. Eisner
GE Corporate Research & Development Center, Schenectady, NY 12301
*Eye Research Lab. and **Dept. of Radiology, New York Medical Ctr., Valhalla, NY 10595

Several components of the human eye, including the len and iris are located within 1 cm of the body surface. Other crucial structures, e.g., the retina and the optic nerve head, are only slightly deeper - being 2-3 cm from the surface. This location makes the eye an attractive subject for improved high resolution surface coil imaging. If the clinical interest is in the anterior eye structures, we have found that a substantial advantage may result from the use of very small coils, approximately one inch in diameter, that are designed to fit into the orbital recess and to be positioned within one to three mm of the eyelids.

The enhanced SNR makes it possible to produce high resolution images and simultaneously reduce the scan time. We have found it possible, at 1.5 T, to produce high quality (128x256 matrix, 3 mm slice thickness) 8 cm field-of-view, multi-echo, multi-slice images using only a single excitation. Satisfactory scan times can be as short as 51 seconds (T_R of 400 msec). By increasing the gradient field strength, the FOV has been further reduced to 4.8 cm while maintaining satisfactory image quality.

The higher resolution makes possible T_1 and T_2 relaxation measurements on the lens with reduced partial volume interference. We have measured lens relaxation times in several normal volunteers. A typical result (male, aged 32) is T_1 = 600 msec T_2 = 23 msec. The lens has a remarkably short T_2 relaxation time - one of the shortest of any of the soft tissues in the head. This presumably reflects an intense cross-relaxation with crystallin proteins.

Difficulties with blinking and eye motion are among the current limitations of this technique. Consequently, we are examining eye tracking techniques to provide a means of gating the image to reduce or correct for motion artifacts. Given the high resolution and sensitivity of this new coil system it is likely that a complete MR eye exam for diseases such as cataract and glaucoma could be completed within fifteen minutes.

► **355** 16:09PM

CONTRAST OF ULTRAFAST FLASH IMAGING IN THE UPPER ABDOMEN

K.Wicke, S.Felber, W.Judmaier, G.Laub*
University of Innsbruck, Department of Magnetic Resonance;
*Siemens Medical Systems, Erlangen, FRG

Ultrafast gradient echo sequences yield to further improved image quality in the upper abdomen by eliminating motion artefacts often compromising SE-images. Their complex signal behaviour however requires a careful selection of scan parameters.

In normal volunteers the contrast behaviour of a newly developed ultrafast FLASH sequence was investigated.

The Snapshot FLASH Sequence allows a single slice acquisition with a 128 x 128 matrix in less than 2 seconds. A standardized program with varying combinations of flip angles and preparation pulses was performed in all volunteers. Quality rating of images was mainly done in respect to soft tissue contrast and signal to noise ratio in comparison to a standard FLASH and T_1 weighted SE sequence.

Overall signal intensity and soft tissue discrimination was considered best at a tip angle in the range of 20 to 40 degrees. Preparation pulses preceding the excitation pulse at an interval time of 250 to 750 ms led to higher T_1 weighted images.

Since conventional single slice breathhold gradient echo sequences are a useful tool in imaging cooperative patients, the ultrafast Snapshot FLASH Sequence can also be used in critically ill patients to achieve comparable image quality. The clinical value of high time resolution contrast perfusion studies using this sequence is under current investigation.

PULSE SEQUENCE DEVELOPMENT & OPTIMIZATION

MODERATORS: W. T. DIXON, Ph.D., M. I. HROVAT, Ph.D.

► 356 14:45PM

EXTRACTION OF CHEMICAL SHIFT INFORMATION IN THE PRESENCE OF A GRADIENT

M.I. Hrovat, G.J. Moore, G. Gonzales
Dept. of Radiology, Harvard Medical School and Brigham & Women's Hosp., Boston, MA

Extraction of chemical shift information in the presence of a gradient has been a long standing problem in many applications. We have developed a method where a gradient may be present during the acquisition of the signal and still permit a complete separation of chemical shift and spatial information without assumptions concerning the chemical shift spectrum.

This method is similar to the technique employed in decoupling chemical shift and J-J spin coupling in 2D homonuclear J-spectroscopy. A series of free induction decays (FIDs) are collected in the presence of a gradient. The only addition is the presence of a gradient read-out encoding pulse prior to the signal acquisition. The function of the read-out encode gradient is similar to the phase encode gradient in a normal spin warp imaging sequence. Each signal is acquired with a different amplitude for the read-out encoding gradient and hence, provides a 2D data set. If a 2D Fourier Transformation (FT) is performed at this point there would result a complicated 2D spectrum with spatial information coupled into both dimensions and chemical shift information coupled along one dimension. By performing a suitable "tilt or shearing" operation on the 2D data set before FT, the spatial and chemical shift coordinates can be made orthogonal to each other.

The extraction method has been successfully applied by our group to data sets acquired using a simultaneous MRI and 3D P-31 Chemical Shift Imaging technique (1). The experimental requirements when using the extraction method for the above application follow the equation:

$$\frac{Gro\ (H\text{-}1)}{SW\ (P\text{-}31)} = \Delta G_{roe}(P\text{-}31) * T_{roe}(P\text{-}31)$$

where Gro is the read-out gradient strength, SW is the spectral width, T is time, and ΔG_{roe} is the change in the read-out encode gradient strength. Using this relation, it is straightforward to show that deconvolution of the data is possible with a simple 45° "tilt" of the acquired data set. This has been confirmed experimentally by our group.

(1) Moore GJ, Hrovat MI, Cheng HM, Gonzalez RG. Simultaneous MRI and 3D Chemical Shift Imaging. Presented at 8th Annual SMRM Mtg., Amsterdam, The Netherlands, 1989.

► 357 14:57PM

T_2 CONTRAST MANIPULATION IN MRI BY A ROTATION "MAGIC ANGLE" RF FIELD

J Zhong, JC Gore and IM Armitage
Dept. of Diag. Radiol., Yale Univ. School of Medicine, New Haven, Connecticut, USA

We have implemented a pulse sequence designed to lengthen tissue transverse relaxation times T_2 and alter the T_2 contrast in spin echo imaging. It uses a RF rotating field applied as a long weak RF pulse of varying duration τ, amplitude H_1 and frequency ω before a regular spectroscopic or imaging sequence[1]. When there is incomplete motional narrowing of the water spins, the decay time of the FID measured with such a sequence is given by $T_{2\rho}=2T_2/|3\cos^2\theta-1|$, where T_2 is the relaxation time that would be measured by a CPMG sequence and θ is determined by $\arctan(H_1/|H_0-\omega/\gamma|)$. If the pre-pulse is on resonance the decay time is $2T_2$, whereas when $\theta=54.7$ (the "magic angle") the decay time is substantially longer. Thus if some of the spins in the sample have significant non-zero dipole interactions arising, for example, from hindrance of the water motion because of their interactions with macromolecules, the measured decay time will be longer than T_2. In an imaging experiment the contrast between such interacting component and other freely tumbling water can be manipulated by varying the length or frequency of the rotating RF field.

In studies of tissue samples we have shown that the decay times elongate in precisely the fashion predicted. In kidney, for example, the decay times are found to be 62, 114, 256 msec from CPMG and $T_{2\rho}$ sequence with $\theta=90$ and $\theta=54.7$ degrees respectively. No changes are seen in decay time of pure liquids. Images recorded at 2.0T with this technique demonstate that novel useful contrast effects can be achieved.

[1] Moses Lee and Walter I. Goldburg, *Phys. Rev.*, **140**, A1261 (1965)

WEDNESDAY p.m.

► **358** 15:09PM

NMR PULSE PROGRAM FOR CARDIAC CINÉ TAGGING

Pearlman JD Reese TG
Massachusetts General Hospital, Boston MA 02114

We have designed and tested a novel pulse program for NMR 'tagging' of myocardium which can be used in cardiac ciné imaging without time delays after R-wave triggering [1]. The placement of the myocardial tag is timed according to the previous R-wave trigger and occurs before the subsequent R-wave. This requires no time delay after R-wave detection and thus allows the acquisition of images to begin at once without the loss of the end-diastolic and early systolic information. The sequence also has sufficient persistence in the myocardium for acquisition of at least 15 frames of one slice at 30mS intervals. This is attributed to the combination of minimizing longitudinal magnetization by excitation at a well-chosen tip angle and minimizing transverse magnetization by phase scrambling in the tagged regions. Unlike previous "saturation" techniques [2,3], we are able to form a full ciné series in one NMR acquisition beginning immediately after the R-wave.

This pulse program was used to assess the myocardial twist and torsion of normal volunteers [1] and confirmed our ability to place tags during late diastole as evidenced by the presence of the tag in left ventricular (LV) blood pool of the first frame. Rotation of myocardium during systole is clearly seen when the ciné study is viewed as a 'movie' and can be measured in timing and magnitude at any arbitrary LV short axis section.

References

[1] Reese TG, Pearlman JD; **Circulation Suppl 78:**II-591, 1988.
[2] Zerhouni EA, Parish DM, Rogers WJ, Yang A, Shapiro EP; **Radiology 169:**59-63, 1988.
[3] Axel L, Dougherty L; **Radiology 171:**841-845, 1989.

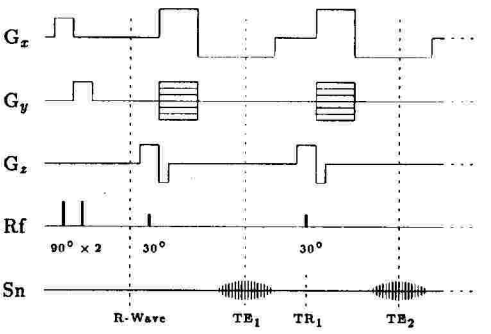

Figure 1 - Pulse Sequence

► **359** 15:21PM

Faster Acquisition of 2D MR Angiographic Data Sets

PJ Keller, Ph.D., EK Fram, MD, KD Williams, MD, BP Drayer, MD
Barrow Neurological Institute, ST. Joseph's Hospital and Medical Center, Phoenix, AZ 85013

Previously we reported on the development of a new method for acquisition of magnetic resonance angiography (MRA) source images. (1) In this method a volume data set is obtained by sequential acquisition of thin contiguous 2D slices. To maximize stationary-to-flow contrast a spoiled gradient echo pulse sequence employing a 50° flip angle, TR = 50, TE = 10 is used. New transceiver hardware permitting phase locking of the receiver to the transmitter was recently installed in our MR instrument (GE Signa, Milwaukee, WI). With this transceiver one can spoil the steady-state by RF phase shifting rather than by using gradient spoilers. This significantly shortens the time necessary to play out the pulse sequence; thus a two-slice interleaved acquisition is possible with a TR = 60. **This decreases the overall acquisition time by 40% without compromising resolution, contrast, or SNR.**

To avoid loss of stationary-to-flow contrast, the first pass pair consists of slices at one end of and at the middle of the imaging volume. The spatial relationships between the two slices of an acquisition pass and an optional presaturation slab are held constant, i.e. all three are incremented to a new location upon completion of a pass. This strategy in combination with the fact that the acquisition is not synchronized with the cardiac cycle, makes it unlikely that blood which was excited (and thus partially saturated) in one thin slice will be present in the distal thin slice of the pass pair at the time of its excitation.

(1) Keller PJ, Drayer BP, Fram EK, Williams KD, Dumoulin CL, Souza SP. Radiology, Nov. 1989, In Press

► **360** 15:33PM

OPTIMIZATION OF PULSE SEQUENCE PARAMETERS IN "SNAPSHOT-FLASH" IMAGING

JP Mugler III, JR Brookeman
Dept. of Radiology and Biomedical Engr., University of Virginia, Charlottesville VA

The recently introduced "snapshot-FLASH" technique[1] can produce T1 or T2 weighted images in less than 1 second. This novel imaging method offers many new and interesting applications for both research and clinical imaging.

We have implemented a version of the snapshot-FLASH technique on our 1.5 Tesla standard commercial whole-body imager (Magnetom 63SP, Siemens Medical Systems, Iselin, NJ). Our implementation employs a repetition time of 5-6ms and an echo time of 3ms. A 128x128 image is measured in 650-750ms, with a minimum field-of-view of 260mm. We use inversion or driven equilibrium preparation pulses to generate T1 or T2 weightings, respectively [2].

Currently, we are investigating the application of this technique to imaging of the brain, C-spine, and abdomen. We have studied the effect of varying the flip angle and the delay between the preparation pulse(s) and the snapshot acquisition on the desired image contrast. Optimum parameter combinations for generating heavily T1 weighted images in the brain and abdomen, and myelographic images in the C-spine are also under investigation.

The optimization of the flip angle for a given preparation to acquisition delay is of particular concern. One of the problems inherent to snapshot-FLASH is a T1-dependent decay of the signal across the phase-encoding steps. This is analogous to the well known T2-dependent decay that occurs in echo-planar imaging. For a given initial value of the longitudinal magnetization and a given T1, it is (sometimes) possible to balance the regrowth of the longitudinal magnetization during TR against the longitudinal component reduction caused by the excitation pulse. With a specific set of tissue T1s, an intermediate value for the flip angle would minimize the T1-dependent decay artifacts. Competing factors include the Ernst angles for the particular tissues and TR (to maximize the SNR), and the increase in transverse coherence artifacts with increasing flip angle. We are investigating this optimization problem with phantoms and a Bloch equation simulation.

Our initial results with snapshot-FLASH are encouraging for a number of potentially useful clinical applications.

1. A Haase, D Matthaei, D Norris, D Leibfritz, 8th SMRM, 364 (1989).
2. B Kiefer, M Deimling, D Finelli, 8th SMRM, 367 (1989).

► **361** 15:45PM

SINGLE-SHOT LOCALIZATION OF VERY SMALL OFF-AXIS REGIONS OF INTEREST BY PROJECTION PRESATURATION

S Singh, BK Rutt
Departments of Medical Biophysics and Radiology, University of Western Ontario, Canada

We have developed an accurate single-shot localization technique called Projection Presaturation for multi-dimensional spatial localization. The technique uses short, small tip-angle, selective saturation RF pulses of cossinc waveform applied multiple times at stepwise equal angular intervals during one half cycle of a constant amplitude rotating gradient to localize a cylindrical region of interest (ROI) by presaturating a hollow outer cylindrical volume. We have further extended and generalized the technique to localize a very small ROI (*e.g.* diameter $\leq$ 4 mm) which can be moved anywhere in three-dimensions at predetermined positions within the sample. To improve the sharpness of the ROI edges especially in the case of a very small ROI, we have used a pair of narrow and wide band excitation cossinc RF pulses instead of a single cossinc RF pulse with negligible overlap in their one-dimensional profiles. To move the cylindrical ROI off-axis with its axis parallel to the axis of rotation and intersecting orthogonally the plane of gradient rotation at (r_o, θ_o), the pulse-pair was frequency-offset by $[\gamma/2\pi\ G_r\ r_o][\cos(\theta_o - \theta)]$ at different angles of repetition $\theta \rightarrow 0\text{-}180^o$. Full movement of the ROI in three-dimensions within the sample was achieved by frequency-offsetting the 90° readout pulse of a standard 2DFT imaging sequence, selective along the axis of rotation, following 2D off-axis localization. To dephase the existing transverse magnetization completely after each pulse-pair in a short time (~ 1 ms), the amplitude of the rotating gradient G_r was increased in the interpulse interval. The outer volume signal was 99.9% suppressed using 36 RF pulse-pairs of 30° tip-angle showing that the technique is not prone to off-resonance effects. Alternately, allowing only partial dephasing of the transverse magnetization of the outer volume, we obtained spatially modulated signal intensity from the outer region in concentric circular bands around the ROI which may be used to study motion (*e.g.* cardiac wall motion, blood flow *etc.*). Applications of the technique include study of short T_2 species from a localized volume by *in vivo* spectroscopy, signal contamination/motion artifact suppression, localized relaxometry, MR angiography, and flow studies.

WEDNESDAY p.m.

► **362** 15:57PM

INTRA-ACQUISITION MODIFICATION OF TR AND TE IN SPIN-ECHO IMAGING

RK Butts, F Farzaneh, SJ Riederer, RL Ehman
MR Laboratory, Mayo Clinic, Rochester, MN 55905, U.S.A.

Conventional T2-weighted spin-echo imaging remains a popular diagnostic method despite long scan times. We describe a method for reducing this scan time while retaining, and in some cases enhancing, the diagnostic quality of the images. This method reduces the TR and TE value of the sequence **during** the scan as a function of the phase encoding "view" being acquired. TR and TE for the low frequency views remain at their prescribed values while they decrease to lower values for the high frequency views. Since the lower frequency views determine contrast, T2 contrast is maintained. The net effect of decreasing both TR and TE is an increase in signal at the higher spatial frequencies, thereby providing an enhancement of edges and small objects. This technique was tested in a sequence in which TR/TE were changed during the scan from 2000/80 to 1000/20. Human images display similar contrast to the standard (2000/80) spin echo images, but with the expected edge enhancement and up to a 30% reduction in scan time. This time savings is due to the progressive reduction in TR during the scan.

As an alternative, the raw data can be filtered before reconstruction to reduce the aforementioned edge enhancement effect. Specifically, the raw data at the higher frequency views can be weighted by an amount inverse to the expected degree of edge enhancement. The resultant signal response for all views is the same as that for a scan at fixed TR/TE. However, the noise in each view is reduced in accordance with the square of the filter response at that view. With some potential loss in contrast in the high spatial frequencies, the result is a simultaneous time savings of up to 30% and an increase in SNR of 30%. We describe the theory of this technique and present experimental in vivo results.

► **363** 16:09PM

IMPROVED T1 CONTRAST IN ULTRA-FAST SCANS

AE Holsinger, F Farzaneh, SJ Riederer
MR Lab, Mayo Clinic, Rochester, MN 55905 USA

MR imaging with ultra-short repetition times typically suffers from decreased contrast. In this paper, we present a method by which the contrast of short-TR images can be enhanced and in which the contrast is independent of the data acquisition. This work is based on our previous experience in MR fluoroscopy (1) in which TR values of 6 msec or less are used, and is similar to that proposed by Haase (2).

Figure 1

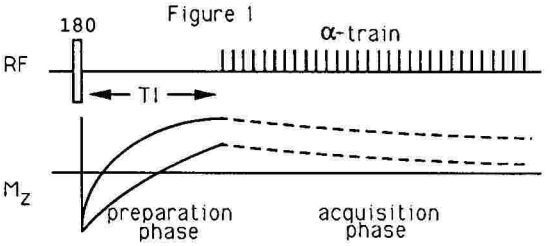

The RF pulse sequence and corresponding magnetization behavior are shown in Figure 1. The contrast is set during the preparation phase (here, an inversion pulse followed by time TI gives T1 contrast) and the data are acquired in one shot with a short-TR sequence during the acquisition phase, when we effectively sample the relaxation curve. We can quantitatively describe the effect of the flip angle and the TR of the acquisition sequence on the approach to steady-state and the perturbation of the T1 curve. It is important that the lower order phase encodings be acquired while the T1 contrast is large in order to ensure that the bulk structures of the image are T1-weighted.

We have implemented this pre-inversion "snapshot" sequence on a GE Signa 1.5T system with 128x128 resolution and TR/TE of 6/3.5 msec for the acquisition sequence. Preliminary results show effective T1 weighting with a scan time of approximately 700 ms per slice. This technique can be extended to gain other contrasts and is potentially useful in abdominal imaging where conventional T1-weighted images can be corrupted by motion due to the long scan time.

1. Farzaneh F, et al. MR Fluoroscopy: Initial Clinical Studies. Radiology 1989; 171:545-549.
2. Haase A, Matthaei D, Norris D, and Leibfritz D. Proc. 8th Mtg. SMRM, Amsterdam, 1989, p. 364.

P001

ABDOMINAL MR IMAGING: INFLUENCE OF SEQUENCES AND CONTRAST AGENTS

S. Kaminsky, M. Gogoll, K. Neumann, M. Langer, R. Felix
Freie Universitat Berlin, UKRV Charlottenburg, Dept. of Radiology

In abdominal MRI lack of suitable bowel contrast agents is regarded as a significant drawback. Various positive and negative contrast agents have been proposed. The purpose of this study is to investigate the efficacy of Gadolinium-DTPA (Gd-DTPA) and air (A) as bowel contrast agents. 125 patients with abdominal tumors or inflammatory diseases were imaged at 0.5T after oral (n=120) and/or rectal (n=20/5) application of Gadolinium-DTPA (1.0 mM, 6-16 ml/kg, 15 g mannitol/l, Schering AG). In 68 cases pre- and postcontrast images we obtained. Various T1- and T2-weighted spin-echo sequences and a multislice gradient-echo sequence were used. To reduce peristaisis scopolamine was IV injected in 98 cases. Contrast of the enchanced gastrointestinal tract (GI-tract) versus pathological structures and lesion delineation were visually assessed. Using a region-of-interest technique signal intensities of intraluminal Gd-DTPA and air, abdominal fat (F), lesion (L) and image noise (N) were measured in 33 cases. According to Stark (10) contrast to noise ratios (CNR) of Gd-DTPA and air versus lesions and abdominal fat were calculated as

$$\text{CNR Gd/L} = \frac{\text{Gd-DTPA} - \text{L}}{\text{N}} \quad \text{CNR A/L} = \frac{\text{A} - \text{L}}{\text{N}} \quad \text{CNR Gd/F} = \frac{\text{Gd-DTPA} - \text{F}}{\text{N}} \quad \text{CNR A/F} = \frac{\text{A-F}}{\text{N}}$$

Gd-DTPA provided hyperintense opacification of the entire GI-tract. In 101 cases Gd-DTPA was in the region of interest. Regardless of the imaging sequence marked positive contrast versus liver, pancreas and kidneys was obtained, whereas contrast towards abdominal fat was either low or not existing (CNR -0.1-2.8, Av 0.5). High contrast of Gd-DTPA-enhanced bowel loops towards pathological tissues was observed in all imaging sequences (CNR 0.3-3.9, Av 2.1). Air showed significantly smaller contrast versus lesions (CNR -0.9 - -0.1, Av -0.8). Tumor delineation was improved in 44 of the 68 cases imaged before and after application of Gd-DTPA. The high signal intensity if intraluminal Gd-DTPA resulted in good delineation of gut wall thickening and in reliable labeling of incompletely filled bowel loops. In 37 of the 57 patients having received postcontrast images only opacification of the GI-tract was found to be diagnostically useful. In the remaining 20 patients Gd-DTPA did not contribute to lesion delineation due to either lack of lesion-bowel interfaces, lack of contrast material in the region of interest or excellent lesion demarcation by peritoneal fat. Mild diarrhea and meteorism were the only side effects in 31 patients. No pathological changes in blood parameters were found. Image artifacts from bowel motion were effectively reduced by the use of scopolamine. Ref. 1 Stark, D.D. et al: Radiology 159, 365-370, 1986

P002

MRI of the Knee:3D FISP Imaging with Multiplanar Reconstruction.

D.L. Mushinsky, R.M. Keiser, J.D. Reeder, S.M. Andelman.
Whitesquare Imaging, Baltimore, Maryland.

POSTER ABSTRACTS

Multiplanar Reconstruction (MPR) images have only recently begun to be recognized as an important diagnostic tool in the visualization of the knee joint. 3D volume acquisition offers not only exquisite detail in thin, contiguous slices but also an increase in signal to noise which fosters a more precise view of small knee joint entities. The reconstruction of orthogonal and oblique orientations from the original data acquisition permits retrospective choice of imaging geometry promoting improved definition of structures not well visualized on conventional spin echo sequences.

P003

MRI OF THE KNEE: CORRELATION OF RADIAL SCANS WITH SAGITTAL AND CORONAL SCANS

Robert C. Hewes, M. D., Ted Miller, M. D.
Kettering Medical Center

Traditional MRI scans of the knee have been performed using Spin Echo T1 images in the sagittal and coronal plane. However, to optimally visualize the entire meniscus, radial scans centered on each condyle were developed. We use a fast scanning (GRASS) to optimally enhance the meniscal pathology. We now have done 100 cases where both radial fast scans and sagittal and coronal T1 weighted images were obtained of the knee joint. We evaluate the accuracy of diagnosis by seeking clinical follow-up in as many cases as possible including surgical and clinical evaluation. We independently correlated the findings on the coronal, sagittal, and radial scans to determine accuracy by each scanning parameter and also the scan sequence that was most definitive of the abnormality.

We find that the radial scans provide more complete evaluation of the meniscus and with the GRASS scans, the contrast is better to define meniscal pathology.

P004

MR FINDINGS IN THE FOOT IN DIABETES MELLITUS

TE Moore, WTC Yuh, MH Kathol, GY El-Khoury
Department of Radiology, College of Medicine, The University of Iowa

In chronic diabetes mellitus, the feet are frequently involved with various interrelated pathologic processes. Together, these complications represent the most common reason for hospital bed occupancy in diabetic patients. Peripheral neuropathy, vascular insufficiency, or a combination of both, are the primary factors in the development of these complications which include bone and soft tissue infections and the various sequelae of neuropathic disease.

MR studies of the feet in 40 patients with diabetes mellitus were reviewed retrospectively. The studies were assessed for features of the following categories: edema, joint effusions, deformity, ulcers, cellulitis, abscesses and sinus tracts, osteomyelitis, neuroarthropathy, ischemia, postoperative changes, progression of disease, and response to treatment. Many of the complications were subtle and were not always appreciated by other modalities. Soft tissue edema, especially in the plantar aspect, was noted in all our patients, with or without infection. We believe this may be one of the earliest manifestations of diabetes mellitus in the foot. Abscesses were frequently detected but cellulitis could not be easily differentiated from the frequently coexistent edema. STIR imaging was found superior to T_2-weighted imaging in the diagnosis of osteomyelitis, whereas T_2-weighted imaging was superior in the delineation of abscesses. MR was found to be an excellent method for detection of osteomyelitis and its differentiation from cellulitis. However, the differentiation of osteomyelitis from neuropathic changes was sometimes difficult, although often suggested by location and associated surrounding soft tissue changes and/or ulcers.

In this poster we demonstrate typical MR features of diabetic foot complications and attempt to explain how these relate to the underlying pathophysiology and chronological progression of the disease process. We also discuss the clinical relevance of accurate diagnostic findings.

P005

MUSCULOSKELETAL HEMORRHAGIC LESIONS: MRI FINDINGS

TE Moore, WTC Yuh, MH Kathol, DP Hawes
Department of Radiology, College of Medicine, The University of Iowa

Hemorrhage in the musculoskeletal system can be of various etiologies. It frequently presents with non-specific signs and symptoms mimicking other pathologic processes. In contrast to intracranial hemorrhage, hyperdense CT appearances of hemorrhage are often not seen in the musculoskeletal system. Musculoskeletal hemorrhage does, however, generally demonstrate typical MR signals which can differentiate it from other processes such as tumor, edema, and abscess.
46 hemorrhagic lesions in 32 patients aged 6-75 years (21 males and 11 females) were reviewed. Attention was paid to etiology, site, extent, and signal characteristics. Hemorrhage was the result of trauma(11), surgery(4), bleeding diathesis(6), tumors and tumor-like conditions(6), unknown etiology(5). Hemorrhage was seen in the following locations: intramuscular(15), intrafascial(13), intratendinous(6), intraarticular(4), intramedullary(6), intervertebral disks(2). Hemorrhage was observed as either localized (hematoma)(15), diffuse(13), or other, such as intraarticular clot(4). The MR appearances of hemorrhage were found to be more specific and more easily characterized in some sites (intramuscular, intrafascial, intratendinous, juxtacortical) than in others (intraarticular, intramedullary). This is attributed to multiple factors including the presence of other fluids, the signal characteristics of adjacent tissues, and the fact that many cases were imaged in the acute phase when the signal characteristics of blood tend to be less specific.
Six representative cases are presented. These were selected to illustrate the changing signal characteristics of blood at different ages, to show localized and diffuse hemorrhage, and to present examples of different etiologies such as hemophilia and hemorrhage within tumors.

P006

A series of color and pen and ink half tone drawings of normal and abnormal knee anatomy are presented to help simplify MRI interpretation. These demonstrate the relationship of the menisci, collateral and cruciate ligaments and the popliteus muscle and tendon. Additional half tone diagrams with corresponding MR images demonstrate common pathologic entities including medial collateral ligament tear, bucket handle tear, anterior cruciate tear, meniscal tear and meniscal degeneration. Brief textual descriptions are included.

P007

SIMPLIFIED ANATOMIC APPROACH TO MRI OF THE SHOULDER

PP Stockhausen, AA Fraizer, BB Kuzma, DO Davis, TS Dina
George Washington University Medical Center

A series of color and pen and ink half tone drawings of normal and abnormal shoulder anatomy are presented to help understand MRI interpretation. These illustrate the relationship of the muscles about the shoulder whose tendinous insertions make up the rotator cuff. Half tone diagrams with corresponding MR images demonstrate the normal anatomy and common pathologic entities including partial tear, complete tear, and acromioclavicular joint impingement. Brief textual descriptions are included.

P008

A NEW STRESS TEST DEVICE FOR CARDIAC NMR

Av Smekal, S Silber, MW Weiner
Magnetic Resonance Unit, VA Medical Center, UCSF, San Francisco, CA

The goal of this work was to develop a technique to exercise human subjects during MRI and MRS in order to determine functional and metabolic changes which occur when cardiac work is increased. For this we developed a unit which is based on a pneumatic system and stresses both legs of the patient in the limited space of the magnet (43 cm diameter). Each leg is alternately extending in order to depress a pneumatic pedal. Using a complex valve system it is possible to maintain a constant pressure in the system over the working cycle and also to change continuously the pressure in the system. This allows rapid step increases in the resistance of the system while the patient is exercising. The pressure range of the system is from 5 to more than 100 psi per leg. The device is easily mounted on the magnet table without hardware changes. The patient lies in a supine position. To avoid motion artefacts while acquiring NMR data, a foam mold was designed which stabilizes the upper body and reduces motion of the chest and shoulders of the patient. The patient's blood pressure is measured with a modified digital sphygmomanometer. The data acquisition is gated with the cardiac cycle (plethysmograph). The unit can be used for both imaging and spectroscopy studies. Images obtained with FFE pulse sequences while stress testing allow measurement of the cardiac ejection fraction and wall motion. With this device it is possible to perform cardiovascular stress studies with patients while acquiring NMR data to measure functional changes in the human heart.

P009

TORQUE OF PROJECTILES AT 1.5T

M. L. Schiebler, L. Robertson, M. A. Mauro, M. A. Koomen, R. A. Whaley

Department of Radiology, University of North Carolina at Chapel Hill

Twelve different projectiles were assessed for torque at 0.5T and 1.5T: seven bullets, three sizes of shotgun pellets, and two BB's. Bullets (the projectile portion) are made of lead (or a copper/zinc alloy), unless they are armor piercing - then they are steel. Shotgun pellets are either lead or steel. New federal legislation requires that steel shot be used on federal land. BB's are made of steel.

Only the steel shot and the BB's demonstrated any torque. The seven common projectiles, including 44 magnum, 38 special and 357 magnum, showed no deflection consistent with their composition (lead; or copper 80% and zinc 20%).

MR imaging in patients with identifiable projectile types should be safe, in that all are composed of lead or a copper/zinc alloy. Shotgun pellets are no longer entirely lead based and a detailed patient history is necessary to ensure that the accident occurred prior to 1985. All BB pellets are composed of steel (99% iron) and will, therefore, have a significant amount of torque at either 0.5 T or 1.5T.

P010

RAPID SPIN ECHO IMAGING (RASE): A NEW TECHNIQUE IN REDUCTION OF ARTIFACTS AND ACQUISITION TIME

SA Mirowitz, JKT Lee, JJ Brown, JP Heiken, SS Eilenberg
Magnetic Resonance Imaging, Mallinckrodt Institute of Radiology

In this poster we introduce a method in which a series of 11 T1-weighted spin echo images can be obtained in a 23 second period. This rapid imaging technique incorporates a very short TR and TE as well as half-Fourier sampling. This allows for screening of the entire upper abdomen (or other comparable body region) during a single suspended respiration. As a result, respiratory artifacts are virtually eliminated. Other significant advantages of this technique include improved patient throughput and potential for performing dynamic contrast studies. Contrast-to-noise measurements in phantoms, normal volunteers and patients indicate a substantial advantage for the RASE technique vs standard multiacquisition T1-weighted sequences. Images obtained with this method were also compared subjectively by three experienced MR readers to standard multiacquisition T1-weighted spin echo sequences. A total of 84 examinations in 18 patients were evaluated blindly in terms of severity of artifacts in phase-encoding direction, edge sharpness and overall image quality. Results indicate that, in addition to a marked reduction in imaging time, the RASE technique allows for considerable improvement in image quality.

P011

IMAGING THE ABDOMINAL AORTA USING DOUBLE-SPATIAL PRESATURATION AND GRADIENT MOMENT REPHASING TO MINIMIZE MOTION ARTIFACTS.

SS Berr,[1,2] JP Mugler III,[2] C Ayers,[1] JR Brookeman[2]
Cardiology,[1] Radiology,[2] Box 190, MRI Facility, UVa, Charlottesville, VA 22908

INTRODUCTION

Atherosclerosis results in more deaths than any other cause in Western Societies. MRI offers a potential means by which this disease could be detected and quantified, offering the possibility of routine screening and the ability to monitor and improve upon diet/drug treatments.

METHODS

A hindrance to obtaining usable MR images of the abdominal aorta arises from motion artifacts due blood flow and breathing. These artifacts can be minimized with appropriate pulse sequences. We have designed a pulse sequence which incorporates gradient moment rephasing (GMR) to limit artifacts. GMR increases the minimum echo time. In order to optimize image intensity, we keep the readout time of the first echo as short as possible and extend the readout time of the second echo in order to compensate for lost S/N (mixed bandwidth).

GMR is good at reducing phase-dependent artifacts, but has limited success with flow artifacts that result from variable-inflow enhancements due to pulsatile blood movement and from the motion of high-signal subcutaneous fat. In order to limit these artifacts, spatial presaturation pulses are incorporated orthogonal (phase encode direction) and parallel to the slice select direction. The orthogonal presaturation pulse is placed through the subcutaneous fat, while the parallel presaturation pulse is placed 5mm upstream from the first imaging slice to limit variable-inflow artifacts.

Images were obtained on a 1.0 Tesla Siemens Magnetom (Siemens Medical Systems, Iselin, N.J., USA) clinical imager. The tip angles of the spatial presaturation pulses applied in the phase encode and slice directions giving the best cancellation of signal were empirically determined.

RESULTS AND DISCUSSION

Several persons have been imaged with a standard double spin-echo sequence and with the above discussed sequence. The resulting proton density and T2 weighted images clearly demonstrate the improved image quality with the combination of motion-artifact limiting measures incorporated into the sequence. This sequence should prove useful for subsequent use in the detection and quantification of atherosclerotic lesions.

POSTER ABSTRACTS

P012

3-D FISP IMAGING OF THE KNEE: VALUE OF MULTIPLANAR RECONSTRUCTION

J.D. Reeder, D.L. Mushinsky, R.M. Keiser, T.R. O'Donnell, S.M. Andelman
White Square Imaging, Baltimore, MD

Recent studies have investigated the use of 3-D gradient-echo techniques as applied to musculoskeletal imaging. In addition to providing truly contiguous, thin sections, relatively high signal-to-noise images, 3-D volume acquisitions sequences also permit post-processing manipulation of the original data set in the form of multiplanar reconstruction. The clinical value of these reconstructed views, however, remains largely untested. In this study, 3-D FISP images were obtained in the sagittal projection on 12 patients who subsequently underwent arthroscopic surgery. Axial and coronal images through the menisci were reconstructed from the original data. Additional oblique coronal reconstructions were obtained parallel to the anterior cruciate ligament (ACL). Of the 24 menisci studied, tears were discovered at surgery in 12 and of the 12 ACLS examined one tear was identified. The sagittal 3-D FISP sequence demonstrated 10 of the meniscal tears. The reconstructed images identified 9 of the 10 tears evident on the sagittal scans and additionally demonstrated one of the tears not seen on the original images. The ACL tear was observed with both techniques. Reconstructed images proved to be of value both in confirming the presence of meniscal or ligamentous injury and in documenting normal anatomy. Considering the diagnostic information derived from the multiplanar reconstructed images at the expense of only minimal additional processing time (approximately one minute), orthogonal and oblique views reconstructed from the original data acquisition provide a complementary, clinically useful perspective relevant to imaging of the injured knee.

P013

THE VALUE OF STIR METHOD AND GD-DTPA IN THE BONE AND SOFT-TISSUE MASSES

H Nishimura, M Uchida, T Abe, M Koganemaru, H Ohtake
Department of Radiology, Kurume University School of Medicine

Magnetic resonance(MR) imaging is already established as an important modality for examination of musculoskeletal lesions and it has been shown that MRI is superior to any other modality for delineation of bone and soft-tissue masses.
STIR(short inversion time inversion recovery) method may be particularly useful for evaluating bone and soft-tissue masses. Since in STIR, T1- and T2-weighted contrast are additive, it could be possible to perform STIR method alone and have the sensitivity of a T1WI for the fatty bone marrow and that of a T2WI for the soft-tissues.
Intravenous administration of the para-magnetic MR contrast agent Gd-DTPA improves the delineation of the lesion in brain and spinal cord. As yet the effect of Gd-DTPA on the MR imaging of musculoskeletal masses has been few reported.
STIR images and Gd-DTPA enhanced MR images of 30 bone and 48 soft-tissue masses were reviewed with pathologic findings.
(Material and Methods)
All patients ranging in age from 6 to 81 years(mean, 46.2 years) underwent MR imaging between June 1987 and August 1989. Our studies were performed using a Shimadzu SMT-50 superconductive magnet(0.5 Tesla). In 78 patients, in addition to the conventional MR-examination(T1WI-SE 460/35, T2WI-SE 1800/100), STIR method(IR 1500/100/40) and T1 weighted scans following intravenous injection of Gd-DTPA(0.1mmol/kg) were performed.
(Results)
STIR method had a good delineation of the disease extent. Gd-DTPA enhanced MRI was sensitive for depiction of internal structure, estimation of vascularity, and accurate detection of lesions. Gd-DTPA was able to help to differentiate clearly the necrotic and inflammatory portions of inflammatory masses, as well as the necrotic and viable portions of tumors.
(Conclusion)
The results of this study indicate that STIR method and Gd-DTPA enhanced MRI are helpful for evaluating the bone and soft-tissue masses and increase the specificity of diagnosis.

P014

MRI OF SCIATIC NERVE IN DIABETICS WITH PERIPHERAL NEUROPATHY

LK Misra, DGK Varma, EE Kim, LE Todd, G Elizondo-Riojas
UT M D Anderson Cancer Center
Univ Nuevo Leon Sch of Med, Monterrey, Mexico

Peripheral neuropathy is a major complication of diabetes. Its detection and evaluation is uncertain by the conventionally used diagnostic techniques. Using animal models we showed that MR relaxation times were sensitive in detecting early signs of nerve impairment. The objective of this study was to determine the effectiveness of MRI to evaluate peripheral neuropathy in diabetics. The sciatic nerve of 7 diabetic patients and 6 age and sex-matched nondiabetic volunteers were imaged in axial planes from about the level of the greater trochanter of the femur to the mid-thigh using FONAR Beta 3000 unit. The nerve in the volunteers exhibited medium signal intensity on all pulse sequences (TR/TE: 500/28; 2000/56; 2000/28). By visual inspection no definite change in signal intensity of the nerves was observed between the diabetics and volunteers. However, the calculated signal to noise ratio was approximately three-fold and two-fold higher in the T_1 weighted (35 ± 9 vs 10 ± 3) and T_2 weighted (24 ± 6 vs 10 ± 2) images in diabetics, respectively. The cross-sectional diameter of sciatic nerve in diabetics (9.7 ± 2.2mm) was significantly reduced ($P<0.01$) than that of the volunteers (14.1 ± 1.3mm). These results suggest that signal to noise ratio and cross-sectional dimensions of sciatic nerve may be helpful in evaluating lesions of peripheral nerves.

Supported by Diabetes Research and Education Foundation.

P015

DIFFERENTIATING SKELETAL NEOPLASM FROM NON-NEOPLASTIC PROCESS: MR AND GD-DTPA

KL Harkens, WTC Yuh, MH Kathol, TE Moore, CW McGuire, DR Hawes, GY El-Khoury
Department of Radiology, The University of Iowa College of Medicine

Thirty patients with skeletal lesions, 12 neoplastic and 18 non-neoplastic, were studied using MR imaging. Each of the neoplastic tumors was examined with and without contrast enhancement using gadolinium (Gd)-DTPA. Five patients with non-neoplastic processes were also administered Gd-DTPA. In contrast to brain neoplasms, neoplastic processes in the musculoskeletal system showed minimal surrounding edema in subcutaneous or fascial tissues, whereas the non-neoplastic lesions, including inflammation, infection, hematoma, and vascular occlusion, produced significant edema and vascular prominence. The lack of surrounding edema demonstrated by the noncontrast MR imaging appears to be useful in the differentiation of neoplastic from non-neoplastic processes. Because of minimal edema, T2-weighted images are usually sufficient to demonstrate the extent of tumor involvement. Therefore, in spite of their enhancement by Gd-DTPA, contrast MR images may not be superior to the T2-weighted image. However, in the complicated case, such as tumor with acute hemorrhage, Gd-DTPA may provide essential information for a definitive diagnosis. When compared to contrast-enhanced CT, both contrast-enhanced T1-weighted images and unenhanced T2-weighted images showed the extent of tumor in soft tissue and bone marrow to better advantage.

P016

HIGH DENSITY BARIUM SULPHATE AS AN MR ORAL CONTRAST

L Martí-Bonmatí, J Vilar.
Department of Diagnostic Radiology. Hospital Dr Peset. Valencia. Spain.

Oral contrast medium is not routinely used in abdominal MR studies. However, it is sometimes difficult to differentiate the stomach or the duodenum, from hepatic or pancreatic lesions. Most oral MR contrast mediums, now under research, are paramagnetic or superparamagnetic particles.

After a sugestion by Dr P.Ros (1) we studied the use of high density barium sulphate as MR contrast medium. 15 persons (10 volunteers and 5 patients) were fasted for at least 4 hours prior to the study. A suspension of 196 g of commertial barium sulphate (BS) (Barigraf A.D. Juste S.A.Q.F. Madrid, Spain) on 130 ml of cold water (85% w/w, 259% w/v) was administered to them 30 minutes prior the examination. An anticholinergic drug (N-butyl bromide of hyoscine, 20 mg) was given 15 minutes before the study.

In the upper GI tract, BS suspension was uniformly dark on SE sequences weighted in T1 and T2, and STIR. The stomach and the two first portions of the duodenum were routinely filled. In 3 patients, there was a liquid-barium level in the stomach (probably due to gastric hypersecretion). The very low intensity of the BS is probably due to its low mobile proton density. We believe that, since BS is inexpenseve, harmless and at hand in all X Ray Departments, its proven effectiveness makes it highly recomendable as an oral MR contrast agent.

(1) P.Ros, personal communication, 1989.

P017

VARIANT MR ANATOMY OF THE IMMATURE KNEE

VM Tartar, MJ Siegel, WG Totty
Mallinckrodt Institute of Radiology, Musculoskeletal Radiology

The skeletally immature knee presents a range of MR appearances differing from adults and varying with age. Age-related differences in configuration and signal intensity of peri- and intra-articular structures of the knee need to be recognized so that they are not mistaken for pathology. We present a spectrum of normal MR appearances in skeletally immature knees to demonstrate observed anatomic variations from adults.

Three general stages of maturation are identified, including the very young, the maturing, and the near-adult. The very young demonstrate markedly thick articular cartilage, within which we have frequently observed a thin low signal linear band. Other anatomic variations we have noted are a relatively low insertion of the posterior cruciate ligament into the condylar notch and a broader region of high signal at the capsular attachment of the menisci than seen in the adult. With increasing maturation, the articular cartilage becomes relatively thinner until in the near-adult knee, it assumes normal adult thickness. The thin low signal line seen within the articular cartilage of the young is identified less frequently with maturation. The near-adult knee demonstrates an adult intra-articular appearance, but is characterized by the persistently open physis.

Against this background of varying normal MR anatomy in the immature knee, we present typical examples of pathology encountered, including meniscal and ligament tears, and bone contusions and tumors.

P018

CONTRAST ENHANCED BREATH-HOLD LIVER MR IMAGING

DG Gelblum, VM Runge, ML Wood
Division of Magnetic Resonance,Tufts-New England Medical Center Hospitals

The use of GD(HP-DO3A) (Squibb Diagnostics); presently in clinical trials; is evaluated at a dose of 0.5 mmol/kg for the purpose of improving detection and delineation of liver disease in a rabbit abscess model. Two types of breath-hold scans are compared with traditional nonbreath-hold spin echo(SE) scans for improved demonstration of contrast enhancement.

To date, 12 New Zealand white rabbits have been studied. The rabbits are anesthetized for sterile laporotomy with a Ketamine/Acepromazine mixture (10:1, 0.6mg/kg). The abscess is created by the insertion of a feces filled gel capsule(no. 4) into the right lobe of the liver. Imaging is performed 7 days following surgery. Pre-contrast images are obtained with standard T1-weighted and T2-weighted SE sequences (scan times of 4.32 and 13.1 minutes respectively) followed by breath-hold imaging performed with FLASH (TR/TE/FA=38/10/50; scan time=9.7 sec) and SE (TR/TE=100/13;256x72 matrix;Half-Fourier technique; scan time=12 sec) sequences. A pre-saturation pulse is applied to the FLASH sequence and a nonselective 180 degree pulse to the SE pulse sequence to minimize vessel pulsation artifacts. Breath-holding is achieved by paralyzing the rabbit with succinylcholine (1 mg/kg) and hand ventilating the animal. Gd(HP-DO3A) is injected through an ear vein and the breath-hold scans repeated immediately and again 5 and 10 minutes after injection. Paralyzation wears off in 15 minutes without the need for chemical reversal. The study is completed with a traditional T1-weighted SE scan. At the finish of the exam the rabbits are euthanized with T-61 and an autopsy is performed.

In this ongoing study, the entire imaging protocol has been successfully performed in 3 of 12 animals. The initial group of rabbits was used to optimize experimental design prior to the start of actual data collection. Review of these images indicates equivalent to superior delineation of enhancement of the abscess and identification of the abscess focus with immediate post-contrast breath-hold imaging.

$Gd(DTPA)^{2-}$ enhancement is a well established technique for the improved detection of CNS lesions . Looking to improve tissue contrast in hepatic imaging the use of contrast agents in liver imaging has been proposed. Preliminary studies reveal the potential of immediate post-contrast breath-hold MR imaging for the detection of liver disease.

P019

Changes of ^{31}P-MRS during development and aging in human brain

C Tanaka, T Higuchi, S Naruse*, Y Horikawa*, S Ueda*, H Yoshioka**, T Sawada**
Dept. of Neurosurgery, Meiji College of Oriental Medicine
Dept. of Neurosurgery* and Pediatrics**, Kyoto Prefecturtal University of Medicine

The purpose of this study is to clarify the changes of ^{31}P-MRS on brain tissue during the course of dvelopment in infancy as well as to know the changes accompanied by aging in adults. For the semi-quantitative analysis of ^{31}P-MR spectra, we obtained the ^{31}P-MRS with long repetition time (15 sec) to eliminate T1 effects on the spectra. Futhermore, in order to analyze T1 effects on the ^{31}P-MRS, we measured also ^{31}P-MRS with short Tr (2sec), and compared those data with these obtained with 15-sec-Tr. Thirty-two healthy volunteers, the range of age from 1 month to 83 years old, were examined by a clinical 1.5 T MRI/S (Gyroscan S15:Philips). Localized ^{31}P-MRS was obtained from brain using ISIS method. The peak integral of spectra were calculated by the curve-fitting software (NMR1:NMRi) using Sun 3/60 (Sun Microsystems).

Fot the semi-quantitative analysis, ratios of each PME, Pi, PDE, PCr and ATP peak integral to the total peak integral of those peaks were calculated in each ^{31}P-MR spectrum with 15-sec-Tr. Then those ratios were compared in infant and adult groups. Infantile brain contains a large amount of PME compared with adults brain and a small amount of PDE and PCr compared with adult brain. Pi did not show significant changes between those two ages.

Peak integral ratio of each signal with 15-sec-Tr to it with 2-sec-Tr, which was corrected for the difference of number of acumulation, is considered as a parameter of T1 value. Both PME and PCr of infantile brain showed a long T1 compared with it of aged brain. PDE and Pi showed no significant changes among different ages.

In conclusion, ^{31}P-MRS of normal human brain showed two remarkable changes during the course of development and aging. One is the quantitative changes of brain metabolites, especially membrane phospholipids metabolites. The other is the changes of relaxation time of brain metabolite, which may imply a changes of micro-circumstance of metabolites. Therefore, to evaluate the pathophysiology of brain disorders using ^{31}P-MRS, we must consider these P-MRS changes associated with development and aging in human brain.

P020

Parameter Relations For the Shinnar-Le Roux RF Pulse Design Algorithm

JOHN PAULY, DWIGHT NISHIMURA, AND ALBERT MACOVSKI
Information Systems Laboratory, Stanford, CA 94305

The Shinnar-Le Roux algorithm [1,2] allows the exact design of RF selective excitation pulses. The pulse design problem is converted into a polynomial approximation problem, which is then solved with digital filter design techniques. This polynomial is transformed back into the desired RF pulse. The algorithm is very efficient; most designs take ten to twenty seconds on a Sun 3/50 workstation.

This efficiency means the design process can be repeated until a satisfactory pulse has been produced. We propose here a better alternative. Empirical parameter relations have been developed for the digital filter design problem [3]. These can be adapted to RF pulse design. The basic relation is $TBW = D_\infty(\delta_1, \delta_2)$ where T is the pulse duration (ms), B is the pulse bandwidth (kHz), and W is the transition width (kHz) divided by B. D_∞ is a measure of the profile ripple, increasing as ripple decreases. Usually it is on the order of 1. With this relationship the designer can trade off the pulse parameters. The time-bandwidth product is proportional to power, so it is usually chosen first. The transition width can then be traded off against the in-slice and out-of-slice ripples.

D_∞ must be compensated for the geometry of the RF pulse being designed. No compensation is necessary for small-tip-angle pulses. Significant (and different) compensation is needed for $\pi/2$, inversion, and spin-echo pulses. Analytical compensation expressions are presented here for each type of pulse. Plots of these expressions allow the visual evaluation of design trade-offs. For example, D_∞ can be plotted as a function of out-of-slice ripple for a range of in-slice ripples. Once a set of pulse parameters have been chosen it is easy to calculate the inputs for the Shinnar-Le Roux algorithm. The resulting pulses reliably meet the predicted design parameters.

The main advantage is that the pulse parameters can be easily traded-off using only the simple design relation and the appropriate plot. No pulses need be designed until a satisfactory pulse profile has been identified. This capability is unique among RF pulse design techniques.

[1] SHINNAR, M., L. BOLINGER, AND J. S. LEIGH, *Proc SMRM VII*, p 659, 1988
[2] LE ROUX, P., *Proc SMRM VII*, p 1049, 1988
[3] RABINER, L. R. AND B. GOLD, Theory and Application of Digital Signal Processing, Prentice-Hall, 1975

P021

TISSUE TEXTURE AS A DETERMINANT OF CONTRAST IN MR IMAGES

FS Greensite, R Buxton
Dept. of Radiological Sciences, Univ. of Calif-Irvine Medical Center

Two tissues with similar (or even identical) mean values are still distinct in a mathematical (and presumably biological) sense if their signal values have different statistical properties (i.e if the tissues have different "texture"). In 2dFT MR acquisitions (in which overall noise is nominally homogeneous) this texture could be due to the arrangement of capillaries, connective tissue, parenchymal cells, paramagnetic substances, etc - and these differences can be easily verified by taking ROIs. In standard images, however, such texture differences will generally not be visible in images windowed to the principal anatomical features of the field of view. Further, calculated CNR contains no contribution from texture differences. In the interests of enhancing subtle but possibly important distinctions between adjacent or embedded tissues, we have developed a method whereby images may be created from the acquisition in which image CNR derives from weighted contributions of differences in mean signal values as well as differences in higher statistical properties. The formalism for accomplishing this also includes the standard images as a limiting case. The signal value function in the new image is the convolution of the "characteristic function" of the acquisition (a sum of delta functions, one for each signal value assigned to a voxel) with a Gaussian density whose standard deviation is a user chosen multiple of the noise standard deviation. We have investigated instances using numerical phantoms where the new images are markedly superior to standard images and usual enhancement techniques like histogram equalization. Preliminary investigations with clinical material suggest a possible role for these images in increasing simultaneous distinction of normal and pathological tissues.

P022

MRI OF THE SHOULDER: 3-D FISP IMAGING WITH MULTIPLANAR RECONSTRUCTION

J.D. Reeder, T.R. O'Donnell, S.M. Andelman
Franklin Square Hospital, Baltimore, Maryland

Three-dimensional gradient-echo pulse sequences offer unique strengths relevant to musculoskeletal imaging, including the ability to acquire contiguous, thin section, relatively high signal-to-noise images. Volume acquisition techniques also permit multiplanar post-processing reconstruction of images from the original data set. In this study, 3-D FISP shoulder images were obtained on a 1 Tesla system from both normal volunteers and symptomatic patients. Multiplanar reconstructed images were generated in orthogonal and oblique orientations relative to the original acquisition plane. The FISP sequence consisted of a 15 msec. TE, a 0.04 sec TR, and a flip angle of 50°. A 17.5 cm. diameter Helmholtz receiver surface coil was positioned over the humeral head and the effective slice thickness was 1.5 mm. Multiplanar reconstructed images had a slice thickness of 0.8 mm. This post-processing multiplanar reconstruction program allows retrospective choice of imaging geometry to evaluate orthopedic anatomy and pathology from multiple perspectives following a single data acquisition. Examples of normal anatomy, tendonitis, impingement, and supraspinatus tendon tears are presented.

P023

IN VIVO P-31 NMR STUDY OF SKELETAL MUSCLE ENERGETICS IN ENDOTOXINEMIC RATS

PG Carlier, RJ Gilles, P Jung, N Yerna, GL Rorive
Departments of Medicine and Radiology, C.H.U. de Liège, par B-4000 Liège, Belgium

Skeletal muscle high-energy phosphates metabolism was investigated in an experimental model of septic shock. Wistar rats were injected with endotoxin (0127:B8, Difco) 15 mg/kg intraperitoneally. P-31 spectra were collected 5h, 8h, 10h, and up to 21 h post-endotoxin injection. The biceps femoris was centered on a 15-mm diameter, two turn, double tuned surface coil. Arterial blood pressure was monitored invasively (femoral catheter) or non-invasively (tail cuff method).The data were compared to pre-injection values and to measurements in similar experimental conditions on untreated control rats. We also introduced a stress procedure and imposed 40-min ischemia to the leg, followed by 13-min reperfusion. The procedure was systematically applied 8 hours after endotoxin injection. Endotoxin-treated rats mean survival time was 19±4 hours. The P-31 spectra collected at rest did not show significant differences in the distribution of the muscle P-compounds between normal and endotoxin-treated rats. Skeletal muscle baseline pH was identical in the two groups. During ischemia, high-energy phosphates degradated at the same rate in the leg muscles of the two groups. There was no differences in the time-course changes of the PI/PC ratio. Acidosis was more profound in the endotoxin-treated rats than in the controls. Upon reperfusion, phosphocreatine recovered less rapidly in the endotoxin group than in the controls. Conversely, inorganic phosphate decreased at a slower rate in the endotoxin group. It also plateaued at a higher level late into recovery. When measured, femoral blood pressure was found to be identical in the two groups at any time during recovery. Also, muscle pH remained more acidotic in the endotoxin group.

Conclusions. 1. Skeletal muscle P-31 spectra appeared normal at rest in endotoxin-treated rats, when compared to control animals. 2. Ischemia resulted in similar alterations of the high-energy phosphates in the two groups. However, leg muscle became more acidotic in the endotoxin group. 3. Reperfusion revealed signs of impaired oxidative phosphorylations in the endotoxin-treated rat muscle, which could not be simply attributed to a lower perfusion pressure.

P024

The Value of MR Imaging in Pediatric Airway Obstruction

Th.Vogl, MD • C.Wilimzig, MD • U.Hofmann, MD • D.Hofmann,MD • J.Lissner, MD

Pediatric airway obstruction due to vascular anomalies can be related to a disease producing respiratory distress. Up to now, several diagnostic modalities have been used in the evaluation of tracheal stenosis. It has been shown that MR imaging has substantial capability for demonstrating the anatomical structures and has the added advantages of not requiring intravascular contrast medium nor x-ray exposure. Bronchoscopy allows the evaluation of the lumen of the trachea, and the degree and location of collapse, however it may be difficult to determine the etiology of the tracheal narrowing.
Fourty patients ranging in age from six weeks to five years ten months were examined with MR imaging after bronchoscopy. The MR imaging diagnoses were subsequently compared for accuracy with the diagnoses determined by direct surgical observations or by the combination of other examinations and clinical findings. Diagnosis included aortic arch anomalies, innominate artery compression, pulmonary artery compression and tracheomalacia.
MR imaging was performed with a 1,0T MAGNETOM (Siemens) using ECG-gated single-echo sequences.
In seventeen patients the tracheal narrowing by the innominate artery was demonstrated as a focal compression of the trachea. In these cases transaxial planes showed the innominate artery originating from the aortic arch distally on the left and passing in front of the trachea to the right side. Sagittal plane by demonstrating the entire thoracic trachea revealed best the site and extent of the tracheal narrowing.
Nine patients had aortic arch anomalies. Some of them had a right descending thoracic aorta and a markedly dilated arch compressing the trachea at the level of carina. The arch runs dorsal of the trachea displacing and compressing it. Eight patients were diagnosed by bronchoscopy to have distal tracheal or bronchial compression.
Several conditions may cause tracheal stenosis which produces respiratory distress, wheezing and stridor. In the cases with tracheal compression by aortic arch anomaly or innominate artery transaxial projections provided most precise estimates of tracheal narrowing in addition to a detailed demonstration of the mediastinal anatomy. Sagittal planes were useful for localizing tracheal stenosis and for evaluation of tracheomalacia demonstrating a non-focal conical tracheal narrowing.
In summary, MR imaging appears to be an imaging modality, appropriate for demonstrating tracheal stenosis. For evaluation of the cause of airway obstruction, MR imaging is an ideal method depicting detailed anatomic structure without employing ionizing radiation or intravenous contrast medium.

P025

MR IMAGING WITH GD - DTPA IN TUMORS OF LARYNX AND HYPOPHARYNX

Th.Vogl, MD • W.Steger, MD • G.Grevers, MD • A.Schramm,MD • J.Lissner, MD
University of Munich, Department of Radiology

30 Patients with tumors of the larynx and hypopharynx were investigated by different MRI - techniques and with paramagnetic contrast medium Gd - DTPA. The results of preoperative MRI were compared with clinical laryngoscopy and the pathological tumor classification. MR examinations were performed at 1,0 T Magnetom with T1 - weighted (TR/TE = 500/17 ms) and T2 - weighted (TR/TE = 3000/25/90 ms) sequences in spin - echo technique. Most patients underwent three slice orientations to find out best diagnostic methods in different tumor Localisations. Laryngeal tumors were subdivided into supraglottic, glottic and subglottic lesions, additionally hypopharyngeal tumors, laryngoceles, amyloid and inflammatory structures were found. In laryngeal lesions transversal and coronar slices proved to be helpful, in hypopharyngeal expansions transversal and sagittal slices were preferred. The most accurate diagnostic findings could be achieved in T1 - weighted images with Gd - DTPA. The combination of plain images, contrast enhanced images and subtraction technique made exact judgement of deep infiltration possible. Due to short scan - times images showed high contrast and subtle anatomical details. T2 - weighted images conveyed more information in liquid filled structures, but there were more artefacts than in T1 - weighted images. The clinical laryngoscopy had advantages in T1 - classified tumors as the morphological outfit of the tumor could be seen, and it offers histological information via biopsy. Diagnostic findings of MRI correlated in 85,7 % with the pathological statement, laryngoscopy proved exact classification in only 71,4 % of all patients. Sensitivity of tumor - containing lymphnodes was 82,1 %, the specivity was 85,7 %. In patients with good condition or unclear diagnostic findings it may be justified to use long T2 - weighted sequences and three slice orientations, but in most cases T1 - weighted sequences in two orientations and the contrast medium Gd - DTPA optimized the examination. In combination with laryngoscopy MRI was the method of choice for the staging of laryngeal and hypopharyngeal tumors.

P026

^{7}LI IMAGING AND LOCALIZED SPECTROSCOPY IN-VIVO

S Ramaprasad*, JEO Newton**, D Cardwell*, P Mohanakrishnan*, J Sprigg*, RA Komoroski*
*Departments of Radiology and Pathology, University of Arkansas for Medical Sciences, and **VA Medical Center, Little Rock, AR 72205

Lithium-7 in vivo NMR spectroscopy has been used to follow the pharmacokinetics of Li uptake and elimination in humans and animals. As with most in vivo NMR spectroscopy, precise localization of the signal anatomically is important. We and others previously have reported Li-7 DRESS slices for human brain. We are currently developing Li-7 imaging for rats at 4.7 T and Li-7 chemical shift imaging (CSI) for humans at 1.5 T. Using concentric H-1 and Li-7 birdcage coils, the corresponding images were obtained on rat head at 4.7 T. Li-7 images were acquired in about one hour using a spin-echo pulse sequence as a 32 x 32 matrix (zero-filled twice to 128 x 128), slice thickness of 20 mm, TE of 12 -15 ms, FOV of 100 - 120 mm, and TR of 1 - 2 s. Anatomic correlations were made to the H-1 image, and regional differences in Li concentrations were seen. Images were taken at various times after a single 10 mEq/kg IP dose of LiCl. In this case the maximum Li level in brain occurs at about 10 hours after injection. At 1.5 T (GE Signa) we have obtained Li-7 8 x 8 chemical shift images (4 x 4 x 4 cm voxels) in 1/2 hour for a phantom of 1 L of 1.1 mM LiCl in agarose with a linear birdcage head coil tuned to 23.84 MHz. These results suggest that Li-7 CSI is possible in human brain at therapeutic dosages.

P027

IN VITRO ADRENAL MRI WITH PATHOLOGIC CORRELATION FOR DETECTION AND MEASUREMENT OF THICKNESS OF ADRENAL CORTEX

ALI SHIRKHODA, M.D., AL-REZA ARMIN, M.D.

WILLIAM BEAUMONT HOSPITAL

Purpose: To measure the thickness of the adrenal cortex and determine its signal intensity as seen on the specimen MRI and correlate that with the measurement obtained by the pathologist in order to determine the ratio of medullary tissue over cortical tissue on MR scans.
Materials and Methods: Ten adrenal glands from five cadavers without any known adrenal disease were carefully dissected within seven hours of death and then scanned in a 1.0 Tesla magnet using a three inch surface coil. Each adrenal gland was removed with the Gerota's fascia and the ipsilateral kidney. The surface coil was placed over the adrenal gland at approximately two inches distance and direct coronal images were obtained using T1 (TE/TR, 600/25) and T2 weighted (TR/TE, 2,000/90, 25) pulse sequences.
Results: While additional 10-15 cadavers are planned to be the subject of this investigation, so far we have found that there is minimal contribution of adrenal cortex to the thickness of the gland as seen on MR images of specimens. The cortical part of adrenal measured only 1-3 mm in most of the cases while the thickness of medullary portion was approximately 2 cm. The signal intensity of the adrenal cortex was also different from that of the adrenal medulla. On T1 weighted image, the adrenal cortical tissue displayed brighter signal than the medullary portion. On T2, it was often difficult to determine the adrenal cortex because of its isointensity to the perirenal fat.
Conclusion: The adrenal cortex provides a fraction of the thickness of the adrenal as seen on the MR images. It also displays different signal intensity than the medullary portion.

POSTER ABSTRACTS

P028

MRI evaluation of gallbladder carcinoma

Paolo Pavone MD, Silvia Giuliani MD, Marco Mastantuono MD, Sandra Tella MD, Roberto Passariello MD

MRI was employed in 15 patients with gallbladder carcinoma. Histological proofs of the diagnosis was obtained at surgery. Ability of MRI to provide complete staging of the tumor was evaluated. The examinations were performed with a 0.5 T superconductive magnet, using short TR, short TE T1 weighted SE sequence with multiple averages (TR 260, TE 20, NSA 8) and 256x256 matrix, and T2 weighted SE sequence (TR 2000, TE 30-70-120, NSA 2). Only axial slices were obtained. CT scans were performed for comparison only in 4 cases, while in the other patients the diagnostic information obtained with MRI were felt sufficient for pre surgical staging. Diagnosis of gallbladder carcinoma was made according to the side of the lesion (gallbladder and relative hepatic fossa in all cases), invasion of the gallbladder (n=8) or intraluminar mass (n=7) and to the presence of intraneoplastic calculi (n=7). Hypointensity of the stones was seen in all sequences employed. Hepatic invasion was evident in 6 patients with involvement of the 4th segment in 4 and diffuse liver metastases in 2 patients. Hileal infiltration was evident in 5 cases, presenting all dilatation of the bile ducts and thrombosi of the portal vein in 3. Perihilor or portocaval lymphonodes were present in 6 cases and showed an high intrinsic contrast with the surrounding liver. In the present experience MRI was able to correctly stage gallbladder carcinoma in all patients, as confirmed at surgery. Its role in substitution of CT can be proposed.

P029

QUANTITATIVE 31P MRS STUDY OF THE EFFECTIVENESS OF CHEMOEMBOLISATION ON HUMAN HEPATIC CANCERS

DJ Meyerhoff, GS Karczmar, AP Venook, M Wilkinson, F Valone, MW Weiner
VA Medical Center and University of California, San Francisco

Chemoembolisation is used in the treatment of patients with extensive metastatic cancer of the liver. In the chemoembolisation procedure, a gel foam containing a combination of chemotherapeutic agents is injected into the hepatic artery to occlude hepatic vasculature and destroy normal and neoplastic tissue. It is hoped that liver function will recover after several weeks, while tumor growth is retarded or eliminated. Currently, there is no method for directly monitoring the effectiveness of the chemoembolisation procedure. Therefore, we have used quantitative 31P MRS to *directly* monitor the effects of chemoembolisation on liver metabolism. The goals of this study were: 1) to determine whether 31P MRS could be used to provide an early indication of the effectiveness of chemoembolisation; 2) to monitor regrowth of tissue in the embolised area; 3) to determine whether regrowing tissue is normal or cancerous; and 4) to correlate spectroscopic findings with results of standard clinical tests.

Patients were studied with a whole body 2T MRI/MRS system, using an ISIS MRS localization technique modified for use with surface coils. Patients were examined prior to and 1 to 5 times after chemoembolisation over a period of 1 to 9 weeks. Localized 31P MRS detected an acute drop in ATP levels following chemoembolisation. Inorganic phosphate and phosphoesters were increased relative to ATP. In some cases, a gradual recovery of ATP was noted over a period of 2 to 9 weeks, while in other cases ATP levels did not recover. Further MRS studies should show whether recovery of ATP is due to recovery of tumor or normal liver tissue.

These preliminary results demonstrate that 31P MRS can be used to directly and non-invasively assess metabolic consequences and effectiveness of the chemoembolisation procedure, and that 31P MRS may ultimately be useful for guiding patient treatment.

P030

Gd-DTPA ADRENAL GLAND ENHANCEMENT AT 1.5 TESLA

WC Small, ME Bernardino
Department of Radiology, Emory University Hospital

Recent reports have appeared in the literature describing MR adrenal imaging using multiple pulse sequences at varying field strengths. These studies have in all cases demonstrated overlap in attempting to differeniate adenomatous from nonadenomatous lesions in the range of 20-30%. Gd-based contrast agents may provide increased adrenal lesion specificity. However, detailed information about adrenal enhancement after Gadolinium is lacking. We report results of a study evaluating the Gadolinium induced changes in signal intensity in normal adrenal glands in a group of 31 patients at 1.5T using both T1-weighted gradient echo and spin echo pulse sequences. A total of 1670 signal intensity data points were acquired in completing the study. A comparison of pre- and post-Gd DTPA enhanced T1-weighted gradient echo images obtained within 5 minutes of 0.1 mg/kg IV bolus contrast administration shows an average increase in signal intensity as referenced to a MnCl2 solution phantom (27 patients) or to body fat (31 patients) of 430% and 416% respectively. Comparison of pre- and post-enhancement signal intensities from T1-weighted spin echo imaging sequences at times more delayed following contrast administration were also obtained averaging 149% referenced to the MnCl2 phantom (21 patients) and 151% referenced to body fat (25 patients) at a 4-9 minute delay, 156% and 153% as referenced to the MnCl2 phantom (26 patients) and body fat (30 patients) respectively at a 10-20 minute delay, and 135% and 150% as referenced to the phantom (7 patients) and body fat (7 patients) respectively at a 21-30 minute delay. These results demonstrate significant adrenal enhancement after Gadolinium and will provide an important baseline in the use of contrast agents in adrenal lesion differentiation.

P031

SCROTAL MRI, REVIEW OF 125 PATIENTS

CB Semba, MA Trambert, RF Mattrey
Department of Radiology, University of California, San Diego; UCSD/AMI MRI Institute

131 scrotal MR examinations were performed on 125 patients between 1985 and 1989, to evaluate scrotal pathology. The patient age ranged from 3 days old to 76 years old (mean of 36 years). The patients presented a variety of intra and extratesticular pathologies, ranging from possible mass lesions to infections or acute or chronic pain. Ultrasound was performed in approximately 50% of the cases prior to the MR examination. The MR studies were evaluated for clinical diagnosis, as well as depiction of normal scrotal structures. Clinical and\or surgical follow-up was available on most of the cases. All MR exams were performed on a GE 1.5 tesla Signa system using a 5 inch surface coil.

MR has higher sensitivity than ultrasound for infection, but similar sensitivity for scrotal abnormalities. However, due to tissue characterization capabilities MR appears to have greater specificity than does ultrasound. The ultrasound diagnosis and therapeutic path was altered by the MR examination interpretation in nearly 10% of patients. For example: there was 100% accuracy in differentiating epididymitis from torsion in the subacute setting. There was a 92% accuracy in determining seminomatous from nonseminomatous testicular tumors. The one error made in the 13 cases was interpretive.

Ten cases done before and after Gadolinium-DTPA suggest that this intravenous contrast material adds further specificity when evaluating scrotal pathology, and may allow for shorter examination time.

MR of the scrotum contributes significant diagnostic data to the sonogram, adding specificity and an easier anatomic display to the referring physician.

P032

MR IMAGING OF THE LUNG PARENCHYMA

CJ Bergin, J Pauly, A Macovski
Department of Diagnostic Radiology and Nuclear Medicine, and MRSRL Department of Electrical Engineering, Stanford University Medical Center, Stanford, Ca 94305

MR imaging of lung structures is limited by problems of motion and susceptibility artifact. A pulse sequence has been developed which uses very short echo times,[1] and can therefore image tissues with very short T2 relaxation times, such as the lungs (T_2 = 4 ms). The very short TE minimizes artifacts due to respiratory motion, susceptibility effects, and flow dephasing. Using this pulse sequence, the TE is limited only by the time required to shut down the radio frequency system (TE = 250 μs on GE 1.5T Signa). The phase encode lobe, dephase lobe and first half of the read-out lobe are eliminated by using projection reconstruction acquisition gradients. Tissues with T2 as short as 1 ms can be imaged.

This technique demonstrates 7th order pulmonary vessels in the lung periphery with reasonable imaging times (approx. 4 mins). We have compared this technique with standard spin-echo and gradient recalled MR images in the lungs. In vitro MR imaging studies with non-inflated and inflated lung specimens demonstrate the limiting effect of susceptibility[2]. The shortened TE used in this sequence can effectively overcome this problem. Preliminary in vivo studies of a spectrum, of lung abnormalities demonstrate the new pulse sequence to be effective in localizing parenchymal abnormalities.

1 - Pauly J, Conolly S, Nishimura D, Macovski A. Slice selective excitation for very short T2 species. Abstract: Society of Magnetic Resonance in Medicine. Amsterdam, August 1989
2 - Kveder M, et al. Water proton NMR relaxation mechanisms in lung tissue.

P033

CARDIAC CINE MRI: PARAMETER OPTIMIZATION AND APPLICATION IN 54 PATIENT STUDIES

P Wozney
University of Pittsburgh, Department of Radiology and the Pittsburgh NMR Institute

Gradient-echo cine-MRI provides dynamic evaluation of the heart and great vessels. This investigation examined the effect of parameter choice on image quality, resulting in a set of optimal parameters. When these results were applied to patient studies, the number of diagnostic cine-MRI studies increased from 30% to 95%.

Studies were performed on a 1.5 T General Electric Signa system initially equipped with pre-production software and then equipped with the production cine-MRI package (including self-shielded gradient coils).

Optimal parameters were: 128 phase-encoding steps, slice thickness of 10 mm for large vessels, and 5 mm for small vessels. Although 4 excitations was optimal, diagnostic studies were routinely achieved with 2 excitations, for a study time of 3 to 7 minutes. The optimal flip angle without self-shielded coils was found to be 20°, and with self-shielded coils 30°. Gradient moment nulling was essential to correct for phase flow artifacts. The minimum number of phases during the R-R interval for diagnosis was 9, although increasing the number of phases improved overall quality.

Several options had unexpected image quality effects. Although a 256 matrix provided sharper (and noisier) images compared with a 128 matrix, it did not result in increased conspicuity for even small pulmonary vessels. ECG gating was nearly indistinguishable from pulse gating. Magnevist (Gd-DTPA) had no effect on image quality. Respiratory compensation in general produced only marginal improvement, and occasionally markedly decreased quality. Prospective triggering was often superior to retrospective gating, although a change in ECG parameters was necessary for adequate diastolic imaging.

P034

"DOUBLE POSTERIOR CRUCIATE SIGN" OF MEDIAL MENISCAL BUCKET HANDLE TEAR

KL Weiss, IM Levy, HT Morehouse
Radiology and Orthopedic Surgery, Albert Einstein College of Medicine

Sagittal knee MRI images were retrospectively reviewed in 55 consecutive patients who subsequently underwent arthroscopy. The presence or absence of a "double posterior cruciate sign", defined as an abnormal curvilinear low signal band lying above the tibial cortex anterior inferior to and somewhat paralleling the course of the posterior cruciate ligament was noted. These results were then compared to arthroscopic findings of "bucket handle" tears.

Seven cases of "double posterior cruciate sign" were retrospectively noted on sagittal MRI images and proved to correctly represent "bucket handle" medial meniscal tears by arthroscopy. One of the cases required stretching the definition of the sign to include the appearance of a "double posterior cruciate" taking in account two adjacent sagittal images rather than a single image. No additional medial meniscal "bucket handle" tear was identified in the remaining 48 cases examined arthroscopically. Of two lateral meniscal "bucket handle" tears noted arthroscopically, sagittal MRI of one demonstrated a small crumpled displaced fragment extending anterior to the PCL. This, however, did not have the orientation or configuration of the "double posterior cruciate sign" and could be clearly traced back to a torn lateral meniscus. The sign was also readily distinguished from the ligament of Humphrey noted as a small, ovoid low signal focus immediately anterior to the PCL or discretely bulging from the concave surface on at least two consecutive sagittal sections. 26 of the 54 cases were felt to demonstrate this ligament.

The "double posterior cruciate sign" appears to be a reliable indicator of a medial meniscal "bucket handle" tear. Since the sagittal projection is often the primary MR imaging plane, attention to the sign may be helpful when evaluating medial meniscal derangement for the presence of a "bucket handle" tear.

P035

APPLICATIONS OF ECHO OFFSET WITH CHEMICAL SATURATION IN ABDOMINAL IMAGING

T Chan, J Listerud, P Chao, HY Kressel, B Milestone
Devon MRI Center, Hospital of the University of Pennsylvania, Philadelphia, PA

The ability to selectively image fat or water protons in the abdomen can suppress unwanted signal from fat which may degrade the image due to respiratory motion, and has the potential to characterize lesions spectroscopically. Various groups have reported on alternatives such as chemical shift saturation and echo offset methods. We are evaluating these options singly and in combination.

10 normal volunteers were imaged on a 1.5 T GE magnet using the 4.0 upgrade as well as with a research pulse sequence developed for our 3.2 system. The images were graded visually for homogeneity and effectiveness of fat suppresion, and conspicuity of various organs. Signal intensities and contrast between the various organs and adjacent fat were compared. 10 patients with abnormalities of the liver, adrenals, pancreas, or adnexa were also studied. The addition of echo offset with chemical saturation to standard T1 and T2-weighted spin echo seqences was evaluated for its role in diagnosis.

We found that the combination of echo offset with fat saturation increased the conspicuity of the pancreas and adrenals which appear as bright structures against the dark retroperitoneal fat. Various techniques, singly or in combination, differed in their sensitivity to shimming and ability to combine with real time respiratory compensation methods such as EXORCIST and ROPE. One patient with a low density adrenal lesion on CT exibited inhomogenous signal intensities within the lesion using chemical shift selective MR imaging.

P036

CHONDROBLASTOMA; THE CONFUSING AND CLASSIC MR APPEARANCE

PT Weatherall, GE Maale, H Jayson, HR Pascoe, P Nurenberg
University of Texas Southwestern Medical Center, Dept. Radiology

We reviewed MR exams on 8 patients with chondroblastomas and found that MRI provided information that was helpful in confirming the diagnosis, but was also frequently misleading. T1 and T2 weighted (T1W and T2W) images were obatined on all patients, with the exams being performed at .35, .5, and 1.0 Tesla. Plain X-ray, CT, and histologic exams were available for correlation. An over estimation of the lesion's aggressiveness was suggested on the MR exams in several cases since they revealed prominent "activity" in the adjacent marrow(n=4), periosteum(n=5), and soft tissues(n=4). A reaction to abnormal mechanical stress is thought to cause marrow inflammation (homogenous low signal on T1W and high signal on T2W images) which estended to the diaphysis in 2 cases and over a large percentage of the epiphysis in the other 2. A prominent adjacent soft tissue "mass" or reactive zone (with increased T2W signal) was seen in 4 of the patients. These features helped cause MRI misdiagnosis in 2 cases (osteomyelitis) and incorrect staging in 2 patients (stage III vs II). None of these patients had extracompartmental extension at surgery and only 2 had evidence of a prior fracture (old in both). MRI is more sensitive to the marrow and periosteal reactions, which in the latter case is associated with 50% of chondroblastomas in a series of JL Bloem et al in Skeletal Radiology 14:1-9, 1985. The MR characteristics of these lesions was otherwise as expected and relatively distinctive. They had well-defined(n=8), finely lobulated(n=5) margins and heterogenous(n=8) internal architecture with occasional(n=3) inner lobulation visible. The MR signal was low to intermediate and homogenous on T1W views. A heterogenous predominently low signal was seen on most T2W images, although 2 tumors had multiple focal areas of high signal, corresponding to hyaline cartilage and cysts (ABC-like). Differential considerations are limited, with GCT and TB generally being excluded on the basis of the fine lobulation. Error can be avoided by attention to the margin and knowledge of the physiologic reaction often associated with chondroblastoma.

P037

MAGNETIC RESONANCE IMAGING AND COMPUTER TOMOGRAPHY IN PELIZAEUS-MERZBACHER DISEASE

PA Caro, HJ Marks
Alfred I. duPont Institute

MRI and CT findings in six patients with Pelizaeus-Merzbacher disease are described. The patients were studied with a high field (1.5T) MRI unit. Sagittal T1W images, multiecho axial, and T2W coronal views were obtained. CT examinations were performed with a GE 2800 unit. Complete case presentation and representative images will be displayed. The patients ranged in age from 1 to 36 years and have the classical X-linked recessive form of the disease. Their clinical presentation and course closely follows the initial description of the disease made by Merzbacher in 1910. As it has already been stated in the literature, Computed Tomography of the brain is unable to detect subtle abnormalities in the white matter, where MRI is strikingly sensitive. All our patients had normal CT examinations when diagnosed in early childhood and evidence of cerebral atrophy later in the course of the disease. MRI, however, was abnormal in all our patients showing a reversal of the normal gray/white matter signal intensity relationship on T1W images and T2W images that can be considered diagnostic in the classical clinical situation. In all our patients the mid brain and upper cervical spinal cord is atrophic and in one patient in which the complete cervical spine was imaged, there is atrophy of the entire cervical cord and the pons. All the patients have an abnormal configuration of the corpus callosum (thin with an undulated shape). Depending on the degree of dismyelination the cortical gray matter is collapsed in deep folds over the white matter giving the appearance of cerebral atrophy. Three patients have a unusual degree of low signal intensity in the basal ganglia, red nuclei, sustansia nigra, and dentate nuclei. This has been described with iron deposition and is indicative of degeneration.

P038

FOLLOW-UP MRI EVALUATION IN WERNICKE'S ENCEPHALOPATHY

Massimo Gallucci, Alessandro Bozzao, Alessandro Splendiani, Anna Cifani, Remo Feliciani, Roberto Passariello
Department of Radiology, University of L'Aquila, Italy

Wernicke's Encephalopathy (WE) is the most severe neurological complication of chronic alcoholism. It is due to a nutritional deficiency of thiamine and for this reason it can be observed mainly but not exclusively in alcoholics. The real incidence of WE is higher than clinically diagnosed since pathognomonic lesions were found up to 2.2% of consecutive autopsies series of adults. Pathological findings described in WE are represented by demyelination, petechial hemorrages and astrocytic, microglial proliferation with relative neuronal sparing. These are especially evident around the 3rd ventricle and involve the mannillary bodies, the periacqueductal, the periepifisary regions and the brainstem. The lesions are always symmetrical and typically interest areas lacking the blood-brain-barrier. Nowadays diagnosis of WE is mostly based on anamnesiac data, clinical symptoms and laboratory essay. For this reason too, many cases are misdiagnosed during life as already reported by Harper. The use of CT scan is usually of little help in the diagnosis of this disease.

For this reason we performed a Magnetic Resonance (MR) follow-up study of 5 patients affected by WE. All the subjects underwent MR in the acute phase of the disease and were re-examined 6-12 months later, when in good health. Three of them also underwent Computed Tomography (CT). Evolutive patterns, described at our knowledge for the first time, were demonstrated by MRI. Very typical hyperintense areas on long TR/TE and long short TE Spin Echo sequences were demonstrated surrounding the 3rd ventricle and the acqueduct in the acute phase of the disease in all patients. Follow-up evaluations showed the disappearance or the reduction of the previously described periventricular and periacqueductal hyperintensities. Third ventricle and acqueduct were dilated at that phase. In our patients, MR was able to show many of the pathological findings described in literature since typical changes were present both in the acute and chronic phase in circumventricolar areas of all patients. Although the hyperintensitities seen on long TR/TE sequences were not specific or able to characterize the pathology (demyelinization, gliosis, tissue degeneration), they can be considered typical of WE, expecially because of their symmetrical distribution which allows the differential diagnosis with other diseases. The reduction of the above mentioned hyperintense areas also confirmed by ventricular and acqueductal dilatation underlines the benign evolution of the pathology when an appropriate therapy is applied. This is made easier when a correct diagnosis is performed and MR may help clinicians in this way.

P039

IMPROVEMENT IN SPINE IMAGING

S Vinitski, A Barbaria, A Flanders, T Tasciyan
Thomas Jefferson University Hospital, Philadelphia, PA

Cardiac and respiratory motion requires improvement in spine MR imaging, especially in the thoracic region. We redesigned "T1 and T2 weighted" spin echo (SE) techniques, and tested them on eight normal volunteers. In T1 weighted SE imaging of the thoracic spine, the high signal intensity near the region of the surface coil saturates the dynamic range, suppressing the contrast between the spine and CSF. We have modified presaturation RF pulses so that their two parts can be moved independently from each other in any given plane. We presaturated both the heart region and the area adjacent to the surface coil, resulting in simultaneous suppression of motion artifact and improvement of the contrast between the spine and CSF. Since noise also increased in the same proportion, we shortened echo time from 20 msec to 12 msec, using symmetrical data acquisition. Consequently, both the sharpness and the contrast to noise ratio of T1 weighted spine images were improved significantly.

One of the significant problems of "T2 weighted" cardiac gated imaging is that during conventional two or three RR intervals, there is not enough time for CSF magnetization to relax fully. This results in T1 contamination of "T2 weighted" images and degradation of the myelographic effect. However, small (45°-60°) excitation RF pulses, in conjunction with two refocusing RF pulses, drive CSF magnetization much closer to equilibrium, eliminating the need for long TR intervals. In addition, the use of mixed bandwidth increases SNR of the second echo. Chemical shift artifact was suppressed by selective excitation. As a result of these modifications, we reduced motion and chemical shift artifact, increased SNR, and significantly enhanced the myelographic effect in "T2 weighted" spine imaging. Clinical trials of this method have begun.

P040

MRI STUDIES OF INTRAVITREALLY PLACED GASES

T. Vullo, J.Sparrow, A. Gershbein, M.J.B. Stallmeyer, S. Chang, P.T. Cahill
The New York Hospital-Cornell University Medical College New York, N.Y.

MRI was performed to investigate the fate of intravitreally placed gases (IPG), which are often used clinically as an adjunct in retinal reattachment surgery to maintain the neural retina in apposition of the retinal pigment epithelium. MRI is potentially the imaging method of choice as compared to ultrasonography, which has significant limitations in the presence of a gas bubble, or to fluoroscopy which is invasive.

An expansile gas (perfluoropropane or perfluoroethane) was injected into the inferior vitreous cavity 2-3 mm. posterior to the limbus in 2-3 kg., albino rabbits. Gas bubble formation was observed with an indirect ophthalmoscope, and in some cases an anterior chamber paracentesis was performed to return the intraocular pressure to normal. MRI spin-echo, multi-slice studies were performed on a 2.0 Tesla, 30 cm diameter magnet with a slice thickness of 1.25 mm. and intraplanar resolution of 350 microns. Through serial MRI studies, changes in the volume of the expansile IPG was measured over time.

For example, with an injected volume of 0.4 cc the volume of IPG (204 mm3 at day 0 in the eye) was increased by 82% on day one and 53% on day 6. Volumes of IPG were measured to a precision of 8%. The IPG then often fragments into smaller bubbles concomitant with the appearance of filaments and intense local MR signal changes. The use of intravenous Gd-DTPA is under investigation to evaluate whether breakdown of the blood-ocular barrier occurs, and if so, at what time and gas pressure.

P041

MRI AND PATHOLOGIC CORRELATION OF CANINE HIPPOCAMPUS VOLUME

M.J.B. Stallmeyer, T. Vullo, V. Deo-Narine, F. Pannizzo, D. GOmez, P.T. Cahill
The New York Hospital-Cornell University Medical College New York, N.Y.

Decrease in hippocampus area and volume has been associated with short term memory loss, amnesia, and Alzheimer's disease. To date, no quantitative pathological studies have been performed to verify hippocampus volume as measured by MRI. In this study, we assessed the technical problems of measuring the hippocampus in canines by MRI with respect to RF pulse sequence, imaging planes, and slice thickness. In addition, a variety of anatomic landmarks for determining the borders or extent of the hippocampus were evaluated. The hippocampus was imaged in three planes: two planes tangential to and the third transverse to the long axis of the hippocampus. Measurements were made by three independent operators using a region of interest. In vivo and in vitro canine studies were imaged on a 2.0T, 30 cm bore magnet at a slice thicknesses of 1.25 mm. Five dog brains were sectioned along planes coinciding with those from MRI and differentially stained for contrasting gray and white matter (V. Deo-Narine et al. Neuroradiology 4:197 (1972)). The hippocampus stained similar to gray matter and cross sectional area was measured by the same operators.

Among the technical problems encountered in MRI were the visual discrimination of the hippocampus from the fornix on views transverse to the long axis and determing the ends of the C shaped hippocampus. The optimum MRI images are those that follow the long axis of the hippocampus. Using the two long axis images of the hippocampus, in vitro MRI measurements were in agreement to within 6% and pathology agreed within 13%.

P042

MR IMAGING IN INTRACRANIAL EXTENSION OF EXTRACRANIAL MASSES

M Hemmati, P Schoettle, S Doundoulakis
Michael Reese Hospital Chicago, Illinois

The majority of inflamatory and neoplastic masses involving the base of the skull and sinonasal cavities are symptomatic while extracranial. Some of these remain silent until they invade intracranially; become symptomatic by compressing cranial nerves or brain substance. Utilizing MRI, we studied 15 patients with intracranial extension of such lesions to evaluate the route of invasion and exact anatomical location. All of the studies were correlated with surgical and pathological specimens.

The 15 surgically proved cases were evaluated using a 1.5T Signa scanner. Multiplaner,spin-echo images were obtained. Post-contrast T1 weighted images were obtained in 8 cases.

The review demonstrates MR imaging is important not only in defining the site, size and origin of the primary lesion but the exact route and location and size of its intracranial component. Four of the patients with symptoms of intracranial disease had silent extracranial primary lesion.

P043

ESTIMATION OF VESSEL LUMEN SIZE WITH MRA: PHANTOM AND CLINICAL STUDIES

TC Kerner, RP Price, DR Pickens, JL Creasy
Department of Radiology, Vanderbilt University Medical Center

Magnetic Resonance Angiography (MRA) is a powerful new technique for the non-invasive study of vascular anatomy and disease. However, the method must accurately gauge the degree of vessel stenosis.

We have developed a vessel phantom in which varying degrees of stenosis can be produced. This is powered by a pulsatile pump with varying flow rates. MRA studies of this phantom are performed with a three-dimensional FISP sequence with flow compensating gradients to enhance vascular contents. We utilize a flip angle 20°, a TR 40 msec and a TE of 8 msec, 64 or 128 partitions and a single acquisition. Slices range from 1-2½ mm. Each of the 64 slices is reconstructed and projection angiogram views are then performed with a maximum intensity ray projection algorithm from any arbitrary angle through the 3-D volume of data. With phantom lesions of varying degrees of narrowing, comparison was made between actual lumen diameter and the imaged lumen diameter over a range of flow rates. In addition, similar comparison was made in several patients undergoing evaluation of carotid artery disease by arteriography and by MRA.

The ability to accurately assess vessel diameter in patients with a range of stenoses is obviously critical to the potential use of MRA as a screening modality.

P044

QUANTIFICATION OF MRI CHANGES IN PATIENTS WITH ACUTE SINUSITIS

MA Jack, B Borah, DS Respler, DJ Beste, GL Wolfe
NEPI, Norwich NY; United Hosp Med Ctr, Newark; Children's Hosp, Milwaukee; Pittsburgh NMR Institute

The objective of this study was to characterize the course of acute sinusitis treated with standard antimicrobial therapy and to correlate symptomatic improvements with resolution of intrasinus pathology monitored by MRI. Analysis of MR images can provide quantitative parameters (volume and viscosity related T2) that have potential for use in clinical studies of sinusitis.

In six patients with acute sinusitis, serial MR images (up to 8 scans over a 14 week period) were collected at 1.5 Tesla. Measurement of the volume of abnormal mucosa and/or free fluid in the maxillary sinuses was made from MRI films using the IBAS 200 image analysis system (Kontron Electric Group). The pattern of decreasing volume of swollen mucosa and/or fluid generally followed the pattern of resolution of signs and symptoms of acute sinusitis. While most signs and symptoms of sinusitis resolved within two weeks, MRI measurements of swollen mucosa/fluid remained elevated for three to four weeks in four of six patients. In some patients evidence of mucosal edema persisted for several weeks.

Four multiple-echo axial T2 images were used for T2 analysis. Intensity data from a 3-4 pixel area of swollen mucosa or fluid in each echo image were analyzed by single exponential decay function to obtain T2 relaxation times. Analysis of the viscosity-related T2 parameter was used to evaluate potential decreases in sinus fluid viscosity over time which would allow drainage through the sinus ostia. In the only patient identified with free fluid, an increase in T2 from 62 to 112ms was observed during resolution; the T2 of the facial fat control stayed constant. This increase in the T2 of free fluid may be indicative of a decrease in fluid viscosity and may represent a unique way to evaluate sinus mucosecretory response during treatment.

P045

MEASUREMENT OF CHANGE IN SIZE OF THE CEREBRAL VENTRICLE BY CARDIAC GATED CINE MRI

T Abe, K Kojima, H Nishimura, M Uchida, M Koganemaru, H Ohtake
Department of Radiology, Kurume University School of Medicine

During the last few years, a number of magnetic resonance imaging(MRI) have been used to image cerebrospinal fluid flow. Cardiac gated cine MRI, one of good techniques for imaging of cerebrospinal fluid flow, demonstrates the change in size of the cerebral ventricle. We measured the ventricular size by cardiac gated cine MRI in 20 normal volunteers and 6 patients who had diffuse cerebral atrophy. From the change in size of the cerebral ventricle by the cardiac phase, we got the ventricular systolic ratio(VSR). The VSR of each cerebral ventricles, the relationship to the aging and the difference from the patients with diffuse cerebral atrophy were studied.

[MATERIALS AND METHODS]

Twenty normal volunteers(8 aged 27-43 years, 12 aged 55-78 years) and six patients who had diffuse cerebral atrophy were examined. The cardiac gated cine MRI were performed on an imaging system(SMT-50, Shimadzu, Kyoto, Japan) that use a superconductive magnet operated at 0.5 tesla. The cardiac gating trigger with R wave was produced by electrocardiographic device. The 16 phased images in a same slice and in one cardiac cycle were made by a field echo technique(STAGE: Short Tip Angle Gradient Echo, 128 X 128 acquisition matrix, TE=14 msec, Flip Angle=30°).

According to the smallest size(VSA: ventricle systolic area) and the largest size(VDA: ventricle diastolic area) of the ventricle on the different phase, VSR was calculated.

$VSR = \{(VDA-VSA)/VDA\} \times 100$

The VSR was measured at the each body of the lateral ventricle by axial image, the each anterior horn of the lateral ventricle by axial image and the fourth ventricle by midsagittal image.

[RESULTS]

1) The negative correlation in the VSR and the aging was noticed at the body of the lateral ventricle.

2) The patients with diffuse cerebral atrophy had lower VSR than normal volunteers at bilateral body of the lateral ventricle and fourth ventricle.

P046

GD-DTPA ENHANCEMENT OF 3D T1-WEIGHTED GRADIENT ECHO SEQUENCES: A QUANTITATIVE COMPARISON TO SPIN ECHO PROTOCOLS

S. Felber, A. Kampfl, G. Birbamer, G. Laub*, J. Haustein**
University of Innsbruck, Department of Magnetic Resonance
Siemens Medical Systems, Erlangen*
Schering AG, Berlin**

T1 weighted 3D gradient echo sequences enable isotropic imaging of the entire brain with the capability of arbitrary postprocessing. The previous drawback was signal loss due to susceptibility changes has been successfully compensated using very short TE's.
T1 weighted GE protocols may require paramagnetic contrast agents for adequate demonstration of parenchymal alterations.
In order to assess the sensitivity of a 3D Flash sequence in combination with Gd-DTPA, 25 patients, harbouring intracerebral tumors, have been investigated by conventional post-contrast SE images and 3D Flash, after informed consent was obtained.
The parameters of Flash-3D were adjusted to optimize T1 contrast (α = 40 , TR = 40 ms, TE = 5 ms). After the routine SE imaging protocol Gd-DTPA was administered (0.1 mmol/kg/BW). T1 weighted images (TR = 550/TE = 15) were performed in two orientations, immediately followed by the volume study. Total examination time was 60 to 90 minutes and tolerated well by all patients.
First 3D Flash was visually compared to precontrast T1 and T2 weighted images. Then the acquired 3D images were reconstructed in similar orientations to T1 SE images. Contrast enhancement on T1 WI and 3D Flash images was evaluated quantitatively by calculating signal intensity ratios between enhancing pathology and grey/white matter.
3D Flash showed comparable or better enhancement than T1 post-contrast SE images in all patients with extraaxial tumors (4 neurinomas, 7 meningeomas).
Enhancing intraaxial neoplasms (n = 14) had higher ratios on T1 SE images, however, Gd-DTPA uptake was also sufficient for diagnosis on 3D Flash in all cases. The 3D examination offered additional information considering tumor composition (calcifications) in 17 (25) patients, and superior anatomic location for surgical and irradiation planning. Thus, 3D Flash combined with Gd-DTPA may replace at least T1 weighted SE sequences in future.

P047

THE MAGNETIC-RESONANCE HYPOINTENSE SPINE OF AIDS

Geremia, GK, McCluney K, Adler A, Charletta D, Hoile R, Huckman,M, and Ramsey R.
Rush-Presbyterian-St. Luke's Medical Center

PURPOSE: We recently observed a substantial reduction in the signal intensity of vertebral bodies on T1 weighted magnetic resonance (MR) scans in ten patients with AIDS. Review of bone marrow samples available in seven patients suggests that the abnormality we detected results from markedly increased amounts of storage iron in the marrows of these patients. The MR findings in these ten AIDS patients with correlative bone marrow samples will be presented.
MATERIALS and METHODS: The case histories of ten patients with AIDS, nine men and one woman, without any known cancer were reviewed, retrospectively, after each was found to have reversal of the usual signal relationships between the vertebral bodies and the adjacent intervertebral discs on T1 weighted images (T1WIs) i.e., the discs displayed higher signal than the vertebral bodies. Seven of the ten patients has histological studies of the bone marrow. The marrow samples were evaluated for cellularity, the presence of foreign cells, fibrosis, fat content and for the presence of stainable iron.
RESULTS: The vertebral bodies demonstrated two characteristic signal patterns, a homogeneously low signal (eight patients) and a low inhomogenous mottled appearance (two patients), on T1WIs. None of the biopsied specimens were detectably infiltrated with fibrous tissue, tumor elements or granulomas. All marrow specimens had markedly increased amounts of stainable iron.
CONCLUSION: Storage iron in the marrow is primarily in the form of hemosiderin. Markedly increased amounts of iron are commonly encountered in diseases which impair red cell iron utilization such as megaloblastic disorders, thalassemias, aplastic anemia, myelodysplastic disorders, chronic renal disease and chronic inflammatory disorders. The latter is a major cause of anemia in patients with AIDS and has been referred to as the anemia of chronic disease.
In all of our cases bone marrow iron was markedly increased. This concentrated form of iron may produce sufficient preferential T2 proton relaxation enhancement on the T1WIs such that the vertebral bodies exhibited relative hypointensity.

P048

MR OF HEAD AND NECK CYSTIC HYGROMAS

LS Buehner, WTC Yuh, Y Sato, SD Gray, SCS Kao, WL Smith, KD Dolan, RA Robinson
Depts. of Radiology, Otolaryngology, Pathology, Univ. of Iowa,
Iowa City, IA 52242

Cystic hygroma is a rare, benign developmental mass of lymphatic origin, representing 5-6% of benign pediatric tumors. Lesions usually present as asymptomatic fluctuant neck masses.

MR was performed in 7 surgically proven cystic hygromas of the head and neck in 6 pediatric patients with focus on configuration, signal intensity, fluid-filled levels, anatomic location, and post-surgical follow-up. Cyst contents were available for MR and chemical analysis in 1 patient.

All lesions were multicystic. Five of 7 had fluid-filled levels best demonstrated on axial T2WI due to various combinations of lipid and proteinaceous contents. On T1WI, lesions had an average signal intensity greater than that of muscle. On T2WI, lesions had an extremely high signal intensity. Anatomic location was best outlined by coronal T2WI, mapping the extent of involvement. Residual or recurrent tumors were clearly demonstrated. All these MR findings were indicative of cystic hygromas and helpful in differential diagnosis.

MR is a useful tool in the detection, characterization, localization and post-operative evaluation of cystic hygromas.

P049

EVALUATION OF MENINGEAL ENHANCEMENT WITH GD-DTPA

ME Phillips, TJ Ryals, WTC Yuh, S Kambho
Department of Radiology, The University of Iowa College of Medicine

Forty-three consecutive patients demonstrating abnormal meningeal enhancement were studied. All patients had at least one T1W and T2W sequence prior to gadolinium administration. Post-contrast sequences were obtained immediately after injection of 0.1 mMol/kg Gd-DTPA. Images were reviewed with special attention to: dural/arachnoid vs. pial involvement, diffuse vs. localized distribution, and nodular vs. linear pattern.

Patients were divided into the following categories: suspected meningeal carcinomatosis (16), inflammatory (11), and postoperative (16). Positive pathologic correlation could be obtained in 12 of 16 tumor patients, and 11 of 11 patients with inflammatory meningeal conditions. Dural/arachnoid membrane involvement was present in all but one case. Pial enhancement was demonstrated in 7 of 11 inflammatory, 4 of 16 tumor, and 2 of 16 postoperative patients. Diffuse meningeal distribution was most commonly present with neoplastic and inflammatory conditions. Localized enhancement predominated in the post-operative population, unless complicated by a subdural fluid collection. A nodular appearance was present in only two patients, both proven malignancy.

In our series, Gd-DTPA enhanced MRI is very sensitive to the presence of meningeal pathology, but nonspecific for any disease entity. MR performance is better in inflammatory disease (100% detection) than neoplastic conditions.

P050

The Major Salivary Glands : MRI Evaluation

S. RAJU, M. MAFEE, R. KINGSLAND, L. CHEKURI, R. AIZENSTEIN

Univ. of Illinois- Eye and Ear Infirmary

The role of MRI in the evaluation of salivary glands will be illustrated. The normal MR appearance of the salivary glands as well as the relevant adjacent anatomy will be discussed, with emphasis on the tissue planes which offer clues to the nature of a lesion in the region of the salivary glands. Proven examples of common inflammatory, benign , malignant and cystic lesions of the salivary glands will be illustrated. Specific entities to be discussed include Pleomorphic adenomas, Warthins tumors, Ranulas and parotid cysts (including those associated with AIDS). MRI is most useful for the evaluation of non inflammatory lesions. The relative insensitivity of MRI for detecting calcifications is a disadvantage when evaluating inflammatory disease.

P051

DIFFERENTIAL DIAGNOSIS OF CEREBELLAR ATAXIA: THE VALUE OF MRI

Massimo Gallucci, Alessandra Splendiani, Alessandro Bozzao,
Anna Cifani, Ornella Migliori, Massimo Maldassarre,
Roberto Passariello
Dept. of Radiology, University of L'Aquila, Italy

The aim of the study is to evaluate by means of Magnetic Resonance Imaging (MRI) the possibility of an "in vivo" diagnosis and nosological classification of patients affected by progressive ataxias.
32 patients affected by progressive ataxias (Friedreich ataxia (FA) 6, Non-Friedreich ataxia (NFA) 7, Olivo-pontocerebellar atrophy (OPCA) 8, Cortical-cerebellar atrophy (CCA) 7, Cerebellar mioclonic dissynergia (CMD) 4) and 40 normal volunteers of the same age and sex were admitted to the study. All subjects underwent MRI by means of a 0.5 Tesla superconducting magnet. Standard surface measurements of cerebellum (verm and hemispheres), pons, medulla, cerebellar and cerebral peduncle, spinal cord and posterior fossa were taken on sagittal, axial and coronal planes. The ratio between all measurements and posterior fossa was performed in order to make data comparable each other. Statistical analysis (Scheffe' procedure, p values below 0.05) was made.
Statistically significative mean values were found in each group. In particular, in FA only spinal cord measurements were affected; in OPCA, cerebellum, pons and cerebellar peduncle were involved; in CCA, cerebellum alone was affected. Our experience confirms that typical specific involvement can be detected by MRI in the different kinds of progressive ataxias. This efforts the clinical diagnosis and, in some cases, may differentiate single subtypes of the disease. More precise diagnostic differential criteria will derive from larger and comparable case histories.

P052

THE RELATIONSHIP BETWEEN THERMODYNAMICS AND THE ACUTE TOXICITY OF Gd(III) COMPLEXES

WP Cacheris, SC Quay, SM Rocklage
Salutar Inc., Sunnyvale, CA

In order to understand the toxicity of Gd(III) complexes we have employed a broad thermodynamic approach. The Gd(III) stability constant should not be the only stability constant important in considering the toxicity of Gd(III) complexes. If one assumes that most of the toxicity of such complexes arises from release of the highly toxic Gd(III) ion in vivo, it is important to know the stability of the ligand with endogenous metal ions such as Zn(II), Cu(II) and Ca(II). In addition, the stability constants of Gd(III) with biological ligands such as amino acids, citrate and albumin must be known.

The difference in stability constant between Gd(III) and the competitive metal ions for the same ligand is termed selectivity. The differences in toxicity for various Gd(III) complexes would be expected to be related to the ligand's affinity for other endogenous metal ions, i.e. its selectivity. In a thermodynamic context, the different stability constants for these endogenous metal ions provide an explanation of the observed stability of the gadolinium complexes in vivo.

The consequences of Gd(III) selectivity of a ligand over other endogenous metal ions can be understood through in vivo speciation calculations. A computer calculation of the speciation of Gd(III) complexes was performed incorporating the metal ions Zn(II), Cu(II), and Ca(II). The in vivo "ligands" used in the biospeciation calculations included the monoamine monocarboxylate amino acids, citrate and human serum albumin. For GdEDTA, GdDTPA, GdDTPA-BMA, and GdDTPA-BP, the amount of Gd(III) released was calculated as a function of dosage.

The results of the biospeciation model are in agreement with the observed LD(50) values (IV, mice) for GdEDTA, GdDTPA, GdDTPA-BMA, and GdDTPA-BP. Despite a 50-fold range in LD(50) values based on administrated dosage for these four complexes, each complex becomes lethally toxic to half the population of mice when they release ca. 13-15 uM Gd(III). Since Gd(III) has been shown to inhibit Ca(II) binding to mammalian cardiac sarcoplasmic reticulum at about 20 uM Gd(III), the actual mechanism of toxicity could involve hemodynamic disruption. The conditional stability of such complexes (based on the selectivity of each ligand), in the form of in vivo speciation of the complexes, provides an excellent correlation to toxicity.

This study describes a detailed thermodynamic characterization of the relationship between in vivo stability and measured acute toxicity for gadolinium polyaminopolycarboxylates. The prior concept of a direct relationship between the thermodynamic stability constant of the complex and observed toxicity is demonstrated to be incomplete. Ligands, like DTPA-BMA, that exhibit enhanced selectivity for gadolinium over competing endogenous metal ions such as zinc, copper and calcium yield highly stable, and hence relatively non-toxic, complexes The results of the biospeciation calculation have also led to formulation design for GdDTPA-BMA that should minimize the amount of Gd(III) released in vivo. Such considerations have resulted in formulations of GdDTPA-BMA that consistently have LD(50) values > 30 mmole/kg (IV, mice,).

P053

128-ECHO CPMG IMAGING FOR SAMPLING TRANSVERSE DECAY CURVES OF WHITE MATTER LESIONS

F.A. Jolesz, R.V. Mulkern, S.T.S. Wong, A.R. Bleier, T. Sandor
Dept. of Radiology, Harvard Medical School and Brigham & Women's Hosp., Boston, MA

We have implemented a 128-echo CPMG sequence for imaging at 1.5 T; this method is now applicable for routine clinical as well as research use. Its spatial resolution is on a par with the current double echo spin echo sequences. The temporal resolution, which is determined by the interpulse spacing (9.6 msec) is sufficient to reveal abnormal compartments with longer than normal T2, and it is now possible to compare in vitro with in vivo measurements.

We applied this method to compare transverse decay curves (TDCs) determined in vivo and in vitro, obtained from experimental white matter edema in animals (cold-induced, and infarct associated). We also obtained 128-echo CPMG images depicting normal human brain and lesions from multiple sclerosis (MS).

TDCs extracted from CPMG image data sets of photochemically induced brain infarction in rabbits demonstrated a biexponential T2 relaxation within the lesion with T2(1) = 168 msec (92%) and T2(2) = 1300 msec (8%). In the corresponding intact area in the contralateral hemisphere, T2(1) = 88 msec (94%) and T2(2) = 1700 msec (6%). In human brain, normal white matter TDCs were essentially monoexponential (T2 = 76 msec), while TDCs sampled from the region of MS plaques were clearly biexponential [T2(1) = 124 msec (87%) and T2(2) = 1200 msec (13%)]. Comparison with previously obtained in vitro measurements of animals with experimental WM edema confirmed that the in vivo results are comparable, notwithstanding the difference that for in vitro studies a shorter tau can be used for sampling, and therefore an even faster relaxing component can be revealed.

Multiecho CPMG imaging is a practical way to further characterize white matter lesions and thereby increase the specificity of MRI.

P054

T1 AND T2 SHORTENING WITH IODINATED CONTRAST AGENTS IN MR IMAGING OF THE CNS

JR Jinkins, L Sisk, RF Williams, G Fullerton
Radiology Department, University of Texas HSC at San Antonio, San Antonio, TX

INTRODUCTION: It was noted clinically that iodinated contrast agents administered intrathecally or intravenously immediately prior to the MRI examination (<1 hr), appeared to modulate MR contrast in the CNS. The effects of iodinated contrast agents in MRI were investigated. Evaluation of intrathecally and intravenously administered iodinated agents as well as in-vitro determinations of effects form the basis of this report.
MATERIALS AND RESULTS: Two patients were evaluated after the intrathecal administration of a water-soluble iodinated contrast agent (Iopamidol) and 5 subjects with cranial tumors after the intravenous administration of iodinated contrast agents (Iopamidol or Renografin). Both patients with intrathecally administered iodinated contrast demonstrated T1 and/or T2 shortening, while only 2 of 5 of the subjects with intracranial tumors illustrated a visible effect. Confirmation of the in vivo observations were obtained by in vitro measurement of T1 and T2 versus concentration in saline and CSF. T1 and T2 relaxation rates were measured in a GE GN300WB (7.05T) and a GE CSI 2T/45 imager (2T). All agents showed a concentration dependent shortening of T1 and T2.
DISCUSSION: All CT contrast agents shortened T1 as the concentration of the agent increased; however, Renographin and Reno M60 showed greater T2 shortening then Omnipaque or Isovue. Two explanations for this effect are proposed based upon the molecular structures of the contrast agents. The first is the effect of nitrogen quadrapolar relaxation on the surrounding water and the second is sequestering, by hydrogen bonding, of a portion of the water surrounding the agent. The observed T1/T2 effects suggest that administration of iodinated contrast agents immediately prior (<4 hr) to MR scanning may be contraindicated in selected cases.

P055

RECURRENT BRAIN TUMOR: COMPARISON OF UNENHANCED AND GD-DTPA ENHANCED MR IMAGING

W Schoerner, H Henkes, T Mitrovics, N Hosten, B Sander, R Felix
Dep. of Radiology, University Clinic Rudolf Virchow/Charlottenburg, Freie Universitat, Berlin

Purpose: The differentiation between normal postoperative changes and recurrence of tumor is a major problem after surgical treatment of intracranial tumors. In the present study, we compared the diagnostic value of unenhanced and contrast enhanced MR imaging in the postoperative follow-up in brain tumor patients.
Materials & Methods: MR examinations were retrospectively evaluated in 21 cases with recurrent brain tumors confirmed by contrast enhanced CT and/or histology. MR studies (0.5T Magnetom) were performed using T2-weighted images (SE 1600/30,70) and unenhanced as well as Gd-DTPA enhanced T1-weighted sequences (SE 400/30, FLASH 315/14, α=90°).
Results: Unenhanced MR studies showed areas of abnormal signal intensity in 21 cases, signs of mass effect in 16 cases, and presumed edema in 9 cases. Based on the results of unenhanced MR scans, recurrence of brain tumor was evident in 7/21, presumed in 8/21 and equivocal in 6/21 cases. Except the 7 patients in which recurrent brain tumor was demonstrated on unenhanced MR images contrast enhanced MR imaging was helpful for the diagnosis of intracranial tumors in 8 patients. In 6 patients, a recurrence of brain tumor could only be identified on Gd-DTPA enhanced MR.
Conclusion: I.v. administration of Gd-DTPA clearly improved the detection and identification of recurrent intracranial tumors and should be a standard procedure in postoperative MR follow up studies.

P056

ENHANCED MR STUDIES OF PITUITARY TUMORS BEFORE AND AFTER SURGICAL AND/OR MEDICAL TREATMENT

MA Mikhael
Evanston Hospital, McGaw Medical Center of Northwestern University, Evanston, IL

Of the 559 MR studies for suspected sellar/suprasellar masses, 45 small pituitary adenomas, 50 large sellar/suprasellar pituitary tumors and 20 sellar/suprasellar meningiomas were diagnosed. Fourteen cases of large pituitary tumors were medically treated and the remaining lesions were surgically removed. Pre- and post-treatment MR scans were obtained for all cases. In surgically treated cases serial scans were obtained every 6 months, and in medically treated cases serial scans were obtained every 4-6 months depending on the condition of the patient.

Post-gadolinium MR studies were superior to pre-enhanced MR scans for pituitary lesions: (1) they facilitated the differentiation between sellar/suprasellar meningiomas and pituitary tumors, an important point for the surgeon, as the surgical approach is different for the two lesions; (2) post-gadolinium MR scans showed very clearly the small intrasellar microadenomas and small pituitary tumors, making the transsphenoidal surgical approach easier and more efficient with less complications; (3) coronal MR slices can visualize the carotid siphon and can rule out the possibility of intrasellar aneurysms without the need for carotid angiography; (4) invasion of the cavernous sinus by intrasellar tumors can be easily visualized after gadolinium enhancement and followed-up after surgery to evaluate the need for radiation therapy; (5) postoperative MR with gadolinium is more diagnostic for visualization of the residual tumor and normal pituitary tissue, and/or any recurrent growth of the lesion with invasion to the bones and/or the cavernous sinus; (6) cases treated with bromocriptine were more accurately followed-up by enhanced MR for visualization of the response of the pituitary mass to the medical treatment.

On the other hand, acute postoperative complications, such as, hemorrhage and swelling are better visualized by noncontrast enhanced MR.

From our series, post-gadolinium enhanced MR is the study of choice for long-term follow-up of cases of pituitary lesions after surgical or medical treatment.

P057

ROLE OF POST-GADOLINIUM ENHANCED MR SCANS IN CASES OF SUSPECTED SPINAL LESIONS

MA Mikhael
Evanston Hospital, McGaw Medical Center of Northwestern University, Evanston, IL

We reviewed 84 cases (17-78 years) of spinal lesions studied with MR scans before and after gadolinium enhancement (Gd-DTPA). They include: 24 cases of metastases to the spine and/or the spinal cord, 6 cases of primary spinal cord tumors, 20 cases of multiple sclerosis of the cord, 4 cases of osteomyelitis of the spine, 10 cases of congenital cord abnormalities, 15 cases of postsurgical changes following laminectomy and diskectomy for recurrent pain, 3 cases of craniocervical meningioma and 2 cases of posttraumatic cord changes. From our series, post-gadolinium MR scans were necessary to visualize: (1) primary cord tumors, especially if they are not large enough to enlarge the cord, (2) intramural cord metastases, (3) active multiple sclerosis plaques of the spinal cord and to follow-up such plaques with clinical changes and treatment, (4) early meningitis secondary to osteomyelitis of the spine, and (5) recurrent spinal cord tumors following surgery and radiation therapy. Moreover, MR scans were helpful in the differentiation between congenital syringomyelia and syringomyelia secondary to spinal cord tumor. They were also helpful in diagnosing postoperative epidural and subarachnoid adhesions from recurrent herniated disc following spinal surgery as the cause of recurrent radicular pain following laminectomy.

Pre-gadolinium enhanced MR of the spine was necessary in cases of suspected metastases to the bones, because in 18 out of 24 cases, post-gadolinium enhanced MR masked early bone metastases. At the same time post-gadolinium MR of the spine showed 2 cases of metastases to the bone, which could not be seen in the pre-enhanced MR. As a result, when metastases are suspected to the bones, a T1 and T2 precontrast MR series should be obtained, and if the diagnosis cannot be reached, a post-gadolinium enhanced series is recommended.

In cases of suspected multiple sclerosis of the spinal cord a T2-weighted series is needed for the diagnosis, and enhanced T1 series is necessary to visualize the active acute plaques that necessitate starting medical treatment.

P058

COMPARISON OF 2D AND Gd-DTPA ENHANCED 3D CEREBRAL VENOUS MR ANGIOGRAPHY

P Schmalbrock, DW Chakeres, VA Davis, C Yuan, PJ Keller

Ohio State University, Columbus, OH, General Electric, Milwaukee, WI
Barrow Neurological Institute, Phoenix, AZ

The goal of this study is a direct comparison of Gd-DTPA contrast enhanced 3D and 2D-time-of-flight MR angiography for deep and superficial venous anatomy.

The studies of 15 patients were carried out on a 1.5T GE SIGNA system using a 2D-imaging sequence allowing a minimal section thickness of 1.5mm, and a 3D-sequence allowing 0.7mm. Both sequences employ shortest possible rf pulses, compact gradients and fractional gradient recalled echos, thus achieving very short TE (9.5ms for 2D, 7ms for 3D with flow compensation).

Very high contrast between stationary and flowing material is observed with the 2D-images, resulting in excellent angiograms of small vessels, but poor visualization of brain anatomy. Gd-DTPA enhanced 3D-imaging yields excellent brain anatomy and sufficient, but decreased contrast for flow. Differentiation between arterial and venous structures can be confusing. Depending on the selected image plane, this problem may be resolved for 2D-imaging by spatially selective presaturation, which is not effective in T1 contrast based 3D-images. Furthermore, 3D is hampered by the additional cost for the contrast agent, signal loss due to saturation effects and slice aliasing, but permits imaging with higher resolution.

Initial results indicate, that 2D-MRA may be better for studies, where definition of venous flow dynamic is important, such as dural sinus thrombosis. 3D-imaging may be the preferred method, where simultaneous information regarding the brain and associated venous anatomy is desired.

P059

DURAL SINUS EVALUATION WITH 3-D MRA WITH GD-DTPA

KM Link, P Margosian, W Sattin, C Souder
Bowman Gray School of Medicine and Picker International

An evaluation of the dural sinuses was performed with 3-D MRA compared FLASH and FISP sequences in normal volunteers. The study was performed on a 1.5T system (Picker International, Highland Heights, Ohio) with a 12mT/m gradient capacity. The studies were performed using a circularly polarized head coil which operated in both the transmit and receive modes. One mm - 2 mm thick slices were performed with slab thickness varying from 32 mm to 64 mm. Minimal FOV was 25 cm with an acquisition matrix of 256 x 256. Sequences employing MAST through first order correcting for velocity in two axes (readout and slice select) and three axes were used with both the FLASH and FISP techniques. The TE was kept at 14 msec while various TR times and flip angles were evaluated. Imaging was performed in both the sagittal and transaxial planes.

Either the FLASH (TR 55 msec; flip angle 12^{o}) or FISP (TR 55 msec; flip angle 20^{o}) sequences correcting for velocity in three axes could demonstrate the dural sinuses. The sagittal sinus can be seen in its entirety on sagittal images, however, there is a consistent signal loss in the mid aspect in the sinus. This situation is partially but not completely corrected by performing transverse imaging. The signal fallout is thought to be secondary to the congregation in this area of many draining veins. Administration of Gd-DTPA prior to scanning revealed no evidence of signal fallout in over 95% of normal volunteers. Although uncommon, sagittal sinus thrombosis is a potential life threatening entity that is difficult to evaluate with conventional techniques. One can potentially demonstrate sagittal sinus thrombosis in a noninvasive way with MR angiography in conjunction with Gd-DTPA.

P060

FIELD MAPPING FROM SPIN WARP IMAGES

T Morrone, JR Benevento, WC Maloney, RK Shenoy, TD Datsikas, M Thompson
Fonar Corporation

Mapping the static magnetic field in a MRI magnet usually involves either point methods, phase images or 3 or 4D acquisition. Point methods have relatively low signal to noise and with phase methods care must be taken to separate out eddy current effects. 4D methods are slow and 3D methods although faster than 4D require a plane phantom and special pulse sequences.

Here we describe our experience with a method based on the distortions in spin warp images. We gain freedom from eddy current effects, speed and simplicity in the pulse sequence at the expense of phantom complexity. In addition the method can be automated. We have employed it a system where an operator need only place the phantom in the imaging space and run a protocol which maps the field and changes shim coil currents to improve it.

The phantom consists of 5 planes each containing 25 rectangular cubes arranged in grid patterns. We make a multislice scan with a positive read out gradient and another scan with this gradient reversed.

The center pixel of each cube is determined by finding its edge locations in a narrow band of pixel through the cube centers. We employ 3 different edge detection algorithms. A test is made of the accuracy of each by fitting a polynomial to the edge pixel values as a function of coordinate. We accept the data if it fits on a smooth curve. Except in very unusual circumstances at least one of the methods gives accurate results.

The magnetic field value at the center of a cube is simply related to the sum of its pixel values in the 2 scans. Eddy current induced fluctuations either cancel in the summation of pixel values or can be shown to be unimportant.

P061

SLICE PROFILE IMPROVEMENT FOR A CLINICAL SYSTEM

J Mao, JR Fitzsimmons, H Yan*

Radiology Dept, Univ of Florida, *School of Elec Eng, Univ of Sydney

Recently several optimized selective pulses that can produce excellent slice profiles have been reported. However, these pulses usually require high peak rf amplitudes to implement. Because of the specific absorption rate (SAR) and the limits of the rf power amplifier their utilization in a clinical system is limited. Therefore, the peak amplitude of a selective pulse is a major restriction for improving the quality of a slice profile.

We have a Siemens 1.5T MRI clinical system. Several pulse files which consist of the bandwidth matched 90^{o} and 180^{o} selective pulses are provided. Some of these can produce excellent slice profiles. However, they can only be used in the pulse sequences with the pulse length of 5.12 ms, because the shorter 2.56 ms pulse requires excessive rf peak amplitude. The pulse length of 5.12 ms is too long for most of the sophisticated clinical pulse sequences. There is a pulse file producing a good slice profile with an allowable peak voltage in the Siemens system, which is commonly used in the pulse sequences with the pulse length of 2.56 ms. Applying the conjugate gradient method we have found an optimized pulse file that can be substituted for the Siemens pulse file to produce an obviously improved slice profile. The experimental results show that the slice profiles and images are improved by the optimized pulse file with a lower peak voltage. Fig 1 shows the experimental result of the slice profile. The slice profile a is obtained by the Siemens pulse file; the slice profile b is obtained by our optimized pulse file at the same experimental conditions as the profile a. The proposed pulse file can also be utilized in the pulse sequences with a short pulse length of other clinical systems. The detail of the optimized pulse file will be presented in the poster.

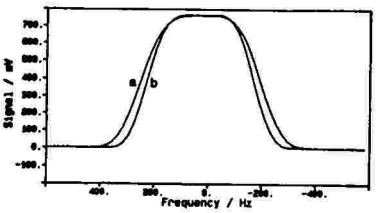

Fig 1

P062

MRI SIGNAL HYPERINTENSITIES IN THE AGING BRAIN: GROSS AND HYSTOPATHOLOGIC FINDINGS

M. Gallucci, A. Bozzao, A. Splendiani, *E. Nardecchia, A. Cifani, E. Passariello
Dept. of Radiology, University of L'Aquila and *Dept. of Forensic Medicine, University of Rome, ITALY

Confluent or isolated foci of abnormal high signal intensity are commonly seen in elderly patients on MR images with long TR and TE sequences. The aim of our study was to evaluate the presence, the rate and the differential aspects of such foci evaluated on non-fixed brain specimens, thus preventing the data from being biased by formaline-induced modifications. 20 brains were taken from 20 cadavers from subjects older than 60, these subject had an apparently normal aging. For this purpose these subjects were excluded which, at our knowledge, had been affected by previous clinically apparent cerebrovascular disorders, demielinating diseases, neurological symptoms, head traumas. The specimens were taken off with 24 hours after death, entirely or sliced along corpus callosum. They were placed in a cool bag and examined within the following 4 hours. The examinations were conducted by means of 0.5 tesla magnet, acquiring long TR/TE and long TR short TE Spin-Echo sequences. Slice thickness ranged from 0 to 5 mm. At the end of the examinations, the specimens were fixed in a formaline solution, and examined for gross and hystopathologic analyses after 3-8 weeks. The cuts were performed by a pathologist, taking into account the planes of MRI scans. Our study demonstrated the presence of hyperintense foci in 9 out of 20 specimens studied. In the basal ganglia we found the higher incidence of lesions (about in 40% of the subjects). In 58% of cases they represented enlarged Wirchow-Robin spaces. Morphology and dimensions were considered unable to differentiate lacunar infarctions from status cribrosus. The only lesion bigger than 5 mm in diameter was an infarct. In periventricular white matter we found 9 lesions, mostly related to the presence of periventricular foci of myelin and axonal degeneration (44% of cases) with associated gliosis and sclerotic vessels. They were likely due to the critical blood-flow in the wathershed areas supplied by the most distal branches of the cerebral arterioles. Ependimitis granularis, as described by Sze and Zimmermann, was also found in a high percentage (33%) more tipically located in subependimal white matter adjacent to the frontal horns. The lesions found in centrum semiovale and in infratentorial territory were referred to infarcts. In our study they involved 12% of subjects, regarding centrum semiovale, and only 6% regarding infratentorial territories. In the last phase of our study, we tried to correlate the morphologic and dymensional aspects of the lesions with the hystopathologic diagnoses, with the aim of underlining eventual differential aspects. Our data showed that it is often difficult to differentiate the groups each other and that clinical hystory and evaluation must be correlated with imaging to reach the correct diagnosis.

P063

A METHOD TO DECOUPLE THE TUNING AND MATCHING CONDITIONS IN AN NMR PROBE

GX Shen, PW Reittinger, RL Nunnally
Biomedical Magnetic Resonance Ctr., UT Southwestern Med. Ctr. at Dallas

The adjustment of the tune and match of an NMR probe can, at times, be a tedious task. There are situations in which it is not possible to have a probe simultaneously tuned and matched. These difficulties arise from the fact that the impedance at the feed point and the resonant frequency of a typical NMR probe circuit are functions of the same parameters. Therefore, it is possible to write the tuning condition as a function of the impedance matching condition, and vice-versa, for this circuit. This paper will show that the resonant frequency and the impedance matching conditions of an NMR probe may be decoupled through the use of an impedance divider for the transmission line feed point. The only design requirement for the impedance divider is that the total reactance of this component must remain constant. The impedance at the feed point to this divider is a function of the ratio of the reactances of the two paths through the divider. Since the total reactance of the divider remains constant, there is no change in the reactances which establish the resonant condition of the circuit. Initial results have been obtained with a differential capacitor constructed from four 33 pF fixed value capacitors. The feed point to the circuit was varied to show an order of magnitude change in the input impedance. The resonant frequency remained constant within three percent, however. Additionally, a design for a differential capacitor will be presented.

P064

HIGH FREQUENCY EFFECTS ON TUNING AND MATCHING IN NMR PROBE CIRCUITS

GX Shen, MP Chwialkowski, RL Nunnally

Biomedical Magnetic Resonance Ctr., UT Southwestern Med. Ctr. at Dallas

Tuning and impedance matching are crucial aspects of NMR coil design for clinical applications. Increased image resolution and contrast to noise are obtained by using greater field strengths. The increase in the resonant frequency which is due to the increased field strength in turn causes a variety of problems in both the tuning and matching conditions of the resonant circuit. Some of these problems can be attributed to the distributed capacitance of the circuit. The distributed capacitance is negligible at low frequencies, but becomes a significant factor at higher frequencies. Two models of distributed capacitance are considered: (1) between the turns of the coil, and (2) between the coil and ground. Both models have been developed to analyze a circuit's behavior at higher frequencies, and to calculate the resonant frequency and input impedance of the circuit. In addition, the frequency dependence of the self and mutual inductances in the circuit has been evaluated.

At higher frequencies, the decrease of the quality factor, Q, of the inductor causes a shift of the resonant frequency and phase. The model indicates that in order to minimize these shifts, the value of Q shoul be larger than 10.

Another phenomena which occurs at the higher frequencies is due to the wire leads of the capacitors used in the circuit. The wire leads always introduce a small amount of inductance in series with the capacitor. Therefore, the leads of the capacitor introduce a series resonance at the higher frequencies. This series resonance will result in more attenuation than expected.

P065

MR IMAGING OF PULMONARY PARENCHYMA AND EMBOLI BY PARAMAGNETIC AND SUPERPARAMAGNETIC CONTRAST AGENTS

S Vinitski, M Thakur, PM Consigny, D Mitchell, R Blob, S Lin, CSG Eley*, M Rifkin

Thomas Jefferson Hospital, Philadelphia, PA; *Vestar, Inc., San Dimas, CA

The high susceptibility gradient between air and lung tissue, as well as the low proton density of lung, deteriorate pulmonary NMR signal. The objective of this study was to investigate the use of paramagnetic and superparamagnetic agents in MR imaging of peripheral lung tissue and its alteration by pulmonary embolism (PE). Three contrast agents, Gd-DTPA albumin microspheres, Gd-DTPA liposomes, and superparamagnetic ferrosomes were examined. Preparations of Gd-DTPA microspheres, Gd-DTPA liposomes (10-30 um in diameter) and ferrosomes (60 nm) are described elsewhere (1,2).

Pulmonary embolism was induced in six rabbits by injection of blood clots (labeled with radioactive Indium-111) into the jugular vein. The presence of pulmonary emboli was verified by gamma camera both in vivo and in vitro (after MR imaging, using excised lungs). The MR imaging was performed on a 1.5 T GE scanner before and after induction of PE. Contrast agents were administered via the jugular vein. Axial and coronal T1 weighted (single RR interval, TE=12 msec, 3 mm thick) images were obtained.

Gd-DTPA albumin microspheres entrapped in lung capillaries did not enhance the signal intensity of lung parenchyma. Liposomes carried less Gd (10 ug/mg vs. 39 ug/mg), but doubled the parenchymal signal intensity, presumably because of their water content. Injection of 8 ml of ferrosomes dramatically decreased the intrapulmonary NMR signal, significantly enhancing contrast between PE and lung parenchyma. In addition, flow artifacts and intravascular signal were also reduced.

In conclusion, superparamagnetic contrast agent appears promising for vascular imaging and detection of PE, and merits further evaluation.

1. Thakur, M. et al. J Nucl Med 30:901-902, 1989.
2. Skarnulis, A.J., William, R.J.P. Chem Comm 1067-1068, 1979.

P066

ONE YEAR OF DAILY QA MEASUREMENTS

Edward F. Kubiez and Deborah D. Cross-Blancke
Department of Radiology, MetroHealth Medical Center, Cleveland, Ohio 44109

One year of daily signal-to-noise measurements have been accumulated in a quality assurance program begun with the installation of our MRI system in September 1988. Our database records forward and reflected transmitter power, transmitter attenuation, receiver attenuation, mean signal value, and noise. For the first two months, two methods of measuring noise, subtraction of images and image acquisition without excitation, were compared; the latter was more consistent, probably from smaller sensitivity to some system instabilities.

Multiple occasions of accelerated troubleshooting demonstrate the value of a QA program for minimizing downtime. An additional benefit is increased operating confidence. As MRI matures, and incremental image quality improvements become smaller, an accurate baseline of system performance becomes more important.

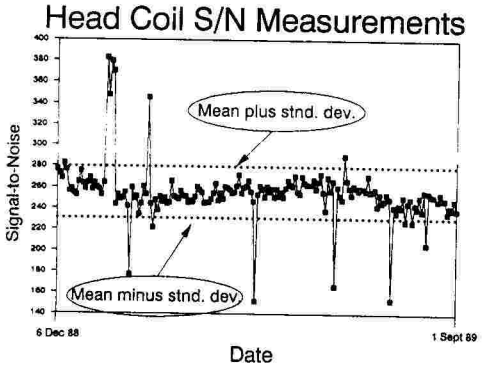

Coil	Number of Measurements	S/N	
		Mean	Stnd. Dev.
Head	171	255	26
L-Spine	43	92	23
C-Spine	36	101	15
Knee	35	100	23

P067

MR QUANTITATIVE FLOW IMAGING WITH 3D COMPUTER SIMULATION CORRELATION

H Yamagata, MH Buonocore, JA Sanders
Division of Diagnostic Radiology, UC Davis Medical Center

Results of quantitative flow imaging using an even echo rephasing pulse sequences have been compared with 3D computer simulation of blood flow. The simulation is based on Peskin's finite difference method for time dependent incompressive Navier-Strokes flow within compliant vessels. MR experiments and computer simulation were carried out for a plastic flow phantom of a stenotic vessel, a plastic flow phantom of a bifurcating vessel, and for carotid artery flow imaging of normal volunteers. The time dependence of plastic phantoms was generated by a pulsatile pump and accurately modeled in the computer simulation.

Velocity vectors and pressures were calculated at each of 32x32x32 voxel points, in the presence of a vessel boundary model consisting of 32x32 curvilinear surface patches. The simulation was implemented initially on a Stellar GS-1000 graphics computer, but transfered to the Cray YMP at the Pittsburgh Supercomputing Center for more realistic flow parameters. Excellent correlation was obtained between the in the simulation with those obtained in MR flow imaging.

POSTER ABSTRACTS

P068

EXPERIMENTAL DESIGN AND FABRICATION OF BIRDCAGE RESONATORS

T. Vullo, R.T. Zipagan, J.P. Whalen and P.T. Cahill

The New York Hosptial-Cornell University Medical College, New York, N.Y.

The RF birdcage coil is popular in clinical imaging due to its inherent high signal to noise ratio and B1 field uniformity approximating 80% of its diameter in the transverse plane. This type resonator has been described theoretically (e.g. Hayes, et al, (1985) J. Magn. Reson. 63:622; Tropp, (1989) J. Magn Reson. 82:51); however, little experimental data is available involving the practical aspects of fabrication, tuning and testing. In this study, an experimental approach was taken to evaluate the design and performance characteristics of the low pass symmetric birdcage.

Ten eight rail birdcage coils were constructed of various diameters and length/diameter ratios using 3/8 inch wide, 16 mil copper strips mounted on rigid plastic frames. The inductance for each coil was calculated from impedance measurements of a single circuit segment (L1) and also for the total coil (Lg). The rail capacitance (C1) was determined, the four resonant modes were measured, and the effects of different types of coil coupling, shielding and loading were evaluated.

Calculation of C1 becomes straightforward when using Lg and a modified Hayes formula ($C1 = (a)*1/[(\omega**2)*Lg]$), where (a) is an experimentally determined constant. Likewise, corrections for sample loading and the effects of shielding associated with the magnet are considered. Images were acquired both on a 0.6 T clinical and 2.0 T imaging system to demonstrate the high degree of B1 uniformity at mode one and non-uniformity at modes 2, 3 and 4.

P069

IN VIVO QUANTITATION OF WATER CONTENT IN MUSCLE TISSUES BY MRI

V. Rajanayagam*, M. E. Fabry# and J. C. Gore+

*Huntington Med Res Insts, Pasadena CA; #A. Einstein College Med, Bronx NY; +Yale Univ Sch Med, New Haven CT

One possible clinical application of MRI is in the quantitation of tissue water content. We have determined water contents of thigh muscle tissues *in vivo* directly from MRI measurements on a whole-body scanner operating at 0.179 T for protons.

The method initially involves the calculation of the corrected proton densities from multiple echo and partial saturation images of phantoms that have been imaged simultaneously with the animal. A calibration plot of these proton densities against the water content is then generated. From this plot, the water content of the muscle tissues are read off directly. The water content values are in good agreement with the reported values in the literature. Comparison with values obtained from the oven-dry method on the same animal yields variations up to 8.5% on normal tissue data.

P070

The Continuous Formulation of the VERSE Technique

D.P Lewis, B.M.W. Tsui, P.R. Moran[1], and D. Saloner[2]
Univ. of North Carolina, Chapel Hill, NC 27599, [1]Bowman Gray School of Medicine, Winston Salem, NC 27103, [2]Univ. of California, San Francisco, CA 94121

Two major concerns in the design of an RF pulse are the peak power and the integrated power of the pulse. Because of hardware limitations and patient safety concerns, it is desirable to keep the power low. The VERSE technique [1], a method for pulse refabrication, meets these concerns by modifying both the RF and gradient waveforms in such a way that the rf power is significantly reduced while the pulse duration and the resultant slice profile are unchanged. The technique as described in [1] assumes that the RF and gradient waveforms are piecewise-constant and produces variable-rate waveforms. It is possible to formulate VERSE using continuous waveforms [2], as we show here.

Under an arbitrary transformation $t \rightarrow f(t)$, the Bloch equation transforms back into itself provided that the RF and gradient waveforms and the magnetization are redefined as

$$B_1'(t) = B_1(F(t)) \cdot dF(t)/dt,\ G'(t) = G(F(t)) \cdot dF(t)/dt, \text{ and } M'(x,t) = M(x,F(t)),$$

where $F(t) = f^{-1}(t)$. As a result, the waveforms $B_1'(t)$ and $G'(t)$ give rise to the same slice profile as do $B_1(t)$ and $G(t)$. The goal of pulse refabrication is to find the "best" pair of waveforms $B_1'(t)$ and $G'(t)$ which yield a particular slice profile. The criteria for "best" depend on the application and are related to peak and integrated power, pulse duration, and implementability.

The continuous formulation of VERSE readily permits the incorporation of maximum gradient and gradient slew rate constraints and, unlike piecewise-constant formulations, does not suffer from degradation of the slice profile due to interpolation from variable-rate to uniform-rate pulses.

Reference
1) Conolly, S., Nishimura, D., Macovski, A., Glover, G., J. Magn. Reson., **78**, 440, 1988.
2) Conolly, S., Ph.D. Dissertation, 1989.

P071

A NEW TECHNIQUE FOR VERY HIGH RESOLUTION IMAGING WITHOUT CHEMICAL SHIFT ARTIFACTS

JP Mugler III
Dept. of Radiology and Biomedical Engr., University of Virginia, Charlottesville VA

There has been much progress in the field of MR microscopy over the past several years, particularly in conjunction with very high field imaging systems (>2 Tesla) equipped with specialized gradient and RF coils. There have also been notable advances in the use of high resolution imaging for clinical purposes using standard commercial equipment [1].

In our particular application, we need to obtain high resolution, thin slice images of excised vessels diseased with atherosclerosis. This investigation is part of an on-going project at our institution on MRI of atherosclerosis [2]. We do not have a high field microscopy imaging system available, and prior techniques[1] employed on commercial imagers which modified standard spin-echo sequences produce unacceptably large chemical shift artifacts when one is trying to quantify volumes of specific plaque types and the spatial relationships between the plaques and the vessel wall.

We have developed a new technique for producing high resolution images on our whole-body 1.5 Tesla imager (Magnetom 63SP, Siemens Medical Systems, Iselin, NJ) that eliminates the in-plane chemical shift artifacts. The pulse sequence is based on the standard spectroscopic imaging sequence [3,4], where all spatial dimensions are phase encoded. As compared to a typical spectroscopic imaging acquisition where the voxel sizes are relatively large to provide sufficient signal-to-noise in the spectra, we significantly extend the duration of the phase encoding to allow voxel dimensions of less then 100 microns. The spectra are post-processed to collapse the information to a single value, thus removing spectral shifts from inhomogeneities or chemical shift from the image. This entails gleaning the high signal points from the spectra until the addition of further points fails to increase the SNR. The acquisition time is comparatively long since a 3D (or 4D) data set is required to generate a 2D (or 3D) image. To minimize the time, imaging is performed using a low flip angle, gradient echo technique such as FLASH or FISP.

To date, we have implemented a version of this technique which produces 2D images. A 128x128 image is acquired in about 10 minutes. This may seem unreasonably long, but when imaging specimens a much longer acquisition time is tolerable in exchange for image quality. Using test phantoms, and a standard 10cm diameter surface coil supplied with the imager, we have acquired images with 1mm thickness, 85x85 micron in-plane resolution, and reasonable SNR (approximately 10). We anticipate much improved results using surface coils more closely adapted to the sample size.

1. A Jesmanowicz, JS Hyde, JB Kneeland, 7th SMRM, 1041 (1988).
2. MB Merickel, CS Carman, JR Brookeman, CR Ayers, 8th SMRM, 1043 (1989).
3. TR Brown, BM Kincaid, K Ugurbil, Proc Natl Acad Sci USA, 79:3523 (1982).
4. AA Maudsley, SK Hilal, WH Perman, HE Simon, *J Magn Reson*, **51**, 147 (1983).

P072

"ROTATED-GATED" CARDIAC IMAGING MADE PRACTICAL

Thomas A. Spraggins
Siemens AG, Medical Engineering Group, Erlangen, FRG

In spite of the gains in temporal resolution afforded by gradient-echo sequences, there is still the need for spin-echo images in cardiac MRI studies. The "dark blood" appearance of these images can greatly facilitate endocardial border detection. A method of "rotated gating" has been described by Crooks, et al.(1), which allows the acquisition of multiple phases of multiple slices. Unfortunately, the temporal resolution is usually poor, and operator intervention may be required for running several sequences.

An improved technique for rotated gating is presented, which provides greater temporal resolution without any increase in imaging time, and which requires only one sequence to be loaded and run, which may reduce image registration problems caused by patient movement between scans.

One can imagine imaging slices 1,2,3,4, and 5 after a trigger pulse, and then 2,3,4,5, and 1 after the next trigger, and so on, and then repeating for each Fourier line. However, due to the long interval between excitations of, in the example here, slice 1, image contrast will vary greatly from one heart phase to the next. It is possible to image slices 1,2,3,4,5 and then (again) 1 during one heart cycle, then 2,3,4,5,1, and 2, and so on, and thereby keep the image contrast nearly constant. Furthermore, an extra phase is thus imaged with no increase in imaging time. By extension, one can image a large number of phases, up to a limit determined by the acquisition time per slice and the patient's heart rate. This method can produce heavily T1-weighted images, which is not possible using conventional rotated gating.

In order to maintain nearly constant image contrast, it is necessary only that the number of phases exceeds the number of slices, and that the number of phases and the number of slices are prime conjugates, i.e., have no common factors. The overall imaging time is determined only by the number of slices desired; the extra phases are "free". For example, it is possible to acquire 16 phases of each of five slices in approximately ten minutes. This method can also be applied to gradient-echo sequences, in order to obviate the need for sequence reloading.

(1). Crooks, L. E., et al., Radiology **152**, 459, 1984.

P073

A SIMPLE PHANTOM FOR PROTON DENSITY MEASUREMENT IN MAGNETIC RESONANCE IMAGING

Ramesh Chandra
Department of Radiology, N.Y.U. Medical Center, New York, N.Y. 10016

Even though proton density images have not been found to be useful clinically, for accurate T_1 and T_2 determinations, an accurate measurement of proton density is essential as it is a fundamental parameter in any equation describing MRI signal. Existing proton density phantoms consisting of mixtures of water and heavy water (relatively expensive substance) have long T_1's which therefore require a time consuming step of adding different but exact amounts of paramagnetic ions to reduce these long T_1's (3 to 6 s) to a short but equal T_1. Short T_1 is needed to keep the imaging times in acceptable limits (15 minutes or less). We have developed and successfully tested a proton density phantom which is less expensive, simpler and faster(10 minutes or less to prepare) to construct than the existing phantoms. This consists of different volume to volume ratio mixtures of alcohols (propanol, pentanol or hexanol) and carbon tetra -chloride. These chemicals are inexpensive and easily available (Aldrich Chemical Co.).

Research grade CCl_4 is mixed with 2-propanol or 1-hexanol in 0,10,20,30,40% ratios (v/v), respectively. Since CCl_4 does not contain any hydrogen, these represent 100, 90, 80 , 70, and, 60% proton density solutions-a range normally found in tissues. T_1 of these solutions was measured with saturation recovery pulse sequence at 10.7 MHz on a Praxis NMR unit. To measure the proton density accuracy of a 1.5 T MR Imager, 20 cc vials of these solutions placed inside a beaker filled with water, were imaged with multislice (slice thickness - 1 cm.) SE sequence for proton density (TR - 4 x T_1 and TE - 20ms) and the observed intensity values in a 1 cm^2 ROI located inside each vial, are correlated with proton density.

Measured values of T1 ranged from 1.1 s for pure to 1.3 s for 60% 2-propanol and 0.55 s for pure to 0.75 s for 60 % hexanol . Regression analysis of the intensity values from the Imager with the proton density showed them to be linear with a correlation coefficient of 0.999. It is concluded that simple incremental solutions of two commonly found chemicals, CCl_4 and 2-propanol or CCl_4 and 1-hexanol, can be used to calibrate proton density measurements with a MR Imager.

P074

NEIGHBORHOOD CRITERION FOR IMPROVEMENT OF MR PROJECTION ANGIOGRAMS

A. V. Lakshminarayanan, P. M. Margosian
Dept.of Rad.,Univ. of AL, Birmingham, AL; MRI Div.,Picker Intl.,Highland Hts.,OH

A robust method for making MR Angiograms is to acquire many thin slices in a way that makes blood vessels the brightest objects, then make a maximum amplitude ray projection reconstruction from several view angles to make a series of images that can be viewed in a cine display to give a three dimensional effect (1). Visibility of the blood vessels is improved by suppressing "background" pixels, either by sequence methods (2) or by postprocessing (3). Postprocessing methods have the advantage of minimizing patient examination time.

The idea presented here is to combine the ray projection calculation with blood vessel identification criteria incorporating a priori information such as typical size ranges and shapes. The method we have tested works as follows:

(a) Find the maximum pixel amplitude and its location along each ray projected through the imaged volume (one from each pixel of the desired output image).
(b) Count the number of pixels within a spatial neighborhood (volume) centered at each maximum which have intensities within a few percent of the intensity of the ray maximum.
(c) If only a few percent (threshold) of the pixels in the local region are within the specified intensity band, then classify this ray maximum as blood vessel and keep it; reject all others.

The effects of the various threshold parameters on visibility of blood vessels will be illustrated with a variety of images.

References:
(1) Laub, G., Mueller, E., et. al., Proc SMRM, p876, 1988.
(2) Dumoulin, C., Souza, S., Proc SMRM, p725, 1988.
(3) Laub, G., Rossnick, S., et. al., Proc.SMRM, p508, 1986.

P075

DIRECT MEASUREMENT OF INTERNAL GRADIENT DUE TO SUPERPARAMAGNETIC PARTICLES USING DIFFUSION STUDIES

J Zhong and JC Gore
Dept. of Diag. Radiol., Yale Univ. School of Medicine, New Haven, Connecticut, USA

We have previously shown[1,2] that superparamagnetic iron oxide particles are extremely effective at reducing T2 in spin echo imaging as well as T2* in gradient echo sequences. Such agents may be useful as MRI contrast agents, but the relative importance of different relaxation effects may vary with the design and application of the particles[2]. An important characteristic is the distribution of magnetic field gradients induced by the particles in the medium because of their different susceptibility. Diffusion of water amongst these field gradients produces a dephasing of the transverse magnetization. We have attempted to measured these gradients directly using a modified pulsed gradient diffusion sequence, in which the decay of the magnetization at fixed TE was measured as a function of diffusion time t. The apparent diffusion coefficient D* decreases with t and this decrease can be used to estimate the internal gradients present. Gels, solutions and tissues containing AMI25 (Advanced Magnetics, Cambridge, MA) were studied at 2.0T. D* is smaller in samples with higher concentration of AMI25. We have estimated the variances of the internal gradient distributions in different samples. In gels and tissues, D* is further reduced at long diffusion times as restricted diffusion becomes important. The implications of these measurements of internal gradients for explaining the contrst mechanisms that are important in practical imaging have been estimated.

[1] S. Majumdar, S. S. Zoghbi, C. F. Pore and J. C. Gore, *Mag. Res. Med*, **9**, 185 (1989).
[2] S. Majumdar, S. S. Zoghbi and J. C. Gore, *Mag. Res. Med*, **10**, 289 (1989).

POSTER ABSTRACTS

P076

The Effects of Gradient Timing and Spatial Resolution on the Signal from Flowing Blood

Jia-Hong Gao, Scott K. Holland, and John C. Gore**
*Departments of Applied Physics and *Diagnostic Radiology, Yale University*

The dependencies of the NMR signal from flowing blood on the precise timing of rephasing gradients and image spatial resolution have been studied theoretically, by computer simulation and experimentally. In principle, the rephasing gradient following slice selection can be applied at any time before signal acquisition, and it is often placed after the 180^0 pulse in a spin echo sequence so it can serve other purposes as well. However, for flowing blood the precise placement of the rephasing lobe may strongly affect the signal intensity, even when the flow velocity does not vary with time(no acceleration). For laminar flow, the velocity gradient within a pixel produces intravoxel incoherence that is more effectively reversed by an early rephasing lobe than a later one. Images have been acquired of flowing $MnCl_2$ solution(T1=500 msec, T2=50 msec) at 2.0T, for different velocities using a flow phantom, and using each of three different spatial resolutions over a fixed field of view. The experimental results are in good agreement with the results of a computer simulation that considers both time of flight effects as well as phase dispersion within each pixel. The NMR signal decays much more rapidly with increasing velocity in the case of late rephasing, but this difference in less marked as the spatial resolution becomes finer and intravoxel phase differences are smaller.

P077

FLASH IMAGING WITH A SINGLE SURFACE COIL

N Bansal and RL Nunnally
Biomedical Magnetic Resonance Center, UT Southwestern at Dallas

Garwood *et al.* have developed a method to acquire images in extremely inhomogeneous radiofrequency (rf) field using adiabatic pulses. Since adiabatic pulses most suited to slice selection are the inversion type, the method involves subtraction and is prone to artifacts from receiver and analog-to-digital conversion saturation and subtraction errors. Previously, we have demonstrated that these problems are substantially reduced by using a pseudo-noise-modulated selective (PNMS) prepulse to randomize the unwanted spin magnetization. However, this approach still involves subtraction and cannot be used for imaging large objects like human trunk. Pulse sequences which incorporate small excitation flip angles using sinc or Gaussian pulse and gradient-recalled echoes (*e.g.* FLASH) can be employed for surface coil imaging. With this approach no subtraction is involved and images with excellent signal-to-noise ratio can be obtained within few seconds. Other major advantages of the technique is the absence of motional artifacts and low rf power deposition.

P078

EFFECT AND EXPLOITATION OF J-MODULATION IN ^{19}F MRI

RP Mason, EE Babcock, N Bansal, RL Nunnally, and PP Antich
Department of Radiology, University of Texas Southwestern Medical Center at Dallas

^{19}F-labeled compounds are being investigated by magnetic resonance for the assessment of biodistribution and metabolism, as well as for the measurement of physiological functions (*e.g.*, pH, PO_2, temperature). Many of these fluorine compounds are perfluorinated and therefore have fluorine homonuclear couplings. With the increase in ^{19}F spin-echo projection images using longer TEs (for improved spatial resolution, increased T_2 contrast, and reduced eddy current distortions), J-modulation effects may occur.

The effect of J-modulation on spin-echoes of homonuclear J-coupled resonances is well known in spectroscopy, but is rarely observed in *in vivo* images. J-modulation of the spin-echo signal causes the disappearance of signal at TE=1/(2J) with reappearance of the signal at TE=1/J. Demonstration of the effect in ^{19}F images of phantoms and perfluorocarbon-loaded mice emphasizes the importance of the proper selection of echo times.

Exploitation of this effect is demonstrated by selectively obtaining images of either a non-coupled or coupled ^{19}F resonance, both present in the sample. Specifically, separate images of either 5% trifluoroacetic acid (TFA) (non-coupled) doped with $GdCl_3$ or an *in vivo* emulsion of perfluorotributylamine (coupled spin system) have been obtained. The image of TFA was obtained at TE=1/(2J) when the coupled signal was suppressed by J-modulation, and the image of perfluorotributylamine was selectively obtained when that signal reappeared (TE=1/J) and the TFA signal had decayed by T2 processes.

P079

3D SEGMENTATION OF BRAIN TISSUE USING CONNECTIVITY

HE Cline, WE Lorensen, F Jolesz*, R. Kikinis*

GE Corporate Research and Development, Schenectady NY 12301

*Brigham and Women's Hospital, Harvard Medical School, Boston MA 02115

We present a method for visualizing MR data of the head that uses segmentation, connectivity, 3D surface construction and color display. For surgical planning applications it is important to extract and create multiple surfaces without tedious, manual intervention. Furthermore, the same high quality 2D slices can be used for both routine diagnosis and 3D imaging. Data is acquired using a two echo SE pulse sequence giving 60 3mm thick slices in 14 minutes. Both short and long echo data sets (TE 30 and 80) are examined for pathology and used in the segmentation procedure. Brain tissue, cerebrospinal fluid, and the scalp are segmented by setting the range of intensities in a selected image from each echo. The segmented data set, represented by an integer for each tissue type, is smoothed by 3D Gaussian filtering to establish a surface normal direction and reduce step artifacts. A 3D connectivity algorithm (1) follows and marks selected tissues. Surface display lists for each marked region are created with the *dividing cubes* algorithm (2). The face, brain, lateral ventricle, and eye globe are displayed using color coding and gradient shading. Color improves the visual ability to separate segmented tissues, while gradient shading enhances the perception of geometry. The 3D model is manipulated interactively to plan surgery using a workstation with an accelerator board that is connected to a 1.5T MRI system (GE Medical Systems, Milwaukee WI). Sulci and gyri are clearly visible to map the functional brain regions relative to the pathology for surgical planning.

1. HE Cline, CL Dumoulin, HR Hart, WE Lorensen, S Ludke. Magn. Res. Imag. 5, pp 345-352,1987

2. HE Cline, WE Lorensen, S Ludke, CR Crawford, BC Teeter. Medical Physics 15(3), pp 320-327, 1988.

P080

MRI OF LASER EFFECTS ON TISSUE

F.A. Jolesz, N. Higuchi, A.R. Bleier, P. Jakab
Dept. of Radiology, Harvard Medical School and Brigham & Women's Hosp., Boston, MA

Because reversible and irreversible photothermally-induced changes in tissue can be detected on magnetic resonance (MR) images, MR has the potential to be used for monitoring and control of energy deposition during interstitial laser therapy.

To increase our knowledge about the MR appearance of laser-induced tissue damage, we applied MR imaging to detect the changes induced in brain and liver tissue of rats and rabbits by radiation from an Nd:YAG laser at 1060 nm wavelength delivered interstitially through a fiber optic waveguide. A range of laser energies was applied, and laser pulse parameters were varied.

Photothermally-produced lesions were seen on both T1- and T2-weighted images. The overall size of the lesions correlated with the magnitude of the energy applied. The MR image appearance depended not only on the total energy deposition, but also on the laser pulse parameters, on the type of tissue, and the MR pulse sequence applied. While T1-weighted images adequately demonstrated an area of tissue destruction, T2-weighted images showed a more heterogeneous and more extensive lesion which could be better correlated with the complex histological representation of these lesions. The 3D extent of the lesions was well demonstrated on multislice images, providing correlation of the affected volumes seen on MRI with volumes seen in histological or histochemical preparations.

We conclude that MRI can demonstrate the 3D extent of the lesions induced by lasers and can be used to investigate and optimize the control of induced tissue change for more precise destruction of preselected targets while minimizing damage to surrounding tissues.

P081

FLASH: THE OPTIMAL PULSE SEQUENCE FOR CONTRAST ENHANCED CNS STUDIES ?

B Sander, W Schörner, R Felix
Dept. of Radiology, University Clinic Rudolf Virchow, Berlin, W.-Germany

In contrast enhanced CNS studies conventional T1-weighted spin echo sequences have several disadvantages. The limited number of slices rarely allows for complete imaging of the whole volume of interest, or with a longer repetition time and a higher number of slices the T1-weighting of image contrast is insufficient. The 180 degree pulse makes slice gaps necessary due to inaccurate slice profiles. And the radio frequency power absorbtion of the patient can exceed the limitations. With FLASH these disadvantages can be reduced.

A multislice 2D-FLASH sequence (TR 400 msec, TE 5 msec, flip angle 90 degrees, 23 slices, 1 NEX), a 3D-FLASH sequence (TR 40 msec, TE 5 msec, flip angle 40 degrees, 63 slices, 1 NEX) and a T1-weighted spin echo (TR 400 msec, TE 15 msec, 11 slices, 1 NEX) sequence were compared in clinical CNS studies (1.5 T Magnetom). The FLASH sequences yielded higher lesion contrast and higher sensitivity to contrast enhancement compared to the conventional spin echo sequence. The multislice 2D-FLASH sequence yielded the highest effectivity (number of slices per acquisition time). The 3D-FLASH-sequence seemed to be the method of choice, when very thin slices were necessary. The sensitivity to artifacts (susceptibility) was higher on FLASH images but did not significantly reduce the diagnostic information. Image quality of the spin echo images was only superior to the FLASH images in patients with metallic implants after surgery.

The multislice 2D-FLASH sequences and 3D-FLASH sequences can replace conventional T1-weighted spin echo sequences in contrast enhanced CNS studies.

P082

MAGNETIC PARTICLES FOR THE ASSESSMENT OF PERFUSION

PA Hardy, MJ Belanger, MJ Bronskill, RM Henkelman
Department of Medical Biophysics, University of Toronto, and The Ontario Cancer Institute, 500 Sherbourne Street, Toronto, Canada, M4X 1K9

Magnetic particles are known to enhance transverse relaxation in tissues by creating a magnetic perturbation through which water molecules diffuse*. The relaxation rate can be further enhanced by moving the particles during the NMR experiment. Even confined to capillaries, the particles can influence a significant fraction of the total spins because the magnetic perturbation extends several times the particle's diameter. Thus, flowing particles can significantly reduce the signal from tissue despite being confined to the vascular system which may represent only 5% of the total volume of a tissue.

These features offer a means for assessing tissue perfusion by measuring the signal reduction in a spin echo sequence from a region containing particles flowing in the vasculature. We have constructed an artificial tissue capillary system consisting of a bundle of hollow, Teflon® fibers (ID = 100 μm) contained in a cylinder (ID = 1.4cm) around which a tuned coil is wrapped. Particles of pure iron (average diameter 5 μm) were imbedded in an agar matrix within the capillaries while water was pumped smoothly around the outside of the capillaries. The extent of signal reduction was determined by measuring the transverse relaxation rate in a CPMG sequence; T_2 decreased monotonically with increasing water flow rate.

A computational model was developed to predict the enhanced relaxation rate. The model considers the perturbation to the frequency of precession of water protons surrounding a capillary which is induced by the relative movement of a nearby magnetic particle. The model predicts a decrease in T_2 with increasing flow rate similar to that observed. The extension of these experiments to imaging tissue with intravenously injected particles could result in a quantitative estimate of perfusion.

* PA Hardy, RM Henkelman, Mag Reson Imaging 7:265-275 (1989)

P083

^{19}F NMR OF FLUOSOL FOR REAL-TIME, *IN VIVO* STUDIES OF RAT LIVER OXYGENATION.

SK Holland and JC Gore
Yale University School of Medicine, Dept. Diagnostic Radiology, New Haven, CT., USA

The potential for *in vivo* oxygen sensitive ^{19}F NMR imaging using perfluorocarbons as biocompatible fluorine agents has been realized for some time (1). ^{19}F NMR images of Fluosol™ phantoms, as well as *in vivo* images of the reticulo-endothelial (RES) system of Fluosol™ infused rats, have demonstrated a linear dependence of ^{19}F, $R_1(=1/T_1)$ on pO_2 (2,3). In long term studies with male Sprague-Dawley rats which have received serial infusions of Fluosol™ up to a total volume of 20ml, we have examined the oxygen sensitivity of ^{19}F NMR images of the RES quantitatively. Multiple partial saturation images have been acquired on a GE 2.0T CSI system, with rats breathing gas mixtures varying in pO_2 from 21% to 100%. Oxygen maps have been computed from the acquired images and reflect the oxygen distribution in the RES of the liver and spleen of the animals. The ^{19}F NMR pO_2 maps reflect variation in local oxygen tension in the RES at the level of 1 mm. We will present *in vivo* pO_2 maps of Fluosol™ infused rats and discuss correlations between the pO_2 values measured with this non-invasive technique and established methods of localized pO_2 measurement.

The oxygen sensitivity of the fluorine NMR signal from Fluosol has also been used to detect sudden changes in liver oxygenation associated with acute occlusion of the portal vein an/or hepatic artery. ^{19}F NMR spectra, acquired at 0.5 sec intervals with a surface coil on the liver of a laparotomized rat infused with Fluosol, demonstrate changes in spectral intensity which directly correlate with the period of blood flow interruption. Waterfall plots of 256 spectra, sequentially acquired while the hepatic artery or portal vein or both are occluded with a pneumatic cuff for an interval of 30-60 seconds and then released will be presented. A qualitative discussion of these results will be offered together with a design for a more quantitative procedure for studying the effects of acute insults on tissue oxygenation using ^{19}F NMR.

1) LC Clark, JL Ackerman, SR Thomas, et al, Adv. Exp. Med. Bio., 180, 835-45, 1984.
2) JE Fishman, PM Joseph, TF Floyd, et al, Mag. Res. Imag. 5(4), 279-85, 1987.
3) SK Holland, R Soto, CC Jaffe, E Gordan, JC Gore, Mag. Res. Imag., 6(S1), 238, 1988.

POSTER ABSTRACTS

P084

THE HOUGH TRANSFORM APPLIED TO 3D MRA DATA SETS

CH Wood, PM Margosian, KS Denison
MRI Division, Picker International, Highland Heights, Ohio

High quality Magnetic Resonance Angiograms rely on the blood vessels being the brightest features in each slice. To help suppress signal from static tissue and background noise, a three dimensional segmentation technique was implemented. Each voxel of the data set was examined with respect to the voxels surrounding it.

Blood vessels are brighter than the surrounding tissue, and are connected by a curve in three dimensional space. A local thresholding technique was implemented which takes advantage of both of the properties of the blood vessels yet does not rely on the curves in space being connected.

The technique is based on original work by Hough in 1962. The Hough Transform can be used to map voxels into a coordinate system where voxels belonging to given curve curve map to a single point. A matrix is used to represent this Hough space which has the same dimensions as the number of parameters needed to describe the curve. Each time a pixel maps to a point in this matrix, the matrix element is incremented by one, or an amount proportional to the strength of the voxel in question.

Using this technique, background noise and signal is removed from the three dimensional data set which can now be ray traced using conventional techniques. Parallel rays are projected through the data set and the brightest voxel each ray encounters is returned to the viewing matrix.

P085

AN INDIRECT METHOD FOR MEASURING LIVER IRON USING MAGNETIC SUSCEPTIBILITY

RW Holt, PJ Diaz and EM Bellon
MetroHealth Medical Center and Case Western Reserve University, Cleveland, OH

We have developed a new method for non-invasively deriving liver iron levels by measuring the field warp induced by the high magnetic susceptibility of the iron-loaded liver in a phantom located adjacent to the liver.

Iron overload syndromes eventually cause organ damage and death by cardiac failure. Precise measurement of the iron concentration in the liver is necessary for rational management of the overload burden. Iron detection by MRI has previously been found to show low correlation with biopsy-determined iron concentration. The source of error may be due to large susceptibility based magnetic gradients formed by iron-loaded ferritin and hemosiderin which cause a non-linear term in T_2. In our method, rather than measuring iron effects directly in the liver, we measure the effect the entire iron loaded organ has on the homogeneous field in a water bath adjacent to the patient (Fig. 1).

Magnetostatic theory predicts the changes in a homogeneous magnetic field caused by the flux though regions of different susceptibility. These field warps are directly related to the differential susceptibility $\Delta X = X_{liver} - X_{bath}$, the external field, H_o and the geometry of the regions. For a perfect sphere in a homogeneous field, the change in the observed field would be, $\Delta H = -H_o \Delta X R^3 (2z^2 - x^2 - y^2)/3(x^2 + y^2 + z^2)^{5/2}$, where R = the radius of the sphere, and x, y, and z are the distance from the center of the sphere. A similar geometrical term must be used when imaging the human liver and torso as in Fig. 1. MRI susceptibility maps, which are derived from the phase reconstruction of Gradient Field Echo images (as $\phi = \gamma \Delta H t_E$), are used to plot the magnetic field. To reduce noise and to provide a known reference, we measure the field warp outside the body in a homogeneous solution of known susceptibility. This field measurement, along with geometric parameters of the torso obtained from spin echo images, is used to calculate the mean liver susceptibility.

Preliminary experiments were conducted on phantoms consisting of either paramagnetic iron chloride or super-paramagnetic iron particles (AMI-25, Biomagnetics) whose susceptibility was verified on a magentic biosusceptometer. The estimates obtained using these studies showed high correlation (r=.9975) with known concentrations (Fig. 2).

We believe that the non-invasiveness and the accuracy of this technique indicate its potential for use in clinical liver iron quantitation studies.

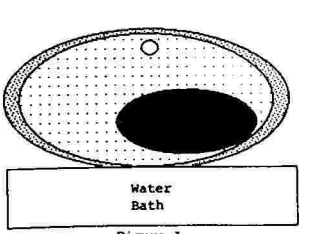

Figure 1

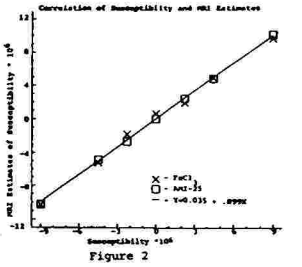
Figure 2

P086

Improved Parametric Imaging In the Presence of Objects Less Than One Pixel in Length

E.M. Haacke, F. Boada, Z.-W. Rong, Z.-P. Liang+
Case Western Reserve University, Dept. of Radiology, Cleveland, OH 44106
+BMRL and NCSA, UIUC, Urban, IL 61801

Parametric image reconstruction holds the promise for improved resolution (sans Gibbs artifact) and optimal signal-to-noise. Its use is to improve image quality for reduced data set acquisitions. Previous described techniques (1,2) cover rather flexible image shapes, but do not include imaging very narrow objects (less than one conventional pixel in width). We have extended the previous methods to handle the otherwise singular cases of narrow objects for realistic signal-to-noise values. This is done by allowing delta-function like objects to enter the class of acceptable functions. This prevents the previous problem of non-local artifacts from occurring when image spikes or narrow objects are present. The role of S/N in determining the type of object function is also considered.

(1). E.M. Haacke, Z-P. Liang, S.H. Izen
Constrained reconstruction: a superresolution optimal signal-to-noise alternative to the Fourier transform.
Medical Physics 16:388-397, 1989.

(2) M.R. Smith, S.T. Nichols, R.M. Henkelman, M.L. Wood
Application of autoregressive moving available parametric modeling in MR imaging reconstruction.
IEEE Trans. Med. 5:132-139, 1986.

P087

Macromolecular MR Contrast Media: Synthetic Rationale and Initial Imaging Results

P Sieving, A Watson, J Hooper, J Francisco, M Carvlin
Georgetown Univ Hosp, Dept of Radiology and Salutar, Inc.

Since Gd-DTPA and Gd-DOTA distribute throughout the extracellular fluid compartment as dictated by capillary permeability they have relatively short plasma half-lives and little tissue selectivity. Poly-chelate analogues of Gd-DTPA and Gd-DOTA have been developed to determine whether macromolecular agents afford improved intravascular enhancement for liver and blood pool imaging.

High molecular weight (MW=75,000) congeners of Gd-DTPA (Gd-R301) and Gd-DOTA (Gd-R401), synthesized by Salutar, Inc., employed a poly-l-lysine platform to which approximately 90 Gd-DTPA or Gd-DOTA molecules were bound. Higher molecular weight (MW=140,000) species (Gd-R302, Gd-R402) were generated by linking Gd-R301 or Gd-R401 moieties to human serum albumin (HSA). Biodistribution data were collected at 1 and 7 days post-injection using 153 Gd radiolabeled compounds. Spin echo images (TR=400/TE=15 msec) of rabbits and rats were obtained at 1.5 Tesla (Siemens) pre- and post-IV bolus (0.033 mmol/kg).

These agents caused enhancement of liver parenchyma and vasculature up to 10 times longer (t=104 minutes) than did monomeric Gd-DTPA. At 30 minutes post-injection, relative enhancement was: Gd-R402 (204%) > Gd-R302 (162%) > Gd-R401, Gd-R301 (130%).

Gadolinium poly-chelate complexes appear to be retained in plasma for an extended period with DOTA chelation and HSA conjugation producing more prolonged vascular enhancement.

P088

Contrast Agent Enhanced MR Imaging of the Diabetic Rat Kidney
R Mazurchuk, RJ Fiel, MA Acara, M Carvlin
Roswell Park Memorial Institute, SUNY at Buffalo, Buffalo, NY.

Male Sprague-Dawley rats were imaged before and after receiving a dosage of 60 mg/kg of streptozotocin IP. These animals were divided into three groups with each group receiving intravenous administration of a single contrast agent: 100 umoles/kg of Gd-DTPA, 100 umoles/kg of Mn(III)-mesotetraphenylporphine sulfonate ($Mn(III)TPPS_4$), 6 umoles/kg Mn(II) acetate. Short TR/TE (500/50 msec) and long TR/long TE (2000/50,100 msec) spin echo images were acquired on a 0.35 Tesla (Diasonics) system using an 8 cm diameter extremities coil before and at 11-14 days post-streptozotocin. Pre-contrast and serial post-contrast images were obtained for up to 3 hrs after injection.

In the pre-contrast short TR/TE images, the kidney/muscle ratio for diabetic rats was increased with respect to non-diabetic controls with the greatest increase seen in the cortical region. T2W images were characterized by a loss of cortico-medullary differentiation with respect to controls. After administration of the paramagnetic chelates, $Mn(III)TPPS_4$ and Gd-DTPA, the signal intensity of the inner medulla consistently increased with respect to pre-contrast images. The magnitude of the observed signal intensity change was greater for diabetic kidneys than for normal controls. Intravenous injection of $Mn(III)TPPS_4$ and Gd-DTPA resulted in the cortex appearing hypointense and the outer medulla isointense compared to pre-contrast images. Injection of the non-chelated manganous salt produced a qualitatively different pattern of signal intensity change than that seen after injection of the chelate complexes. Mn(II) caused the cortex to appear hyperintense with respect to the pre-contrast images.

The differences in signal intensities on pre-contrast MR images of the diabetic kidney are consistent with an altered state of hydration within the renal parenchyma. Administration of paramagnetic ions and chelate complexes indicates that the biodistribution and time sequence for renal handling of these agents is disturbed in the diabetic state. The degree to which these observed effects may be specific to diabetes and what relation, if any, they may share with other renal diseases are under investigation.

P089

FOUR AND EIGHT ECHO INTERLEAVED DIAGONAL CARTESIAN ECHO PLANAR IMAGING*

G. Kashmar and O. Nalcioglu

Department of Radiological Sciences, Division of Physics & Engineering, University of California-Irvine

Results were recently announced[1] showing clear two and three echo interleaved images made with the diagonal Cartesian echo planar method. Blurred four echo interleaved images were also shown. Further improvements now make it possible to produce clear four and eight echo interleaved images with imaging times in the 3 to 10 second range. This makes it possible to reduce a large number of spin warp scans to times less than a breath hold. The current images were taken with 90 and 180 pulses with a field of view of either 24 or 48 cm. and dimensions in pixels of 128 x 256. All images were done using the half Fourier phase map method with a separate phase map for each echo. The use of "per echo" phase map correction is found to make it quite simple to interleave data from different echoes. The SNR is found to be low and pictures appear noisy at fast imaging times. In addition, bright objects are found to produce half Fourier artifacts. No other obvious image quality problems are evident. An eight echo image was produced with a computer speed limited TR of 130 milliseconds at 3.12 seconds total imaging time and another at the desirable high contrast TR of 300 milliseconds in 6.9 seconds total imaging time. This gives a speed improvement slightly better than five and a half over full Fourier single echo spin warp. Eight echo interleaving required 16 TR periods for the phase map and 7 TR periods to cover the rest of the data space. With four echo interleaving a 24 cm. phantom image was produced at 2.9 second and 3.5 seconds using TR periods of 90 and 110 respectively. Repetition times lower than this were found to be unacceptably noisy and TR periods will be even longer for acceptable head and body images. Four echo interleaving required 16 TR's for a phase map and 15 TR's for the rest of the image. One additional dummy TR was used for a total of 32 TR periods. A kidney image of moderate quality was produced with four echoes at 9.3 second and a TR=300. A low contrast brain image at TR=2000 was also made which took 62 seconds. An important observation to be made from this study is that it is not productive to think of FLASH and GRASS technology as competing with echo planar technology but to realize that even with multi-TR echo planar and hybrid imaging, GRASS/FLASH considerations must also be accounted for. In particular, spoilers are very important for low TR times in hybrid imaging, especially phase encode spoilers to prevent differing phase encodes from destroying the steady state.

References
1. Kashmar, G., Nalcioglu, O., Proc. 8th Annual Meeting SMRM, p.921, Amsterdam 1989
* supported in part by grant CA45229 and CA41307 awarded by NCI, DHHS

P090

F-19 CHEMICAL SHIFT IMAGING UTILIZING PFOB*

H. K. Lee, O. Nalcioglu and D. Long**
Department of Radiological Sciences, Division of Physics & Engineering, University of California-Irvine

The spectrum of PFOB consists of multiple peaks and causes certain complications in F-19 imaging[1,2]. These multiple peaks result in chemical shift artifacts and a loss of spatial resolution in the images. One simple solution to this problem would be to utilize chemically selective excitation but this would have to be at the expense of the already low signal-to-noise ratio(SNR) . In order to improve the SNR , we utilized the two upfield peaks separated by 1.05 Khz and the Dixon technique[3]. The pixel misregistration along the readout direction due to chemical shift was 11mm (17 pixels) for a 256X256 image at a FOV of 16cm. The actual in-phase and out-phase offset intervals for a 180° pulse were measured repeatedly by calculating the area under a one dimensional projection profile. The offset values were 0.3ms for in-phase and 0.53ms for the out-phase. The in-phase and out-phase images were kept as complex arrays after the 2D Fourier transform so as to preserve both the magnitude and phase information. The images of the two peaks were calculated by complex addition and subtraction of these arrays. The main difficulty in the complex addition/subtraction method is due to the fact that the complex images may suffer from other effects causing additional phase shifts such as the inhomogeneity of the static field and other local field deformations . Since there is a considerable amount of shift between the two peaks (17ppm), the complex operation approach may be applicable to a large field of view if the field inhomogeneity is moderate. Currently, two additional techniques one utilizing a phase correction method and another one using a signed bit map based on the absolute pixel values are under investigation. In the present study, the selection gradient was 0.9G/cm with a slice thickness of 1.5cm. The other group of closely coupled peaks were suppressed by a long TE time of 50ms.

References
1. P. M. Joseph et al, JCAT **9**,1012(1985).
2. S. Thomas , Proc. SPIE **626**, 7(1986).
3. W. T. Dixon, Radiology **153**, 189(1984).

* Work supported in part by grant CA45229 awarded by the National Cancer Institute, DHHS.
** Department of Radiology, University of California-San Diego.

P091

MRI ACCEPTANCE TESTING: THEORETICAL AND PRACTICAL ASPECTS

S.M. Dyer (1), D.J. Goodenough (2)
(1) The Institute for Radiological Image Sciences, MD (2) George Washington UMC, Wash. DC

Introduction - Our acceptance testing of MR systems consists of three targeted parts: (A) Image quality, (B) Software functions, (C) Site accessories/peripheral equipment.

Of the three categories, part C involves determining agreement between the purchase order and actual equipment installed. Part B consists of system conforming to specifications for performing specific sequences, acquisition/display matrices, and timing requirements. Testing for part A is more rigorous and usually represents the most critical portion in the acceptance routine that evaluates system integrity. Although there is movement to consistent methodologies for testing, additional clarifications are needed.

Discussion - To complete the section of tests for evaluating image quality the vendor phantoms or the IRIS, Inc. phantom have been used for testing the following parameters: Spatial Resolution, Signal to Noise Ratio (SNR), Slice Width, Uniformity, Spatial Linearity, Slice Alignment, and Artifacts.

This paper will discuss our experience of testing many MR sites including both public and private installations. In particular we will consider some 15 specific sites with almost all vendors represented. We have confronted issues of appropriate test methods for: SNR, Uniformity, Spatial Linearity, and Artifacts.

Non acceptance of systems, specific to image quality has been a factor of degraded image uniformity and or evidence of artifacts. Consistent methodologies for uniformity and artifact definition need clarification. For instance, uniformity testing, is without consistency between advisory group, vendor and testing group as to the percentage of field of view used in measurement. In particular, in the case of artifacts, how is it defined, and what method is used to quantify the severity, needs clarity in definition.

Conclusion - It is our intent to review our testing experience and to examine areas of acceptance testing specific to image quality. These parameters have presented problems in converting theoretical determinations into on site procedures that can be uniformly accepted and consistently applied to all vendors' systems.

P092

WHY THE POSTERIOR PITUITARY IS BRIGHT IN MR IMAGES

RM Henkelman, W Kucharczyk
Departments of Medical Biophysics and Radiology, University of Toronto

The posterior pituitary appears anomalously bright on T_1-weighted MR images appearing similar to fat. The signal intensity of the posterior pituitary has been compared to that obtained from doped buffered water, oil, liposome vesicles, and liposome vesicles containing vasopressin using a variety of imaging pulse sequences. Images have been performed with proton density, T_1-weighting, T_2-weighting, fat suppression, and increased chemical shift in several directions. The sequences demonstrate clearly that the brightness of the posterior pituitary does not arise from lipid components. The signal intensity correlates best with a sample of liposome vesicles and is not dependent on the presence of the vasopressin hormone. It is the presence of a high concentration of membranes that serve as an additional relaxation sink for longitudinal relaxation but which has a proportionately smaller effect on T_2 that leads to the anomalous signal intensity in the posterior pituitary.

P093

MAGNETIC RESONANCE IMAGING STUDY OF THE PHARMACODYNAMICS OF GADOLINIUM-DTPA POLYLYSINE IN THE RABBIT

GJ Marchal, P. Van Hecke, C. Van Ongeval, K. Johannik, H. Bosmans, P. Aerts, A.L. Baert and U. Speck*
Depart. of Radiology, Univ. Hospitals K.U. Leuven, Belgium and Schering AG*, Berlin, FRG
Department of Radiology, University Hospitals K.U. Leuven, Belgium

Gadolinium-DTPA Polylysine is a new blood-pooling NMR contrast agent with potential applications for liver enhancement. The specific properties of this molecule relate to increased molecular weight (50000), enhanced relaxivity (13 $Lmmol^{-1}s^{-1}$) and good acute intravenous tolerance LD_{50}, mice 15 mmol Gd/kg). Pharmacokinetic studies in rats and rabbits have shown that the compound is subject to renal excretion.

The pharmacodynamics of this new compound were studied in three normal rabbits injected intravenously at a dose of 0,1 mmol/kg. The NMR experiments were performed on a 1.5 T Siemens Magnetom. Images were acquired using a T1 weighted sequence with TR/TE = 300/15 ms. The corresponding measuring time was about 5 min. Signal intensities of the liver, the kidney cortex and medulla and the dorsal muscle were measured from these MR images prior to, and after contrast injection every 7 min. during the first hour, then after 2, 4, 6 and 8 hours and further after 2, 3, 7 and 16 days.

Signal intensities and decay times were similar for the three rabbits. The liver signal intensity increases with a factor 1.7 immediately after injection and drops to half the maximum value in about one hour. The kidney cortex also reaches maximal intensity during the first measurement (factor 2.8) and decays with a halfvalue time of about 1 hour. The medulla however peaks 40 min. after injection with an enhancement factor of 3.7 ; the half-value time is reached 80 min. later.

The cortex decay is slowed down and crosses the medulla after about 8 hours. Signal intensities return to normal in the liver after 3 hours, in the renal medulla after 1 day and in the renal cortex after 3 days. Muscle signal intensities do not show significant changes. The delay in medulla uptake probably reflects the slower diffusion of the contrast agent through the glomerular membrane.

P094

STRIPE PATTERN IMAGING FOR FLOW MEASUREMENT

H.Matsuura, M.Yamada, N.Iriguchi and O.Takizawa
Siemens Asahi Medical Systems, TOKYO

The detection of the internal motion, blood flow or organ movements, is one of the interesting subjects using MRI technique.

To display those motions in the MR images, many pulse techniques using RF are used such as bolus imaging, tagging or presaturation method.

In this paper we discribe the tagging method for the tissue or blood by using the gradient pulse followed by the 90 degree rf pulse. The phase difference in the X-Y plane generated by the gradient fields are converted into the difference of the Z-conponent magnetization.

By changing the strength of the gradient pulse, the stripe pattern was generated. This method has an advantage in tagging the spins in three dimensional space.

This method enabled us to describe the complex movements in three dimension. This method can be utilized together with any other tagging technique.

P095

EVALUATION OF MYOPATHY BY MAGNETIC RESONANCE SPECTROSCOPY

LK Misra, EE Kim, LW Dennis
Diagnostic Imaging, University of Texas M.D. Anderson Cancer Center, Houston, Texas and Exxon Research and Engineering, Baytown, Texas

MR spectral changes of degenerating muscles were evaluated in a well-characterized avian model of myopathy. The ^{1}H (water suppressed) and ^{13}C spectra at 200 MHz and 50 MHz, respectively, were obtained first from the intact pectoralis major muscles and then from their methanol-chloroform extracts. Distractionless Enhancement by Polarization Transfer technique was used to assign peaks. Both ^{1}H and ^{13}C spectra showed distinct differences between the normal and dystrophic muscles (Fig.1). Normal muscles showed fairly complex spectra. The spectra of dystrophic muscles had only peaks due to netural lipids (not labeled), reflecting fat infiltration. Assignment of the major peaks in the ^{1}H and ^{13}C NMR spectra is as follows: 1- lactic acid, 2-creatine or phosphocreatine, and 3- carnosine and anserine. The spectra of methanol-chloroform extracts suggested a higher degree of unsaturation in the fatty acid chains of normal muscles, presumably due to phospholipids, than in those of dystrophic muscles. Extracts provide insights into muscle degeneration as the disease progresses. (Supported by RO1AR 38741 and General Electric Medical Systems).

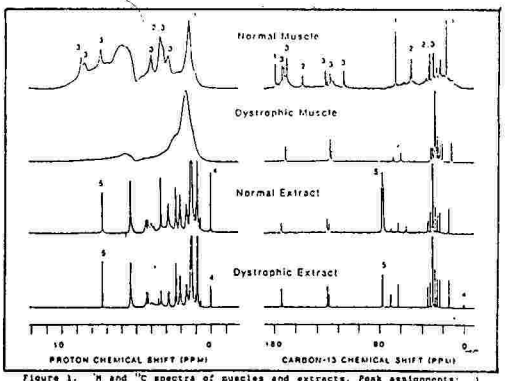

Figure 1. ^{1}H and ^{13}C spectra of muscles and extracts. Peak assignments: 1. lactic acid, 2. creatine (or phosphocreatine), 3. carnosine and/or anserine, 4. tetramethylsilane (reference), 5. deuterochloroform (solvent).

POSTER ABSTRACTS

P096

Small Unilamellar Paramagnetic Liposomes as MR Contrast Agents

Unger E, M.D., Fritz T, M.Sc., McCarver R, MS IV, Tilcock C, Ph.D.
University of Arizona, Department of Radiology (EU, TF, RM)
University of British Columbia, Department of Biochemistry (CT)

MR contrast agents such as Gd-DTPA or Gd-DOTA are non-specific and their use in the body has been disappointing. To improve the use of gadolinium for body imaging we have incorporated paramagnetic complexes into liposomes resulting in targeted MR contrast agents which are confined to the blood pool until accumulated by specific cells such as the reticuloendothelial system and hepatocytes. Some of our results may be summarized as follows: 1) Diffusion of water across the lipid bilayer is the limiting factor to relaxivity; small vesicle size increases the ratio of surface area to entrapped internal volume facilitating water exchange. 2) Incorporation of cholesterol into the lipid bilayer stabilizes the membrane but at the cost of decreased relaxivity, however, we have developed alternative means of stabilizing the membrane at no cost in relaxivity. 3) Biodistribution and clearance studies show that the half-life for clearance from the liver of liposomal Gd-DTPA is about 3.5 days. 4) Acute toxicity studies show that liposomal Gd-DTPA has lower acute toxicity than unencapsulated Gd-DTPA (subacute data will be presented). 5) Use of the liposomal MR contrast agent significantly improves the detection of hepatic metastases in rats and will likely be useful for blood pool imaging and detecting tumors in the spleen and bone marrow.

P097

AN EFFICIENT DOUBLE TUNED SURFACE COIL SYSTEM FOR 4.7T

S.P. Kingsley, C.D. Smith*, G.S. Thomas*

Center For Biomedical Engineering
* Magnetic Resonance Imaging and Spectroscopy Center

Surface coils tuned to two different frequencies are of considerable interest in MRS and MRI. Here we introduce an efficient 1.6cm double tuned surface coil system resonating at the P31(81MHz) and H1(200MHz) frequencies in a 4.7T magnetic field. The coil system consists of two coaxial single turn coils of AWG18 wire, each having a variable capacitor (Voltronics) in series. The inner coil tunes to the H1 frequency and the outer to the P31 frequency. The coil system is inductively coupled to the transmitter/receiver via a coupling loop and is matched using a transmission line, its length experimentally determined so that the real part of the coil impedance could be matched to 50 ohms using a variable capacitor at its end, and placed in a "T" configuration to allow adjustment outside the bore of the magnet. The coils could be tuned using the variable capacitors and matched to the first order by small variations in the angle and displacement of the coupling loop. The final match could be obtained by varying the capacitance at the end of the transmission line. The double tuned coil system was compared with single tuned coils of the same diameter and gauge wire. The 90 degree flip angle pulse power and the S/N for the single tuned coils and the double tuned coil system were determined, using 1.46M H_3PO_4 treated with 0.05mM $CuSO_4$ in a glass sphere of diameter 1.4cm. The profiles of the coil system in the two frequency modes were also obtained, using a rectangular 0.5cm slab phantom containing NaH_2PO_4. The pulse powers and S/N indicated that the double tuned coil system has the same efficiency and S/N as the single tuned coil in the low frequency mode, and is less efficient (-3.5dB) and has less S/N by 38% in the high frequency mode . The profiles indicated that the coil system was looking at the identical volume of interest for both frequency modes. The double tuned coil system has given successful results for in vivo spectrocopy from gerbils and has the novelty of being tuned and matched to other resonant modes by changing the capacitance in the coils and the length of the matching line.

P098

SPECTROSCOPIC IMAGING OF ^{31}P IN THE HUMAN BRAIN

JW Hugg, AA Maudsley, DB Twieg*, GB Matson, D Sappey-Marinier, B Hubesch, and MW Weiner
MRS Unit, VA Medical Center, Depts. of Radiology and Medicine, Univ. of California, San Francisco and *Philips Medical Systems, North America

Three-dimensional Magnetic Resonance Spectroscopic Images (3D-MRSI) have been obtained of human brains at 2 Tesla using ^{31}P in normal volunteers and in patients with strokes and brain tumors. Variations in metabolite concentrations are clearly observed in diseased regions, principally reduced concentrations of ATP, PDE, and PME. Smaller variations in Pi, PCr, and pH are also apparent. These changes in the diseased brain regions are in general agreement with those observed using single volume ISIS localization.

Spin-echo MRSI acquisition avoids the problem of spectral distortion encountered by Fourier-transform techniques which observe an FID after a necessary delay for phase-encoding gradients. Our spin-echo method consists of non-selective excitation, followed by gradient phase-encoding periods before and after a non-selective 180° refocusing pulse, and is concluded by acquisition of the second-half of the spin echo. The TE is typically 2.7 to 3.2 msec. Nominal voxel resolution is typically $(2.2\ cm)^3 = 11$ cc, which is reduced by smoothing during data processing, with a $(12)^3$ 3D-data matrix acquired in 20 to 40 minutes.

Data reconstruction includes zero-filling and smoothing, resulting in a processed data set of 8 transaxial slices with a $(32)^2$ image matrix. We have developed an interactive MRSI utility for display of spectra and color or gray-scale images of ^{31}P metabolite distributions. We are developing techniques for quantitating metabolite concentrations by using reference standards, B_1 field maps, relaxation and off-resonance corrections. In addition, our homebuilt birdcage coil is being further developed for quadrature acquisition to optimize the naturally low ^{31}P NMR sensitivity.

P099

MONITORING REDISTRIBUTION OF CEREBRAL IONS BY NMR SPECTROSCOPY

J Pekar*, RC Lyon**, CTW Moonen*, and AC McLaughlin**
*Biomedical Engineering and Instrumentation Branch, National Institutes of Health, and **Laboratory of Metabolism and Molecular Biology, National Institute on Alcohol Abuse and Alcoholism

Metal ion NMR spectroscopy was used to follow the redistribution of ions in the rat brain following death. Upon death, the sodium NMR signal decreased, while the potassium NMR signal increased. These changes are consistent with a partial intracellular "NMR visibility" for these spin 3/2 quadrupolar nuclei, and the well-known equilibration of ion gradients after death. In contrast, the relaxation-allowed multiple-quantum (MQ) NMR signals changed in the opposite directions: Following death, the sodium MQ NMR signal increased, while the potassium MQ NMR signal decreased. This is consistent with the basic theory of relaxation-allowed MQ NMR, which predicts that strongly-relaxed ions, which have reduced "NMR visibility", will have increased "MQ NMR visibility". These results suggest that MQ NMR may be complementary to conventional NMR for the study of compartmentalized metal ions.

P100

OBSERVATION OF F-19 NMR SIGNALS FROM ANESTHETIC IN HUMAN BIOPSIES

CT Burt, G Jendrasiak, G Browne, RL West

NIEHS, Rsch. Triangle,Depts. Radiation Oncology and Clinical Pathology and Diagnostic Med., E. Carolina U. Med. School, Greenville, North Carolina

Previous studies in the rat both in vivo and in vitro showed a distinctive pattern of the F-19 NMR spectra from halothane in an adenocarcinoma compared to normal tissue. The spectra from tumor generally showed two peaks separated by about 0.5 ppm whereas normal tissue had a single narrower resonance. To see if a similar phenomenon could occur in humans, samples of therapeutic surgical procedures obtained under anesthesia were examined using the anesthetic remaining from the procedure as the probe. Samples of colon (5), lung (3) and breast (2) tumors and nearby control tissue have been measured. The anesthetic used was isoflurane (forane = CF_3-CHCl-O-CH_2F_2) which contains two classes of fluorine that give rise to two resonances about 6 ppm apart. In general the biopsy was frozen within ½ hour after removal. Anesthetic will remain in the frozen tissue for several days. Within that time the spectra were recorded at 336 MHz.

There are distinctive differences between the pathologic and control samples. First, the peak due to the -CH_2F_2 shows a distinct shoulder about 0.5 ppm from its major peak suggesting two resonances. This behavior is not present in matched samples. Second, there is a general tendency for the separation between the fluorine class resonances to be smaller (ca. 6.0 ppm) in the pathological compared to 6.3 in the matched samples. More specifically, in some of the colons (2) the CF_3 peak is also seen to be split. In the colon biopsies the signal to noise and hence the concentration of anesthetic is less in the tumor than in the control. These results point toward a practical MRS use of anesthetic or anesthetic-like compounds as neoplastic probes reporting on membrane environments.

P101

BIO-EFFECTS OF HIGH MAGNETIC FIELDS; A STUDY USING A SIMPLE ANIMAL MODEL

J Weiss, RC Herrick, KH Taber, GA Plishker
Magnetic Resonance Center, Baylor College of Medicine

The desire to do clinical imaging and spectroscopy at field strengths greater than 2 T necessitates investigation of possible bioeffects and biohazards at these high fields. There have been anecdotal reports of some individuals experiencing vertigo while working around 4 T whole body magnets. In order to study effects of magnetic field on behavior a simple animal model was employed. Twenty eight Long-Evans Hooded rats were run in a T-maze. The right arm of the maze extended to the center of a 30 cm horizontal bore magnet, while the left arm extended into a mock magnet bore with the same dimensions. The magnet is of a unique self-shielded design, developed through a collaboration between Baylor College of Medicine and the Houston Area Research Center, which reduces the fringe field to zero within 1 meter of the bore. This makes it possible to place the intersection point of the maze at zero field and the end of the arms at high field. Each animal performed a total of ten trials. Three sets of trials were examined: a zero-field control set, a set at 1.5 T field, and a set at 4 T field. A followup subset was run at 4 T with the maze reversed. No significant differences from the control were observed at 1.5 T. At 4 T, however, in 97% of the trials the rats would not enter the magnet. In a maze-reversed subset a majority of the rats turned toward the magnet, indicating that they had learned an aversive response from the previous trials at 4 T. However, in only four decisions out of fifty eight did the rats enter the magnet. Eighteen decisions were made to turn around just outside the magnet, in a region of strong field gradients, on the order of 10 G/cm and reaching a field strength of 300 G at the magnet bore.

P102

QUANTIFICATION OF MYOCARDIAL INFARCTION:COMPARISON BETWEEN MRI, Tl-201 SPECT DEFECT AND RADIONUCLIDE EJECTION FRACTION

Kastler, Ph Germain, G Roul, G Zöllner, A Sacrez, A Wackenheim
University hospital, Strasbourg - FRANCE

AIM: In 12 patients with acute myocardial infarction (AMI: 10 anteriors, 2 inferiors) we compared the infarction size evaluated by MRI with stress test Tl-201 tomoscintigraphy and at rest Tc-99m ventriculography (performed during the third week after MI onset).

METHOD: The % of injured myocardium is planimetered from the highlightened area depicted on the MRI third echo image (10mm thick adjacent slices, spin echo, TE=28ms). Tl-201 defect is computed from 22mm thick short axis views divided in 12 sectors using a 50% activity threshold. Left ventricular ejection fraction (EF) is determined in the 45° LAO projection.

RESULTS: Infarction size evaluated with MRI (33.1±9%) is greater than with Tl-201 (23.8±15%) $p<.005$. However the linear correlation between both methods is good: $r=.82$ $p<.0012$. A less close but still significant correlation is found between MRI and EF: $r=.61$ $p<.038$.

CONCLUSION: In spite of an overestimating tendancy, T2 weighted MRI is a valuable method for clinical AMI sizing as compared with radionuclide techniques.

NOTES

SPECTROSCOPY: APPLICATIONS

MODERATORS: J. A. INGWALL, Ph.D., M. W. WEINER, M.D.

PS 01 08:00AM

^{13}C STUDIES OF METABOLIC PATHWAYS IN HUMAN MUSCLE AND BRAIN

R.G. Shulman, D.L. Rothman, G.I. Shulman, and J.W. Prichard
Yale University, New Haven, CT

^{13}C gives a very weak NMR signal and in addition is only 1.1% abundant so that low signal-to-noise has limited its use in metabolic studies. We have shown that it is possible to overcome these limitations of ^{13}C spectroscopy first in cellular suspensions and perfused organs and animals studies and more recently in studies of humans. The low natural abundance of ^{13}C can be neutralized by using 1-^{13}C glucose labeled to about 99% as substrate and this has been done inour muscle and brain experiments. In the human muscle we measured ^{13}C spectra of glycogen studying the rate of glycogenesis from the labeled blood glucose. This has the additional sensitivity advantage that peaks from all the glucose moities of glycogen reinforce each other so that very high concentrations of glucose moities are obtained in vivo (around 100mM in muscle). These quantitative muscle glycogen studies have shown that during a hyperglycemic-hyperinsulinemic clamps in both normals and in non-insulin-dependent-diabetics all of the non-oxidatively metabolized glucose is stored as muscle glycogen. The important difference is kinetic in that the diabetics synthesize glycogen at about one-half the rate of the normals and also have a delay before synthesis starts.

In the brain it has been possible to improve the signal strength by detecting the ^{13}C by its influence upon the ^{1}H spectra which has the sensitivity of ^{1}H spectroscopy. We have developed these methods in rats and rabbits following our demonstration that ^{1}H spectra could be obtained from the mammalian brain. We are able to follow the flow from 1-^{13}C glucose into lactate or glutamate pools in rats and rabbits and to measure the time course of pool turnover by these proton observe carbon edit (POCE) methods. These results are being interpreted so as to determine the glycolytic flux and the TCA cycle flux in the animals and in humans.

PS 02 08:30AM

SPATIALLY LOCALIZED NMR SPECTROSCOPY STUDIES OF CARDIAC BIOENERGETICS

K Ugurbil, PM Robitaille, G Path, J Zhang, M Yoshiyama,
M Garwood, AHL From, RJ Bache
Departments of Biochemistry, Radiology and Medicine,
University of Minnesota

The energy requirements for the work performed by the cardiac muscle are met primarily through oxidative synthesis of high energy phosphate (HEP) compounds. This process is tightly coupled to the mechanical output of the heart. Pathosphysiological conditions, such as ischemia induced by coronary stenosis perturbs this process. Since the HEP compunds and inorganic phosphate (P1), the product of HEP hydrolysis are detectable by P-31 NMR spectroscopy, the oxidative synthesis of HEP under both normal and pathological conditions can be studied non-destructively by NRM. However, the left ventricular wall of the cardiac muscle is not homogeneous with respect to systolic stress development, O2 consumption, distribution of key enzymes involved in bioenergetics and in blood flow. Especially during coronary stenosis, the transmural distribution of blood flow can become severely nonuniform. Therefore, studies of cardiac bioenergetics both in the presence or absence of ischemia must utilize spatial resolution provided by spectroscopic localization. Accordingly, spatially localized P-31 NMR studies were performed together with simultaneous measurements of mechanical function and blood flow to examine myocardial bioenergetics with transmural differentiation, under control conditions and in the presence of sustained coronary stenosis. The results, which will be presented, document the presence of significant transmural heterogeneities in myocardial bioenergetics, especially during coronary stenosis, and demonstrate the power of spatially localized NMR spectroscopy in physiologic and biomedical applications.

PLENARY SYMPOSIA INVITED TALKS

PS 03 09:00AM

GRADIENT-LOCALIZED NMR SPECTROSCOPY IN HUMANS

J Frahm, H Bruhn, ML Gyngell, KD Merboldt, W Hanicke
Max-Planck-Institut fur Biophysikalische Chemie, Gottingen, FRG

Clinical interest in magnetic resonance spectroscopy results from its potential to non-invasively detect steady-state concentrations of tissue metabolites in focal regions of the human body. At present, however, it is not yet clear whether major achievements of spectroscopy will be in the early or more accurate diagnosis of diseases and in the access to metabolic control of treatment, or whether long-term benefits may result from its use as a basic research tool for studying in vivo biochemical aspects of, for example, pathology and pharmacology.

In all cases, technical issues such as localization, quantitation, and motion problems (liver, kidney, heart) are still of primary concern: any conclusion drawn from spectroscopic data needs certainty about the spatial origin of the spectrum, and of course it would be helpful to translate the data into metabolite concentrations.

This presentation focuses on gradient-localized spectroscopy of single voxels, i.e.,the recording of one spectrum at a time from one image-selected volume-of-interest (VOI). Single voxel localization techniques take advantage of the same principles as employed for slice selection in MRI. The use of such methods offers easy control and reliability of size, shape, and position of the VOI as well as localized shimming to achieve excellent magnetic homogeneity. In addition, shorter measuring times as compared to global or multi-voxel techniques allow multiple spectral recordings with different T_1-T_2-weightings in the limited time of a patient investigation.

Examples will deal with stimulated echo (STEAM) sequences applied to localized proton and phosphorus spectroscopy of the human brain (including the effects of broadband proton decoupling). In vivo spectra of brain tumors will be compared to high-resolution in vitro spectra of tumor biopsies.

SPECTROSCOPY: IMAGING

MODERATORS: J. A. INGWALL, Ph.D., M. W. WEINER, M.D.

PS 04 13:30PM

ADVANTAGES AND PROBLEMS OF CHEMICAL SHIFT IMAGING

Ian R. Young
Hirst Research Center, East Lane, Wembley, Middlesex U.K.

The use of chemical shift imaging (CSI), often in conjunction with other localization methods is becoming increasingly common. The advantages of the method lie in its easy coverage of normal and abnormal tissues, extending to volumetric acquisition, and its relative simplicity of implementation. The problems with its application lie in the extended acquisition times which are often needed (which complicates the recovery of relaxation time constant data), on the need for heavy spatial filtering, and in its proneness to motion artifacts. However, localization per se can deliver higher signal-to-noise ratios that might otherwise be expected (because, in effect, it improves the quality of the field in the region from which the signal for any one spectrum is recovered) and, in conjunction, with susceptibility mapping progress can be made towards improved spectral processing.

PS 05 13:50PM

EXPERIENCE WITH SPECTROSCOPIC IMAGING AT VAMC/UCSF

A.A. Maudsley, D.B. Twieg*, J.W. Hugg, B. Hubesch, D. Sappey-Marinier, G.B. Matson and M.W. Weiner
Radiology, Medicine and Pharmaceutical Chemistry, University of California at San Fransisco, and VA Medical Center, San Fransisco, CA, and *Philips Medical Systems

Spectroscopic Imaging (SI) techniques have been implemented for human brain studies at 2.0 Tesla, and for animal studies at 7.0 Tesla. Spatial discrimination by Fourier encoding in two or three dimension is used. For 31P SI studies of the human brain, a short spiOn echo sequence is used with TE of 2.7 msec and half echo sampling. This enables P SI data to be obtained without the baseline distortion of the FID acquisition method, while incurring minimal signal losses from T2 relaxation.

The acquired SI data is transferred to a dedicated workstation for data processing and display. A display utility has been developed which allows rapid review of the large 4 dimensional data sets typically produced with SI. The spectral data may be viewed from any individual voxel or integrated over any volume. Images of the distributions of integrated signal intensities over any frequency range may also be viewed. Additional capabilities allow for additional data analysis or image processing functions.

PS 06 14:10PM

SPECTROSCOPIC IMAGING OF PROTON METABOLITES

Peter R. Luyten
Philips Medical Systems, The Netherlands

Recently, considerable progress has been made with water suppressed image localized human 1H NMR spectroscopy. Nowadays localized proton spectra obtained in humans show the same detailed spectral information as in vivo 1H spectra previously obtained from animals. The advantages of 1H spectroscopy are obvious. The NMR signal is significantly more intense than that of most other nuclei due to the high gyromagnetic ratio and natural abundance, thus enabling shorter measurement times and smaller volume sizes. The problems which have to be overcome are the interference from the very intense water signal and lipid resonances that may obscure the metabolite signals in the proton spectra completely.

A number of techniques have been uses to localize the proton signals from a single voxel. These techniques have been very successful in measuring several metabolites under normal and pathological conditions in the human brain. Tumors and cerebral infarcts reveal differences in the signals obtained from N-acetyl aspartate, creatine, choline, lactate and alanine. These pathologies often show very inhomogeneous tissue characteristics around the affected lesions. 1H NMR spectra of single voxels ranging from a 5 to 30 cc lack the spatial resolution to reveal the inhomogeneity of the tissue.

We have applied proton spectroscopic imaging techniques to study stroke and tumor pathologies, resulting in spectra and spectroscopic images that show the spatial distribution of metabolic alterations around and within affected regions of the brain.

By the introduction of these new techniques and the technical improvements of the existing localization schemes, localized proton spectroscopic imaging can be applied to obtain detailed biochemical information from brain lesions measuring a few cubic centimeters or even less.

PS 07 14:30PM

APPLICATION-DRIVEN SPATIAL LOCALIZATION PROTOCOLS FOR CLINICAL SPECTROSCOPY IN THE HEART AND BRAIN

PA Bottomley*, CJ Hardy, PB Roemer, RG Weiss, G Gerstenblith, JP Cousins
*GE Research and Development Center, PO Box 8, Schenectady, New York 12301

To optimize the sensitivity of metabolic information derived from human *in vivo* spectroscopy studies, localization protocols should be designed to match the size and shape of voxels with those of the pathology within time-limits imposed by any dynamic testing: optimum sensitivity is achieved with the largest acceptable voxel size. Full 3D spectroscopic imaging may be crucial for focal diseases like tumors and infarctions, but can usually only reliably demonstrate *relative* metabolic changes due to compromises involving T_1, T_2, and RF uniformity needed to achieve the desired spatial resolution. For nonfocal disorders like dementias, myopathies and transplant rejection, fine resolution is less important, and enlarging the voxels can buy enough sensitivity to avoid the troublesome T_1, T_2 and RF field corrections. We have used this strategy to measure significant decreases in absolute high-energy phosphate concentrations in whole brain sections in AIDS dementia. Similarly, in heart, 3D localization requires about 20 min for 20 cm^3 voxels and is probably unnecessary for studying cardiomyopathy and transplant-rejection. With 1-D phase-encoding, surface-coil ^{31}P spectra can be acquired from 1 cm slices through the anterior cardiac wall and septum in such patients in just 5-15 min. This timing also allows exercise stress-testing of patients with coronary artery disease. Our clinical findings demonstrating metabolic correlates of neurological dysfunction in AIDS dementia and ischemic myocardium in exercising patients with compromised anterior blood flow, argue strongly for the treatment of voxel size and the localization technique that defines it, as an adjustable variable which should be set to optimize *metabolic* rather than *anatomical* information. In each case the anatomy is best defined by conventional ^1H imaging which becomes an integral and essential part of the spectroscopy exam.

MUSCULOSKELETAL MRI/S

MODERATORS: H. K. GENANT, M.D., F. G. SHELLOCK, Ph.D.

PS 08 08:45AM

MAGNETIC RESONANCE IMAGING OF THE SHOULDER

Harry K. Genant, M.D.
University of California, San Francisco, CA.

Magnetic resonance (MR) imaging, because of its ability to demonstrate a wide range of tissue contrast with excellent resolution, has revolutionized imaging in many areas of the musculoskeletal system generating excitement among those interested in the painful shoulder. Correct diagnosis in shoulder impingement syndrome requires the use of appropriate pulse sequences and imaging planes, proper patient positioning, and a satisfactory surface coil. In addition, the imager must have a thorough understanding of shoulder anatomy and pathology.

The most significant early finding in shoulder impingement syndrome is increased signal in the supraspinatus tendon near its insertion which can be seen on T1-weighted or proton density images. Presumably this is due to an increase in free water protons in the tendon secondary to inflammation, edema, hemorrhage, or a combination of the three. Typically this signal is located approximately one cm from the tendon insertion. In stage II shoulder impingement, there is progressive signal increase in the supraspinatus tendon. It has not yet been established whether the tendon is actually thinned at this point or whether such an appearance is produced by the inflammatory or degenerative process with its resultant signal changes involving certain fibers of the tendon with adjacent portions having a more normal signal. Although investigators have not conclusively demonstrated MR's ability to detect partial tears, it is plausible that MR will be able to demonstrate erosion of the supraspinatus tendon at the level of the critical zone as Codman originally described the lesion. If a joint effusion is present it is conceivable that fluid might flow into an undersurface of the tendon demonstrating the defect. This has yet to be proven. Other findings in Stage II impingement may include changes in size or in signal intensity in portions of the subdeltoid bursa. The fat plane between acromion, AC joint and the superior surface of the supraspinatus may be obliterated or displaced by osteophytes. In stage III shoulder impingement syndrome which is associated with complete rotator cuff tear, the supraspinatus tendon is interrupted or replaced by high signal on both T1 and T2*-weighted images and fluid may be seen in the subacromial-subdeltoid bursa. In addition the supraspinatus musculotendinous junction may be retracted. Eventually the supraspinatus muscle will atrophy and be predominantly replaced by fat which will be seen as increased signal on T1-weighted images. Isolated infraspinatus tears are uncommon but are diagnosed most easily when fatty atrophy of the muscle belly is present. In most patients with stage II or III disease, the supraspinatus muscle and tendon will be obviously impinged along its course between the humeral head and the undersurface of the acromion with its associated spurs.

A summary of the current status of MR imaging of the shoulder including technical, anatomic, and pathologic considerations and a review of the pertinent literature wil l be presented.

PS 09 09:15AM

MR OF THE KNEE

SE Harms
Division of Magnetic Resonance, Department of Radiology
Baylor University Medical Center, Dallas, Texas

Recent advances in knee imaging are reviewed. Improvements in pulse sequences have made three dimensional imaging of the knee a clinical reality. Conventional gradient echo sequences such as GRASS, FISP, FLASH, etc. can be used with a shorter TE (less than 5 msec) for improved contrast and a shorter TR (less than 20 msec) for faster scan times. High signal intensity fluid resulting from T2/T1 contrast is reduced with RF spoiling (Spoiled GRASS). Spoiled GRASS is used for heavily T1 weighted image contrast. A new sequence, 3D FASTER employs nonselective composite RF to achieve a 50% improvement in SNR and better contrast than conventional GRASS. T2 weighting is produced with a steady state sequence that spoils the gradient echo and uses the RF echo for imaging. These T2 weighted fast scan sequences are called SSFP or CE-FAST. When this method is combined with 3D FASTER, it is called CE-FASTER. RF spoiling can be also combined with 3D FASTER for better SNR and T1 weighted imaging. When the 3D data are loaded into an image processor, images are calculated in near real-time for accurate and efficient image analysis. All image planes including oblique planes are calculated from the same set of data. The rapid display of images allows the radiologist to quickly review images and "cone in" on areas of abnormality. Normal knee anatomy as displayed on a 3D workstation is reviewed. A spectrum of clinical abnormalities as seen on 3D images are presented using a variety of 3D optimized pulse sequences. The general advantages of fast 3D include efficient patient thruput, 3D analysis, and higher resolution. In clinical terms these features translate into improved definition of meniscal tears, greater sensitivity for ligamentous injuries, and a significant advantage in the diagnosis of osteochondral disease.

PLENARY SYMPOSIA INVITED TALKS

PS 10 09:45AM

MR OF MUSCLE

W. A. Murphy
Mallinckrodt Institute of Radiology, St. Louis

Normal muscles are easily identified and fully displayed in longitudinal and cross-section due to investing fat that both separates individual muscles and provides contrast between them. Most intrinsic pathological states of muscle are readily differentiated from normal muscle on the basis of both morphological and signal intensity alterations. Among the most dramatic conditions affecting skeletal muscle are the muscular dystrophies, the neuromuscular disorders and the metabolic myopathies.

The metabolic results of exercise induce changes in muscle that are detected as lenghtened tissue relaxation times and revealed as increased signal intensity on pulse sequences that emphasize water content (edema). This pattern can be used to study normal muscle function and to evaluate normal responses and injuries in athletes.

Trauma to skeletal muscle results in a spectrum of conditions and MR patterns. Among the patterns observed are sprain, rupture, hemorrhage and hematoma. Various patterns of myositis may develop and at times be associated with infections. Pyomyositis may be impossible to diagnose without a culture.

Many neoplasias arise within and between muscles. Chief among these are angiovenous dysplasias, lipomas and sarcomas. MRI is effective for detection, localization, characterization and staging of all benign and malignant soft tissue masses. It demonstrates their existence, their local relationships and their extent. Longitudinal sections establish compartmental localization. Cross-sections define local relationships. Combined morphologic and signal characteristics in conjunction with clinical circumstances are often diagnostic of the tissue type. Most investigators recommend MRI as the primary imaging method for evaluation of masses found in muscle.

MRA, FLOW AND PERFUSION

MODERATORS: E. M. HAACKE, Ph.D., T. J. MASARYK, M.D.

PS 11 13:30PM

MR Angiography: An Overview of Current Technology

Paul J. Keller, Ph.D.
Chief Staff Scientist, Magnetic Resonance Research, Barrow Neurological Institute

The study of flow by NMR methods indeed has a long and venerable history. A subset of the myriad of techniques that have been applied produces images of blood vessels--hence the term MR Angiography. A review of all of the members of this subset is not feasible; however, the techniques currently being investigated will be discussed. There are two broad classes of MR Angiographic methods: phase contrast and time-of-flight.

Phase contrast methods as introduced by Dumoulin and co-workers incorporate a bipolar gradient pulse into a gradient-echo sequence. The action of the bipolar pulse results in no net phase change for stationary spins; however, moving spin will acquire a phase advance. On the subsequent excitation, the amplitude of the bipolar pulse is inverted. As before, stationary spins are unaffected, while flowing spins experience a phase change in the opposite direction as previously. Upon subtraction of the signals from the two acquisitions, the contribution from stationary spins cancels; however, the signal for flowing spins is retained proportional to the sine of the phase advance.

Time-of-flight methods rely upon "tagging" spins outside of the imaging volume, and then detecting the tag inside the imaging volume. The tag may be inversion of longitudinal magnetization, presaturation, or simply the in-flow of fresh spins. Early work in this area by Masaryk and others concentrated on in-flow tagged spins flowing into the region of a 3D-volumetric acquisition. Recently, we have explored 2D-sequential slice acquisition. There are many variations on the theme which will be presented.

PS 12 14:00PM

MRA APPLICATIONS

Jeff L. Creasy, M.D.
Vanderbilt University Medical Center

MR angiography (MRA) is becoming increasingly useful in imaging vascular disorders of the head and neck. The various MRA methods allow the visualization of flowing blood within patent vascular structures. While the resolution as yet does not rival cut film angiography or high resolution DSA techniques, it can be used in the noninvasive evaluation of a number of vascular diseases.

Current neuroradiological applications of MRA include demonstrated or promising utility in the assessment of the patency of dural venous sinuses, the delineation of major feeding vessels of AVMs, the evaluation of cerebral aneurysms, traumatic vessel occlusions, and atherosclerotic disease.

Examples will be presented of each of these disorders, as will the optimal MRA techniques for specific disease classes. There will be a brief discussion of uses of MRA outside the central nervous system.

PLENARY SYMPOSIA INVITED TALKS

PS 13 14:30PM

Perfusion and Diffusion Imaging

Thomas J. Brady, MD
Massachusetts General Hospital
Boston, MA 02114

The effect of diffusion on MR images has been recently introduced as a mechanism to induce contrast differences between tissues or physiological states. Diffusion "weighted" images are commonly acquired using a modified Stejskal-Tanner spin-echo sequence or similarly-modified rapid 2-D FT steady-state free precession sequences. Both single and multi-compartmental models have been proposed to take into account the effect of restricted diffusion and microscopic flow. Methods for perfusion imaging have been proposed which utilize extensions to diffusion imaging techniques. In addition, rapid imaging following intravenous injection of high-magnetic-susceptibility contrast agents has yielded kinetic parameters of tissue/organ perfusion. The various approaches to diffusion/perfusion imaging will be presented and discussed.

FAST & 3-D IMAGING

MODERATORS: R. E. HENDRICK, Ph.D., J. TKACH, Ph.D.

PS 14 08:00AM

IMAGE CONTRAST IN GRADIENT ECHO SEQUENCES

FW Wehrli
Hospital of the University of Pennsylvania, Philadelphia, PA

Gradient echo imaging refers to a family of pulse sequences in which an FID or echo is sampled from a train of eqidistant RF pulses of some arbitrary flip angle. Any such stream of RF pulses creates an FID following the excitation RF pulse as well as an echo centered at the site of the RF pulse. The parent of the pulse sequences in which the FID is collected is referred to as FLASH, with two possible variants of implementation: one in which the steady state resulting from residual transverse magnetization is maintained (GRASS, FISP) and one in which the transverse coherences are destroyed (spoiled GRASS, spoiled FLASH). Whereas in the high flip angle regime the former affords contrast in which the signal is approximately proportional to T2/(T1+T2), the use of spoiling enables generation of pure T1 contrast at moderate to high flip angles. A salient feature of this family of pulse sequences is their ability to minimize the degree of saturation by appropriately lowering the pulse flip angle and thus generate images which have the characteristics of proton density weighting, even when TR/T1<<1. Thus, the pulse flip angle is the counterpart of pulse repetition time in spin-echo imaging. A very different class of pulse sequences exploits the echo (SSFP-echo or CE-FAST) with the signal proportional to exp (-2TR/T2), thus enabling generation of T2-weighted images in the very short-TR regime. Each of the pulse sequence classes discussed can be implemented in a 2D or 3D mode. Other characteristic features of gradient echo images are their sensitivity to vascular and CSF flow, discontinuities in magnetic susceptibility and the chemical shift. These phenomena will be discussed and illustrated with clinical images.

PS 15 08:30AM

High-speed MR Imaging: From Fast to Instant

Mark S. Cohen
Advanced NMR Systems, Inc. Woburn, MA

MRI speed improvement methods are important because:

- Motion artifacts severely compromise image quality for many patients and exam types
- Patient tolerance of long exam times is limited
- MRI equipment cost is high on a per exam basis and imaging speed restricts throughput
- For certain organs spatial resolution - and therefore diagnostic value - is limited by motion

The intrinsic physical processes which yield the MR signal are relatively slow in biological tissues. The longitudinal relaxation rate (T1), in particular, poses fundamental limits on the rate at which the signal can be repeatedly excited to form images. Two general classes of imaging methods are presently utilized to circumvent these limitations: partial saturation techniques (small RF flip angles) which disturb the magnetization less and therefore require less time for signal recovery, and rapid encoding methods which decrease the time for position-encoding by acquiring several, or all, lines of phase encoding after each echo.

Clinical image quality, determined by spatial resolution, contrast and temporal resolution, differs greatly for the several speed enhancement methods. The partial flip angle techniques generally trade contrast, and to a certain extent signal to noise ratio, for imaging time. They maintain high spatial resolution and are often, therefore, excellent methods for the rapid detection of anatomical abnormalities. The rapid encoding techniques, such as Instascan, generally pay a price of spatial resolution for their improved speed and contrast; they may also require special hardware. Recent technical advances in Instascan have allowed the acquisition of images with resolution comparable to that of conventional MRI but with a temporal resolution which allows both motion free imaging and direct visualization of the time course of contrast agent uptake and distribution, in turn enabling assessment of e.g. cerebral blood flow and volume. The instant techniques offer the potential for clinical diagnosis based on functional differences and for the replacement of time-consuming conventional scans with their instant equivalents.

PLENARY SYMPOSIA
INVITED TALKS

PS 16 09:00AM

ACQUISITION AND PROCESSING OF 3-D MR IMAGES

ML Wood

Tufts University and New England Medical Center, Boston, MA 02111

Three-dimensional (3-D) MRI can cover extensive regions of anatomy with high resolution in all three directions. Gradient echo techniques that use short repetition times (TR=10-30 ms) can complete the acquisition of data for a 3-D image of 256x256x128 voxels in five to 16 minutes. Recent improvements in data acquisition will be reviewed first, including the spoiling of transverse magnetization, steady state free precession (SSFP), and MR angiography. Components of transverse magnetization can persist over several TR intervals when TR is much shorter than T2. Such transverse coherences can cause artifacts and influence the contrast in 3-D MR images, similarly to two-dimensional (2-D) images. Transverse coherences must be spoiled for T1-weighted contrast. Spoiling is accomplished by shifting the phase of the transverse magnetization by a linearly increasing amount at the end of each phase encoding step. Instead of spoiling transverse magnetization, SSFP techniques attempt to maintain it in a steady state. The intensity of tissues with long T2, such as cerebrospinal fluid (CSF), becomes enhanced with SSFP, especially when TR is short. The imaging of CSF appears to be a promising application for 3-D SSFP. Gradient echo images become distorted near abrupt magnetic susceptibility changes, but 3-D images are affected less than their 2-D counterparts. The use of non-selective RF pulses instead of selective RF pulses provides more uniform excitation and also a shorter $TE_{,}$, which reduces degradations caused by susceptibility changes and motion.

The second part of the presentation concerns recent image processing developments for visualizing 3-D MR images and obtaining volumetric measurements. Although these applications are not unique to MRI, they are challenging, because it is difficult to segment MR images into tissue components. Techniques for reformatting and rendering 3-D MR images into surfaces or volumes are being applied to diagnosis, surgery and radiation therapy planning, and physician education. These applications are becoming more practical, because of engineering advances that have been incorporated into new MRI systems and workstations.

CARDIOVASCULAR MRI

MODERATORS: R. M. HENKELMAN, Ph.D., R. J. HERFKENS, M.D.

PS 17 13:30PM

New Developments in Dynamic Cardiac Cine MRI

Michael S. Silver, MD
Philips Medical Systems
Shelton, CT 06484

Dynamic cardiac cine MRI is rapidly becoming accepted as a tool for cardiac function and structure evaluation. Left and right ventricular function, ventricular mass, valvular function, and wall motion abnormalities can all be evaluated easily in multiple planes within a reasonable scan time. Cine MRI can add valuable information to that provided by echocardiography and cardiac catheterization in the assessment of complex congenital heart disease. Several additions to the standard velocity-compensated gradient echo sequences have been introduced recently, expanding the potential of the method. Techniques such as spatial modulation of magnetization allow for potentially quantitative assessment of wall motion abnormalities. Creative gating strategies such as phase-gating and retrospective ECG-referenced gating improve image quality in the presence of arrhythmia or decreased R-waves. Saturation techniques which enhance contrast, reduce blood flow artifacts, and permit the quantitation of blood flow within the heart have also been presented. The combination of ultra-fast imaging techniques and the use of contrast agents promises to open the way for MR myocardial perfusion measurements currently available only with PET and SPECT. Display and analysis methods for the vast quantity of data acquired in an exam are being developed. Four-dimensional analysis and display are currently possible, but not yet practical for routine examinations.

PS 18 14:00PM

MRI OF CONGENITAL HEART DISEASE

R.D. WHITE, M.D.
DEPARTMENT OF RADIOLOGY, SECTION OF CARDIOVASCULAR IMAGING, CLEVELAND CLINIC FOUNDATION

Because of its non-invasive nature and the high-quality anatomic detail provided, MRI has been popularized for the evaluation of congenital heart disease (CHD). ECG-triggered spin-echo (S-E) MRI has already become established for the detection of simple (e.g.,ASD) and complex (e.g., single ventricle) forms of CHD, as well as for congenital anomalies of the great arteries (e.g., coarctation). The most unique anatomic capabilities of S-E MRI are seen in the setting of complex cardiovascular anomalies in which segmental assessment of situs, systemic and pulmonary venous return, atrioventricular and ventriculoarterial connections, and chamber morphology is required. In addition, because of the ability to evaluate the great arteries and their branches within the mediastinum and lungs, it has been particularly useful in evaluating related congenital abnormalities (e.g., pulmonary atresia).

With the advent of ECG-gated dynamic gradient-echo ("Cine") MRI, the ability to derive physiologic information about CHD has become possible. Because of the good temporal resolution and the characteristic appearance of abnormally turbulent or stagnant flow, information about ventricular contractility, valvular function, unidirectional or bi-directional shunting, and post-stenotic or diminished flow within the great arteries can be assessed. Cine MRI also appears useful in the anatomic evaluation of simple congenital abnormalities at the cardiac (e.g., VSD) or great artery (e.g., coarctation) levels.

In this presentation, representative S-E and Cine images will be shown to demonstrate how these techniques can assess the anatomic and physiologic abnormalities found in a wide range of CHD, respectively. In addition, other MRI techniques which may have valuable roles in the evaluation of CHD will be described.

PLENARY SYMPOSIA
INVITED TALKS

MRI Evaluation of Cardiac Function

Charles B. Higgins, MD and Stefan Wagner, MD
University of California, San Francisco, CA 94143

Functional evaluation of the cardiovascular system is now practical using cine MR. Several reports have indicated the capability of multiphasic ECG-gated (image acquired in both diastole and late systole) or cine MR imaging for the evaluation of abnormal blood flow patterns, left ventricular and right ventricular dimensions and stroke volumes, left ventricular mass, and regional myocardial function.

By achieving a temporal resolution of more than 30 frames per cardiac cycle, cine MR successfully captures end diastole and end systole, such that end diastolic and end systolic volumes and ejection fractions can be accurately calculated. It should be noted that the temporal resolution of cine MRI does not capture a single heart beat, but rather separates an average heart beat into many components. The imaging data for this average heart beat is acquired over 256 cardiac cycles. Normal values for left ventricular volumes and ejection fraction using cine MR imaging have been reported. A good correlation has been found between LV volumes calculated from cine MRI and those measured from 2-D echocardiography and angiography. It should be noted that those volumes measured from cine MR are smaller in general than those that have been traditionally accepted based on angiographic measurements. The advantages of MR imaging for such measurements are that this technique is a truly 3-D imaging technique when tomographic images are acquired encompassing the entire chamber being interrogated. However, angiographic measurements depend upon geometric assumptions, which have variable validity, depending upon the shape of the chamber.

Measurement of left ventricular mass using MR imaging has shown a close correlation with postmortem measurements in animals and estimates from angiography in man. Accurate measurement of left ventricular mass is important, since changes in mass may be the most effective way to monitor the response to therapy in diseases causing left ventricular hypertrophy. Sequential measurements of mass could be used to effectively monitor the myocardial response to aortic valve replacement or pharmacologic treatment of hypertension.

Functional evaluation in ischemic heart disease is achieved using MR by monitoring wall thickening during the cardiac cycle. A study in normal individuals and patients with prior myocardial infarction demonstrated that MR imaging distinguished the site of previous myocardial injury by a diminution or absence of wall thickening during systole.

NEURO, MR AND PET

MODERATORS: R. B. LUFKIN, M.D., V. M. RUNGE, M.D.

PS 20 08:00AM

NEUROSURGICAL APPLICATIONS OF INTEGRATED 3-D DISPLAY OF MRI AND PET

D.N. Levin et al.
Dept. of Radiology, U. of Chicago, Chicago, IL 60637

Image processing and computer graphics techniques have been used to create 3-D views of the brain surface from data acquired during a single 10 minute MR scan (1). This made it possible to see the pre-central (motor), post-central (sensory), left inferior frontal (speech), and left superior temporal (hearing) gyri, which could not be identified with certainty on cross-sectional images. Neurosurgical planning benefited from this new information.

Most patients with medically-intractable epilepsy have normal MR scans and abnormal PET images of brain metabolism. However, the PET scans are insufficiently resolved to depict the anatomical location of the lesion. Software was developed for using the PET data to create a 3-D model of brain surface metabolism. This model was fused with an MR-derived model of brain anatomy (2) by means of a program for retrospective image registration (3). The result was an integrated 3-D model of brain anatomy and function which showed the location of PET-detected seizure foci with respect to MR-depicted gyral anatomy.

MR "angiographic" images are usually reformatted as maximum intensity projections, which demonstrate the vasculature against a background of featureless brain signal. Software was developed for using MR angiography data to create a 3-D model of the isolated vascular tree, which was merged with a highly resolved model of brain anatomy (4). The observer could then assess the 3-D relationship between vessels and brain parenchymal anatomy.

Physicians could interactively manipulate these multimodality 3-D models in order to perform electronic "rehearsals" of neurosurgical procedures. They could also "roam" through a model, examining any anatomical or functional attributes at any point in the patient's brain. A video clip will be shown to illustrate the clinical application of these techniques.

1. Levin DN, Hu X, Tan KK, and Galhotra S. Radiol 1989; 171:277-280.
2. Levin DN, Hu X, Tan KK et al. Radiol 1989; 172:783-789.
3. Pelizzari CA, Chen GTY, Spelbring DR et al. JCAT 1989; 13:20-26.
4. Hu X, Tan KK, Levin DN et al. Proc of Chapel Hill Workshop on Volume Visualization, 1989; pp 45-49.

PS 21 08:30AM

Neuro-correlative Studies: MRI/MRS/PET

Robert M. Kessler, MD
Vanderbilt University, Nashville, TN 37232-2675

PET and MRI have been utilized in many of the same disorders, i.e., cerebral tumors, peripheral sarcomas, head and neck tumors, colon cancer, epilepsy, dementia, movement disorders, and ischemic coronary artery disease. To date, MRI has predominantly relied upon proton imaging to produce high resolution, high contrast anatomical studies with some information related to chemical composition and flow. PET has utilized a variety of tracers to study glucose metabolism (^{18}F2-fluorodeoxyglucose), cerebral blood flow ($H_2{}^{15}O$, $C^{15}O_2$, $C^{15}O$), protein synthesis (^{11}C leucine and methionine), neurotransmitter synthesis (^{18}F6-fluoro-DOPA) and receptors (^{18}FN-allcylspiperone, ^{11}C-raclopride, ^{11}C-N methyl spiperone), as well as regional myocardial blood flow ($^{13}NH_3$).

The study of gliomas illustrates how these modalities often interact. MRI is an exquisitely sensitive means of detecting and often categorizing cerebral tumors. PET allows one to predict the grade of glioma and, for high grade gliomas, survival times of patients. It is particularly useful in defining the extent of tumors and differentiating post-surgical and post-radiation changes from recurrent tumor. These are areas where MRI has proved less useful. Partial seizures, movement disorders, stroke, dementia and ischemic coronary artery disease will be discussed as well.

The ability of MRS to study levels of tissue metabolites, particularly related to energy metabolism, will be discussed in relation to the capability of PET to study metabolic changes in disease. The potential for MR spectra to specifically characterize CNS neoplasms and ischemia will also be explored.

PLENARY SYMPOSIA INVITED TALKS

PS 22 09:00AM

CLINICAL SPINE MRI: PULSE SEQUENCES, GRADIENT ECHO TECHNIQUES AND CONTRAST AGENTS

JS Ross
University Hospitals of Cleveland, Cleveland, Ohio

The role of MRI in the spine has gone far beyond its original clinical expectations, and today has multiple well defined applications. MR's value has been established by comparative studies with conventional modalities in degenerative disease involving the cervical and lumbar spine, vertebral osteomyelitis, congenital malformations, and intramedullary lesions such as syringomyelia and neoplasm. The modality is still evolving, and research in coil technology and pulse sequences continues to improve our approach to spinal pathology. MRI has an accuracy of greater than 80% compared to surgery in defining lumbar disk herniation and stenosis. In cervical radiculopathy, MR agrees with surgical findings 75-80% of the time, compared to 80-85% for CT myelography. Improvements in the evaluation of degenerative disease depend upon decreasing slice thickness, and the ability to image directly the oblique course of the foramina. 3D GE imaging has the potential for increasing the accuracy of MR in the cervical spine. The use of contrast is essential in the evaluation of the postoperative patient with a question of recurrent disk herniation versus epidural fibrosus, where MRI's accuracy is 96% when compared to surgical findings. Spine MRI has become an integral part of the imaging armamentarium, with a resultant decrease in the need for invasive myelography. Improvements in MRI should limit the role of intrathecal contrast in the evaluation of spinal pathology.

ABDOMINAL/PELVIC MRI

MODERATORS: D. D. STARK, M.D., H. D. SOSTMAN, M.D.

PS 23 13:30PM

NEW DEVELOPMENTS IN MR IMAGING OF THE UPPER ABDOMEN

HERBERT Y KRESSEL, M.D.
HOSPITAL OF THE UNIVERSITY OF PENNSYLVANIA

The role of high field magnetic resonance imaging of the abdomen has been somewhat controversial. A number of initial concerns, namely lack of sufficient contrast at higher fields, and lack of adequate RF penetration, have not proved to present a significant problem. However, a number of the generic problems in the magnetic resonance imaging of the abdomen, namely motion effects, the lack of optimal gastrointestinal contrast material, and chemical shift artifacts still are problematic.

Artifacts due to motion, namely blurring and the presence of periodic ghost images serve to markedly degrade the image quality obtained in the upper abdomen and liver. Respiratory motion, cardiac pulsations, peristaltic motion, and gross patient motion during the time of data aquisition all contribute to the image degredation. A number of different technical approaches to controlling and reducing motion related artifacts have been employed to improve image quality in the liver and upper abdomen. These include: cardiac and respiratory gating, short TR/TE scans with extensive signal averaging, respiratory ordered phase encoding, short T1 inversion recovery, selective saturation, gradient moment nulling, and gradient echo fast scan techniques have been employed to reduce flow related artifacts. With improved artifact control, morphologic information is superior and improved diagnostic specificity can be obtained.

PS 24 14:00PM

KIDNEYS AND RETROPERITONEUM: CLINICAL EXPERIENCE WITH MRI AND CORRELATIVE IMAGING WITH MRI/US/CT

THOMAS A. POWERS, M.D.
VANDERBILT UNIVERSITY MEDICAL CENTER

Magnetic resonance is a nearly ideal imaging modality for examination of the retroperitoneum. The ability to image in coronal and sagittal planes allows MR to better evaluate retroperitoneal masses for possible invasion of contiguous structures. In the case of renal or adrenal tumors, spin echo sequences can usually document presence or absence of renal vein and caval extension, eliminating the need for inferior vena cavagrams. Renal masses may be differentiated to some degree based on their signal characteristics. Newer fast scan sequences, e.g. Turbo-Flash, allow dynamic imaging of a contrast (Gd-DTPA) bolus through the kidneys and adrenals and may prove useful in further defining mass lesions.

PLENARY SYMPOSIA
INVITED TALKS

PS 25 14:30PM

FEMALE PELVIS: MRI/US/CT

Shirley McCarthy, M.D., Ph.D.
Yale University School of Medicine, New Haven, CT

Gynecologic anatomy is reliably demonstrated and optimally seen with T2 weighted scans. MRI is a valuable tool in the classification of abnormal uterine development since the amount of interposing myometrium, the external contour of the uterus, and non-communicating segments can be directly demonstrated. Although US is a good screening technique, MRI is the procedure of choice in the therapeutic evaluation of leiomyomas because the number, size, vascularity, location and degeneration is demonstrated. Additionally, precise quantitative assessment of response to conservative medical therapy is possible. Adenomyosis, not seen with other techniques, can be prospectively identified with MRI and appears as a focal or diffuse thickening of the junctional zone. Foci of high signal on T2 and some T1 weighted images can also be seen which represent the heterotopic endometrium. MRI is very useful in localizing masses equivocal on US to a uterine or ovarian location. The signal behavior of most ovarian masses in non-specific except for benign masses such as dermoids and endometriomas. Endometriomas being hemorrhagic exhibit characteristic signal behavior on MRI. However, MRI is not useful in the routine diagnosis or staging of endometriomas since adhesions and small implants are not routinely identified. Dermoids typically exhibit signal behavior similar to fat. Contiguous chemical shift artifact is diagnostic. MRI is not useful in staging ovarian cancer since the long imaging times result in motion obscuration of peritoneal implants. MRI is superior to CT in staging endometrial and cervical cancer.

INVITED TALKS

RECENT DEVELOPMENTS IN IVIM MR IMAGING

D. Le Bihan, R. Turner, C. Moonen, P. Van Zijl, J. Delannoy.
Diagn. Radiology Dept. and Biomed. Eng. and Instr. Branch, NIH, Bethesda, MD20892.

Intravoxel incoherent motion (IVIM) MR imaging was proposed several years ago to measure and image diffusion-like motions of spins occuring in each voxel. These motions are expected to be represented mainly by molecular diffusion and microcirculation in pseudo-randomly orientated capillaries (perfusion). In the presence of magnetic field gradients, incoherent motion produces intravoxel dephasings which destructively interfere and result in signal attenuation. This attenuation, usually negligible with conventional MR sequences, can be dramatically enhanced by adding a strong gradient pulse pair. Images where contrast depends only on IVIM can be calculated from a series of images differently sensitized to IVIM by gradient pulses differing in strength or duration. IVIM imaging has been shown to be compatible with any MR imaging sequence, namely spin echoes, stimulated echoes, or steady-state free precession using 2DFT reconstruction schemes, and more recently echo-planar. The latter technique has the advantage of overcoming the problem of motion artifacts that may arise with 2DFT type sequences due to temporal variations in macroscopic motion.

Diffusion imaging may be useful in many areas. Clinically, cystic lesions and edema present diffusion coefficients close to that of pure water and can be separated from solid lesions where diffusion coefficients are much smaller due to viscosity or restricted diffusion effects. By using high performance gradient coils, low diffusion coefficients can be determined more accurately. It becomes then possible to demonstrate restricted diffusion effects. When molecular displacements are limited by microscopic barriers, the measured diffusion coefficients are apparently decreased as a function of the size of the restricted volume, possibly of value for tissue characterization. In these conditions, diffusion coefficients may appear different along different directions of measurement (anisotropy) as it has been shown in brain white matter, varying with the direction of the myelin fibers. Using IVIM-spectroscopy, diffusion of metabolites can be determined *in vivo*. Diffusion coefficients are also temperature dependent and diffusion imaging has been used for temperature mapping.

The effects of perfusion in IVIM imaging are more controversial. As microcirculation involves only a very limited number of spins, care is required in both hardware and experiment control. Qualitative clinical perfusion images and quantification of perfusion in IVIM images have been obtained in the cat brain using a very simple model. Perfusion imaging using IVIM techniques has the advantage of working without contrast agents, of interest for functional imaging.

Biodistribution, Toxicity and Imaging of Small Unilamellar Paramagnetic Liposomes

Evan Unger, M.D., Thomas Fritz, M.Sc., Robert McCarver, MS IV, Colin Tilcock, Ph.D.
University of Arizona, Department of Radiology (EU, TF, RM)
University of British Columbia, Department of Biochemistry (CT)

We synthesized limit size vesicles 30 nm in diameter from egg lecithin and cholesterol to encapsulate either Gadolinium-DTPA (Gd-DTPA) or Gd-DOTA. We performed biodistribution of the Gd-DTPA liposomes in rats yielding a half-life for clearance of the liposomal 153-Gd-DTPA from the liver of about 3 1/2 days. In these experiments we also perform biodistribution, clearance and toxicity testing in mice for both Gd-DTPA and Gd-DOTA liposomes. To answer the question as to whether liposomal Gd-DTPA may decomplex once in the liver we perform biodistribution with Cl4 labelled DTPA-Gd. The final concentration of gadolinium in the liposomal preparation was 150 mM. In mice, because of volume constraints, the highest dose that could be injected IV was 1.35 mmoles weight with no sign of any acute toxicity at this dose, which is almost 60 times higher than the effective imaging dose of liposomal gadolinium which we have shown to be 0.025 mmoles Gd per kg body weight. Subsequent acute toxicity testing at higher doses of gadolinium had to be administered via IP injection and the liposomal Gd-DTPA had lower acute toxicity than free Gd-DTPA.

The results of these experiments may be summarized as follows:

1. To maximize the relaxivity of entrapped gadolinium the liposomes should be as small as possible (limit size = approx. 30 nm).
2. Both Gd-DTPA and Gd-DOTA function effectively when entrapped in vesicles as liposomal MR contrast agents.
3. Acute toxicity of the liposomal contrast agents is no greater than either Gd-DTPA or Gd-DOTA without liposomal encapsulation.
4. Results of chronic toxicity and decomplexation will be presented.

NOTES

NOTES

NOTES

INDEXES AND INFORMATION

NOTES

SMRI 1990 TECHNICAL EXHIBITS INDEX

3M Medical Imaging Systems Division
Building 223-2W-03,
3M Center
St. Paul, MN 55144-1000
612-733-2154

Agfa Matrix Division, Agfa Corporation
100 Challenger Road
Ridgefield Park, NJ 07660
201-641-9566

Berlex Imaging
300 Fairfield Road
Wayne, NJ 07470
201-305-5082

C.V. Mosby Company
11830 Westline Indiana Drive
St. Louis, MO 63146
314-872-8370

CompHealth
4021 South 700 East
Salt Lake City, UT 84107
801-264-6400

Diagnostic Imaging Magazine
500 Howard Street
San Francisco, CA 94105
415-397-1881

Diasonics, Inc.
280 Utah Avenue
S San Francisco, CA 94080
415-872-2722

Eastman Kodak Company
343 State Street
Rochester, NY 14650
716-724-2689

Elscint, Inc.
930 Commonwealth Avenue
Boston, MA 02215
617-739-6000

E-Z-EM, Inc.
7 Portland Avenue
Westbury, NY 11577
516-333-8230

GE Medical Systems
P.O. Box 414 (W-439)
Milwaukee, WI 53201
414-548-2223

Hitachi Medical Systems America, Inc.
70 West Streetsboro,
Ste. 106
Hudson, OH 44236
216-656-9336

Instrumentarium/ Ausonics
900 West Edgerton Avenue
Milwaukee, WI 53207
414-747-1030

Medical Advances, Inc.
10431 Watertown Plank Road
Milwaukee, WI 53226
414-258-3808

Medrad, Inc.
271 Kappa Drive
Pittsburgh, PA 15238
412-782-4600

New Methods Research, Inc.
719 East Genesee Street
Syracuse, NY 13210
315-424-0329

Nonin Medical, Inc.
12900 Highway 55
Plymouth, MN 55441
612-553-9968

Pergamon Press
395 Saw Mill Road
Elmsford, NY 10523
914-592-7700

Permanente Medical Group
1814 Franklin Street
4th Floor
Oakland, CA 94612
415-987-4972

Philips Medical Systems North America Company
710 Bridgeport Avenue
Shelton, CT 06484
203-926-7647

Picker International
595 Miner Road
Highland Hts., OH 44143
216-473-3544

PME, Inc.
1315 Union Plaza Court,
#201
Oceanside, CA 92054
619-967-8518

Radiology Today/ Slack Inc.
6900 Grove Road
Thorofare, NJ 08086
609-848-1000

Resonex, Inc.
720 Palomar
Sunnyvale, CA 94086
408-720-8600

Siemens Medical Systems, Inc.
186 Wood Avenue,
South
Iselin, NJ 08830
201-321-4500

Southern California Permanente Medical Group
393 East Walnut Street
Pasadena, CA 91188
818-405-3224

Toshiba America Medical Systems, Inc.
2441 Michelle Drive
Tustin, CA 92681
714-730-5000

Year Book Medical Publishers
200 North LaSalle Street
Chicago, IL 60601
312-726-9733

8TH ANNUAL MEETING ACKNOWLEDGEMENTS

▼

BREAK/LUNCHEON SERVICE

The SMRI has provided complimentary pre-session and afternoon coffee/soda and light luncheon service for Annual Meeting participants. All service will be provided in the rear of the Technical Exhibit areas. Please avail yourself of the services provided.

MORNING COFFEE BREAK

The Society gratefully acknowledges the generous contribution received in support of these events from Picker International.

A TASTE OF AMERICA

The Society gratefully acknowledges the generous contribution received in support of this event from Siemens Medical Systems.

AUTHOR INDEX

▶ X

▶ Y

▶ Z

NOTES

SMRI

MEMBERSHIP INFORMATION

The Society for Magnetic Resonance Imaging is an organization whose purpose is to:

- Provide an equal opportunity to physicians and basic scientists to contribute to the development of MRI.
- Provide an international multidisciplinary forum for the advancement of magnetic resonance imaging.
- Promote the applications of magnetic resonance techniques to medicine and biology, with special emphasis on imaging.
- Prepare and disseminate technical and product information related to research techniques, equipment and clinical applications of magnetic resonance.
- Develop educational and training material and methods for the application of magnetic resonance to medicine and biology.

All individuals involved in the field of magnetic resonance imaging are invited to join the Society. The Full, Associate and Corporate membership rates include a subscription to the bimonthly journal, *Magnetic Resonance Imaging*. Those applying for membership categories of Technologist and Student may obtain a subscription to the journal by remitting an additional $40.

MEMBERSHIP

- The membership of the Society for Magnetic Resonance Imaging is composed of clinical and basic scientists and technologists. These individuals are joined by a common objective—to contribute to the development of magnetic resonance as a diagnostic technique in medicine. New frontiers of research are reached daily by members of the SMRI and are disseminated beyond the Society through its journal, *MRI* and the Annual Meeting.
- Membership in SMRI is open to all basic and clinical scientists and technologists actively engaged in MR. Additionally, certain allied scientists who share the stated purposes of the Society may also join SMRI.
- Residents and fellows in MR training programs are eligible for a subsidized category of membership. Through such membership, and through non-member subscriptions to the *MRI* Journal, the SMRI reaches many residents in such training programs.
- Benefits of all categories of membership include reduced registration fees at the Annual Meeting and a reduced subscription rate to the *MRI* Journal.

MEMBERSHIP REQUIREMENTS BY CLASS AND BENEFITS OF MEMBERSHIP

FULL MEMBER

A person who shares the stated purpose of the Society, who is involved in the field of MRI and who has completed postgraduate studies or equivalent training in any subject or work of significant merit in the area of magnetic resonance.

- subscription to the Journal, *Magnetic Resonance Imaging;*
- reduced registration fee at Annual Meeting;
- right to vote;
- right to hold office.

TECHNOLOGIST MEMBER

A person who shares the stated purpose of the Society and who has technical or professional background in the area of MRI or an allied field.

- journal subscription at member rate of $40;
- reduced registration fee at Annual Meeting.

STUDENT MEMBER

A person who shares the stated purpose of the Society and who is engaged in full-time study, graduate or undergraduate, in the fields of medicine, basic or applied science.

- journal subscription at member rate of $40;
- reduced registration fee at Annual Meeting.

CORPORATE MEMBER

A corporate entity that has a major interest in the development and application of NMR instrumentation in MRI or MRS for medical or biological purposes. Selection to corporate membership must be confirmed by a 2/3 vote of the Board members present at the meeting following application for such membership.

- member of SMRI Corporate Council;
- subscription to the Journal, *Magnetic Resonance Imaging.*

ASSOCIATE MEMBER

A person who shares the stated purpose of the Society, but does not qualify for other categories of membership.

- subscription to the Journal, *Magnetic Resonance Imaging;*
- reduced registration fee at Annual Meeting;
- right to vote.

SMRI CANDIDATE INFORMATION FORM

▼

In order to be considered for MEMBERSHIP, please provide the information requested below. A complete curriculum vitae of your education, employment and publications MUST accompany this application.

1. **Name:** _____ **Degree:** _____

2. **Address:** _____

   City/State/Zip/Country: _____

   Telephone Number: (____) _____ Fax Number: (____) _____

   The above information is your (☐ office or ☐ home) address and telephone number.

   Employed By/Affiliated With: _____

3. **Sponsor I:** _____ **Sponsor II:** _____

   Name _____ Name _____

   Tel. No. _____ Tel. No. _____

4. **Classification Codes:** (Enter code which best describes your professional classification) _____

   1. Clinical scientist
   2. Basic scientist
   3. Resident/trainee (specialty _____)
   4. Radiology Support Personnel and Hospital Staff: (a) technologist, (b) engineer, (c) radiology business manager, (d) radiology administrator, (e) nurse, (f) hospital administrator, (g) radiology educator, (h) hospital purchasing agent.
   5. Qualified Non-Health Sciences Personnel: (a) architect, (b) computer analyst, (c) investment broker.
   6. Non-Hospital-Based Medical Care Provider: (a) purchasing consultant, (b) equipment consultant, (c) imaging center entrepreneur.

5. **Professional Affiliations:** _____

   (a) AAN, (b) AAPM, (c) ACR, (d) ARRS, (e) ASNR, (f) ASRT, (g) ESMRMB, (h) RSNA, (i) SMRM, (j) SNM, (k) Other: _____

6. **Please check your area of specialty from the following fields of study:**

   ☐ M.D.: Radiology, Neurology, Cardiology, Other: _____

   ☐ Ph.D.: Physics, Bio-Chemistry, Spectroscopy, Biology, Other: _____

   ☐ Other: _____

7. **Please check your primary workplace from those listed below:**

   ☐ University Hospital/Medical School ☐ Industry

   ☐ Private Hospital/Clinic ☐ Hospital/Clinic: Number of Beds _____

   ☐ Government Lab ☐ Other: _____

8. **Please check appropriate Membership Classification:**

   ☐ Full ($100.00) ☐ Technologist ($25.00) ☐ Student ($25.00) ☐ Associate ($100.00)

   ☐ I am applying for Student or Technologist Membership and am enclosing an additional $40.00 for a subscription to *Magnetic Resonance Imaging.*

Signature: _____ Date: _____

IMPORTANT

Your application package must include all of the following elements before approval procedures may begin:

- ▶Completed Application
- ▶Curriculum Vitae
- ▶Membership Fee

RETURN TO:

Society for Magnetic Resonance Imaging
213 W. Institute Place; Suite 501
Chicago, IL 60610

SOCIETY FOR MAGNETIC RESONANCE IMAGING

Washington, D.C.
February 24 - 28

CERTIFICATE OF ATTENDANCE

This is to certify that _____ was registered for the educational and/or scientific activities at the 8th Annual Meeting, of the SMRI, February 24 – February 28, 1990, at the Washington Hilton and Towers in Washington, D.C.

SOCIETY FOR MAGNETIC RESONANCE IMAGING
EDUCATIONAL AND SCIENTIFIC PROGRAM

Washington, D. C.
February 24 - 28

As an organization accredited for continuing medical education, the American College of Radiology certifies that this continuing medical educational offering meets the criteria for Category I Credit for up to 33-1/4 hours, provided it is completed as designed.

This form is provided to assist registrants in the recording of Category I Credits earned, hour-for-hour, at the 8th Annual Meeting. The SMRI will not record credits earned by individuals. Please keep this record for your own files. Do not send this to the ACR office or to the AMA office.

Day	Hours Attended/ Credit Earned	Maximum Credit Possible
Saturday	_____	7 Hours
Sunday	_____	6-3/4 Hours
Monday	_____	6-1/2 Hours
Tuesday	_____	6-1/2 Hours
Wednesday	_____	6-1/2 Hours
Total Credits Earned:	_____	Total Credits Available: 33–1/4 Hours

R E Hendrick

Signature of Certifying Official
Society for Magnetic Resonance Imaging